PUBLIC UNIVERSITY OF NAVARRA
Technical School for Industrial Engineering
& Telecommunications

The Potential Integration *of* Distributed Generation *in* Medium & Low Voltage Grids: The Applicability *of* Power Flow *and* Hardware-In-The-Loop Tools *for* Simulation *and* Validation

Author:
Konstantina Mentesidi

Supervisor:
Monica Aguado Alonso, Ph.D.
Department of Electrical & Electronic Engineering
Public University of Navarra (UPNA)

A Thesis submitted to the
Electrical & Electronic Engineering Department
in fulfilment of the requirements for the degree of
Doctor of Philosophy

October, 2014

'Δεν υπάρχουν ιδέες, υπάρχουν μονάχα άνθρωποι που κουβαλούν τις ιδέες, κι αυτές παίρνουν το μπόι του ανθρώπου που τις κουβαλάει...'

Νίκος Καζαντζάκης

Abstract

Lately there is a growing interest towards distributed generation (DG) penetration in medium and low voltage (MV/LV) networks and generally in autonomous power systems. Consequently, the common assumption of a unidirectional power flow and voltage drop along the distribution feeders is no more credible for all the operating conditions.

With renewable electricity generation increasing, there will be some important changes in electric power systems, notably through smaller generators embedded in the distribution network. The introduction of this kind of systems allows a better management of the resources and an optimum planning of the power generation system favouring the reduction or even elimination of inefficient and expensive plants. However, the amount and the location of distributed generation penetration would start to influence the dynamics and stability of the transmission and distribution network respectively.

For instance, voltage control in these power networks is usually restricted to the on-load tap transformer changer at the high/medium voltage substations. Thus, maintaining the voltage levels within specific limits, which is a significant power quality criterion, is a great challenge in electricity supply. Furthermore, voltage deviations induced by load changes and power delivery limitations are observed during reactive power instability. Switched capacitors, reactors and VAR compensating devices such as STATCOMs are used to control reactive power flow and thus maintaining voltage in electrical systems and have proved to be effective since they can reduce these energy transfer limitations. Apart from VAR compensating devices, distributed generators interfaced to power electronic converters are, usually, controllable reactive power sources.

Hence, in order to analyze a grid and examine the impacts of distributed power integration, considerations such as the dynamic behaviour of a power system that entails transient stability analysis, grid capacity and limits characterization need to be taken into account. Besides, this type of study is very important to ensure the network´s secure operation under fault incidents. Therefore, comprehensive analysis of distributed energy resources' integration requires tools that provide computational power and flexibility.

The current thesis is dedicated to the penetration of DG technology into a MV/LV distribution network that may loosely represent an Island or autonomous power system since MV/LV levels are of high interest as most of distributed energy sources (DER) will be connected there. Two simulation tools will be utilised throughout this work to demonstrate the implementation of DG technology on distribution networks; the Siemens PTI, PSS/E software tool that allows for grid penetration and analysis studies and RTDS/RSCAD program that allows for real time simulations and execution of Power Hardware-in-the-loop (PHIL) tests.

Due to the particular structure and characteristics of Islands, the penetration of DG and DER devices may provoke problems and constraints which lead to limitations of their integration level into this type of power systems. In respect to these limitations, the following aspects need to be considered; Voltage deviations, fault ride through capability (FRT) of DG units, short circuits etc.

Accordingly, this research work aims at building the grid model of a real Island system and implementing steady-state and dynamic simulation analysis configurations with the commercial software tool, PSS/E to determine the allocation, maximum capacity of embedded generation that may be inhabited within this autonomous network. Various scenarios are employed with different penetration rates of geothermal and wind generation units in addition to the distribution voltage levels to be connected to in order to study the steady-state limit of distributed generation integration into this system. In this way, it is possible to check the Island's system dynamic behaviour under normal operation and against several disturbances onto the grid.

Additionally, thanks to the limitation of the PSS/E model's library, it was decided to emulate and verify the ''smart'' coexistence of central and decentralised generation very close to realistic conditions. In this context, two sets of tests of real time simulations were developed on hardware-in-loop (HIL) environment in RTDS/RSCAD software tool and Power Hardware-in-the-Loop experiments were executed. The extension in mind was to apply different solutions to increase DG in an Island power system or generally in a LV distribution network. In particular, the utilisation of a VAR compensating device (i.e. STATCOM) and the use of energy storage systems (i.e. DC-capacitor) may prove to be key effective.

Therefore, the first group of tests analyse the application of reactive power compensating devices to distribution networks and the second one emulate the energy management system of a real Microgrid (MG) including a diesel synchronous machine and inverter-based sources in order to examine their dynamic operation within the LV islanded power system.

The PSS/E results discuss the impact may induce any units´ addition on the power system´s load flow, short circuit level (SCL) and transient stability. The major advantage of this work is that proposes the most suitable substations to introduce the dispersed generation with the extension in mind the voltage level to connect these units. The main issues addressed were the total system losses, fault level at the addition and nearby buses, whereas among the most critical perturbations was a three phase fault application at the connection point of the wind farm.

The PHIL results certified the high flexibility in the research of the complex problems which concern the penetration of various energy systems with respect to network stability and security. The first group of tests demonstrate a detailed description of switching inverters' controller design and investigated the effects of an Average Model of STATCOM integrated with a DC-capacitor on voltage control within a low voltage distribution network using RSCAD/RTDS environment. Additionally, the implemented control strategy of the capacitor maintained the inverter's DC bus

voltage constant. The results confirmed that the STATCOM model studied throughout this thesis suited for voltage sag mitigation, since it compensated the reactive power required during a step decrease in the load (hardware inductance) and led to improved steady-state voltages. The second group of test results discuss the energy and control management of a real Microgrid system including a diesel synchronous machine and inverter-based sources. Moreover, their dynamic behaviour was examined within the LV islanded power system and more than that the adequate performance of the laboratory set-up is verified through tests on a real experimental site.

One step further and beyond the PSS/E and PHIL simulations discussed throughout this thesis was the analysis and presentation of the results of power quality measurements in a diesel-powered Island system, since the majority of most small Island power systems and off-grid remote areas are relied on the imported fossil fuels to fulfil their energy necessities. Generally, it is shown that diesel-engine driven generating units which are used as backup power supply in this kind of power systems, are the source of flickering mainly in Island networks, because of the pulsed variation of their torque. Hence, a new control scheme has been developed in this work in order to eliminate the amplitude range of the inherit frequency oscillations that is a permanent problem within a diesel generating unit.

Declaration of Authorship

I, Konstantina Mentesidi, declare that the work presented in this thesis is my own, and generated by me as the result of my own original research. I confirm that:

- This work was done wholly or mainly while in candidature for a research degree at this university;
- Where any part of this thesis has previously been submitted for a degree or any other qualifications at this university or any other institution, this has been clearly stated;
- Where I have consulted the published work of others, this is always clearly attributed;
- Where I have quoted from the work of others, the source is always given. With the exception of such quotations, this thesis is entirely my work;
- I have acknowledged all main sources of help;
- Where the thesis is based on work done by myself jointly with others, I have quoted exactly this contribution.

Konstantina Mentesidi
3rd of October, 2014

To my nephews John and Paul

&

To you, Panos

Acknowledgements

The completion of my Ph.D. thesis has been a long journey which I could not have succeeded without the invaluable support of several people who helped me and stood by my side during these 4 years. It gives me great pleasure in expressing my deep acknowledgements to all these supporters, especially the select few of them I am about to mention, whose contributions made this research work possible.

First and foremost, I would like to express my gratitude towards my supervisor, Dr Monica Aguado, who gave me the opportunity to do my Ph.D. and really provided me with an inspiring guideline to move on my thesis. She demonstrated kindness and patience over the whole project time. Moreover, she arranged tasks for me in an appropriate way and provided me with the right mixture of scholarly precision and infectious enthusiasm.

I must sincerely thank my Professor George Kallos and Ignasio Marti, who initiated my 'research trip' to Spain and helped me to begin my professional career in CENER with their warm encouragement and useful suggestions. In this context, I need to thank Oihana who was my first contact in CENER and helped me with all the non-scientific and necessary paperwork when I arrived to Pamplona.

Moreover, I am grateful to my colleagues in IRE department for their camaraderie, the friendly and warm environment they provided. I need also to thank other past and present group members that I have had the pleasure to work with or alongside of and the numerous graduate and postgraduate students who have come through the department. Thank you for the Spanish tips and being patient all these years with my 'Spanglish' idiom. I have really had enjoyed the time I spent with all of you. The happy hour of the day is the 'nicknames' time'. Thank you Gabriel (the person that I highly admire for his patience and calmness), Sindia, Raquel, Miguel Angel, David, Mikel, Inigo, Luis….

To this select group, I would like to give my special thanks to Raquel and Sindia (my dear friend Sindria) for their constant support, kindness since they have always had offered willing ears to listen to my problems.

Another staunch supporter who I would like to express my gratitude is Mikel, or as I call him, 'tirano'. Although, my Spanish was very poor and his English level-literally at zero, we have had a great collaboration together that led us to two successful manuscripts. Thank you for your critical remarks, suggestions and nationalist songs!!

I gratefully acknowledge the funding source that made a part of my research work possible. This work was co-funded by the European Commission within the Seventh Framework Programme (FP7/2007-2013) DERri under grant agreement no 228449. In this context, I would like to express my profound sense of reverence to Dr. Giorgio Franchioni, Professor Nikos Hatziargyriou, Dr. Stathis Tselepis, Dr. Evangelos Rikos and Dr. Thomas Strasser for giving me the opportunity to participate in the DERri project with two transnational access visits to the ICCS-NTUA and CRES Research Infrastructures in Athens, Greece, supported by the European Commission under FP7.

The members of the research group of the Energy Systems Laboratory have been a very good source of collaboration and advice. I would like to express my gratitude to Vasilis Kleftakis, Athanassios Vassilakis, Panos Kotsampopoulos and Alexandros Rigas. We worked together on PHIL experiments, and I very much appreciated their willingness, ideas, and significant contributions regarding these experiments.

I would also like to give a heartfelt, special thanks to Dr. Evangelos Rikos who has always been ready to help me during tough times in the Ph.D. pursuit. Dr. Evangelos (in him I have made a life-long friend and colleague) has been a source of wisdom, motivation and a booster, especially at the last stage of this research course. He showed genuine caring and concern during the execution of experiments at CRES Microgrid site. Thank you for your patience, the hot cups of coffee and our long inspirational conversations lasting for hours on Skype. Dr. Evangelos has remained a faithful supporter and provided me with insight and direction-up to the end even after the completion of the DERri project. Additionally, he gave me many useful ideas and suggestions that prompted me to think more thoroughly into droop control. His ideas on diesel-powered island systems have been stimulating and enlightening for me. Thank you very much for all your support and humour!!!

During my stay in Pamplona, weekends were usually the times I relaxed and had a good time around and out of office. Therefore, I would like to thank my Pamplonicos 'amigos' (friends) and ex/current flatmates, Sindia, Pablo, Fabienne, Roberto and Fernando.

Moreover, it has been a period of time during which very rarely I have felt I am staying away from home due to the 'Greek colony established in Pamplona'. In this regard, I would like to thank those who came and soon left, Christos (Jesusaki) and Danai.

I cannot imagine my current position without the love and support from my best and entire life friends who have always been 'awaken' and 'alarmed' to my Skype calls. My weeklong visits to Greece the last four years have been invaluable! Thank you my beloved Marilena, Spyros, Papi, Elli, Georgia, Xanthoula, Antoine for your comprehension, patience and faithfulness during this hard working task all these years since my Master in Edinburgh until now…You all kept things bright and me smiling and sometimes even crying because I have been far away from you for a long time…

Above all, I am immensely grateful to my parents, my two lovable sisters, Olga and Fotini and to my adorable nephews, John and Paul. They have been a twinkle in my eye since they were born. Thank you for your support, travelling with me and giving me your love all these years. I am too proud of you and love you more than everything. Thank you mum and dad for giving me a good foundation with which to face life. You have each taught me in your exclusive way about hard work, persistence, self-respect and good attitude towards life difficulties. Thank you for loving me and supporting my decisions and of course for the 'grey cells' you passed onto me!!!!

Konstantina Mentesidi

Public University of Navarra

October, 2014

List of Acronyms

Acronym	Meaning
AC	Alternating Current
ASG	Asynchronous Generator
CHIL	Controller Hardware-in-the-Loop
CHP	Combined Heat & Power
CIGRE	The International Conference on Large High Voltage Electric Systems
CIRED	The International Conference on Electricity Distribution Networks
CP	Connection Point
CRES	Centre for Renewable Energy and Saving of Greece
DC	Direct Current
DER	Distributed Energy Resources
DFIG	Doubly-Fed Induction Generator
DG	Distributed Generation
DGP	Distributed Generation Pack
DILC	Distributed Intelligent Controllers
ESS	Energy Storage System
ETERM	Terminal Voltage
EWEA	European Wind Energy Association
FRT	Fault Ride Through Capability
FSG	Fixed Speed Generators
HuT	Hardware under Test
HV	High Voltage
IC	Internal Combustion Engines
IEA	International Energy Agency
IEC	International Electrotechnical Commission
IEEE	Institute of Electrical and Electronics Engineers
I/O	Input/Output
LV	Low Voltage
MG	Microgrid
MGCC	Microgrid Central Controller
MV	Medium Voltage
NTUA	National & Technical University of Athens
OLTC	On-Load Tap Changer
PHIL	Power Hardware-in-the-Loop
PI	Proportional Integral
PM	Phase Margin
P.O.	Procedimiento de Operacion: Spanish Operation Procedure
P.O.D.	Spanish Operation Procedure of Distribution Level

PPC	Point of Common Coupling
PPC	Public Power Corporation
PV	Photovoltaic Panels
PWM	Pulse Width Modulation
REE	Red Eléctrica de España: Spanish Electrical Utility
RES	Renewable Energy Sources
RPM	Revolutions per Minute
RTDS	Real Time Digital Simulator
SI	Sunny Island
STATCOM	Static Synchronous Compensator
SOC	State-of-Charge
VAR	Volt Ampere Reactive
VPHIL	Virtual Power Hardware-in-the-Loop
VSI	Voltage Source Inverter
WECS	Wind Energy Conversion Systems
WF	Wind Farm
WT	Wind Turbine
WTG	Wind Turbine Generator

Nomenclature

Symbol	Meaning
n_s	Rotational speed of the stator
f_s	Slip frequency
p_s	Number of poles
s	Slip
T	Torque
K_p	Proportional gain
ω_o	Nominal frequency
$\omega_{measured}$	Measured frequency
P	Power output
S	Apparent power
Q	Reactive power /Water flow rate
H	Effective head/Inertia constant
n	Overall efficiency/Speed
ρ	Water density
g	Acceleration gravity
S_{cc}	Three-phase short circuit power
I_{cc}	Short circuit phase current
V_{LL}	Line-to-line voltage
T_f	Transfer function
ω_n	Resonance angular frequency
ξ	Damping ratio
s	Laplace transform, s-domain function
V, i	Voltage, current
Z	Impedance
R, X, L, C	Resistance, reactance, inductance, capacitance
Y	Admittance
G	Conductance
d, q	Subscripts referring to the d, q axis of the rotating reference frame
X_{eq}	Generator equivalent reactance
V_ω	Initial wind speed
$Damp$	Machine damping factor
K_{aero}	Aerodynamic gain factor
$Theta2$	Blade pitch at twice rated wind speed
$Htfac$	Turbine inertia fraction

$Freq1$	First shaft resonant frequency
D_{SHAFT}	Shaft damping factor
Tfv	Filter time constant in voltage regulator
Kpv	Proportional gain in voltage regulator
Kiv	Integrator gain in voltage regulator
Tfp	Filter time constant in torque regulator
Kpp	Proportional gain in torque regulator/ PI regulator
Kip	Integrator gain in torque regulator/ PI regulator
Kpc	Proportional gain of the compensator
Kic	Integrator gain of the compensator
PMX	Max limit in torque regulator/Power reference
PMN	Min limit in torque regulator
QMX	Max limit in voltage regulator
QMN	Min limit in voltage regulator
$IPMX$	Max reactive current limit
$TetaMin$	Lower pitch angle limit
$RTetaMax$	Upper pitch angle rate limit
ω	Rotating speed of the reference frame
a, b, c	Subscripts referring to three-phase power systems
T_ni	Time constant of the PI regulator
τ_{fil}	Time constant of the feedback filter
f_c	Cut-off frequency
R	Droop characteristic/Specific gas constant
i, v	Subscripts referring to current and voltage regulation loops respectively
nom	Subscript referring to nominal value
Ra / Rs	Stator winding
X_a	Stator leakage reactance
X_d	Synchronous-direct axis
Xq	Synchronous-quadrature axis
X'_d	Transient-direct axis
X'_q	Transient-quadrature axis
X''_d	Subtransient-direct axis
X''_q	Subtransient-quadrature axis
T'_{do}	D: open circuit-transient
T''_{do}	D: open circuit-subtransient
T'_{qo}	Q: open circuit-transient
T''_{qo}	Q: open circuit-subtransient

T_{REV}	Period of shaft revolutions
T_{PS}	Period of strokes firing
k_c	Constant
θ	Angle of throttle angle
m_{ai}	Ingoing air mass
m_{ao}	Outgoing air mass
P_m	Manifold pressure
P_{amb}	Ambient pressure
V_m	Manifold volume
T	Temperature
N	Engine speed
T_{eng}	Torque produced by the engine
A/F	Air to fuel ratio
σ	Spark advance
V_f	Field Voltage
V_T	Terminal Voltage
I_{FD}	Field Current
K_F	Exciter Constant Tuning Parameter
K_C	Exciter Constant Parameter
T_F	Exciter Tuning Time-Constant

TABLE OF CONTENTS

Page

List of Figures

Page

List of Tables

Page

Appendix Figures

Page

Appendix Tables

Page

PART I. Research Work Objectives, Scope, Methodology and State-*of*-the-Art

Part one, concentrates the objectives, scope and the motivation for this research study. It further discusses the state-of-the-art of the topic and the methodology utilised throughout this work.

Chapter 1. Introduction

1.1. Introduction

This first chapter gives an introduction to the research work accomplished throughout this thesis. The thesis, motivation, scope, objectives and major areas of contribution are presented. Finally, an overview of the following chapters is given.

1.2. Background of the Study

Worldwide demand for energy is growing at an alarming rate. An average growth rate of 1.8% per year for the period 2000-2030 for primary energy worldwide is predicted. The continuous growth in this load demand has led to the depletion of fossil fuel reserve. Therefore, governments have switched their interest to alternative energy solutions, such as the renewable energy sources [1]. Global warming and environmental policies are the driving force to look for cleaner energy solutions. According to the Kyoto protocol and to the Durban convention [2], a complementary commitment period was launched so as EU, the UK and many other countries have adopted new strategies in order to reduce greenhouse emissions.

The UK government, for instance, is targeting to cut down its carbon emissions to 80% below 1990 levels by 2050, with an intermediate target of at least 26% by 2020 [3]. To reach the 2020 target, around 30% of electricity supply is proposed to be generated from renewable energy sources [4].

Considering as an example the Spanish case study, Spain is in a complicated situation due to its high energy dependency from the abroad, around 80%. As a consequence, the country is quite vulnerable to the variation of some parameters like oil prices and the supply of resources. Spain needs to develop concrete R&D plans and policies about energy in order to achieve the goals adopted by the Kyoto Protocol in 1997 related to the reduction of greenhouse emissions. Moreover, the Spanish grid that comprises a meshed network system has the need for operation control, maintenance and reliability of the system. Red Eléctrica de España (REE) is the Spanish transmission system operator and in 2009 established the new power control centre named CECRE that deals with the control of special regime units at the same point of common coupling (PCC) [5, 6] focusing on wind farms with larger than 10 MW capacities. This good control system allowed Spain being considered among the best countries with proper wind energy integration. It is true that special regime units are normally penetrated to the transmission or the high voltage distribution level [7]. For instance, wind farms are connected to the transmission lines because it was easier to do so.

Distributed generation, synonymously called as embedded or dispersed generation involves wind turbines installed on site load or in offshore, photovoltaic panels, geothermal, biomass plants, micro-hydro turbines and combined heat and power (CHP) generation fuelled by gas or biomass [1, 8]. Lately, there is a growing interest towards wave, tidal power and fuel cells. In general, turbines and reciprocating engines are the most prevalent units for penetration installations (IEA 2002). Distributed technology can offer flexibility and controllability in terms of power profile, which increases system reliability. A variety of industries, such as chemical, petroleum, metal etc. are nowadays more eager to invest in distributed generation to enhance this level of reliability. For instance, fuel cells and backup systems could possibly supply with protection against power interruptions [6, 9].

It is expected that distributed generation (DG) will support the scheme of reducing greenhouses emissions by producing cleaner and more efficient energy. Consequently, the increasing development in non-conventional technology has resulted from security supply issues and poor power quality combined with the economical independence of fossil fuels associated to distributed generation. Therefore, distributed generation has gained a significant interest the last decade. The factors that have contributed to this are numbered as the following [10]; new acquirements regarding the distributed energy resources technologies, limitations on the transmission lines, increased demand, the electricity market liberalization and major concerns about the climate change.

Distributed generators need to be introduced into the distribution networks as embedded generation to meet the requirement of load growth and to help relieve transmission constraints by the means of power flow exchanges, whilst offering higher power quality [11]. Additionally, DG units are located close to the heat loads to minimize the transport losses and thus the capital investment. The introduction of these kinds of systems allows a better management of the resources, the electricity and an optimum planning of the power generation system favouring the reduction or even elimination of inefficient and expensive plants [1, 12]. Besides, embedded generation can be a supplement to the present centralised electrical power systems [13]. Furthermore, in the case of medium and low (MV/LV) networks or islanded power systems, DG generation allows new and smaller scale power generation being produced from low-carbon and renewable-based resources to be connected to these systems.

However, the evaluation of distributed generation characteristics requires an understanding of the technology of prime movers, the appreciation of natural resources and comprehension of the general operation of the dispersed generation plant, since embedded generators increase the complexity of the distribution network. In other words, when the penetration rate is high, the impact on system´s stability is more severe because DG may cause voltage oscillations and interfere with voltage-control process [14, 15]. Subsequently, its integration into the grid is mainly a matter of technical issues, but also of economic and regulatory ones.

Furthermore, Codes at European level are demonstrated to satisfy the operational limitations and ensure the system security of a grid power network. Each country has developed its own codes, since the power networks present different size, generation mix and wind energy potential [16, 17]. In Spain, grid codes that concern the wind power integration state that during faults wind turbines must continue being connected permitting the protection system to clear the fault [13, 18]. Specifically, wind generators connected to the transmission level have to comply with the operation lines of grid code for transport P.O.12.1 and voltage/frequency dips P.O.12.2 that appear in MITYC 2005 [5, 10]. *''Soluciones de acceso para la conexión de nuevas instalaciones a la red de transporte and FP.O 12.2. Instalaciones conectadas a la red de transporte: requisitos mínimos de diseño, equipamiento funcionamiento y seguridad y puesta en servicio. ”*

For instance, wind power penetration at the distribution level mainly concerns local power inefficiencies [19, 20]. One of the major issues is to keep the nodal voltages within their acceptable limits (±5%). According to this reference point, wind integration in distribution level has to encounter the RD 436/2004 as appears in MITYC in 2004 [5, 10]. *''Metodología para la actualización y sistematización del régimen jurídico y económico de la actividad de producción de energía eléctrica en régimen especial. ”*

1.3. Thesis Scope and Motivation

With renewable electricity generation increasing, there will be some important changes in electric power systems, notably through smaller generators embedded in the distribution network. The introduction of these systems into medium and low voltage (MV/LV) networks, which may loosely represent an Island or autonomous power system since MV/LV levels are of high interest as most of distributed energy sources (DER) will be connected there, allows a better management of the resources, the electricity and an optimum planning of the power generation system.

Because of particular structure and characteristics of Islands, the integration of DG and renewable energy sources may provoke problems and constraints which lead to limitations of their penetration level into this type of power systems. In respect to these limitations, the following aspects need to be considered; Voltage deviations, fault ride through capability (FRT) of DG units, short circuits, contribution to the ancillary services etc. The ancillary services concerning voltage and frequency regulation, supply reserves, load following are becoming critical for the secure and reliable operation of the power systems.

Furthermore, power quality measurements are of high concern, especially in a diesel-powered Island system, since the majority of most small autonomous grids and off-grid remote areas are relied on the imported fossil fuels to fulfil

their energy necessities. Generally, one important issue questioned in islanded networks is the transient behavior of diesel gensets during critical disturbances induced by intermittent power sources and load step changes and more than that, the degraded power quality induced by their inherit torque oscillations.

In more details, the amount and the location of distributed generation penetration may influence the dynamics and stability of the transmission and distribution network respectively. Moreover, the common assumption of a unidirectional power flow and voltage drop along the distribution feeders is no more credible for all the operating conditions. For instance, voltage control in these power networks is usually restricted to the on-load tap transformer changer at the high/medium voltage substation. Thus, maintaining the voltage levels within specific limits, which is a significant power quality criterion, is a great challenge in electricity supply.

Furthermore, voltage deviations induced by load changes and power delivery limitations are observed during reactive power unbalances. Switched capacitors, reactors and VAR compensating devices such as Static Synchronous Compensator (STATCOM), commonly advantageous for industrial applications, are used to control reactive power flow and thus maintaining voltage in electrical systems and have proved to be effective since they can reduce these energy transfer limitations under normal and fault conditions. Besides, STACOMs have already been applied to distribution systems, i.e. 400 V and medium voltages, namely 10 kV, 35 kV etc.

Apart from VAR compensating devices, distributed generators interfaced to power electronic converters are, usually, controllable reactive power sources, in addition to the energy storage systems (i.e. DC capacitors or Supercapacitors) which are introduced as backup sources for controlling the active power flow and can be key effective solutions to increase DG in an Island power system or generally in a LV distribution network.

It is accepted that an energy storage system (ESS) connected to the DC bus of a STATCOM in low voltage distribution networks or a micro-grid infrastructure appears to be a very promising solution for power quality issues. Because the STATCOM's traditional operating modes, namely, capacitive and inductive will not be limited to reactive power compensation but it may be also feasible to control the active power flow within the STATCOM and the point of common coupling through charging/discharging the energy storage system [21-24].

Concluding, an effort that this thesis will try to carry out is to analyse MV/LV distribution networks from an electrical point of view and propose the potential and suitable areas for integration of distributed electrical generation in this kind of power systems, either they operate in connected or isolated mode. For this type of analyses, tools that provide computational power and flexibility are necessary. On the one hand, DER integration requires steady-state and dynamic analyses for present and future configurations. On the other hand, the core of such active networks is depicted by the power converters and apart from implementing grid penetration studies, it is important to research on their control performance and the interaction of the devices connected to these grids since they may induce serious impacts on the power quality parameters. Hence, real time simulations will be reinforced and this will not only allow us to size and locate the distributed generation systems, but will also let us optimize MV/LV and in general Island power networks, and likely introduce energy storage.

1.4. Thesis Context

1.4.1. Objectives

The core objective of this thesis is focused on investigating distributed generation integration into MV/LV electrical grids, which aims at defining the suitable areas for an optimal distributed generation penetration into these voltages. A MV/LV voltage distribution network is selected that may loosely represent an Island or autonomous power system since MV/LV levels are of high interest as most of distributed energy resources (DER) will be connected there.

In the points beneath are presented the *specific aims and objectives* of the survey:

1. Propose the potential areas in an Island power system suitable for the introduction of DG (*where*).

2. Apply different potential scenarios (*how much*) of penetration and confirm that these comply with the grid requirements of the region.
3. The Island power system´s steady and dynamic stability is examined with the addition of geothermal power units and with the supplementary addition of wind power units.
4. Identify the impacts of DG on the system.
5. Apply recommendations concerning improvements for the existing grid and possible solutions to advance the penetration level.
6. Investigate the effects of STATCOM on voltage stability and reactive power compensation.
7. Include the STATCOM's controller design and examine voltage regulation at the common coupling of this inverter interfaced source.
8. Integrate the control of a DC capacitor in order to have it on stand-by for power system aid.
9. Analyse a LV islanded power system's energy management, to study its control strategy i.e. droop control.
10. Evaluate the diesel generator's active power droop control and verify the battery inverters' droop curves.
11. Examine the load sharing for parallel operation of the islanded system's generation units.
12. Verify the dynamic operation of the energy units within a real MG infrastructure during step load changes.
13. Propose a new control scheme in order to eliminate the amplitude range of the diesel generator's inherit frequency oscillations.

1.4.2. Project Conceptual Approach

In order to reach the objective mentioned above, the current thesis needs to investigate the conditions and constraints met by DG in Islands and generally in LV distribution networks, thus it is dedicated to study different solutions to overcome some of the existing problems and barriers to a larger development of DG in such grids. The skeleton of the research work followed to achieve this goal is described beneath;

Firstly, a grid model is built in PSS/E software tool (Chapter 4) based on the data from a real Island power system. In continuation, steady-state and dynamic simulation analysis configurations are accomplished to determine the allocation, maximum capacity of embedded generation that may be inhabited within this autonomous network. Various scenarios are employed with different penetration rates of geothermal and wind generation units in addition to the voltage levels to be connected, i.e. 60, 30 and 10 kV within the autonomous power network in order to study the steady-state limit of distributed generation integration into this system. The Island's electricity production mainly comes from its geothermal resources and a small percentage from fossil-fuelled power units. The analytical description of the system's power plants production is given in Chapter 4. In this way, it is possible to check the off-grid system's behaviour under normal operation and against several disturbances onto the grid. Geothermal plants using basic machine model such as synchronous generator, exciter and governor and wind farms employing Doubly-fed Induction Generator (DFIG) technology were chosen throughout this thesis. The adequate stability margin of the system will be investigated upon the fault-ride through capability and frequency response of the network elements, whereas among the most critical perturbations to be considered is a three phase fault application at the connection point of the wind farm.

The simulations in PSS/E are conducted in CENER (The National and Renewable Energy Centre of Spain) premises.

As a continuation to the load flow and dynamic analyses, is to analyze the penetration of distributed generation into distribution networks, i.e. a Microgrid (MG) system as an isolated entity or a LV islanded power system. Moreover, due to the fact that the models' library in PSS/E is not unlimited, for instance the control performance of VAR compensating devices, i.e. STATCOM and energy storage systems (i.e. DC capacitor) that can be used in islanded

power networks cannot be investigated throughout PSS/E simulations, another kind of simulations and field tests are needed.

Thus, it was decided to emulate and verify the ''smart'' coexistence of central and decentralised generation very close to realistic conditions. In this context, certain real time simulations in RTDS/RSCAD software tool and a group of Power Hardware-in-the-Loop (PHIL) tests (Chapter 5) utilizing an impedance as Hardware under Test (HuT) were performed to examine the generation plants integration into LV distribution networks for the reasons explained above, in Section 1.3. More analytically, the first group of real time simulations and PHIL experiments analyse the application of VAR compensating devices to distribution networks and the second group of tests emulate the energy management system of a LV distribution network including a diesel synchronous machine and inverter-based sources. The results regarding the energy management within the distribution power system were, then, verified at a real Microgrid (MG) infrastructure through experiments during which various tests were performed concerning the diesel generator and the battery inverters in order to examine their dynamic operation within the LV islanded power system.

The real time and PHIL simulations described in Chapter 5 were carried out in NTUA (The National & Technical University of Athens) whereas the Microgrid experiments were executed in the real test site in CRES (Centre for Renewable Energy and Saving of Greece) premises under two transnational accesses co-funded by the European Commission within the Seventh Framework Programme (FP7/2007-2013) DERri under grant agreement no 228449.

One step further and beyond the PSS/E and PHIL simulations discussed throughout this research work was the analysis of power quality measurements in a diesel-powered Island system or generally in off-grid applications (Chapter 6). Emphasis is given on frequency oscillations induced by the pulsed variation of the diesel genset´s torque. Broadly speaking, this is an inherit problem of the diesel generators and it was also detected during the onsite Microgrid experiments in CRES premises. The entire system will be simulated in Matlab/Simulink. In more details: A controlled power source, i.e. a dynamic load will be utilised to supply a given active power set-point. The control of the active power flow will be regulated and arranged through a droop characteristic.

In overall, the simulations and tests executed throughout this thesis in order to study distributed generation integration into MV/LV voltage electrical grids and/or in islanded power systems are summarised beneath;

1) Steady-state and dynamic simulations in PSS/E software tool. This kind of testing aims to define the quantity and the allocation of DG integration into distribution networks. Examine the steady-state margin and the dynamic stability of system after the application of fault incidents by the means of voltage, current limits and network losses as described above in Section 1.3.

2) RTDS/RSCAD simulations and PHIL experiments. These simulations and experiments are divided into two groups of tests in order to reach the specific objectives also described in Section 1.4.1, such as voltage sag mitigation, reactive compensation and study the energy management within LV grids.

The first set of tests which elaborate:

i) Simulate in RSCAD/RTDS an Average model of a STACOM, ii) Develop this inverter´s control & examine its effects on voltage stability of a LV three-phase power network, iii) Integrate a DC Capacitor model and its control in the aforementioned network and iv) Perform PHIL tests.

The second set of tests involves two blocks of experiments;

A) RSCAD/RTDS simulations: i) Modeling in RSCDA/RTDS of a three-phase LV network that includes diesel generator, feeders, various resistive loads and Sunny Island (SI) 4500 battery inverter, ii) Calculation of battery inverter´s droop curves (droop f & V), iii) Load sharing for parallel operation, iv) Perform PHIL tests.

B) Execution of Microgrid experiments: i) Diesel generator and battery inverters´ active power droop control, ii) f/P droop calculation for parallel operation of three inverters (master-slave) with step load changes, load asymmetries and with a 24-hr load profile, and iii) Load sharing for parallel operation of two SI Inverters connected both in one phase.

1.4.3. Contribution to Knowledge and Significance

Lately and during the time of performing this research, DG penetration in distribution networks has been of great concern to industrial and academic researchers. The interest is rather focused on the negative effects may induce large amounts of DG connection to this kind of power systems. Moreover, governments feel more initiative towards grid integration studies.

Nevertheless, there are no specific studies about the potential of dispersed technology penetration and the simultaneous real time grid simulations in MV/LV power systems as a whole and therefore, the incentives and proposals are more qualitative than quantitative. This research work tries to cope with those concerns in an alternative way.

The principal advantage of this thesis is that up to now, the existent literature reviews do not analyze an autonomous power grid system as a whole from electrical point of view, employing static and dynamic simulations within PSS/E software to define the quantity (how much) and the allocation (where to add the distributed generation), an effort that is reinforced throughout this study. The conclusions drawn from the steady and transients stability simulations will be investigated to define the correctness of the two sub-objectives above.

On the other hand, the deployment of RTDS/RSCAD simulations and PHIL laboratory tests as a data reference for verification in the domain of DER integration is relatively constrained up to now. Specifically, the existent literature is very limited regarding this kind of tests that study the control strategy of LV islanded power networks with the integration of inverter-based devices and even energy storage systems. The prevalent advantage of this kind of experimenting is that in the end the implementation and development of a methodology that characterizes the energy supply devices and system analysis for decentralised grid services is viable.

Ultimately, this research study involves the analysis of the operation of a diesel-powered Island grid that takes into account the power quality measurements with focus on frequency and voltage oscillations. The majority of the literature reviews that discuss this topic, analyse this phenomenon and state that this flicker is an inherit problem a diesel generating unit induces itself, but without attending to suggest any solutions to sort out this problem. This work proposes a control scheme to eliminate the flickering, and could be very useful for rural and isolated power networks.

Concluding, the expected outcomes drawn through the PHIL, Microgrid tests and the PSS/E simulations could be the basis for analysis and comparison of the dynamic performance among different energy sources and thus, finally choose which best fits in our grid studies. In that way, the developed scheme (s) is postulated to be useful solution for DG planners with the potential to become a tool for fostering DER integration into MV/LV or Island power systems and a provisional step towards smart distribution networks.

1.5. Limitations and Delimitations of the Study

The introduction of DG units presents a number of new challenges, thus the traditional planning and operational practices have to be reviewed with the increased amount of distributed generation into the grids. Beneath are presented the restrictions and limitations that came up during the completion of this research work.

The considerations for the PSS/E simulations are outlined in the following:

I. One of the greatest challenges will be the network data collection in order to complete the study appropriately and with the highest consistence. Information was requested from the public electrical utility of the studied region, manufacturers etc. In case of data deficiency, reasonable assumptions were conducted and thereafter justified.

II. Not only will the operation in the transmission system but also in the distribution network raise much of interest in this project because special regime units are penetrated to the transmission or the high voltage distribution level [7].

III. The increased integration of DG and DER devices in Island grids depends on several factors such as: a) the provision of ancillary services by DG and DER plants, in particular concerning contribution to the control of network voltage and frequency and b) fault-ride through capability of DG and DER units, that's to say their capability to withstand network perturbations such as voltage dips and frequency oscillations.

IV. One of the incentives of the project will be to identify the transient stability with distinct dispersed integration levels and technologies. For instance, under an N-1 (contingency) study, with a supposed generation or line loss; the influences on the transient stability are rather strong [25]. Depending on the technology, in the literature is reported that induction generators have worst effects than the synchronous ones. Alternatively, for long-term stability penetration of distributed systems is expected to raise the frequency level after the disturbance [13, 20].

V. A great consideration in such penetration studies should be the stochastic power output of the distributed generators. Weather, heat, and natural conditions cannot be predicted precisely and if the power system is ''weak'', this may induce instability issues. Thus, a larger spinning reserve is required and according to V. Thong et.al, a 10% of the demand is hold as spinning reserve [5, 20]. The calculation of penetration level in percentage involves the ratio of the DG power generation and the total demand [20].

VI. Grid codes are demonstrated to satisfy the operational limitations and ensure the system security. Each country has developed its own codes, since the power networks present different size, generation mix and wind energy potential. In Spain, grid codes that concern the wind power integration support that during faults wind turbines must continue being connected permitting the protection system to clear the fault [18].

VII. Wind power penetration at the distribution level mainly concerns local power inefficiencies [19]. One of the major issues is to keep the nodal voltages within their acceptable limits $(\pm 5\%)$. According to this reference point, wind integration in distribution level has to encounter the RD 436/2004 as appears in MITYC in 2004 [5, 26]. *''Metodología para la actualización y sistematización del régimen jurídico y económico de la actividad de producción de energía eléctrica en régimen especial. ''*

For the PHIL simulations stability and accuracy issues are of the most importance when executing this kind of experiments. The constraints for this kind of experimenting are described beneath:

I. Before performing a PHIL test, it is crucial to ensure that the experiment will be stable. Therefore a virtual PHIL test should be tested in Matlab/Simulink. Moreover, the protections in the RTDS have to be tested in order to ensure that in case of a possible error in the simulation layer no damage will be done to the equipment. Lastly, before the closed loop tests are performed, it is essential to check that the signals will be inserted to the simulated system having the correct characteristics of amplitude and phase.

II. In order to validate the accuracy of the results, off-line simulations are necessary to be performed in Simulink/Matlab. The entire closed loop system has to be simulated, and the results are compared with the results from the PHIL tests. More specifically, the resulting rms values (current, voltage) need to be compared with the values expected according to the off-line simulation.

1.6. Thesis Outline

This thesis consists of seven chapters, together with the necessary appendices. Chapter 1 introduces the topics that this thesis deals with, the thesis objectives and goals, the major areas of contributions, the thesis statement etc. Distributed generation penetration is the core study of this work since distributed generation and its resultant impact on the grid are of special concern

Chapter 2 presents the state of art of various distributed generation technology types with emphasis on wind power and gives an overview of the restraints and limitations of distributed generation penetration into MV/LV networks. In addition, the impacts of increased distributed generation on system stability are studied which identifies the importance of considering distributed generation penetration within a distribution network.

Chapter 3 introduces the research methodology utilized throughout this work. This thesis is focused on two research areas; a) grid penetration studies in order to define the steady-state and dynamic limit for distributed generation integration into an Island power network. This work is accomplished with PSS/E simulation tool and b) real time distribution grid simulations in RTDS/RSCAD tool and especially Power Hardware-in-the-Loop (PHIL) experiments of an autonomous power network which allow us testing and validating the control performance and interaction of the system´s equipment. A brief description of the two utilised software programs, namely PSS/E and RTDS/RSCAD, as well as the principal hints of the research methodology are given in this chapter.

Chapter 4 describes the implementation of a case study of a real power system model in the commercial software package PSS/E used for dynamic simulations. It details the various scenarios employed to analyze and propose the potential areas in an Island power system, suitable for the introduction of distributed generation into the electrical grid. Static and dynamic simulations are carried out in an example autonomous power grid that is a real distribution network. This chapter examines the results of the case study in PSS/E. Principally, the system´s steady and dynamic stability is evaluated with the addition of geothermal power units and afterwards with the supplementary addition of wind power units. DFIG units are the technology type of wind power utilised throughout this work.

Chapter 5 presents the real time and Power-Hardware-in-the-Loop simulations of a set of tests for DER integration in LV islanded power systems. Moreover, onsite experiments in a real Microgrid installation were performed to verify a part of the simulation results indicated above. In this context, several real time simulations in RTDS/RSCAD software tool and PHIL experiments are executed from which the fist group of tests analyse the application of VAR compensating devices to distribution networks and the second one emulates the energy management system of a real MG including a diesel synchronous machine and inverter-based sources.

Chapter 6 highlights the operation of a diesel-engine generating unit in an Island grid or generally for off-grid applications. It presents the results of power quality measurements with emphasis on voltage flickering and frequency oscillations induced by the pulsed variation of the diesel genset´s torque.

Finally, in Chapter 7 conclusions are drawn regarding the DER penetration in low voltage grids and its role. Several suggestions are presented for possible future work on this subject.

1.7. Associated Published Work

The scientific contributions, namely conference and journal articles evolved from this thesis are outlined below. The full papers are provided in the end, in Appendix V.

1.7.1. Journal Publications & Scientific-Technical Reports

- Konstantina Mentesidi and Monica Aguado, "The potential integration of electrical distributed generation in an island power system," in *International Journal of Distributed Energy Resources and Smart Grids*, vol. 9, no. 4, pp. 341-366, 2013.

- Konstantina Mentesidi, Evangelos Rikos, Vasilis Kleftakis, Panos Kotsampopoulos and Monica Aguado, "Real time Simulation Technique of a Microgrid Model for DER Penetration", in *EAI Endorsed Transactions on Energy Web. In Press.*

- Konstantina Mentesidi, Mikel Santamaria, Athanasios Vassilakis, Alexandros Rigas, Vasilis Kleftakis, Panos Kotsampopoulos and Monica Aguado, "Power Hardware-In-The-Loop experiments of an Average Model of STATCOM for a LV Network", *in International Journal of Renewable Energy Research (IJRER). Under Review.*

- Konstantina Mentesidi, Evangelos Rikos, Raquel Garde and Monica Aguado, "The Operation of a Diesel Genset in an Autonomous Network ", in *Applied Energy, Elsevier. Under Review*.

- Igor Usunariz, Mikel Santamaria, Konstantina Mentesidi, and Monica Aguado, "Secondary Control of Droop-Based Converters for Power Stability Analysis in Microgrids" in *IEEE Transactions on Smart Grid. Under Review.*

- Konstantina Mentesidi, Technical Reporting of the Transnational DEIAgrid project, within the 7th European Framework under the DERri project with No: 228449.

- Konstantina Mentesidi, Technical Reporting of the Transnational DGIV project, within the 7th European Framework under the DERri project with No: 228449.

1.7.2. Conference Papers & Contributions

- Konstantina Mentesidi, "PHIL Tests in support of the studies on the DER Integration," in *Experimental research and DER integration in the EU Energy System*, Milan, Italy, October, 2013. *Prize Invitation. Conference Proceedings.*

- Konstantina Mentesidi, Mikel Santamaria, Athanassios Vassilakis, Alexandros Rigas, Vasilis Kleftakis, Panos Kotsampopoulos and Monica Aguado, "Power Hardware-In-The-Loop technique applied to a LV Network for integrating a Supercapacitor with an Average Model of STATCOM," in *IEEE International Workshop on Intelligent Energy Systems (IWIES 2013)* Vienna, Austria, November, 2013, pp. 167-172. *IEEE Indexed Conference Paper.*

- Konstantina Mentesidi and Monica Aguado, "Dynamic behavior analysis of distributed generation in an off-grid network with power system simulator for engineering (PSS/E)," in *IEEE International Energy Conference, ENERGYCON 2014*, Cavtat, Croatia, May 2014, pp. 1042-1049. *IEEE Indexed Conference Paper.*

- Konstantina Mentesidi, Evangelos Rikos, Vasilis Kleftakis, Panos Kotsampopoulos, Mikel Santamaria, and Monica Aguado, "Implementation of a Microgrid model for DER Integration in Real time Simulation

Platform," in 23rd *International Symposium on Industrial Electronics (ISIE 2014)* Istanbul, Turkey, June, 2014, pp. 2274-2279. *IEEE Indexed Conference Paper.*

- Konstantina Mentesidi, Monica Aguado, Fatima Zahra Harmousch and Khalid Loudiyi, "A PV and CSP integration study experience in a Mediterranean Partner Country," in 4th Solar Integration Workshop, Berlin, Germany, November, 2014. *Conference Paper.*

Chapter 2. Integration of Distributed Generation

2.1. Introduction

This chapter performs a thorough literature report on distributed and renewable generation with emphasis on their integration into distribution networks. The chapter starts with an introduction to distributed generation and generally the distributed energy resources, including the concept of the Microgrid. A background of the electrical network layout is given and the penetration of DG into these system configurations is also described. One of the key surrounding subjects includes types of DG technologies, where emphasis is paid on wind power. The discussions are based on fixed speed and variable double-fed induction machine designs, whereas a closer look is taken on their characteristics and frequency, speed and active power control aspects. In continuation, the benefits of DG penetration are addressed, in addition to the technical considerations and restraints of most concern that arise with the DG connection to distribution and generally to Island power networks. Finally, a brief overview of the embedded generation status in Europe with a detailed analysis of the Spanish case is also given.

2.2. Power System Structure

2.2.1. The built-up of the electrical power system

In a conventional large electric power system, the central generators feed the interconnected transmission system through their step-up transformers and the power being extracted from this high voltage network passes through a series of bulk supply transformers to the distribution network to ultimately reach the customers´ demand (Fig. 2-1).

The electrical networks consist of three main parts; generation, transmission and distribution. The transmission power system is normally the system with the highest voltage, e.g. from 300 kV and above. Transmission networks may transfer the highest energy capacities and are mostly built as meshed networks to enhance the security of the system. Moreover, in this part of network only very large electrical energy consumers and producers are connected, whereas can also be used as connecting lines to other systems for example tying different countries together [27, 28]. The sub-transmission network belongs to the transmission network. It consists of a high or medium voltage network, with the voltage levels ranging between 66 kV and 300 kV. In contrast to the transmission network, the sub-transmission network is built as a radial network or a weakly coupled network.

Distribution networks are systems characterised by medium voltages, normally below 45 kV and are operated at a number of different voltage levels; HV up to 35-40 kV, MV ranging between 10 and 20 kV and LV for voltages smaller than 20 kV. The distribution network is often a radial structure and its function is to transfer power down to the individual customers. Small generation and medium sized units are connected to this range of voltages [27].

EU Electricity Directive 2009/72/EC [29] defines like distribution voltage levels the ones ranging between 132 and 0.4 kV, whereas transmission voltages are considered the ones above the 132 kV threshold. According to EWEA [30], wind power units are connected more than 50% to the transmission level and concentrated solar thermal power units over than 60% at the same voltage level (145-400 kV). The remaining technologies are rather injecting into the distribution level.

The design of traditional transmission and distribution networks have nearly reached their capacity to facilitate dispersed units and impose a unidirectional power flow profile. Future enhancements in distribution network building construction from centralized to decentralized configurations will be needed, thus terms like active networks or smart and micro grid concepts are proposed [31]. This increase in DG and/or RES integration can be followed by decommission of conventional generators and/or an annual growth in load demand by 2% until 2020 [32].

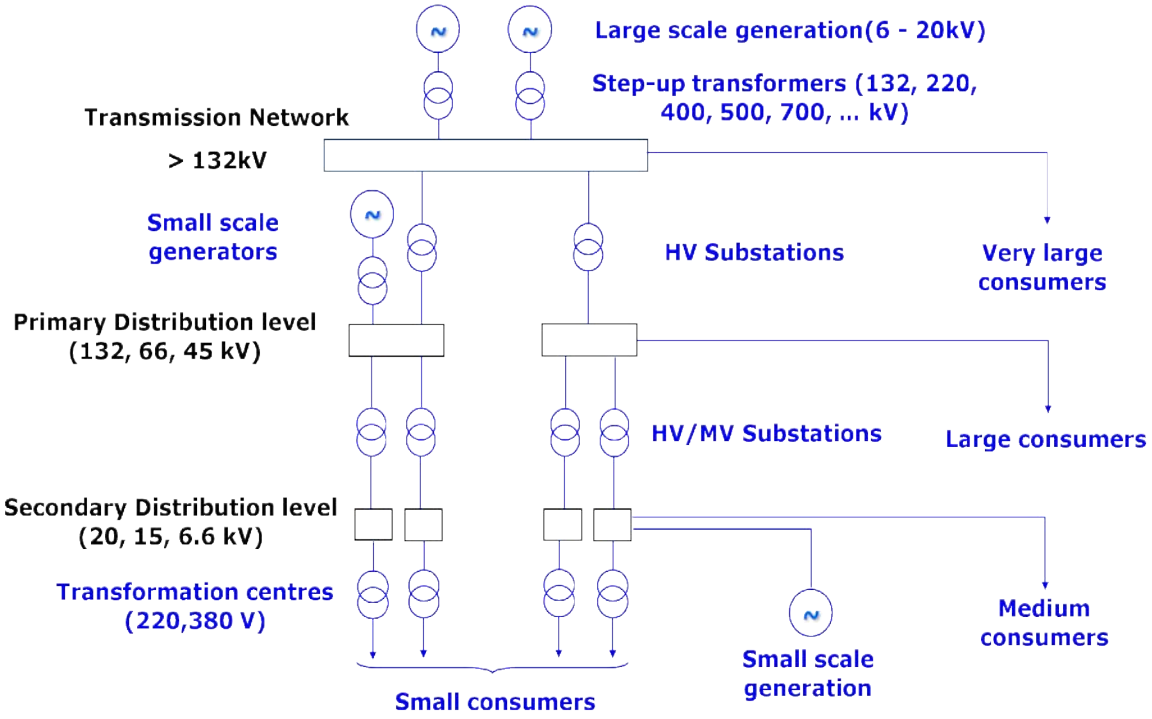

Fig. 2-1: Single-line equivalent of a power system layout.

2.2.2. Layout of Network Configurations

Generally, there are five main distribution network configurations that are commonly used [33, 34]: i) mesh, ii) interconnected network, iii) link arrangement, iv) open loop and v) radial system. These configurations are depicted in Fig. (2-2), where the circles illustrate individual substations. The advantages differ among the various arrangements. In more details, the mesh and interconnected network configurations are rather preferred to high voltage transmission systems (HV) and may ensure security of supply to individual substations. The link arrangement serves as a connection link among two in-feed substations and may operate as two radial substations whilst ensuring supply of one of the in-feed substations is out of service. The open loop configuration can also provide security of supply when a fault incident takes place. In that case, the faulted section is isolated and the open points are closed to operate as backup supply. Finally, the radial arrangement is usually used in LV rural networks where the systems are characterized by less complexity and less fault incidents may occur.

2.3. Distributed Generation at a Glance

2.3.1. An issue with multiple definitions

According to Electricity Act, generation technologies are divided into two specifications; the special and ordinary regime units. Special regime generation units consist of renewable technologies (except large hydraulic plants), waste energy sources and CHP, whereas the ordinary ones are comprised of coal, gas turbines, nuclear and big hydro plants generation technologies [35], [36].

Over the last decade there has been an increasing interest in the generation connection to the distribution network, the so-called embedded or dispersed generation. Both names are synonymous and are used to represent small-scale electricity generation [1], [37].

There is no universally approved definition of what constitutes embedded generation and the way it differs from central or conventional generation. Among the working groups that tried to award some common attributes are CIGRE [38], CIRED, the IEEE and IEA [39]. The first two defined DG as the generation of units normally connected to the distribution voltage level, with a maximum capacity of 50-100 MW. Moreover, the IEEE considers DG as the generation by facilities much smaller than the central power plants, thus the interconnection at any point near the power system is feasible. On the other hand, IEA does not take into account the power capacity level but considers that DG supplies power directly to the customer´s site. Generally speaking, all the reviews seem to converge at least to the small-scale generation definition and the most preferable specification concerns that distributed energy resources (DERs) are ordinarily applied to the distribution system voltages of 230/415 V up to 145 kV [40].

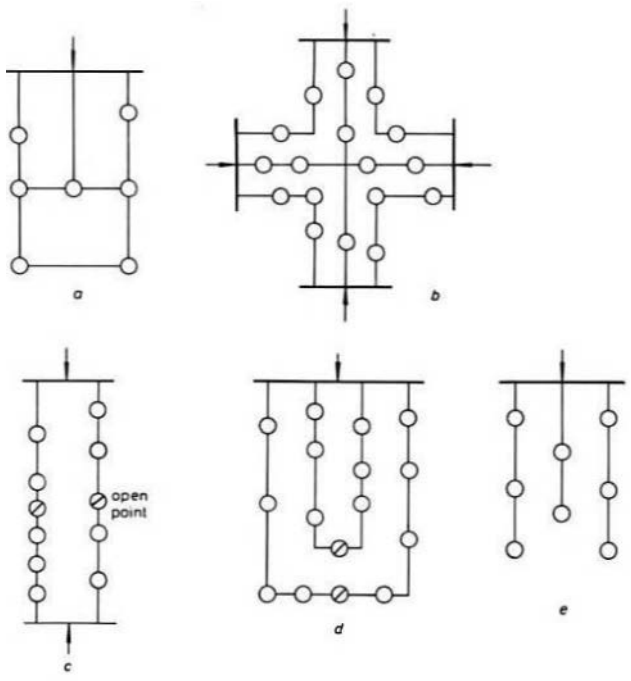

Fig. 2-2: *Network configurations; (a) Mesh network, (b) Interconnected network, (c) Link arrangement, (d) Open loop and (e) Radial [41].*

2.3.2. Distributed Energy Resources and the Microgrid Concept

Microgrids (MG) are small-scale active distribution networks that group small DG systems (PV, fuel cells, micro-turbines and wind turbines), storage devices and loads at LV networks, the so-called microsources (≤100 kW) [42] and feed the electrical and heat loads of a small infrastructure, such as a housing estate or a public community such as a commercial building, an industrial site, an university area etc [37]. Moreover, distributed energy resources (DERs) or in other words microsources are the DG systems that may occupy either conventional primary sources or renewable energy technologies [37].

In this regard, distributed generation may range from micro-CHP systems that employ Stirling engines, fuel cells, micro turbines and internal combustion (IC) engines to renewable energies such as photovoltaic panels, wind turbines, small hydro plants and geothermal plants. Other forms of renewable energy sources like biomass, landfill gas, wave and tidal power plants will not be analyzed in this study, although significant development of these types is reported the last years.

A MG infrastructure is either interconnected to the distribution network or it can be operated in islanded mode. From the customer point of view, MGs supply both the electrical and heat load demanding, whereas ensure system´s

reliability by supporting voltage and frequency and reduce emissions. However, from operational point of view, the DG units that a MG installation occupies need to be equipped with power electronic interfaces and control systems to ensure the flexibility and operation of the MG as a single aggregated system with restricted energy handling capacity [37], [43]. According to IEEE recommendations, their maximum capacity is normally restricted to almost 10 kVA [44, 45].

On the other hand, from the grid´s point of view, a MG can be considered as a controlled unit on its own within the power system and it can be operated as an aggregated load or generator and/or even provide ancillary services to the main network [46].

The most profound differences among a MG infrastructure and conventional systems are the ones outlined beneath:

a. The microsources that a MG contains are of much smaller capacity compared to the one of the large generation units in a conventional power plant.
b. In conventional systems the power is generated far away from the load centers, whereas the power generated within a MG feeds directly the distribution network, thus losses are minimized.
c. The function of the active distribution network is to efficiently link generation units with loads, allowing both to decide on the best operation in real time.

A typical MG configuration is given in Fig. 2-3 beneath, where it is basically coordinated by the Microgrid Central Controller (MGCC) and coupled to the MV utility grid. Several, Microgrids can generally be interconnected to shape a large power system supplying a load pocket through a common distribution network. In this case, each Central Controller has to perform its own control, but in close coordination with the neighboring ones [47].

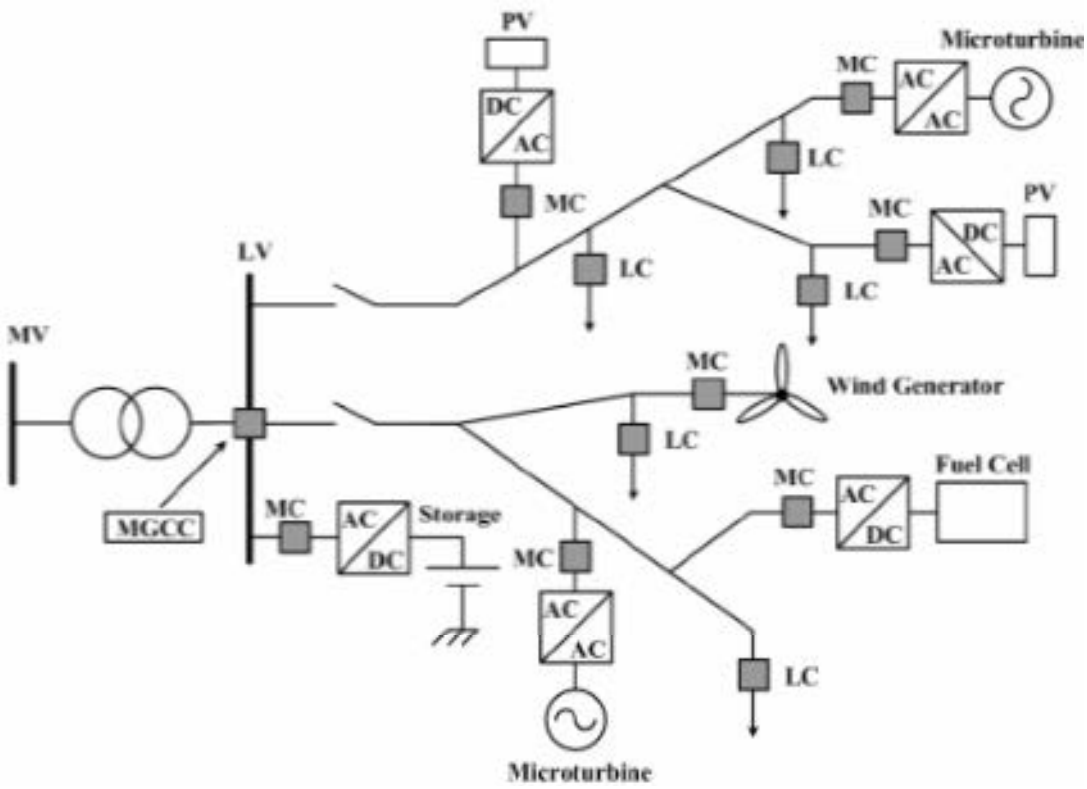

Fig. 2-3: A Typical MG Configuration [46].

2.4. Distributed Generation Technology Types

Currently and in the near future, the most prevalent RES technologies which are involved in the electricity generation are onshore wind and photovoltaic installations. Offshore wind, CSP and biomass are less promising because of logistic and competence issues [48].

This subchapter briefly discusses the next DER technologies, where wind generation units are analysed more in detail:

- Fossil-fuel powered generators (and diesel gensets)
- Cogeneration and micro-CHP systems
- Wind power
- Solar photovoltaic systems
- Fuel cells
- Small-scale hydro generation
- Geothermal plants

2.4.1. Fossil fuel powered generators

Conventional generators belonging to this category are sized below 100 MW, with reciprocating engines and gas turbines being the mostly utilized. Gas turbines that generally apply to micro-applications are more environmentally friendly as are powered by natural gas compared to reciprocating engines which are oil fuelled.

2.4.1.1. Diesel gensets

A diesel genset contains an internal combustion engine and a synchronous generator coupled to the same shaft. Diesel engine generating units have customarily been introduced as backup sources in autonomous power grids or emergency systems for commercial as well as for industrial applications.

The generator can be either a permanent magnet or a wound-rotor machine but with impact on power efficiency, generator losses and of course on the system cost [49].

2.4.2. Cogeneration and micro-CHP applications

Large CHP plants are better employed in big heating systems like industrial areas, hospitals, oil refineries where catch the by-product waste heat. The efficiency of such plants reaches the 80%, especially if they are located close to the thermal loads. On the other hand micro-CHP technologies apply to smaller holdings with a handling capacity from 10 to 100 kW [37] and differ from the larger units not only in terms of energy generated but also in prime mover operation. Micro-CHP utilize as main driver parameter the heat loss and electricity as a by-product [37].

Micro-CHP systems primarily employ internal combustion (IC) engines, Stirling engines and microturbines. Below, a brief description of internal combustion engines is presented since this kind of technology is occupied by diesel gensets and will be analytically discussed later on in this thesis (Chapter 6).

2.4.2.1. IC engines

The combustion process in IC engines involves the burning of fuel with or without oxidizers in the appropriate chambers resulting to high-temperature and pressure air gases which act on movable bodies, like pistons. IC engines differ from external combustion engines, such as steam and Stirling engines since the latter heat externally a separate working fluid during the combustion process. The typically used fuels are diesel oil, gasoline and petroleum gas,

whereas ethanol and biodiesel can also be used. The combustion process is initiated with spark ignition or compression ignition within the engine´s cylinders depending on the type of fuel that runs the engine.

2.4.3. Wind power

Wind energy conversion systems (WECS) extract the kinetic energy from the wind that passes through the rotor blades and convert it into electrical power at the generator side. At their early stage wind turbines were rated at a few kWs, but nowadays the commercially available ones exceed the 5 MW. Wind power remains the most promising renewable energy source because of its capability to generate electricity at a large scale [50].

The nacelle, tower and rotor comprise the main parts in a wind turbine configuration. Two or three blades are attached to the rotor hub and rotate in the direction of the inflow wind. Gearbox and generator lie in the nacelle, where the former adjusts the rotor speed to higher values on the generator side of over 1500 rpm [51]. The generator shaft is driven by the wind turbine to spin and produce electrical power injected into the grid. Beneath, two generator technologies are chosen to be presented whch are occupied in the wind energy market. These are fixed speed asynchronous (FSG) and variable doubly-fed induction machines (DFIG). Variable speed machines convert the mechanical energy into electrical form at a great spectrum of frequencies but then need to be readjusted to the grid frequency of 50 Hz. On the other hand, fixed speed generators is not necessary to be corrected, but are incapable to perform well during wind fluctuations [51].

2.4.3.1. Characteristics of the different Wind Turbine Designs

The stator in AC machines is connected to the three-phase system, while the rotor is short-circuited internally or its slip rings are connected to the grid externally [52]. When balanced three-phase currents are applied at frequency f_s, the stator windings produce an electromagnetic field that rotates at

$$n_s = \frac{120 \times f_s}{p_s} \tag{2-1}$$

where n_s is the rotational speed of the stator in (RPM), and p_s is the number of poles. The induced electromagnetic field of the stator also induces a rotation in the rotor, the n_r. One more element to be addressed is the slip; Slip is the difference among the stator rotating field and the rotational speed of the rotor [52, 53].

$$s = \frac{n_s - n_r}{n_s} \tag{2-2}$$

According to [52] & [54] FSG and DFIG are modelled for dynamic simulations, whereas their differences can be attributed to the physical manufacture of each wind turbine type and to their behaviour against a series of subsystems. These subsystems are the aerodynamic, mechanical, generator and the wind turbine control subsystem. The following figure (Fig 2-4) represents the schemes of a FSG (ASG)[1] and DFIG turbine respectively.

[1] ASG: Asynchronous Generator

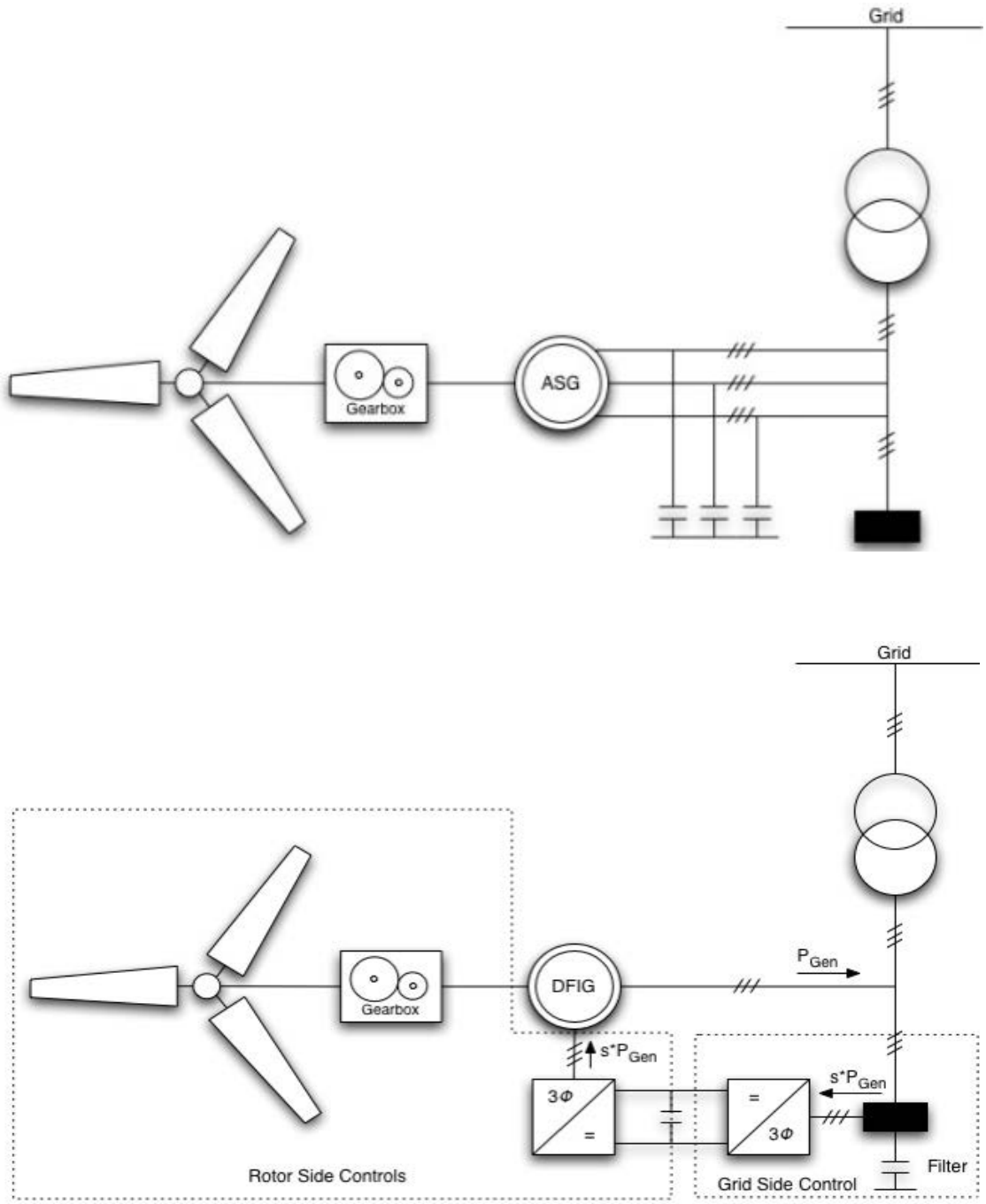

Fig. 2-4: FSG and DFIG Wind Turbine Designs [52].

FSG has its blades coupled directly to the induction generator through the gearbox. The stator is connected to the grid, while the rotor is short-circuited. DFIG has its blades decoupled from the rotor of the electric machine. Consequently, the inertia of the blades cannot be seen by the system and the system cannot respond to a generation loss [55-57]. The ac currents produced by the generator are converted into dc current by an AC/DC converter, and then again converted into ac currents by another AC/DC converter. In FSG there is no speed control and the only way of optimizing the tip speed ratio (λ) lies in the blade pitch angle control. It is difficult to adjust the pitch angle, β, in cases the wind changes rapidly. Thus, this kind of wind turbines are modelled accordingly to the wind characteristics of the region they will be installed that also results to operate more often for optimum λ. On the other hand, in DFIGs

both blade pitch and speed control is possible that permits this kind of generators work for optimum λ in variable wind speeds [52], [58]. This type of technology occupies voltage controlled inverters ac-dc-ac that convert power at varying frequencies to dc and with the utilization of a power converter back to ac at a fixed frequency suitable for the grid connection [59]. Moreover, these generators can participate in voltage control, providing or consuming reactive power without exceeding the rated limits of the machine.

2.4.3.2. DFIG Inertial Response and Speed Control

As mentioned in [52], the inertial response is the basic method of primary frequency control in wind turbines. The above response is implemented through three hierarchical control loops. The electrical one supervises the generator and the converter, whereas the mechanical one supervises the blade pitch angle and the blades´ speed. The figure beneath (Fig. 2-5) represents the speed controller [60]. There are four main steps within this control. 1) Identification of ω_{ref} (generator reference speed) from the P-ω characteristic graph. 2) The error between the measured speed and the reference one is defined as Δω. 3) The error is then sent to PI controller, resulting in the torque speed reference value T_{ref}. This value incorporates the imbalance among the turbine torque and the generator torque, that will result to an accelerating or decelerating torque until the desirable speed is achieved. 4) The torque speed reference and an additional torque inertia term will define the torque reference.

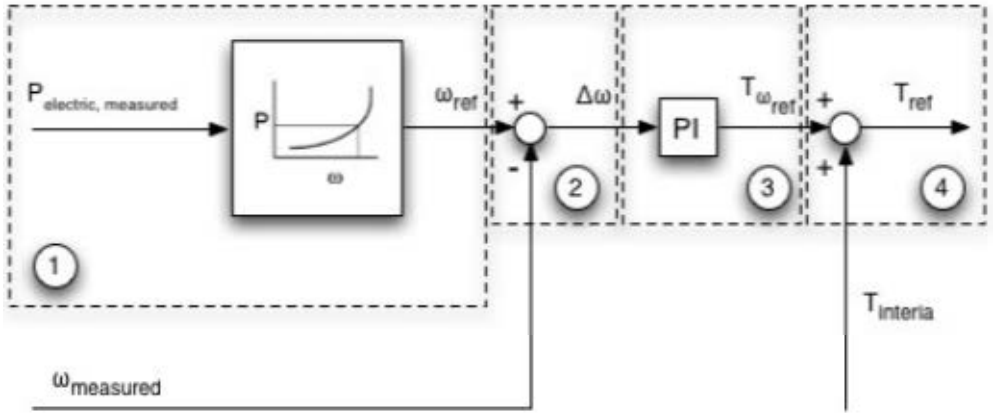

Fig. 2-5: Speed Controller Design [60].

Figures (Fig. 2-6 & Fig. 2-7) beneath represent the inertia and droop controller schemes respectively [57, 60, 61]. The inertia controller–not embedded in the DFIG-is to minimize the mechanical drive train loads, and the rate of power injection by adding a filter that leads to the reduction of electromagnetic torque and the reduction in the peak torque. On the other hand, the droop controller relates the torque to the deviation from the nominal system frequency as follows:

$$T = K_p \cdot (\omega_o - \omega_{measured}) \tag{2-3}$$

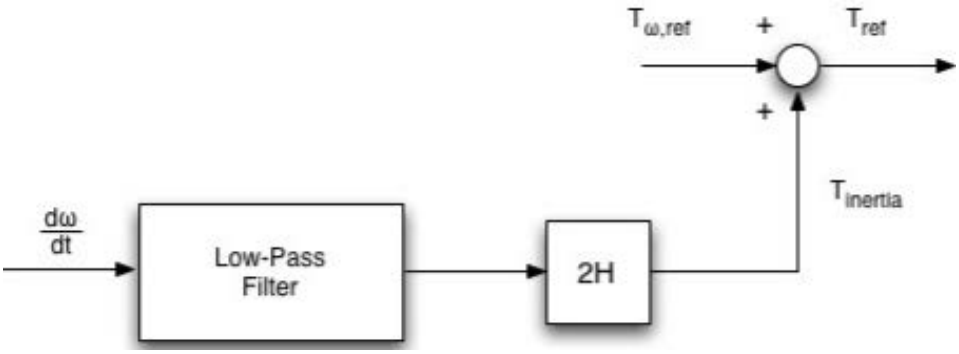

Fig. 2-6: Inertia Controller Design [57, 60, 61].

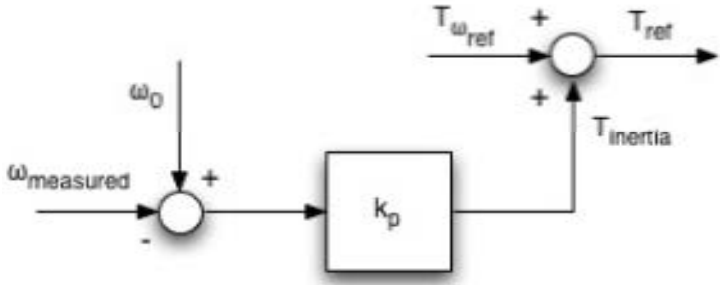

Fig. 2-7: Speed Controller Design [57, 60, 61].

2.4.3.3. Frequency Control and Active Power

Frequency and active power control implementation are analytically mentioned in [52] which are subsequently described in this report. Control of the system frequency is a crucial issue in the operation of a power system. In order to achieve a near constant frequency, it is necessary to keep the balance among the generation and the load in the system. For instance when the system suffers from a generation loss and cannot supply sufficiently the load, the frequency will decline. Frequency response after a system imbalance occupies roughly three time frames and is so called as the primary frequency. A) Proximity effect $t=0^+$, B) Inertial response ($0^+<t<t_g$ sec) and C) Governor response ($t_g<t<t_f$ min). The above responses are essential for eliminating any power imbalance sensed by the system. The proximity effect is rather realized by the machines closer to the load changes and refers to their compensation level according the imbalance. It is independent the machine size and rating. The inertial response refers to the middle time frame after the imbalance and before the governor reaction. In general, after an imbalance, the system will suffer from an overall deceleration, with individual generators react according to their inertial response. The rule is that the larger the inertia, the faster the response will be. It lasts for a slight transient period, usually on the order of a few seconds. In case that the machine does not provide with any turbine governor action, the inertial response will determine the final steady-state frequency following the load imbalance [62, 63].

Turbine governor is generally applied through the use of a droop controller. The droop control replies to a 5% decrease in the turbine speed, due to an increase in the load. Thus, any change per unit in the mechanical power is a relationship to the change in frequency (speed). Here, the share of each machine is based on its rating, so the bigger the machine the higher the contribution to the disturbance will be.

The different kind of designs in machines, like the FSGs and the DFIGs that are commonly utilized in wind turbine technologies define the system frequency response. In more details, the FSGs have inertial response inherent in

contrast to the DFIGs. Subsequently, in the primary frequency control scheme, the FSG will react as a synchronous generator during the inertial response.

2.4.4. Photovoltaic power plants (PV)

PV cells are arranged in series or parallel connection in order to form arrays or panels, with the suitable surface area of high voltage and power rating output. Sun light in the form of photons make electrons on the PV cell surface move towards a specific direction and behave like DC current carriers crossing the p-n layer junctions. The DC nature of photovoltaic systems imposes the requirement of converter circuits which transform the DC power to AC at the granted grid frequency. Factors like solar irradiance/intensity, surface area, light angle incident and converter rating affect at a large extent the performance of a PV farm. It is a common attribute installing fast tracking systems to shift the operating point of the arrays, thus more sunlight is captured and subsequently the power output is maximized [37].

We can meet four main types of PV cells in the market. These are mono-crystalline and multi-crystalline silicon, thin-film silicon and hybrid configurations [37].

2.4.5. Fuel cells

Fuel cell is a generation unit that converts chemical energy into electricity. The electrochemical process requires the presence of a fuel, usually hydrogen and an oxidant (air) are injected into the two electrodes, the anode and the cathode respectively. Reactions take place and DC power is produced. A single fuel cell does not produce more than 1 V as an output voltage, thus more than one cell are stacked on top of each other in series connection to form an array [37]. Fuel cells generally perform well in gas and hydrogen infrastructures. We can discriminate four characteristic kinds of fuel cells dependent on the different electrolytes and operating temperatures. These are the proton exchange membrane (PEMFC), phosphoric acid (PAFC), molten carbonate (MCFC) and solid oxide (SOFC) fuel cells [37].

2.4.6. Small hydroelectric plants

Hydro plants exploit the kinetic energy of a mass of water to produce electricity. The effective water head column and water flow rate define much of the power output. The equation beneath justifies that [37].

$$P = Q \cdot H \cdot n \cdot \rho \cdot g \tag{2-4}$$

Where P is the power output in W, Q is the water flow rate (m^3/s), H the effective head (m), n the overall efficiency, p the water density (1000 kg/m^3) and g the acceleration gravity. Cross-flow impulse turbines are used for small hydro plants rated below 10 MW where the kinetic energy coming from the water movement hits the turbine blades as a water sheet and drive the generator [64]. Induction or synchronous generators technologies may be occupied in these DG arrangements with variable ratio gearboxes [37].

2.4.7. Geothermal power plants

Geothermal power farms convert the heat coming from hot rocks (potential geothermal reservoirs) into electricity. Water is warmed and the produced steam circulates inside the rock reservoir up to the surface and back again to be reheated while it drives the generator turbine to produce electrical power. This natural steam circulation retains the reservoir potential [50].

2.5. Identifying the benefits of DG penetration

Distributed generation has gained a significant interest the last decade. The factors that have contributed to this are numbered as the following: new acquirements regarding the DERs technologies, limitations on the transmission lines, increased demand, the electricity market liberalization and major concerns about the climate change. A brief description of DG integration benefits is given below [65].

a. The continuous growth in load demand has led to the depletion of fossil fuel reserves. Therefore, governments have switched their interest to more efficient and cost effective energy solutions, such as renewable energy sources [1].

b. Global warming and environmental policies are the driving force to look for cleaner energy solutions. According to the Kyoto protocol (1997) and its second commitment phase defined by the Durban convention (2011), EU, UK and many other countries have adopted new strategies in order to reduce greenhouse emissions. It is expected that embedded generation will support this scheme by producing cleaner and more efficient energy.

c. One of the most vital examples is the CHP (combined heat and power) plants which utilize the waste heat for industrial, commercial or domestic applications. Additionally, they are located close to the heat loads to minimize the transport losses and thus the capital investment. It has been reported that CHP generation may result to a 10 up to 30% energy conservation relying on the size and efficiency of the cogeneration units [6].

d. It can offer flexibility in reliability necessities. A variety of industries, such as chemical, petroleum, metal etc. may criticize the grid supplied electricity too low and may want to invest in distributed generation to enhance this level of reliability. For instance, fuel cells and backup systems could possibly supply with protection against power interruptions [40], [38].

2.6. Technical Considerations

The question of power quality and DG is not outspoken. It is a matter of fact that this is one of the major challenges of penetrating high RES amounts. For instance, the DG units may influence the system frequency, while regularly are not equipped with a load-frequency control, they will cumber on the efforts of the transmission grid operator or the regulatory body to sustain system frequency [7]. Consequently, the quality of supply may worsen, unless the appropriate control measures are taken. In addition, embedded generation can prove to have a healing effect on the voltage profile, especially on rather low voltage levels [66]. On the other hand, sudden and extreme increases of voltage figures in radial networks constitute a major connection issue of the distributed generation. Besides, voltage fluctuations result from bi-directional power flows and complex reactive power management. Variations in voltage level can generally be divided into slow and rapid changes-flicker [7], [66], [67]. The former results from power deviations e.g. in case of wind turbines because of variations in wind speed, and the latter occurs due to start/stop activity of a device.

Moreover, distributed generators have regularly difficulties in predicting their power output, especially when we are talking about energy production or renewable energy sources. In case they are unable to meet the power portfolio balance-power injections to be roughly equal to withdrawals, they are penalized [40].

One more difficulty could be detected on the fact that bi-directional flows require for diverge protection schemes at both voltage levels, as increased share of distributed generation may introduce power flows from the low voltage into the medium-voltage grid.

What is worth mentioning is that the majority of embedded plants occupy rotating machines, with induction and synchronous generators increasing the fault level of the distribution system. One way to limit this effect could be the

appearance of impedance as induced by a transformer or a reactor but at the expense of higher losses and bigger voltage variations at the generator side [68].

Distribution Network Operators (DNOs) undertake the operation and maintenance of distribution networks. Each region may belong to more than one DNOs, but only one operator is actually responsible for ensuring reliability and security of supply to its customers [69, 70]. The DG units' penetration into distribution networks is arranged by the DNOs. In overall, their responsibilities are; network protection from fault incidents, voltage stability within statutory limits, avoid thermal and fault overload ratings of protection systems and cables, ensure system reliability and power quality maintenance [71].

2.6.1. An Overview of the Restraints for DG Connection

Distributed units are inhabited into the grid via two different connection points the physical connection point (CP) and the point of common coupling (PCC) as it can be also seen in Fig. 2-8. The latter one is considered as the network junction point or the substation bus bars [66]. However, the CP is the actual connection point that interconnects the substation terminals via a direct line branch. Independently the equipment is going to be used for the installation procedure in a service, the coupling substation consists of protection devices as represented in Fig. 2-8 [66].

With the integration of dispersed generation in the grid is necessary to estimate the expected disturbances beginning with those in the PCC due to a particular DG installation. Dedicated interconnection lines are part of the grid, thus disturbance limits can be also applied in the CP point with more lenient attribute than for the PCC [72],[73]. Specifically, these limits are defined in order to ensure that the resulted faults will not affect other users of the network. The majority of reports comply with the IEC 61000 standards that planning levels are utilized as disturbance limits [18].

Harmonic distortion is a product of power electronics use in variable speed wind turbines, photovoltaic panels, micro turbines etc. A group of different IEC standards is applied to identify the acceptable disturbance limits with IEC 61000-2-2 and IEC 61000-3-6 being the most prevalent [25], [73].

Apart from the power quality issues, additional considerations involve steady-state thermal obligations, network congestion and short circuit capacity. Over currents and overloads may incur with the penetration of high amount of DG not only at the connection point but also and in the area around it [74]. Moreover, the outputs of grid components need to be capable to deal with the power of the dispersed unit.

Attention should also be paid to avoid exceeding the fault level of the network, because embedded generation induce and arise the fault currents and power in the grid [72].

Distribution generation units need to comply with ancillary service issues that involve reactive power compensation and voltage control. Voltage and reactive power are linked to a chicken-and-egg situation: Reactive power intake induces voltage dips in the system with generating plants or capacitor banks participating in this compensation.

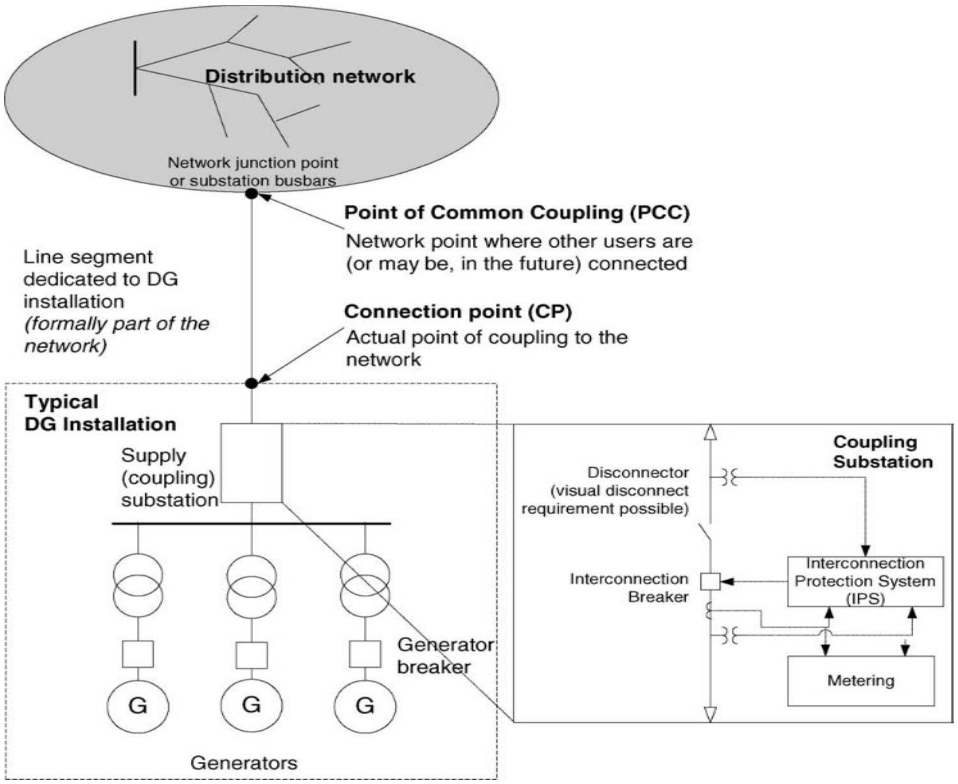

Fig. 2-8: Connection point (CP) and point of common coupling (PCC) [66].

2.6.2. Reactive Power Control & Voltage Regulation

Reactive power control and subsequently voltage control are necessary for regulating the voltage levels across the distribution feeders. In more details, the nodal voltages that represent the connection points of distributed generation must be regulated in order to be maintained within the limits imposed by the statute which define the allowable variations for steady-state voltages in electrical systems.

It is worthy mentioning that public power utilities compensate for the needed reactive power and control voltage at the cost of generating capacity. When stand-alone systems or Microgrids are connected to the distribution network, and given that they can provide this service, the utility generators would produce power at their maximum capacities, enhancing the total generation and in the meanwhile achieving a lower generation cost.

The single-line feeder in Fig. 2-9 beneath depicts the HV, MV and LV electrical power circuits. The voltage tends to drop along the feeder at the load connection point and especially at a far distance from the HV/MV substation where the voltage is boosted. Consequently, nodal voltages need to be regulated so as to remain within specified limits.

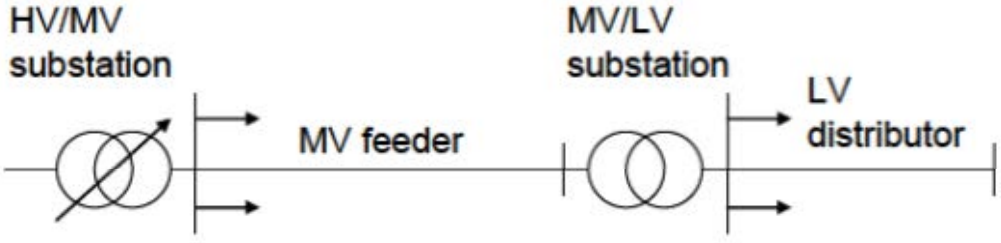

Fig. 2-9: A simplified representation of electrical power circuits [41, 69].

Grid perturbations like voltage sags and swells may be the product of uncompensated reactive power throughout the system resulting in possible damage to equipment due to high currents and overheating. Traditionally, capacitor banks and voltage regulators are used to control the voltage levels across the network feeders. The reactive power supplied by a capacitor bank drops as square of voltage [37]. Apart from the fixed capacitors banks, they do exist various VAR compensator technologies employed for reactive power compensation, such as synchronous condensers, static VAR compensators (SVC), static synchronous compensators (STATCOMs) etc.

Generally, voltage regulation in distribution networks can be categorised into two alternative ways to achieve it; the direct and indirect voltage regulation. Direct voltage regulation is achieved by using on-load tap changer (OLTC) at the substation or distribution transformer and is commonly used in HV/MV power system, notably 132/33 kV and 33/11 transformer substations [75]. Usually, an OLTC transformer contains a group of taps and it accomplishes regulation on its secondary bus bar voltage that varies due to load connection by adjusting the tap position based on the difference among the values of the reference and the measured voltages [41].

Indirect voltage regulation is performed via reactive power compensation at critical points along the line feeders that suffer from severe voltage variations. Shunt capacitors or FACT devices using relays are favoured in these cases to detect voltage variations caused by step load changes etc [76].

2.6.3. Voltage Rise

Variations in voltage and especially voltage rise at the addition node are the greatest impact that DG penetration may induce. In the previous subsection, it was discussed that voltage levels need to retain within acceptable levels beyond the transformers´ substations according to the statute. The uncontrollable addition of generation units may cause voltage fluctuations, especially when talking about variable generation like wind energy in autonomous networks.

Voltage variation between two nodes 1 and 2 (Fig. 2-10) can be approximately given by equation (2-5), where R, X are the resistive and reactive parts of the feeder, respectively and P and Q are the net active and reactive power flows between the two buses across the line [34]. Q_C depicts the reactive power compensation by a shunt device, i.e. shunt capacitor. Subscripts L and DG represent the load and the distributed generation units connected to the second bus feeder.

$$\Delta V = V_1 - V_2 \approx \frac{R_{12}P + X_{12}Q}{V_1} \approx \frac{R_{12}(P_L - P_{DG}) + X_{12}(Q_L \pm Q_{DG} \pm Q_C)}{V_1} \tag{2-5}$$

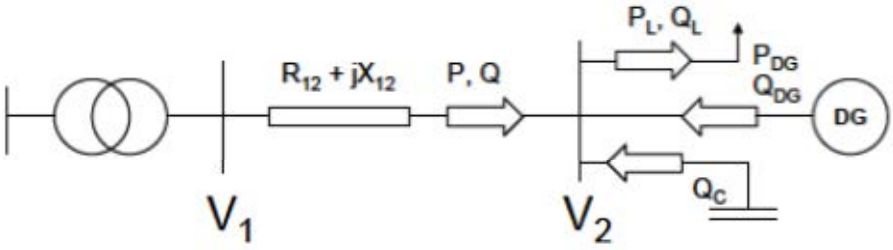

Fig. 2-10: A two nodal system [34].

2.6.4. DG Units in Islands: Physical Impacts and Limits

Interconnected DGs can be efficiently operated as Microgrids both in grid-connected and islanded mode and may be incorporated in an Island power system. The most auspicious facet of Microgrids is their ability to provide ancillary services to reinforce the reliability of ´´weak grids´´ and generally of the distribution networks. Microgrids´ contribution in reactive and thus voltage control depends on their size and allocation since it can provide locally smooth voltage regulation following the controller settings and specifications.

Similarly to the integration of distributed generation in MV/LV distribution networks, the penetration of these units into Islands or autonomous electrical grids influences these power systems in multiple ways since they increase the complexity of the existent networks. The bibliography reports an extensive work [77-81] done on investigating the aforementioned impacts and give possible solutions for DGs penetration into distribution and autonomous grids.

Beneath are outlined the factors that are mostly impacted by the amount of DG that is added.

- Short circuit level and ratio
- Power ratings
- Voltage rise
- Losses
- Power quality
- Reliability
- Protection

Broadly speaking, the penetration of DG fires up the short circuit level and this increase is favorable since it will make stronger and more robust the system. Nevertheless, it is important to ensure that this increase does not exceed the ratings of the breakers and the protection devices because this would be dangerous for the system.

Most evident are the changes of active and possibly reactive power flow which affect the total power flows throughout the network branches. These changes in braches´ power flows influence the network voltage and current limits, network losses and finally the power quality and reliability of the power system. Consequently, as soon as the number of DG units and their size increase, the power injected and dispersed by the formers throughout the power system is no longer negligible.

A voltage rise takes place when the generation exceeds the load demand along branches with high impedance. This problem is more often in rural areas where the demand is rather low. Moreover, the resistive part of distribution lines is higher than the inductive because at the connection points away from the substation area, lines and cables tend to have smaller cross-sectional area. Thus, the ratio of X/R is smaller in distribution networks, i.e. $X/R \leq 5$, whereas it varies between 10 and 20 in transmission networks and worsens the rise problem. Concluding, recalling the formula (2-5), the active power flow has greater impact on voltage level than the reactive one and the voltage rises with more injection of active power generation.

The protection coordination of the distribution system devices is most affected since the transition to active distribution networks modifies the fault currents flows from unidirectional to bidirectional. Additional effects are the false tripping of feeders, change of fault level ratios, unwanted islanding etc [80-82]. For instance, Microgrids, unlike conventional protection schemes that are designed for high fault levels and unidirectional power flows, are characterized by lower fault levels due to the limited microsources´ capacity and their power interfaces, in addition to the bidirectional power transfer from the sources to the load banks.

Considering the above and the fact that DG penetration needs to cope with the requirements imposed by the Distribution Code [70], concrete technical recommendations are applied to MV/LV networks such as G83/1, G59/1, IEEE 1547, and CEI 11-20 specifying the anti-islanding protection feature. In that case, DG units need to be disconnected from these networks, when the circuit breaker supplying the feeder connected to the DG is tripped [83, 84].

According to voltage and power potential of the distributed generation to be embedded, different technical requirements are applied; For instance, G83/1 refers to generators connected to low voltages and with up to 16 A/phase. G59/1 refers to generators of no more than 5 MW capacities that are embedded to lower than 20 kV systems and G75/1 concerns power units of no more than 5 MW generation capacity connected to higher than 20 kV networks [85-87].

2.6.5. Penetration of Microgrids

A numerous of technical considerations need to be encountered with the penetration of Microgrids. These are related to the difficulties experienced in controlling various plug-and-play microsources and energy storage systems. Concrete communication protocols need to be employed within this area. For instance, the IEC 61850 communication standard [1] is started to be deployed in the new-comer concept of a Microgrid which regards mainly the information exchange among Intelligent Electronic Devices. However, the implementation of this protocol requires the existence of appropriate communication infrastructure that the current rural Microgrid installations suffer from. Apart from the communication protocols, standards addressing operation and protection issues are not still widely available, since Microgrid is a rather new area [1], [88].

Furthermore, one of the biggest challenges is synchronizing multiple parallel generators since it is more complex when a power system is relied on a group of components instead of a large generator. In addition to this, without the inertia of the main grid, the system may suffer from frequency and voltage stability problems. The same dilemma appears with the integration and parallelization of the microsources' inverters.

2.7. The Challenge of Rewiring Distribution Networks

Active distribution networks involve bidirectional electricity transportation compared to passive power networks since DG units are penetrated into them. These types of networks need to associate flexible and intelligent control technologies leading to a Smartgrid networks. The key aspects of this research are in the areas beneath: i) extensive area of active control, ii) adaptive protection, iii) management devices, iv) simulation on a time basis, v) upgraded sensors and measurements, vi) innovative conception of transmission and distribution systems.

For instance, the UK industry regulator that is the Office of Gas and Electricity Markets (Ofgem) names the need to upgrade the infrastructure of the existing passive networks to those ones which will encompass distributed generation, the active ones. The so-called ''Rewiring Britain''.

More specifically, three different studies examined the load control across the UK [89]. Firstly, a load manipulation technique was implemented in the North East of England to limit the voltage augment in order to accommodate higher capacity of wind energy. The results showed that with load control more than 600 MW of wind power could be installed. Secondly, Distributed Intelligent Controllers (DILCs) were utilized to control the system frequency in the Scottish island, Rum and the modeling showed that there was a need for advanced development of DILCs, because high voltage fluctuations were marked. The ultimate stage of the case study involved a combination of load control and synchronous compensator tested on an islanded operation of a wind farm. The simulations presented that the frequency and voltage can be controlled within satisfactory limits, although the wind turbine start up may be hard.

2.8. Summary

This chapter discussed the background of distributed generation integration. Distributed and renewable energy sources ranging from small-scale to large-power generating units have gained high interest and attention worldwide,

whereas the enhancements and advances on their technology types have fostered the use of this kind of clean and very promising sources to generate electricity. Undoubtedly, distribution penetration into MV/LV and especially into Island or ´´weak´´ power grids may have a healing effect on the system´s voltage profile, especially in remote areas. The Microgrid concept is another solution for integrating small-scale generation (with their intelligent controllers) and storage devices into LV, as well as MV networks since is an autonomous group of controlled microsources. This configuration can operate as an independent islanded power system or in synchronism with the utility grid, optimally placed to serve the benefit of the customers and thus, enhancing the system´s stability and reliability.

However, the impacts and the technical considerations of the DG penetration into MV/LV distribution networks are apparent and cannot be negligible, as soon as the number of DG units and their size increase, the power injected and dispersed by the formers throughout the power system is no longer negligible.The major affect is on the planning and operation of distribution systems since their unidirectional characteristic places limitations and specific requirements on the amount of embedded generation integration into these systems. Most evident are the changes of active and possibly reactive power flow which influence the total power flows throughout the network branches. These changes in braches´ power flows affect the network voltage and current limits, network losses and finally the power quality due to system incompatibility with different electronic equipment. Hence, the commissioning of future DG installations should follow the Distribution Code guidelines related to specific connection requirements that generators of different voltage and capacity should adhere to.

Chapter 3. Research Methodology

3.1. Introduction

As aforementioned in Chapter 1, Section 1.4.2, comprehensive analysis of DER integration requires tools that provide computational power and flexibility. In this context, this thesis is focused on two research areas; a) grid penetration studies in order to define the steady-state and dynamic limit for distributed generation integration into a real Island power network. This work is accomplished with PSS/E simulation tool and b) real time distribution grid simulations with RTDS/RSCAD tool developed in PHIL environment for LV power networks which allow us testing and validating the control performance and interaction of the system´s equipment. This kind of testing gives the opportunity to analyze the behaviour of the hardware device in real time since the current and voltage measurement signals of the generation unit are fed back.

This chapter discusses the principal hints of the research methodology followed throughout this thesis and gives a brief description of the two utilised software programs, namely PSS/E and RTDS/RSCAD.

3.2. PSS/E Software Tool

3.2.1. Background

In order to analyse a power grid from an electrical point of view, examine its stability and define the potential integration of distributed generation into the grid, static and dynamic simulations need to be carried out. Stability considerations can be divided into two case studies: the steady-state and dynamic stability analyses.

Steady-state analysis and especially load flow analysis involves the calculation of power flows on the network lines, transformers and the voltage profiles of system bus bars. This study is very important for the planning and design of the connection of distributed generation to the transmission and distribution grid [90]. Contingency or N-1 analysis is also essential in order to ensure the security and reliability of power supply [91], [92]. Short circuit calculations introduce the proper selection of high voltage equipment and protection relays. Both contingency and short circuit studies belong to the steady-state or static analyses.

On the other hand, dynamic analysis studies the transient stability of the system in time domain. A transient event occurs undesirably and instantly in a power system and can either be an oscillatory or impulsive disturbance [91]. For instance, branches and bus faults, line, loads and generators tripping may induce frequency, rotor angle as well as voltage oscillations and can lead to the failure of the distribution system where the embedded generation is planned to be connected to or even can cause damage to the power electronics equipment. Therefore, a transient stability study is necessary to investigate the power system response to disturbances and check over its fault ride through capability to see if the network elements have adequate stability margin [92-94].

The collection of the necessary data related to the grid model to be analysed comprised the most important and questioned target of this project. The info that will be introduced into the *Power System simulator for Engineering,* PSS/E in order to apply a static and dynamic analysis of the Island power grid, includes: the nodes of the power system, generators, power plants, transformer and non-transformer branches, loads, fixed and switched shunts, and general representation of the transmission and distribution schemes. Rated power, nominal power, power factors, impedance and admittance figures, iron and copper losses in the transformers, and sequence components consist some of the values to be further asked.

3.2.2. The Program

The Siemens PTI PSS/E simulator is a software tool that allows power flow, short circuit and dynamic modeling in an integrated environment, while permits the development of user defined models based on Python language [95]. The program is more than 30 years in commercial use and the enhancements being done all this time of utilization

made it a powerful tool to optimize the network system. Additionally, PSS/E employs a vast number of algorithms to solve problems of large and small scale [95]. It is a generally acceptable instrument in the area of integration into the power networks. Public electrical utilities such as the PPC (Greece) and Scottish Power (UK) have developed relevant reports about distributed generation on European islands and ´´weak´´ grids. For instance, the Greek islands [9] of Kythnos, Crete, and Chios and in Scottish area Rum, Shetland and Isles of Scilly are simulated in this kind of studies.

Some of the program capabilities are represented beneath;

- *Steady-state analysis:* Facilitate a variety of analyses including power flow, balanced and unbalanced faults, probabilistic and deterministic contingency analysis (N-1, N-2, N-3), PV/QV study and graphical construction.
- *Time Domain analysis:* The program occupies a vast library of machines' models, exciters, governors, stabilizers, load, FACTS equipment, and models of wind turbines. Moreover, it offers the possibility to produce user-defined models with FORTRAN code and with Graphical Model Builder (GMB); the user may create graphical test control diagrams.

PSS/E applies short circuit faults including three-phase faults, single-line-to-ground faults, double-line-to-ground faults, line-to-line faults and also simulates faults based on ANSI standards calculations. Furthermore, performs IEC 60909 [73] standards on the fault computations, requesting only for the zero and negative sequence components if unsymmetrical faults are to be calculated. An advantage of the program is that it can perform one or all sorts of faults on one bus and even on all the system, reducing the computation time.

The following figure (Fig. 3-1) illustrates the program´s elementary interface views.

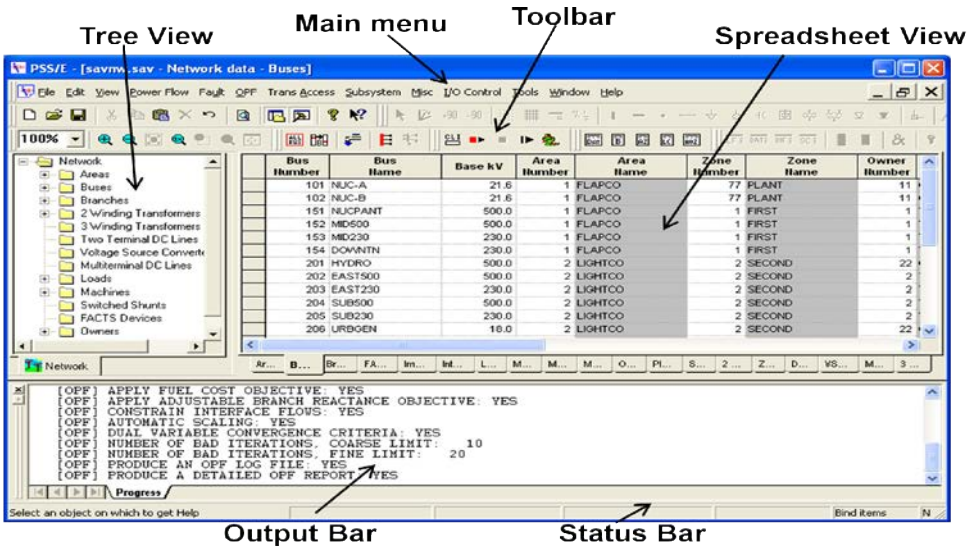

Fig. 3-1: PSS/E Elementary Interface Views.

3.2.3. Steady-State Modeling

3.2.3.1. The Power flow problem: Buses categorization

Power flow calculates the voltage magnitudes and phases angles at each bus throughout the electrical system. Generally, the input data for power flow computations are the voltage magnitudes V, the load angle δ, the net real power P and the reactive power Q. Depending on the buses' classification, two of these parameters are always input data and the remaining two are calculated by the power flow program. Buses or nodes are categorised as follows [27, 96]:

a) Swing or slack bus; this is an artificial reference node that ''acts'' as a starting point in the load flow equations because is the only bus where the voltage and phase angle are specified. Voltage and phase angle retain the value of 1 pu and 0 pu respectively. According to these values, all the other voltages are computed, in addition to line currents and losses. For instance, when we change (increase/decrease) the output of a generator in order to keep the power balance, the slack generator is the one to react immediately (auto-regulation) to these changes. Its variation in active and reactive outputs depends on the other nodes' changes as given by (3-1). Equation (3-1) describes the power balance within a system, where the generation equals the load demand plus the losses occurred this is a chicken-and-egg relationship.

$$Generation = Demand + Losses \tag{3-1}$$

b) Load bus; normally, this is the most common bus within the power system where P and Q are input data and V, δ are computed.
c) Voltage controlled bus; this is also known as generator bus where, usually, a generator is connected to. In this case, P and V are the input data and Q and δ are calculated. As input data can also be considered the maximum and minimum limits of reactive power that the generator can reach. A bus should be designed as voltage controlled bus if a tap-changing transformer is connected to it.

Power flow programs (i.e. PSS/E, Power World Simulator etc) calculate the bus voltages based on bus admittance matrix given by (3-2) together with the voltage and current vectors. Y is the bus admittance matrix, V is the column vector of the bus voltages and I the vector of current sources. The current and bus admittance vectors are the input data.

$$\overline{I} = \overline{\overline{Y}\,\overline{V}} \tag{3-2}$$

The bus admittance matrix consists of the diagonal sum of admittances (Y_{ii}) connected to the studied bus and all off-diagonal elements (Y_{ij}) are the negative sum of the admittances between the specific bus and the remaining buses of the electrical system [27].

Hence, the power injections at any node i can be extracted from (3-3) as:

$$\overline{S_i} = P_i + jQ_i = \overline{V_i}\,\overline{I_i}^{*} \tag{3-3}$$

Diving the real and imaginary parts yield equations (3-4) and (3-5):

$$P_i = \sum_{j=1}^{N} |V_i||V_j||Y_{ij}|\cos(\delta_i - \delta_j - \theta_{ij}) \tag{3-4}$$

$$Q_i = \sum_{j=1}^{N} |V_i||V_j||Y_{ij}|\sin(\delta_i - \delta_j - \theta_{ij}) \tag{3-5}$$

3.2.3.2. Newton-Raphson method

The PSS/E simulation tool employs different power flow solution methods, however this research work is based on fixed slope decoupled Newton-Raphson solution.

As a by-product of the power flow calculations given the voltage magnitudes and phase angles, power flows and losses can be also computed. The power or in other words load flow problem is nothing more than a set of non-linear algebraic equations that can be generally represented in matrix format as follows [97, 98]:

$$f(x) = \begin{bmatrix} f_1(x) \\ f_2(x) \\ \vdots \\ f_N(x) \end{bmatrix} = y \tag{3-6}$$

Where x, and y are N vectors and f(x) is an N vector consisting of functions. For instance, x can be the vector of the unknown state variables like voltage magnitudes and angles, whereas y can be the vector of the inputs, i.e. real and reactive power generations/demands as given by (3-7) and (3-8) respectively.

$$x = \begin{bmatrix} \delta_1 \\ \delta_2 \\ \vdots \\ \delta_{N-1} \\ V_1 \\ V_2 \\ \vdots \\ V_{N-1} \end{bmatrix} = \begin{bmatrix} \delta \\ V \end{bmatrix} \tag{3-7}$$

$$y = \begin{bmatrix} P_1 \\ P_2 \\ \vdots \\ P_{N-1} \\ Q_1 \\ Q_2 \\ \vdots \\ Q_{N-1} \end{bmatrix} = \begin{bmatrix} P \\ Q \end{bmatrix} \tag{3-8}$$

Consequently, for a system with N nodes, the vector of non-linear functions linking power injections[2] with voltage is given by (3-9).

[2] Calc for calculated

$$f(x) = \begin{bmatrix} \sum_{j=1}^{N} |V_1||V_j||Y_{1j}| \cos(\delta_1 - \delta_j - \theta_{1j}) \\ \sum_{j=1}^{N} |V_2||V_j||Y_{2j}| \cos(\delta_2 - \delta_j - \theta_{2j}) \\ \vdots \\ \sum_{j=1}^{N} |V_{N-1}||V_j||Y_{N-1,j}| \cos(\delta_{N-1} - \delta_j - \theta_{N-1,j}) \\ \sum_{j=1}^{N} |V_1||V_j||Y_{1j}| \sin(\delta_1 - \delta_j - \theta_{1j}) \\ \sum_{j=1}^{N} |V_1||V_j||Y_{1j}| \sin(\delta_1 - \delta_j - \theta_{1j}) \\ \vdots \\ \sum_{j=1}^{N} |V_{N-1}||V_j||Y_{N-1,j}| \sin(\delta_{N-1} - \delta_j - \theta_{N-1,j}) \end{bmatrix} = \begin{bmatrix} P_{calc} \\ Q_{calc} \end{bmatrix} \quad (3\text{-}9)$$

Recalling equation (3-6),

$$0 = y - f(x) \quad (3\text{-}10)$$

Adding Dx to both sides of (3-10) where D is a square N x N invertible matrix yields:

$$\mathbf{D}x = \mathbf{D}x + y - f(x) \quad (3\text{-}11)$$

Multiplying by D^{-1},

$$x = x + \mathbf{D^{-1}}[y - f(x)] \quad (3\text{-}12)$$

The iterative method indicates that the old values x(i) on the right side are utilized to calculate the new values x(i+1) on the left side of (3-12) and can be the solution to the non-linear equations [97]. In other words,

$$x(i+1) = x(i) + \mathbf{D^{-1}}\{y - f[x(i)]\} \quad (3\text{-}13)$$

The Newton-Raphson method is used to specify the matrix D and on based on the Taylor´s formula; Expanding f(x) around a given point x_0 and neglecting higher order terms.

$$y = f(x_0) + f'(x_0)(x - x_0) + ... \quad (3\text{-}14)$$

And

$$x = x_0 + \frac{y - f(x_0)}{f'(x_0)} \ldots \tag{3-15}$$

With the Newton-Raphson scheme, x(i) replaces x_0 and x is in turn replaced by the new value x(i+1). Thus, D in (3-13) is replaced by the J(i) which is an N x N matrix whose elements are partial derivatives, and is called Jacobian matrix.

$$x(i+1) = x(i) + \mathbf{J^{-1}}\{y - f[x(i)]\} \tag{3-16}$$

Returning to the load flow problem, there are defined Jacobian sub-matrices of partial derivatives such as:

$$H = \left[\frac{\partial P}{\partial \delta}\right],\ M = \left[\frac{\partial P}{\partial V}\right],\ N = \left[\frac{\partial Q}{\partial \delta}\right],\ K = \left[\frac{\partial Q}{\partial V}\right] \tag{3-17}$$

With elements,

$$H_{ij} = \frac{\partial P_{i,calc}}{\partial \delta_j},\ M_{ij} = \frac{\partial P_{i,calc}}{\partial V_j},\ N_{ij} = \frac{\partial Q_{i,calc}}{\partial \delta_j},\ K_{ij} = \frac{\partial Q_{i,calc}}{\partial V_j} \tag{3-18}$$

Concluding, with the Newton-Raphson iterations yield the voltage magnitudes and phase angles as given by 3-19.

$$\begin{bmatrix} \Delta\delta \\ \Delta V \end{bmatrix} = \begin{bmatrix} H & M \\ N & K \end{bmatrix}^{-1} \begin{bmatrix} \Delta P = P - P_{calc} \\ \Delta Q = Q - Q_{calc} \end{bmatrix} \tag{3-19}$$

3.2.3.3. Lines Representation

The length of the transmission lines defines their modeling and characteristics. A short transmission line, i.e. when its length is less than 100 km is shown in Fig. 3-2 containing a series resistance and inductance. Subscripts S and R stand for the sending and receiving ends of the voltage and current whereas l is the line length [28].

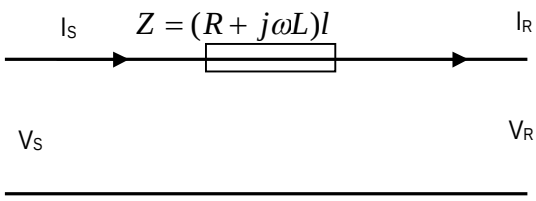

Fig. 3-2: Equivalent circuit of a short length line.

The admittance, Y, for short transmission lines cannot be neglected for a medium length line and is represented by the equivalent Π-circuit where the admittance is connected in parallel with half at each end of the circuit as shown in Fig. 3-3. Normally, medium length lines range from 100 to 300 km [28].

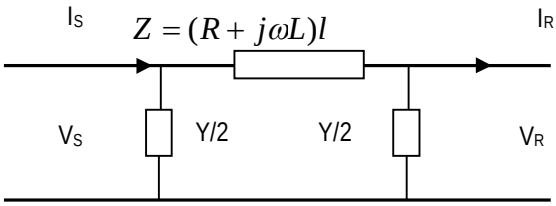

Fig. 3-3: Equivalent circuit of a medium length line.

The admittance depends on the conductance and the capacitance as follows:

$$Y = G + j\omega C \tag{3-20}$$

The relationship between the receiving and the sending ends of the voltage and currents are illustrated in equation (3-21) where the parameters A, B, C and D depend on the line characteristics, R, L, C [28].

$$\begin{aligned} V_S &= AV_R + BI_R \\ I_S &= CV_R + DI_R \end{aligned} \tag{3-21}$$

Rewriting the above equation in matrix form yields (3-22) as follows:

$$\begin{bmatrix} V_S \\ I_S \end{bmatrix} = \begin{bmatrix} A & B \\ C & D \end{bmatrix} \begin{bmatrix} V_R \\ I_R \end{bmatrix} \tag{3-22}$$

For short line equivalent circuits the A, B, C, D matrix is given by (3-23) as:

$$\begin{bmatrix} A & B \\ C & D \end{bmatrix} = \begin{bmatrix} 1 & Z \\ 0 & 1 \end{bmatrix} \tag{3-23}$$

Whereas for the medium length lines the A, B, C, D matrix is defined as:

$$\begin{bmatrix} A & B \\ C & D \end{bmatrix} = \begin{bmatrix} (1+\frac{YZ}{2}) & Z \\ Y(1+\frac{YZ}{4}) & (1+\frac{YZ}{2}) \end{bmatrix} \tag{3-24}$$

3.2.3.4. Contingency Analysis

Contingency analyses are accomplished to ensure that the system´s stability and security is maintained for instance with the outage of a single element in the system. For steady-state regime, security means operation without overloads and that the voltage levels remain within specified grid code levels. There are several types of contingency analyses, from the most basic only considering the outage of a single transmission/distribution line (N-1 criterion) to more complex analyses considering multiple line outages or/and loss or change of generators/loads in the system [99, 100]. Throughout this thesis, only single line outages and loss of generators will be discussed and the respective results will provided in the following chapter (Chapter 4).

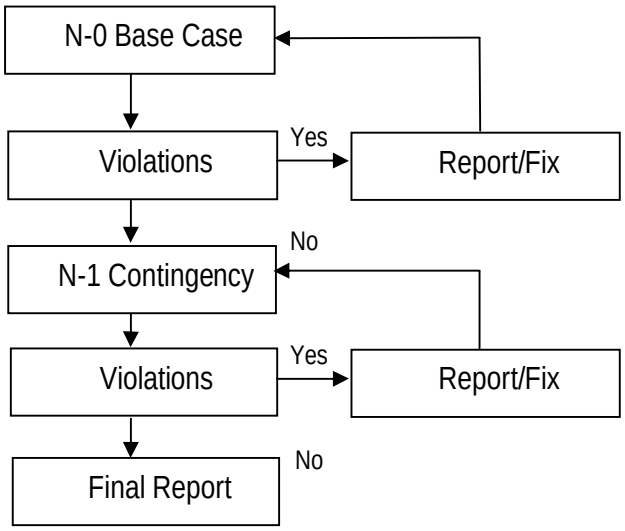

Fig. 3-4: Schematic of a contingency plan [99].

3.2.4. Power System Reliability & Load Flow Requirements

An outstanding power system operation under normal three-phase steady-state regime stands in need for the following [97]:

a) Generation feeds the load demand plus loses (recalling equation 3-1).
b) Nodal voltages remain within acceptable limits.
c) Generators outputs do not exceed specified real and reactive power limits.
d) Transformers and non-transformers branches are not overloaded.

The load flow or power computations allow for investigating on these requirements. Thus, the steady-state and dynamic response of the examined Island power system is evaluated under different potential scenarios by its secure operation under both N and N-1 criteria. This means that all the line flows must be below their limits not only for a given normal operating state, but also when any of the lines is disconnected.

One of the biggest challenges in the current work was to maintain the dynamic security not only at normal operating state, but also following ´´credible´´ contingencies, such as short circuits, tripping a transmission line, and loss of a large unit that will be presented in Chapter 4.

Moreover, throughout this research work we reviewed the prerequisites for safe operation that REE (The Spanish Electrical System Operator) has imposed for the voltage levels and the transformer and non-transformer branches´ current loadings of distribution networks. For normal operation the above should follow the criteria indicated by the dots beneath [5], [101]:

- The distribution voltages at the substations could vary $\pm 7\%$ of the nominal voltage (P.O.D.9).
- The variations in frequency may range around the values of 49.85 and 50.15 Hz at the connection point.

- Under normal operation, are not permitted overloads in the lines and transformers.
- In order to remain the voltage values within the acceptable limits and do not vary, the generators should operate with a power factor between 0.85 inductive to 0.95 capacitive.
- Conventional generators have the obligation to reserve the 1.5% of their nominal potential according to the P.O.1.5.

Under contingencies analysis (N-1), the criteria are the following [5], [101] :

- It is only acceptable a 10% overload at the nominal value of transformers during the winter period time.

In overall, throughout this thesis (Chapter 4), the voltage profile of the distribution network is loosely accepted to reside within the acceptable limits of ±5% of its nominal voltage values (0.95-1.05 pu) and a ±10% under (N-1) operation criterion, which is the typical steady-state voltage limit in MV networks according to [102], during 95% of the time. Furthermore, transformer and non-transformer branches current loadings are checked against their power ratings for overloads. A percent of 80% is set as the maximum default value in the run time options.

3.2.5. Systematic steps for DG penetration

Short circuit calculations define the potential distributed capacity that can be introduced into the grid. Principally, the main objective of such analysis is to check the short circuit power at every substation in order to evaluate the available space in terms of capacity to penetrate dispersed generation units.

These DG units are normally penetrated into the buses with the highest short circuit capacity to induce the minor impacts on the system´s stability. In this thesis, two rules of thumb were examined as where to add the distributed generation.

The former was to introduce these units at the lower voltage buses and the latter to try to add them (i.e. wind energy) to buses with denominator the higher short circuit capacity and the high load demanding and at the meanwhile obtaining the minimum possible power losses. One more criterion to be considered is that the wind potential to be penetrated cannot surpass the 5% of the short circuit capacity at the connection point node (Spanish low voltage electrical regulations, [101]).

In the current study, three-phase symmetrical faults are calculated for the transmission and distribution substations´ nodes of the system rated at voltages of 60, 30 and 10 kV for all the Scenario cases. Short circuit power calculation is based on (3-25).

$$S_{cc} = \sqrt{3} \cdot I_{cc} \cdot V_{LL} \tag{3-25}$$

Where S_{cc} is the three-phase short-circuit power, I_{cc} is the short-circuit phase current in amps, and V_{LL} is the line to line voltage in volts. All the related results are presented in Chapter 4.

3.2.6. Grid Integration Studies in Record

Grid integration studies involving the sizing and sitting of distributed generation into power systems require the analysis of the network in terms of power quality, reliability, grid capacity and limits characterization. This type of analysis may be accomplished via Steady-state and Dynamic Simulations. Different computer packages deal with the modeling of the power systems´ behaviour, such as PSS/E, EMTDC/PSCAD, SIMPOW, DigSilent, etc.

There is a record of several studies [50, 91-94, 103-110] that investigate the penetration and its consequent impacts of DG into the network grids but the majority of them deal with the modeling of wind turbines that employ

Doubly Fed Induction Generator technology (DFIG). Below is given a short review of four literature studies that utilize PSS/E as software simulation tool.

In [91] are described methods for evaluating the penetration levels of wind generation in autonomous power systems. Three different wind turbine technologies are occupied namely; fixed speed wind turbines equipped with induction generators, variable speed wind turbines with doubly fed induction generators (DFIG) and variable speed turbines with a synchronous generator and a full converter (DDSG). The conclusions concerned that wind power introduction at 30% does not apply to all power systems, whereas the penetration level does not depend only on internal parameters of wind turbines, but also on grid parameters. PSS/E and Matlab models were employed for modeling thermal plants, AVR and wind farms.

In [93] is examined the performance of the DFIG wind turbine model. The dynamic behaviour of the wind turbine is checked against a step increase in wind speed and a voltage dip induced by an electrical fault both simulated in the PSS/E software tool. The results were compared to models as developed by others. In all the results was depicted that the DFIG interacts well with the wind park and the power grid.

Paper [103] illustrates the most important characteristics of an aggregated wind farm model rated at 80 MW that occupies DFIG turbine units. Load flow and dynamic modeling in PSS/E of the wind park and the transmission grid considered as an infinite bus are employed. Through these analyses are defined the basic requirements for the wind farm connection to the transmission grid. Moreover, the wind turbine generators ´response is checked against a three-phase fault on the interconnection point.

In [105] was performed a Static Analysis of the Iraqi grid in PSS/E program in order to define upon the buses the distributed units to be added to. Diesel generators of small capacity are introduced extensively into some substations nodes of 11 and 33 kV voltages. The impact of this adds is examined over the power system losses and the short circuit levels at the addition and the nearby buses. A novel finding was extracted as to allocate the distributed generation units to the bus with the highest Thevenin impedance.

In [110, 111] Static and Dynamic Analyses of a real Island grid were performed in PSS/E to check the off-grid system's behaviour under normal operation and against several disturbances onto the network. Geothermal plants using basic machine model such as synchronous generator, exciter and governor and wind farms employing DFIG technology were chosen throughout this research study. The adequate stability margin of the system was investigated upon the fault ride through capability and frequency response of the network elements whereas among the most critical perturbations was a three phase fault application at the connection point of the wind farm. Moreover, two different exciter models (IEET1 & EXST1) were chosen to perform open-circuit set-point step tests and record their field voltage and terminal voltage responses after tuning application.

3.3. Power Hardware-in-the-Loop Technique

3.3.1. Background

The growing integration of power electronic devices interfaced to distributed generation units increases the system´s complexity due to the impact that can be induced onto the power quality and reliability within the hosting networks, which can no longer be considered passive. In addition to this, modern distribution networks need novel and advanced tools for simulation and validation experiments.

Consequently, while the penetration rate keeps increasing, network operators and regulatory authorities impose stricter technical requirements for connection and parallel operation of distributed energy resources in order to safeguard the security and reliability of the system operation, in addition to ensuring the compliance of the voltage standards (e.g. EN 50160) [112]. Besides, in EU grid codes, notably for DER penetration into the MV networks, tolerance restrictions with regard mainly to voltage drops and frequency disturbances increase the demand for

network support by means of provision and control of reactive and active power exchanges respectively [17]. As reported by [113, 114] each generating unit penetrated into network needs a so-called ´´type-specific unit certificate´´ that refers to its electrical characteristics like the connecting voltage, the power capacity, type of generator etc. Moreover, laboratory or field tests in line with system level simulations of each one generating device need to be accomplished to demonstrate its conformity with the technical issues [115] related to grid penetration.

Generally, they do exist two options for performing system experiments; a) testing real devices or b) running a simulation. A sheme that has been lately gaining attraction is the hardware-in-the-loop (HIL) apporach which combines simulation flexibility with hardware testing [116-119] and is a hybrid from these two possibilities (Fig. 3-5). This kind of experimenting gives the opportunity to test repeatedly and analyze the behavior of the hardware under test (HuT) which is a physical equipment, very close to realistic conditions. In other words, the HuT is tested over a simulated system that it is supposed to run in parallel, i.e. a distribution power network etc, and it is not available in the laboratory [119-121].

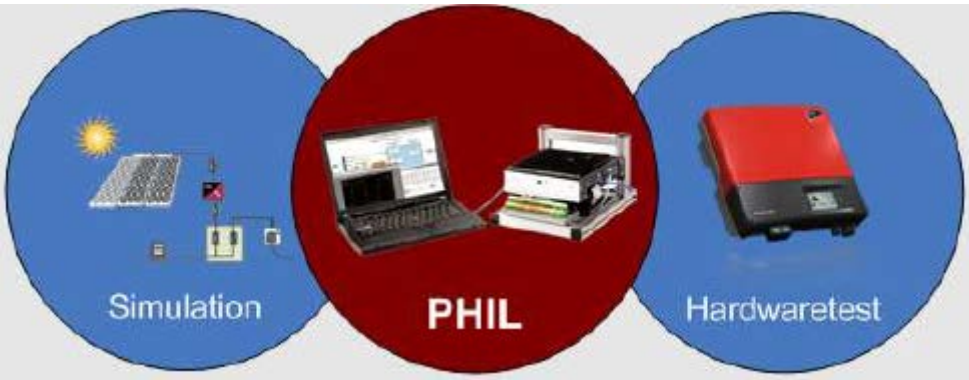

Fig. 3-5: (Power) Hardware-in-the-Loop technique [122]

Hardware-in-the-Loop simulations are traditionally divided into the control HIL (CHIL) and power HIL (PHIL) ones, where in the former the HuT is a hardware controller, such as relays, power converter controllers etc and the latter uses as HuT a power device, i.e. a PV inverter [115]. CHIL simulations have been radically exploited whereas PHIL is a newcomer approach with limited records in the direction for testing DER components and networks up to now, but is increasingly gaining interest.

3.3.2. RTDS/RSCAD Computation Program

The Real time Digital Simulator (RTDS) enables the simulation of electrical power systems and the testing of the laboratory equipment by the means of Hardware-in-the-Loop (HIL) experiments, such as control and protection devices. The hardware architecture is built in parallel units, called racks that consist of several digital and analogue inputs and output channels (I/O).Each rack accommodates various slot mounted cards [123].

A communication backplane links all slot mounted cards within a rack to enable the exchange of information. Moreover, direct card to card communication is also possible through fiber optic links. The communication between racks is accomplished via special inter-rack communication links (Fig. 3-6). Various I/O cards are typically mounted on rails within the simulator cubicle and connected directly to individual processor cards via optical fibers [123].

The RTDS computation program consists of two basic software elements [123]; the RSCAD Software Suite and a vast number of Model Libraries.

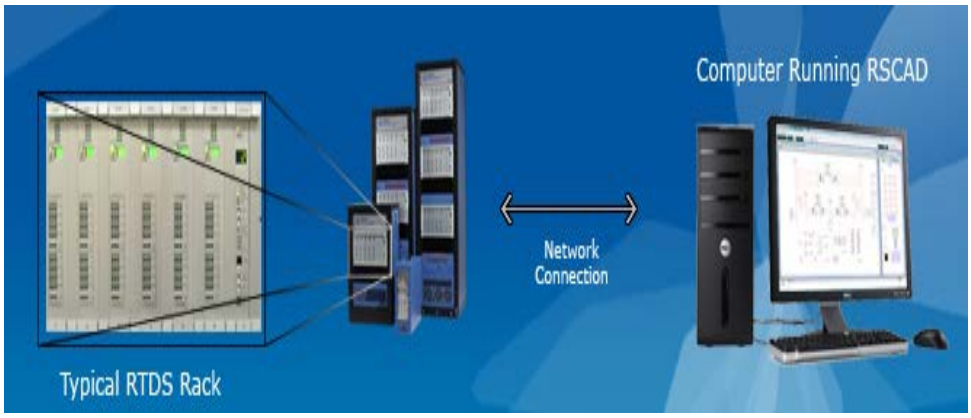

Fig. 3-6: RTDS/RSCAD Hardware [123].

The RSCAD software interface is user-friendly and allows for simulations performance, control and modification of system parameters during a simulation and result analysis. FileManager, Draft, Tline, Cable, RunTime, MultiPlot and ComponentBuilder are its own modules. Furthermore, RSCAD has embedded its own model libraries that include power system, control system, protection and automation component models. Once the system with its own parameters is built in the RSCAD software interface, the compiler automatically produces a low-level code to initiate the simulation. Consequently, it is the software itself that determines which processor card will be in function throughout a simulation [123].

Since the HuT is tested in real time, the simulated system in RSCAD with which it will exchange power signals must also be computed in real time. Hence, the time step of the RTDS needs to be small enough to check over the dynamic behavior of the simulated system.

3.3.3. PHIL Interface Concerns

Power Hardware–in-the-Loop technique employs as hardware part a device that generates or absorbs power, such as a PV inverter or an induction motor. Here, the presence of a power interface is necessary since it exchanges low voltage signals with the simulated system and real power with the HuT, thus the digital to analogue and vice versa converters cannot participate sufficiently in this trade-off (Fig. 3-7). The power interface being used during this thesis for the experimental procedure and its results will be given in Chapter 5 consisted of a single phase (5KVA) AC/DC/AC converter and enables the low power output signal (i.e. I_{HuT_low} and reference voltage labeled as V_{N*}) of the RTDS to be amplified to a higher voltage signal (i.e. V_N). This voltage is applied to the HuT device (in our case an actual load) and provokes a current flow through it. The current waveform is measured by the power interface's sensor and is fed back to the RTDS to close the loop (Fig. 3-8).

PHIL technique is a novel approach and offers great flexibility in arranging and performing various test scenarios for DER devices since the virtually simulated system can be modified without hardware adaptions, in addition to the fact that the tests can be repeated quickly and accomplished very close to realistic conditions.

3.3.3.1. Power Amplifier

The basic components of a power interface is the power amplifier and a sensor. The former amplifies the low level signals received from the RTS to the HuT at higher power ratings, thus high accuracy and small-time delay are key considerations.

The power amplifier used for this contribution is an unconventional single-phase bidirectional AC/DC/AC converter consisting of 3 IGBT half-bridges [124, 125]. The converter is coupled to the utility grid on the one-side and runs as a

voltage source of variable voltage and frequency on the other-side. Additionally, the analogue signals exchanging with the utility grid and the microgrid components is done on a conversion time of about 40µsec, 16 bit resolution and ± 10V range.

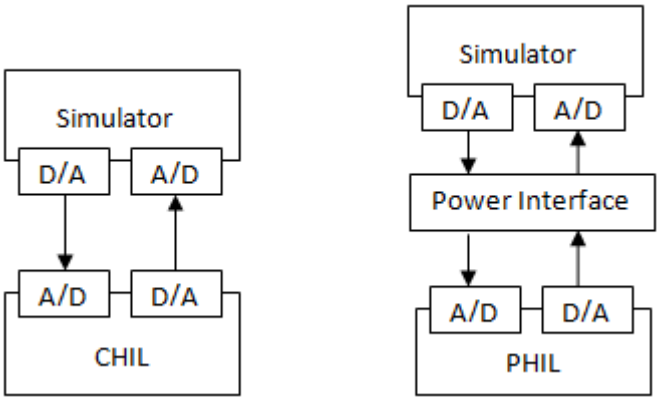

Fig. 3-7: CHIL and PHIL schemes layout [118].

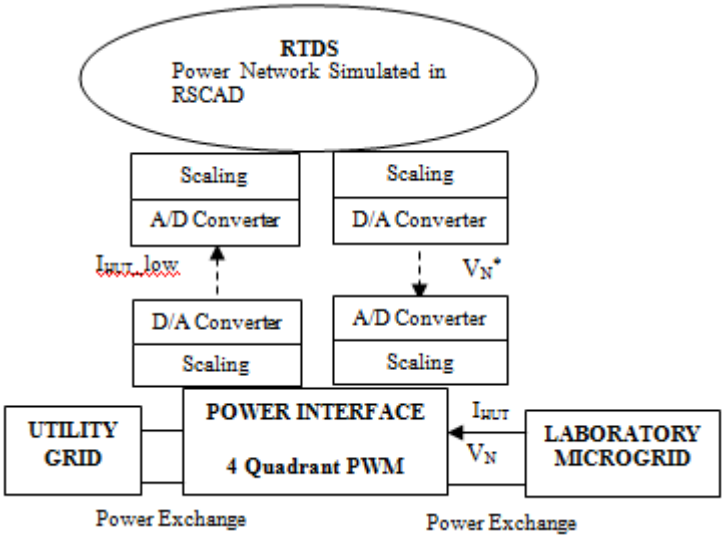

Fig. 3-8: Representation of the PHIL environment [126].

The power electronic converter platform permits the user to model the control scheme in Matlab/Simulink, with access to the available measurements and the possibility to change some control parameters online. In this case, the control algorithm of the given converter was provided by the manufacturer and it was modified in order to fulfill the two basic functions which a power interface needs to provide with during a PHIL simulation, i.e. voltage amplification and supplying current feedback signal [120].

Equation (3-26) gives the transfer function of the power amplifier's second order output filter utilized throughout the experiments (Chapter 5). This transfer function is basically drawn from the introduced time delay and the output filter of the power converter [126].

$$T_f(s) = \frac{{\omega_n}^2}{s^2 + 2\xi \cdot \omega_n \cdot s + {\omega_n}^2} = \frac{(1500\pi)^2}{s^2 + 2100s + (1500\pi)^2} \quad (3\text{-}26)$$

- ω_n, the resonance angular frequency.
- ξ, the damping ratio.

The total time delay in the current PHIL experiments was about 750μsec.

3.3.4. Stability and Accuracy Considerations

PHIL simulations involve a closed-loop interaction. Shortcomings that innately lie in this closed-loop can decrease the accuracy of the simulation and may evoke instability. Thus before performing a PHIL test, it is crucial to ensure that the experiment will be stable. Consequently, throughout this thesis virtual hardware-in-the-loop experiments (off-line simulations) were performed in Matlab/Simulink to check the system's stability for the different test scenarios presented in Chapter 5. Furthermore, stability should be accompanied by an adequate accuracy of the experiments' outcomes. Therefore, the entire closed loop system was simulated, and the results were compared with the outputs from the PHIL tests in order to assess their accuracy.

Apart from the comparison of the PHIL results with the corresponding outcomes from the off-line simulations, the validity of monitored quantities (current and voltage rms values) was also obtained through comparison of several measurements at different points in the system. For instance, the current through the hardware impedance was monitored by measurements of the Power Interface, an oscilloscope, and the software of the RTDS.

3.3.5. Protection Issues

Over-current and over-voltage protection schemes are introduced into the RTDS/RSCAD at the shared node between the simulation and hardware. Fig. 3-9 beneath illustrates the protections implemented for the execution of the PHIL experiments conducted for this thesis. In case the pre-determined limits are exceeded, I_{HuT} becomes zero and the voltage reference sent to the amplifier is held constant to a specific value. Subsequently, the output of the RTDS will be maintained constant and the PHIL test will be terminated. Flip-flops are employed to ensure the safe operation of the system if an instability incident takes place.

3.3.6. PHIL Simulation Studies in Record

PHIL technique is merely a new concept in the domain for DER integration. PVs, wind turbines or even whole Microgrids can be connected to simulated distribution networks that entail various DER devices. Several researches are implemented in this direction using the Real Time Digital Simulation as a comprehensive tool to perform flexible and high speed real time simulations [119-121, 126-131] and some of them are presented below.

In [126] was shown the applicability of PHIL simulations in the domain of VAR compensating devices such as Static Synchronous Compensators. Specifically, within this study an Average Model of a STATCOM is modelled in RTDS/RSCAD. The IGBT Voltage-Source Converter is represented by equivalent controlled voltage sources generating the set of three phase AC voltages, whereas PWM switching frequencies are neglected. In addition, the integration and control concept of a capacitor model is represented which consists of an equivalent series resistance ESR=0.1 Ohms and an equivalent series DC capacitor with large value of C=0.5 F. The objective of the STATCOM controller is to regulate the voltage of common coupling of this inverter interfaced source. In continuation, PHIL tests were executed utilizing an impedance as Hardware under Test (HuT).

The objective of [127] is to execute real time simulations in RSCAD/RTDS of a LV islanded power system's energy management, to study its control strategy i.e. droop control and conduct PHIL laboratory tests as a data reference for verification. The hardware part utilized throughout these experiments was a variable resistive load of 105.8 Ohm. Moreover, for tests aiming at analyzing the energy transfer in an AC Microgrid, a set of experiments were conducted related to the diesel generator and the battery inverters that were available in a real Microgrid infrastructure.

In [120] a thorough description of the design and development of a PHIL set-up for DER devices is validated through laboratory experiments. Specifically, a PHIL implementation of a voltage divider was performed and the closed-loop synergy between a simulated LV network and hardware such as PVs and inverter was demonstrated.

In [131] a grid connected wind farm with a 2-level inverter based STATCOM model was simulated in the RTDS to analyze the dynamic and transient characteristics in realistic conditions. Throughout the proposed study it was shown that the terminal voltage of the wind farm remained at the desired value under different wind conditions and network faults. The above work was performed in the real time RTDS/RSCAD environment; nevertheless PHIL experiments were not conducted.

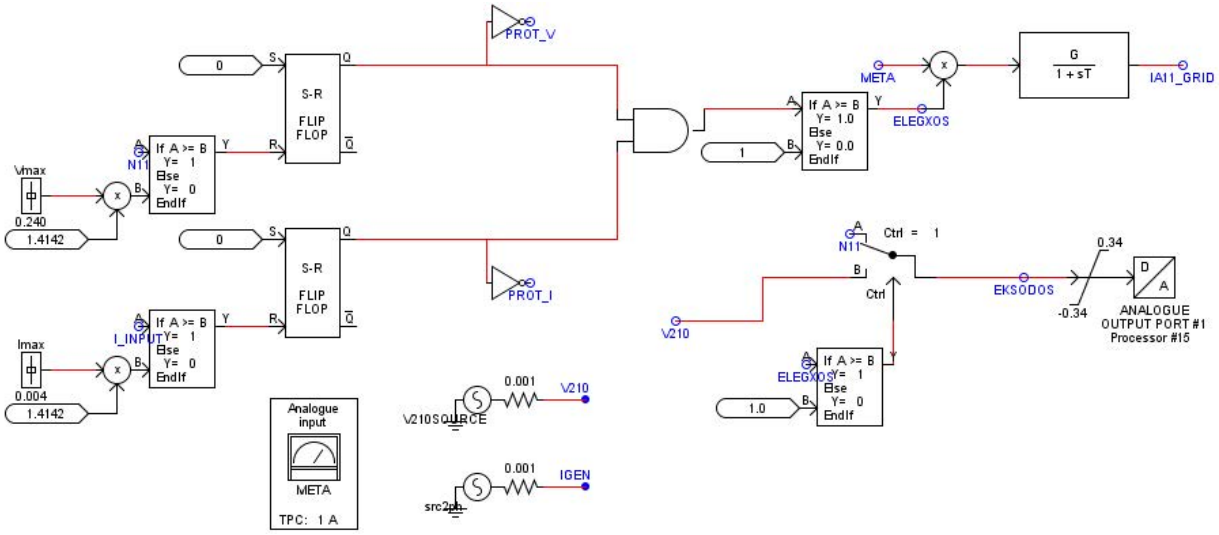

Fig. 3-9: Protection design implemented in RTDS/RSCAD [126].

3.4. Summary

A new electric power production industry is emerging that it wiil rely on a wide array of new technologies. Distributed generation is expected to support this scheme, although the increasing penetration is not done without a new set of problems. The impacts on power stability, namely voltage drop/rise and frequency disturbances due to the high rates of DG integration into distribution grids increases the demand for network support by means of provision and control of reactive and active power exchanges respectively.

Therefore, each generating unit penetrated into MV/LV networks, according to the EU grid codes needs to be tested and to be attributed a so-called ´´type-specific unit certificate´´ that refers to its electrical characteristics like the connecting voltage, the power capacity, type of generator etc. Generally, they do exist two options for performing system experiments; a) testing real devices or b) running a simulation.

This chapter reviews the research methodology followed throughout this thesis and is asscociated to the tolerance restrictions described above. In more details, this work tries to combine laboratory or field tests in line with system

level simulations of DG devices to demonstrate their conformity with the technical issues related to grid penetration into MV/LV networks. Thus, the research lines of this study are directed to; a) grid simulation analyses and b) real time simulations and PHIL experiments for distributed generation integration in MV/LV power networks. The basic features of the utilised programs, namely PSS/E and RTDS/RSCAD software tools are outlined as well as the key points of the research methodology, i.e. systematic steps for DER integration, interface concerns, stability and accuracy issues etc. Moreover, a literature survey on PHIL and grid penetration studies is also provided.

.

PART II. Employment of Power Flow and Hardware-in-the-Loop Tools for Simulation and Test Verification

Part two of this research work gives a detailed analysis, i.e. simulations, experimental tests and results of DG penetration in MV/LV networks. This part is divided into two Chapters, which are Chapter 4 and 5.

Chapter 4 discusses the allocation and sizing of DG within a real Island power system and it is evaluated under several potential scenarios. Steady-state and Dynamic simulation results are performed in Siemens PTI, PSS/E software tool.

In continuation, Chapter 5 presents the Real-Time and Power-Hardware-in-the-Loop simulations of a set of tests for DER integration in LV islanded power systems. Moreover, onsite experiments in a real Microgrid installation were performed to verify a part of the simulation results executed in the Lab environment.

Chapter 4. A Detailed Case Study of DG Embedded in an Island Power System with PSS/E tool

4.1. Introduction

This Chapter performs a detailed case study for distributed generation integration implemented on a real Island power grid. The grid model of the system is derived and static and dynamic simulations were accomplished in order to define the steady-state limit, the potential areas within this autonomous network suitable for DG penetration and the impact these extra generating units may induce onto the system´s stability.

Hence, the specific objectives of this research are as follows:

1) Built the entire grid model in PSS/E;
2) Selection of areas from electrical and resource point of view;
3) Static analysis for identifying the following;
   a) the capacity for the disposal of the network nodes
   b) stability of nodes
   c) voltage levels
4) Accelerate the integration of renewable energy sources;
   a) identify which nodes are the most suitable to connect new distributed network plants and which are the most overloaded ones.
5) Dynamic analysis for investigating on;
   a) system components´ transient stability, especially of DFIG and synchronous generating units
   b) voltage and frequency perturbation during fault incidents
   c) system's fault-ride through capability

The chapter starts with a description of the Island´s power system including the power plants, substations, load configuration and network branches. Moreover, the voltage quality parameters are provided as monitored by the Island´s electric utility. Three scenarios are defined in order to define the impact of DG integration, namely wind and geothermal power. In this context, the first two scenarios, Scenarios 1 & 2 employ steady-state simulations, i.e. power flow, contingency and short circuit analyses in line with their attained results, which are described in section 4.4. In continuation, the power flow and short circuit outcomes for Scenario 3 with wind power included are given. Finally, the simulations and results derived from the transient stability analysis are discussed. Emphasis is addressed on the system´s stability margin and fault-ride through capability during fault incidents such as a three-phase fault application at the connection point of the wind farm, loss of generators, and outage of distribution lines. In addition, as part of the dynamic studies, open circuit set point step tests for two exciter models namely, EXST and IEET1 were performed to identify the exciter that is not well-tuned.

4.2. Characterization of the Electrical System

4.2.1. Power Plants

The electrical system of the islanded power network in 2009 included ten production plants and ten electricity substations. Moreover, the island's transmission and distribution system consisted of a HV transmission network at 60 kV (this voltage level represents the HV distribution network in conventional systems) and a medium voltage (MV) distribution network with voltage levels of 30 and 10 kV. The study will be based on these voltage levels since data of lower voltages than the 10 kV are not provided. The system comprises of 1000 nodes, however it will be simplified due to convergence issues by accumulating the feeders in the distribution substations.

The Island's power system consists of one central fossil fuel power station (CTCL-CPP[3]), of two geothermal power plants, namely CGRG-GPP[4] & CGPV-GPP, and of seven hydraulic power stations ($CHTN_1$, $CHTN_2$, CHTB, CHFN, CHFR, CHRP and CHSC). The names of the power stations are arbitrarily chosen. There are eight generators connected to the central fossil fuel power plant and inject their outputs into the 60 kV network. The biggest geothermal plant, CGRG consists of four machines whereas the smallest one, CGPV consists of one generator and both generate their power at 60 and 30 kV network respectively.

Their general data are presented in Tables 4.1 & 4.2. The total hydro potential amounts for 3.8% of the whole power capacity, thus is not taken into account in the current work. Appendix A concentrates the data of the three power plants.

Table 4-1: Power source share in percentages, year 2009.

Power Plants	Power Installed	Energy
Thermal	73.9%	59.49%
Geothermal	22.3%	36.59%
Hydro	3.8%	3.92%
Total	132.694 (MW)	442 (GWh)

Table 4-2: Central Power Plants, year 2009.

	Primary Source	Groups of Generators			Transformers		
		Voltage level (kV)	Units	Pot. Installed (kW)	Transformation ratio (kV)	Units	Pot. Installed (MVA)
CTCL	Thermal	11	4	67,280	11/60	4	92
		6.3	4	30,784	6.3/60	4	40
CGRG	Geothermal	10	4	16,600	10/60	2	16
CGPV	Geothermal	11	1	13,000	11/30	1	17
CHTN	Hydro	6	1	1,658	6/30	1	2
CHTB	Hydro	0.4	1	94	0.4/30	1	0.16
CHFN	Hydro	3	1	608	3/30	1	0.5
CHCN	Hydro	0.4	1	400	0.4/30	1	0.5
CHFR	Hydro	0.4	1	800	0.4/30	1	1
CHRP	Hydro	0.4	1	800	0.4/30	1	1
CHSC	Hydro	0.4	1	670	0.4/30	1	1
Total	Hydro	[redacted]	20	132.694	[redacted]	18	171.16

Figure 4.1 illustrates the HV/MV layout of the Island's power system with all the transmission branches connecting the power plants to the substation nodes, whereas only some of the distribution branches are also represented.

[3] CPP: Central Power Plant

[4] GPP: Geothermal Power Plant

In addition, node 1 CTCL-CPP of 60 kV (Fig. 4-1) is chosen as the slack node, because it is the most important transmission bus of the electrical system and eight conventional generators (aggregated on the scheme below) are connected to it. The majority of the system´s transmission lines leave this bus which highlights it as the main power injection point.

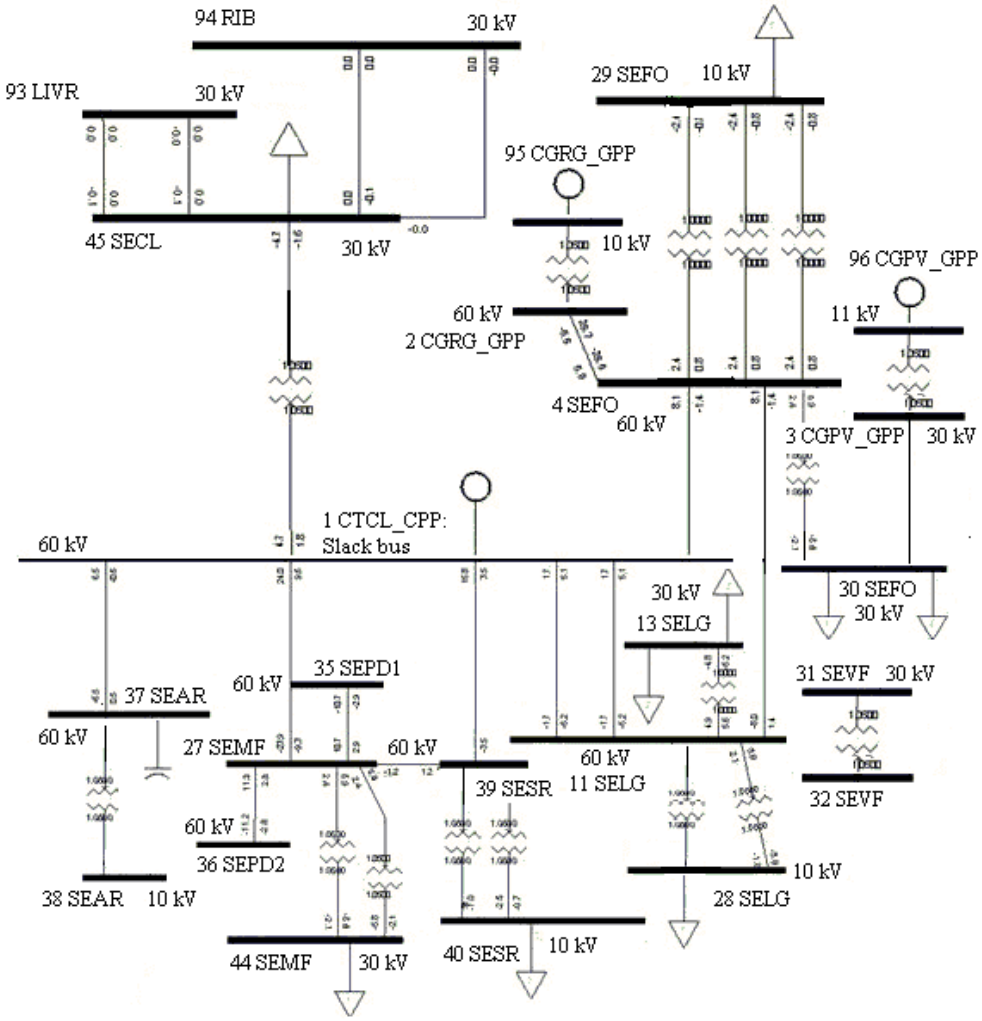

Fig. 4-1: Single-line HV/MV network representation in PSS/E [110].

4.2.2. Substations

The HV/MV transmission network includes five 60 kV substations namely as SEMF, SEAE, SEPD, SELG and SEFO (Fig. 4-1). These are stepped down from 60 to 30 kV and/or 10 kV. The MV distribution network includes 30/10 kV substations in particular, SESR, SEVF and SESC. The main network´s substation is the SEFO since it is the only connected to the three system´s power plants and to the distribution network through its three stepped down transformers of 60/10 kV and one of 60/30 kV. Moreover, it concentrates the highest load demanding within the 30 kV distribution network. The MV/LV distribution network includes four 30/10 kV substations. The PSFU (Fig. 4-2) is the power sectioning point that interconnects the 30kV bus of the SEVF substation to a couple of distribution overhead and subterranean lines and to the hydroelectric plants, and it can be considered as an important node from electrical point of view apart from the substation nodes SEVF and SEFO. The following table (Table 4-3) shows the general data of the substations.

4.2.3. Load Configuration

In the current study, only the summer period with the maximum and minimum load demands of a typical day were taken into consideration. A justification could be attributed to the generality that a summer peak demand scenario corresponds to the most thermally stressed loading on the transmission system. During- the winter season- wind speeds are rather higher, while the loading of the system is lower than in the summer time. For the steady-state analysis, where maximum MW injection is desired, a study based on a summer peak loading is the most appropriate. The tables beneath (Table 4-4 & 4-5) represent the total maximum and minimum values of the active and reactive parts of load demand at the different substation and voltage nodes respectively on a characteristic summer day in year 2009.

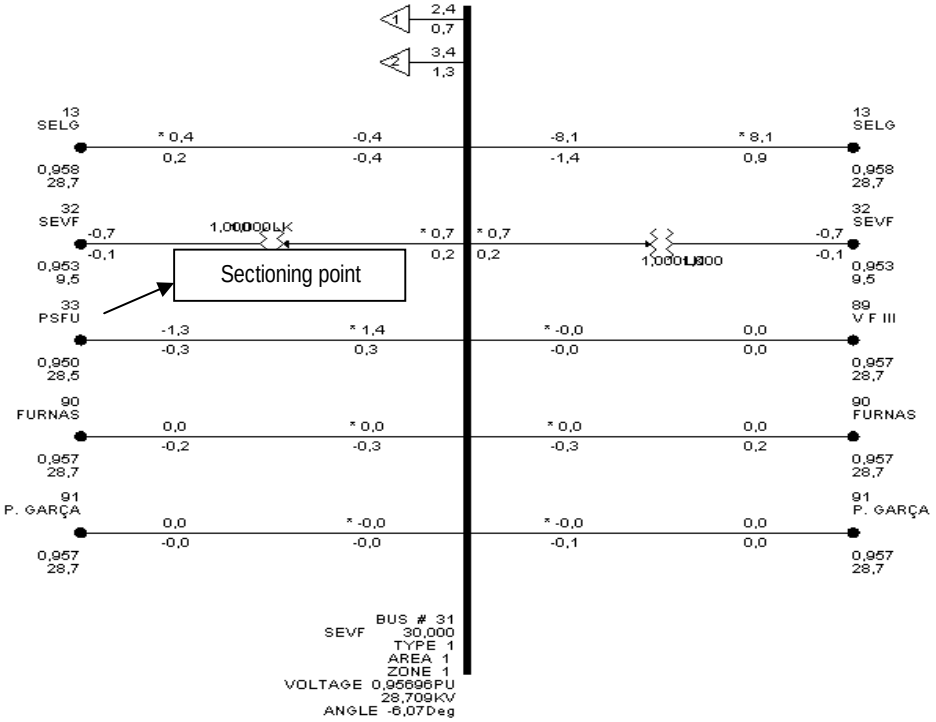

Fig. 4-2: Distribution branches adjacent to SEVF 30 kV substation.

Table 4-3: Substations, year 2009.

Substations			
	Transformation ratio (kV)	# Transformers	Pot. Installed (MVA)
SECL	60/30	1	12.5
SEMF	60/30	2	25
SELG	60/30	1	12.5
	60/10	2	16.25
SEFO	60/30	1	12.5
	60/10	3	20
SEVF	30/10	2	10
SEPD	60/10	2	40
SEAR	60/10	1	20
SESR	60/10	2	22.5
Total	[redacted]	17	191.25

Table 4-4: Summarised load configuration, year 2009.

Voltage nodes (kV)	Pmax (Pmin) MW	Qmax (Qmin) MVAr
10	43.38 (22.46)	16.88 (8.43)
30	50.87 (41.05)	15.56 (10.96)

Table 4-5: Load configuration, year 2009.

		Summer (August 19th 2009)			
		Maximum		Minimum	
	Voltage level (kV)	P(MW)	Q(MVAr)	P(MW)	Q(MVAr)
SEAR	10	6.12	2.35	3.14	1.14
SECL	30	4.36	1.73	1.66	0.52
SEFO	10	4.7	1.95	3.51	1.42
	30	11.35	4.21	11.35	2.69
PSFU	30	0.9	0.51	0.56	0.45
SELG	10	6.14	3.27	2.86	1.65
	30	4.25	1.74	2.51	1.3
SEMF	30	10.63	4.18	6.99	3.11
SEPD	10	19.9	6.97	8.84	2.68
SESR	10	5.48	1.99	3.34	1.25
SEVF	10	1.04	0.35	0.77	0.29
	30	3.13	1.25	1.73	0.96
Hydro(SEFO)	30	11.7	0.44	11.7	0.43
Hydro(PSFU)	30	0.35	0.12	0.35	0.12
Hydro(SELG)	30	2.1	0.69	2.1	0.69
Hydro(SEVF)	30	2.1	0.69	2.1	0.69

4.2.4. Network Branches

At the transmission voltage level, the reactances dominate whereas the low voltage distribution network is rather resistive. Transmission and distribution lines´ resistive, reactive and susceptance (B) characteristics are computed on the system´s power base MBASE=100 MVA.

The transmission non-transformer branches in total thirteen among which the twelve are overhead and one is a subterranean line are all of them at different lengths. The 60 kV network is designated with conductors´ type of Cu 185 & 95 mm^2. Distribution non-transformer branches (72 in number of various lengths and types) up to 10 kV comprise a rather complex low voltage network and their data, as well as the transmission branches' characteristics are provided in Appendix B.

4.3. Quality Parameters of Voltage Waveform

In order to identify the voltage quality, the following parameters were monitored and provided by the Island's electric utility [132, 133];

- RMS voltage
- Frequency
- Flicker
- Harmonic distortion
- Unbalanced three-phase system voltages
- Overvoltage

4.3.1. RMS Voltage

At the level of high voltage (HV-60 kV), Regulation of Quality of Service states that in normal operating conditions, 95% of the effective average of the supplied voltage for 10 minutes duration must be within the range Uc ± 5%, where Uc is a declared voltage (62500 V). For the period reviewed here, there was a compliance of 100% of the values registered with the Regulation of Quality of Service into the network monitored.

At the level of medium voltage (MV-30 kV and 10 kV), 95% of the effective average under 10 minutes for each monitored equipment was within the range defined in the EN 50160 [134], i.e. Uc ± 10%. By analyzing the recorded data, it is concluded that the registered values comply 100% with the ones of EN 50160 points in the monitored network.

At the low voltage level (LV), the EN 50160 sets limits for the variation of the nominal voltage, i.e. 95% of the registered values (Un ± 10%) and 100% of recorded values (Un +10% / -15%) [133].

4.3.2. Flicker

At the level of high voltage (HV) the Regulation Quality of Service states that under conditions of normal rates of flicker severity (short and long term), the 95% for each measurement period throughout a week, should be less than 1.

At the level of MV, EN 50160 states that under normal conditions, for any period of one week, the severity of long-term flicker should be less than 1 for 95% of the time. Moreover, regarding the low voltage level, EN 50160 states that under normal conditions, for any time-period during one week, the severity of long-term flicker should be less than 1, for 95% of the time [133].

4.3.3. Frequency

Regarding the variation of frequency for all, high voltage, medium voltage and low voltage, EN 50160 states that in normal operating conditions, the average frequency, measured in intervals of 10 seconds should be between the following values: 50Hz ± 2% for 95% of a week, and 50Hz ± 15% for 100% of the recorded values during one week. The analysis of the data verified the conformity of equipment to the values recorded during the selected period according to EN 50160 [133].

4.3.4. Amplitude of Voltage

In high voltage, and according to the values recorded in three selected weeks, the greater amplitude recorded was 26.7% with a duration of 0.434 seconds.

For the medium voltage, and according to the values recorded in three selected weeks by equipment, the greatest amplitude was achieved at the number of 48.7% of the declared voltage (with duration of 0.775 seconds) as recorded in the Substation of SEMF affecting the lines connected to it. The amplitude length-peak with the longest duration (55.841 seconds and amplitude of 39.8% of declared voltage) was recorded in the substation of SELG [132].

Finally at low voltage level, higher amplitude was reported with a peak of 93.9% (equivalent time of 0.638 seconds) and was recorded in the transmission line of 60 kV from SEMF to SEPD substations and similarly in the line from CTCL to SEAR (Fig. 4-1).

4.4. Steady-State Simulations

4.4.1. Introduction & Scenarios Designation

In the current study three different scenarios were employed regarding to the generation capacity, the renewable energy engagement and load demanding. The above scenarios were examined under two temporal time frames, one actual of 2009 and one future time-based on 2015. The electricity generation plan [132] includes possible renewable resource at the Island, like a plan to expand geothermal and wind farms up to the year of 2015.

As it has been already mentioned in Section 4.2.1, the hydraulic plants were not taken into consideration, thus it was added to the wind the hydro share too for Scenario 3, which is designated with a wind potential of 14 MW installed by 2015. Scenario 2 will solely investigate the impacts of geothermal plants´ enlargement onto the static behaviour of the system by employing power flow, contingency and short circuit simulations. Scenario 3, beyond the steady-state calculations will also employ dynamic simulations to examine the system´s stability after the integration of wind power into the network. Both Scenarios 2 & 3 experience the same geothermal capacity. Concluding, we could summarize the different schemes to the ones beneath:

- Scenario 1, year 2009 base case
- Scenario 2, year 2015 with additional geothermal power
- Scenario 3, year 2015 with wind energy and geothermal power.

All the scenario cases studied throughout this work are investigated under two loading schemes, the high and the low demand. In Scenario 3, it will be only presented the outcomes of the high demand loading as it is the worst case scenario with focus on power flow and short circuit results. Furthermore, the power flow and contingency analysis results for low demand for Scenarios 1 & 2 are presented in Appendices C-F.

The upper objective is to accomplish power flow, contingency and short circuit analysis for all the defined scenarios in order to determine on the system's disposability in terms of capacity and stability for DG penetration. The results of the simulations will verify the correctness of the initial decision making on the quantity and allocation of the embedded distributed generation.

The examined Island power system is not connected to any major grid or even to other islands. All the following assumptions upon electricity demands were estimated in accordance to various forthcoming case studies related to the actual base case scenario (2009) of electricity consumption on the power system.

In the temporal scheme of 2009, the electrical system´s equilibrium was examined with the participation of the geothermal plants that constitute and the only renewable energy source in the system at the present. The total power installed amounts for 132.69 MW, where the 98.064 (74%) MW belongs to the thermal power capacity and only the 34.63 (26%) MW to the renewable energy sources (geothermal and hydro power). The pie chart below shows these figures in percentages (Fig. 4-3). In addition, in 2009 the electricity production totaled at the number of 442 GWh, where 179.26 GWh was the renewable energy sources participation and 262.94 GWh the conventional systems´ one. The bar graph (Fig. 4-4) represents these values. Table 4-6 also demonstrates the exact share of each one power source to the total energy mix.

In 2015, the energy consumption will reach the figure of 590 GWh with renewable resources holding the 70%. Specifically, the geothermal power output is estimated to be the 89% of the renewable resources share in the energy mix pie.

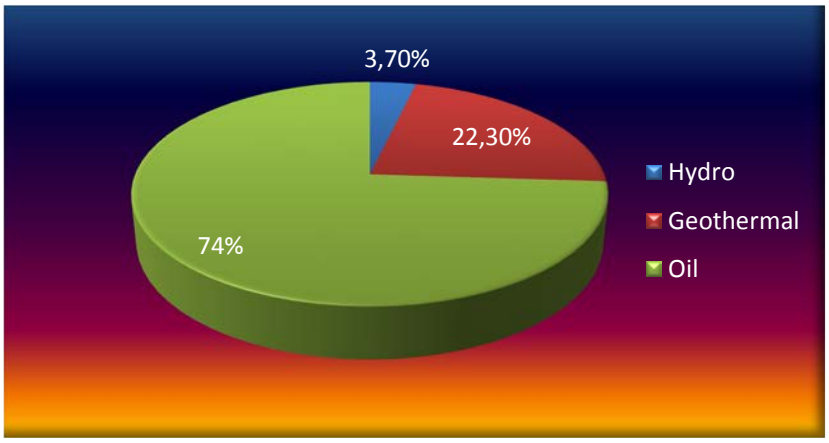

Fig. 4-3: Comparison of the contribution from renewable sources, 2009.

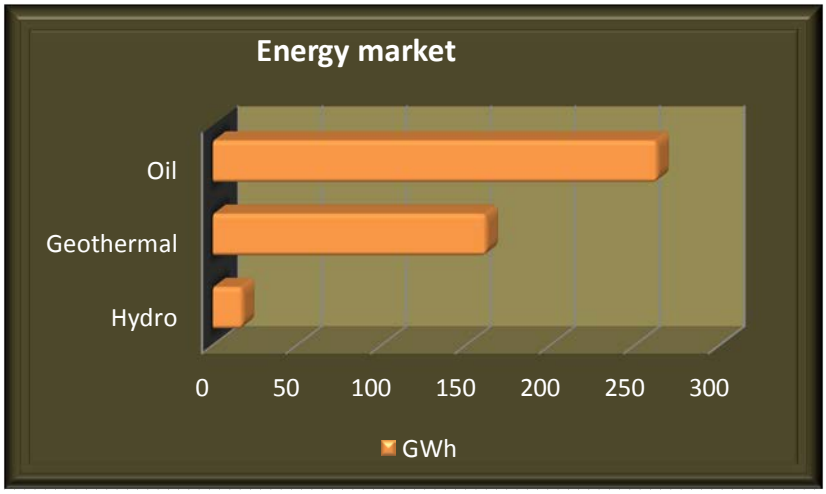

Fig. 4-4: Comparison of the contribution from renewable sources to the regional electricity production in 2009.

Table 4-6: Power source share in the energy mix, 2009.

	Power Installed (MW)	Energy Production (GWh)
Thermal Plants	98.064	262.939
Geothermal	29.6	161.722
Hydro	5.03	17.538
Total	132.69	442

4.4.2. Scenarios 1 & 2- Geothermal Power (High Demand)

4.4.2.1. Power Flow Analysis Results

The geothermal generators aggregated operate for the 70% of their installed capacity for both the high and load demand and with a power factor of ±0.8 (inductive/capacitive) [110, 111]. Geothermal machines are four in number

for the CGRG and one for the CGPV power plants, which are connected to the buses CGRG of base voltage at 10 kV and to CGPV of base voltage at 11 kV respectively (Fig. 4-1 & 4-5). Table 4-7 shows the average output that represents the 70% capacity output of their rated power for each one of the geothermal power plants. The soar in power production will affect the conventional generators (in this study the slack ones), whereas an increase by 9.2% is denoted at the active and by 8% at the reactive load demand rates to also accommodate this increase.

In more details, the rated geothermal power installed in 2009 was 29.6 MW and will increase by 36.8 MW in 2015. This soar in power production will affect the conventional generators of the CTCL-CPP (in our case the slack ones). The 70% of 36.8 MW equals to an increase of 25.76 MW. The modeling configuration in PSS/E is not the same as followed before. Six more generators have been added to the Geothermal Plant of CGRG where two of them are rated at 5.4 MW and the remaining four at 2.9 MW.

Moreover, in the Geothermal Plant of CGPV is introduced one more generator with nominal power of 13 MW. The system is supported by three more transformers, two stepping-up the voltage from 10 to 60 kV at the terminal of the CGRG generators and one from the terminal node of CGPV rated at 11 kV stepping up to 60 kV. Generally, transformers produce magnetic fields and therefore absorb reactive power. The heavier the current loading the higher will be the absorption, especially when we are talking about transformers of high potential. Nevertheless, this absorption is also dependent on the transformers' characteristics. Tables 4-8 & 4-9 illustrate the case summary results resulted from the power flow computations.

According to Scenario 1 (Table 4-8), the total generation produced is at 95.5 MW where the 74.8 MW comes from the slack generators and 20.7 MW from the renewable energy sources, whereas its reactive power delivery amounts for 30.8 MVAr. Charging is at 5.6 MVAr and shunts amount for 0.4 MW and (-3.2 MVAr). High load demand arises to 94.3 MW and 32.4 MVAr, thus the losses are 0.8 MW and 7.2 MVar for the real and reactive power respectively.

On the other hand for Scenario 2 (Table 4-9), load demand has increased from 94.3 MW by 9.2% to 103.7 MW. This rise of 9.4 MW is allocated selectively among the distribution substations and according to their load demand rates (Table 4-5). For instance, the nodes of 11.7 and 11.35 MW load demand will suffer from an increase of 1.17 MW. Nodes that power demand reaches the value of 19.9 MW will have a rise of 1.99 MW and buses of 10.63 MW will reach up to 11.695 MW (1.065 MW increase). All the remaining substation nodes will increase their power demand by 0.31 MW. Reactive load demand also increases by 8%, from 32.4 MVAr nearly to 35 MVAr. This increase of 2.6 MVAr is distributed among the nodes´ according to their reactive requirement with the ones of 6.97 MVAr and 4.21 MVAr suffering from an increase of 0.7 and 0.42 MVAr respectively. The remaining buses will each one increase their demand by 0.131 MVAr.

The case summary results for this scenario (Scenario 2) indicate that the total generation produced is at 104.7 MW where the 59.2 MW comes from the slack generators and 45.5 MW from the renewable energy sources, whereas its reactive power delivery amounts for 36.5 MVAr. Charging is at 5.6 MVAr and shunts amount for 0.7 MW and (-1.9 MVAr). High load demand arises to 102.9 MW and 35 MVAr, thus the losses are 1.1 MW and 8.9 MVar for the real and reactive power respectively.

The numerical difference among the two scenario cases in both reactive and active power losses was prospective as losses have to do with the total system handling capacity and load demand. Branch losses are considered as I^2R and I^2X and exclude the line charging, line connected shunt, and magnetizing admittance components. Moreover, the increase in power losses aligns with the raised load profile.

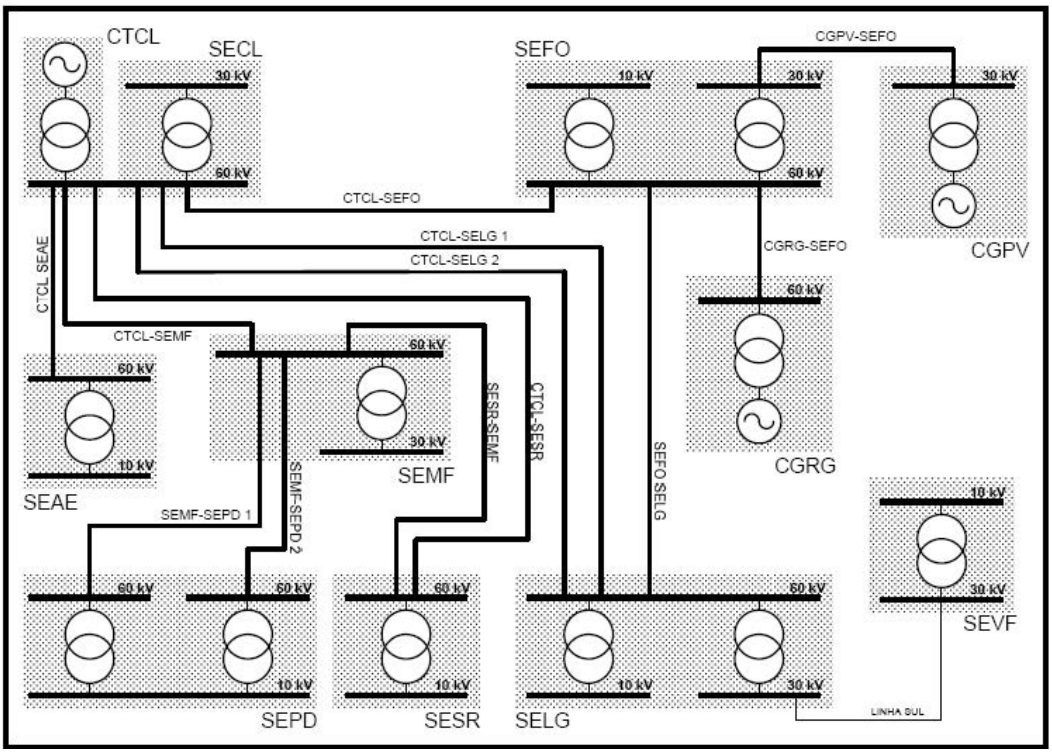

Fig. 4-5: Representation of the island´s transmission network [110].

Table 4-7: Geothermal power output in 2009 & 2015.

	CGRG_GPP	CGPV_GPP
2009	11.62	9.1
2015	26.04	20.45

Table 4-8: Case summary power flow outcomes, Scenario1

Total	Generation	PQLoad	Shunts	Charging	Losses	Swing
MW	95.5	94.3	0.4	0	0.8	74.8
MVAr	30.8	32.4	-3.2	5.6	7.2	22.3

Table 4-9: Case summary power flow outcomes, Scenario 2

Total	Generation	PQLoad	Shunts	Charging	Losses	Swing
MW	104.7	102.9	0.7	0	1.1	59.2
MVAr	36.5	35	-1.9	5.6	8.9	22.3

Following the load flow requirements explained in Section 3.2.4, the voltage profile at the Island´s system nodes needs to reside within the acceptable limits as ±5% of the nominal voltage value, i.e. 0.95-1.05 pu. Moreover, it is loosely accepted that the same voltage limits are applied for the transmission and distribution network. Figures 4-6 & 4-7 illustrate the voltage profile at all the system´s substation nodes.

In the current study there are no voltage violations, except for very slight variations below the value of 0.95 pu at bus 33, at the sectioning point PSFU (Fig. 4-2) and the adjustment to its nodes. SEFO (Fig. 4-1 & 4-5) is the main transformer substation. Moreover, the active and reactive load demand at the bus SEFO of 30 kV belongs to among the highest values (Table 4-5).

According to Scenario 1, the actual voltage of its secondary transformer's winding (nominal 30 kV) appears to have a voltage value of 0.958 pu while the transformer branch SEFO 60/30 experience active and reactive losses of 0.10 MW and 1.46 MVAR respectively. These losses are the highest among all the transformer and non transformer branches. The observed losses and the relevant low voltage at the secondary winding side may be attributed to the transformer's characteristics. Besides, the 30 kV network is rather resistive with high values of the R/X ratio thus the ability to decrease the losses is low. The recalling of the approximate formula (2-5) which is rewritten as in (4-1) may justify the voltage drop within the SEFO transformer branch and proves that the factor QX has greater influence as the transformer leakage reactance is 0.08 pu >>0.0052 pu of the resistance. Moreover and as it was mentioned before, transformers produce magnetic fields and therefore absorb reactive power. The heavier the current loading the higher will be the absorption.

$$\Delta V = \frac{PR + QX}{V} \tag{4-1}$$

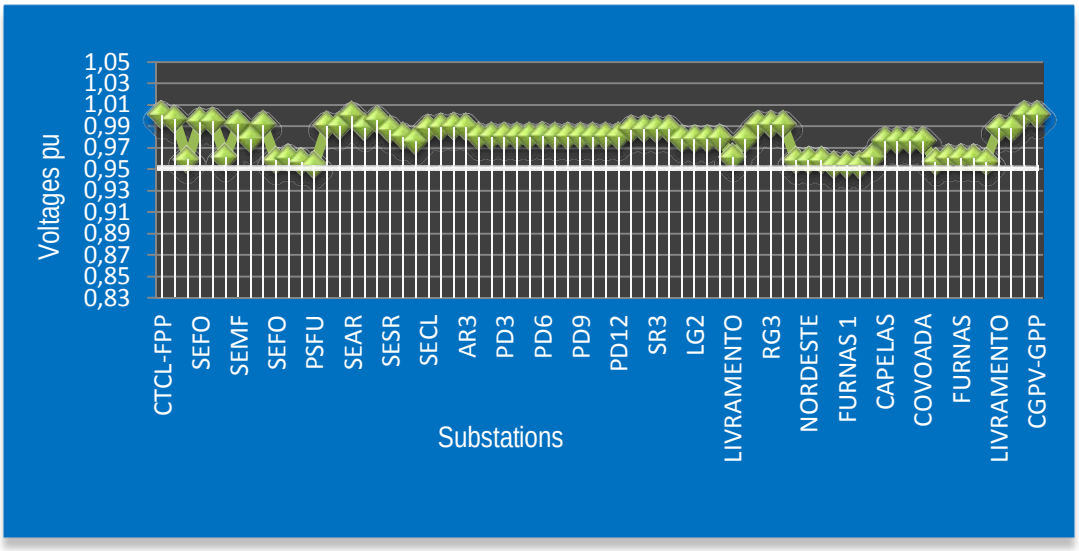

Fig. 4-6: Voltage profile of the transmission and distribution network, Scenario 1.

According to Scenario 2, the 60 kV node of the SEFO network substation appears to have a higher actual voltage value of 0.973 pu while the transformer branch SEFO 60/30 experience active and reactive losses of 0.03 MW and 0.49 MVAR respectively. This figure is much smaller compared to the one in the previous case study of Scenario 1. In general, reinforcement in distributed generation that feed central nodes, like the one of SEFO 30 kV substation, increases the voltages around this area and minimizes the active and reactive losses. However, a simultaneous soar in load demand affects the nodal voltages, especially these that are more isolated and makes them more ´´unstable´´ to changes. The lines that end to these nodes seem to be a sink of reactive power. Additionally, there is a violation of 128.4% against its power rating in the transmission branch rated at 30 kV that interconnects the geothermal plant of CGPV and the substation of SEFO (Fig. 4-1). This was resulted from the increase in the geothermal output and the

subsequent overloading in the step–up transformer of CGPV 30/11 kV. The line can be relieved as the real power output of the synchronous generator connected to this plant can be controlled (Fig. 4-7).

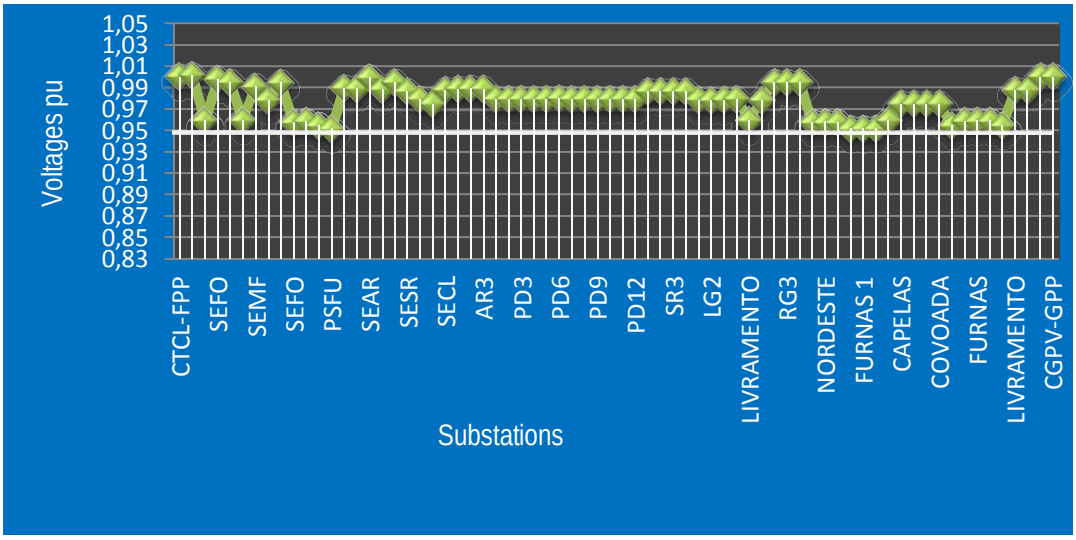

Fig. 4-7: Voltage profile of the transmission and distribution network, Scenario 2.

Load flow computations also involve the calculation of active and reactive power flows for each in-service AC branch, i.e. non-transformer branches and two-winding transformers are calculated. The percent current loading, which depends on the rating set established as the default rating in the run time options is then represented. 80% is set as the maximum default value for the branches' loadings to be checked against their power ratings in the run time options and the default rating is chosen to be the system´s MVA base, 100 MVA.

For Scenario 1 there are no violations in branches, whereas for Scenario 2 there is a slight violation of 128.4% (Fig. 4-8) against its power rating in the branch that interconnects the geothermal plant of 3 CGPV and the substation of 30 SEFO. This was resulted from the increase in the geothermal output and the subsequent overloading in the step–up transformer of CGPV 30/11 kV. Bus numbered as 3 CGPV-GPP of 30 kV inflows 18.2 MW from the generator bus 96 CGPV-GPP of 11 kV (Fig. 4-1). The thermal capacity constraint of this line interconnecting the nodes of 3 CGPV-GPP to 30 SEFO rated at 30 kV is of 14.8 MVA, whereas the line loading reached the value of 19 MVA. The line can be relieved as a generator´s real power output can be controlled.

```
BRANCH LOADINGS ABOVE  80.0 % OF RATING SET A (MVA FOR TRANSFORMERS,
CURRENT FOR NON-TRANSFORMER BRANCHES):

X--------- FROM BUS ----------X X---------- TO BUS ----------X
  BUS# X-- NAME --X BASKV  AREA    BUS# X-- NAME --X BASKV  AREA CKT
LOADING  RATING PERCENT
     3 CGPV-GPP    30.000     1     30 SEFO        30.000*    1  2
19.0    14.8   128.4
```

Fig. 4-8: Branch loadings, Scenario 2.

4.4.2.2. Contingency Analysis (N-1) Results

According to the prerequisites for safe operation reported in Section 3.2.4, the voltage profile of the transmission and distribution network and the transformer and non-transformer branches´ current loadings should follow the criteria beneath:

- ±5% of the nominal voltage value (0.95-1.05 pu) and ±10% of the nominal voltage for N-1 criterion
- 80% is set as the maximum default value for the branches' loadings to be checked against their power ratings in the run time options.

The PSS/E contingency analysis results are given in a table format, which summarises for each monitored element, the selected rating, loading and percent loading in the base case network solution, and the loading in addition to the percentage loading for each of the contingency cases taken into account.

Any percentage loading above the specified percentage threshold is followed by an asterisk (*). An asterisk (*) is printed between the bus number and name of the bus at the end of the branch with the larger current loading.

The system is studied under the loss of each one of its transmission lines of 60 kV and of its distribution branches rated at 30 kV. Loadings over 80% and violations in voltages against the range of ±5% of the nominal voltage value (0.95-1.05 pu) are defined for each scenario. The red parallelogram denotes the contingency voltages whereas the blue one the line violations.

For Scenario 1, tripping the transmission lines of 60 kV one by one, the contingencies with the worst consequences on the system is to open the two transmission lines from bus 1 CTCL-CPP to bus 11 SELG (Fig. 4-5) both rated 60kV as reported in the contingencies legend (Fig. 4-9). As it can be observed in Fig. 4-9 beneath, the effect of this tripping is that all voltage profile drops under the minimum acceptable value of 0.95 pu. It is worthy to mention that the bus 13 SELG rated at 30 kV is connected to the substation of SEVF rated also at 30 kV (Fig. 4-1). The 33, 79, 80, and 81 (Fig. 4-9) are the connecting end nodes of the lines initiating from this bus (SEVF). Thus, the voltages drop at the very end of these lines and not directly at the bus that mediates. Probably, this results from the deficiency of reactive power supply in these remote buses. In addition, violations in lines are presented on two transmission branches with the worst being on the line CTCL-CPP to SESR (Fig. 4-9) of 60 kV rated at 105.3%. Below are represented the contingency results:

```
<---------------- MULTI-SECTION LINE ----------------> <----------------- MONITORED BRANCH -----------------> CONTINGENCY
   RATING     FLOW      %
     37.4     38.8    105.3                          1 CTCL-FPP     60.000     39*SESR        60.000 1  SINGLE 4
     37.4     32.3     89.2                         27*SEMF         60.000     39 SESR        60.000 1  SINGLE 4

MONITORED VOLTAGE REPORT:
SYSTEM                    CONTINGENCY  <-------- B U S --------->   V-CONT   V-INIT   V-MAX    V-MIN
'ALL          '           RANGE SINGLE 2         33 PSFU          30.000  0.94891  0.95379  1.05000  0.95000
'ALL          '           RANGE SINGLE 2         79 POVOAÇÃO      30.000  0.94892  0.95379  1.05000  0.95000
'ALL          '           RANGE SINGLE 2         80 FURNAS 1      30.000  0.94892  0.95379  1.05000  0.95000
'ALL          '           RANGE SINGLE 2         81 FURNAS 2      30.000  0.94892  0.95379  1.05000  0.95000
'ALL          '           RANGE SINGLE 3         33 PSFU          30.000  0.94894  0.95379  1.05000  0.95000
'ALL          '           RANGE SINGLE 3         79 POVOAÇÃO      30.000  0.94895  0.95379  1.05000  0.95000
'ALL          '           RANGE SINGLE 3         80 FURNAS 1      30.000  0.94895  0.95379  1.05000  0.95000
'ALL          '           RANGE SINGLE 3         81 FURNAS 2      30.000  0.94895  0.95379  1.05000  0.95000

CONTINGENCY LEGEND:
LABEL          EVENTS
SINGLE 1     : OPEN LINE FROM BUS 1 [CTCL-FPP     60.000] TO BUS 4 [SEFO        60.000] CKT 1
SINGLE 2     : OPEN LINE FROM BUS 1 [CTCL-FPP     60.000] TO BUS 11 [SELG        60.000] CKT 1
SINGLE 3     : OPEN LINE FROM BUS 1 [CTCL-FPP     60.000] TO BUS 11 [SELG        60.000] CKT 2
SINGLE 4     : OPEN LINE FROM BUS 1 [CTCL-FPP     60.000] TO BUS 27 [SEMF        60.000] CKT 1
SINGLE 5     : OPEN LINE FROM BUS 1 [CTCL-FPP     60.000] TO BUS 37 [SEAR        60.000] CKT 1
SINGLE 6     : OPEN LINE FROM BUS 1 [CTCL-FPP     60.000] TO BUS 39 [SESR        60.000] CKT 1
SINGLE 7     : OPEN LINE FROM BUS 2 [CGRG-GPP     60.000] TO BUS 4 [SEFO        60.000] CKT 1
SINGLE 8     : OPEN LINE FROM BUS 4 [SEFO         60.000] TO BUS 11 [SELG        60.000] CKT 1
SINGLE 9     : OPEN LINE FROM BUS 27 [SEMF         60.000] TO BUS 35 [SEPD1       60.000] CKT 1
SINGLE 10    : OPEN LINE FROM BUS 27 [SEMF         60.000] TO BUS 36 [SEPD2       60.000] CKT 1
SINGLE 11    : OPEN LINE FROM BUS 27 [SEMF         60.000] TO BUS 39 [SESR        60.000] CKT 1
```

Fig. 4-9: Contingency analysis outcomes for the 60 kV lines, Scenario 1.

Tripping the transmission and distribution lines of 30 kV one by one, are observed the two transmission branches between 3 CGPV-GPP and 30 SEFO (Fig. 4-1) rated at this voltage value being overloaded. In more details, the contingencies with the worst consequences on the system is to open the two line from bus 3 CGPV-GPP to bus 30 SEFO, that interconnects the geothermal power plant to this big substation. The effects of this tripping are violations on current ratings by 83.6 % and 94.1 % respectively. Voltage drops are also denoted considering the outage of two

distribution lines as reported in the contingency legend (Fig. 4-10). Generally, the voltage drops are more significant in case of tripping a 60 kV instead of a 30 kV distribution line. This can be justified as follows; the 60 kV lines of our system interconnects the main central power plant to its substation nodes, thus a loss of such a branch creates a sink of active and reactive power supply. Moreover, when a 60 kV line is lost, the power now flows further towards the nodes to satisfy the demand, and the losses are higher. However, with the tripping of 30 kV distribution lines, voltage sags appear on more buses, as the distribution lines link many nodes together. Especially, when the line that interconnects the substation node SELG to the SEVF bus both rated at 30 kV opens, it affects all the voltage values of the buses adjacent to the substation of SEVF. This is denoted in the contingency legend beneath as Single 3 & 4. The results are as follows;

final results

<---------- MULTI-SECTION LINE ---------->					<---------- MONITORED BRANCH		
----------> CONTINGENCY		RATING	FLOW	%			
					3 CGPV-GPP	30.000	30*SEFO
30.000 2	SINGLE 1	14.8	11.8	83.6			
					3 CGPV-GPP	30.000	30*SEFO
30.000 1	SINGLE 2	12.5	11.2	94.1			

MONITORED VOLTAGE REPORT:

SYSTEM	CONTINGENCY	<-------- B U S -------->		V-CONT	V-INIT	V-MAX	V-MIN
'ALL '	RANGE SINGLE 4	31	SEVF	30.000	0.94796	0.96030	1.05000	0.95000
'ALL '	RANGE SINGLE 4	32	SEVF	10.000	0.94445	0.95680	1.05000	0.95000
'ALL '	RANGE SINGLE 4	33	PSFU	30.000	0.94140	0.95379	1.05000	0.95000
'ALL '	RANGE SINGLE 4	79	POVOAHГO	30.000	0.94141	0.95379	1.05000	0.95000
'ALL '	RANGE SINGLE 4	80	FURNAS 1	30.000	0.94141	0.95379	1.05000	0.95000
'ALL '	RANGE SINGLE 4	81	FURNAS 2	30.000	0.94141	0.95379	1.05000	0.95000
'ALL '	RANGE SINGLE 4	88	V F II	10.000	0.94445	0.95680	1.05000	0.95000
'ALL '	RANGE SINGLE 4	89	V F III	30.000	0.94796	0.96030	1.05000	0.95000
'ALL '	RANGE SINGLE 4	90	FURNAS	30.000	0.94812	0.96052	1.05000	0.95000
'ALL '	RANGE SINGLE 4	91	P. GARHA	30.000	0.94797	0.96031	1.05000	0.95000
'ALL '	RANGE SINGLE 4	92	VF I	10.000	0.94445	0.95680	1.05000	0.95000
'ALL '	RANGE SINGLE 17	33	PSFU	30.000	0.94988	0.95379	1.05000	0.95000
'ALL '	RANGE SINGLE 17	79	POVOAHГO	30.000	0.94989	0.95379	1.05000	0.95000
'ALL '	RANGE SINGLE 17	80	FURNAS 1	30.000	0.94988	0.95379	1.05000	0.95000
'ALL '	RANGE SINGLE 17	81	FURNAS 2	30.000	0.94988	0.95379	1.05000	0.95000

CONTINGENCY LEGEND:

LABEL	EVENTS
SINGLE 1	: OPEN LINE FROM BUS 3 [CGPV-GPP 30.000] TO BUS 30 [SEFO 30.000] CKT 1
SINGLE 2	: OPEN LINE FROM BUS 3 [CGPV-GPP 30.000] TO BUS 30 [SEFO 30.000] CKT 2
SINGLE 3	: OPEN LINE FROM BUS 13 [SELG 30.000] TO BUS 31 [SEVF 30.000] CKT 1
SINGLE 4	: OPEN LINE FROM BUS 13 [SELG 30.000] TO BUS 31 [SEVF 30.000] CKT 2
SINGLE 5	: OPEN LINE FROM BUS 13 [SELG 30.000] TO BUS 70 [LIVRAMENTO 30.000] CKT 1
SINGLE 6	: OPEN LINE FROM BUS 13 [SELG 30.000] TO BUS 70 [LIVRAMENTO 30.000] CKT 2
SINGLE 7	: OPEN LINE FROM BUS 13 [SELG 30.000] TO BUS 82 [RIBEIRA CHГ 30.000] CKT 1
SINGLE 8	: OPEN LINE FROM BUS 13 [SELG 30.000] TO BUS 82 [RIBEIRA CHГ 30.000] CKT 2
SINGLE 9	: OPEN LINE FROM BUS 30 [SEFO 30.000] TO BUS 75 [CALHETAS 30.000] CKT 1
SINGLE 10	: OPEN LINE FROM BUS 30 [SEFO 30.000] TO BUS 75 [CALHETAS 30.000] CKT 2
SINGLE 11	: OPEN LINE FROM BUS 30 [SEFO 30.000] TO BUS 76 [NORDESTE 30.000] CKT 1
SINGLE 12	: OPEN LINE FROM BUS 30 [SEFO 30.000] TO BUS 76 [NORDESTE 30.000] CKT 2
SINGLE 13	: OPEN LINE FROM BUS 30 [SEFO 30.000] TO BUS 77 [RIBEIRINHA 30.000] CKT 1
SINGLE 14	: OPEN LINE FROM BUS 30 [SEFO 30.000] TO BUS 77 [RIBEIRINHA 30.000] CKT 2
SINGLE 15	: OPEN LINE FROM BUS 31 [SEVF 30.000] TO BUS 33 [PSFU 30.000] CKT 1
SINGLE 16	: OPEN LINE FROM BUS 31 [SEVF 30.000] TO BUS 89 [V F III 30.000] CKT 1
SINGLE 17	: OPEN LINE FROM BUS 31 [SEVF 30.000] TO BUS 90 [FURNAS 30.000] CKT 1
SINGLE 18	: OPEN LINE FROM BUS 31 [SEVF 30.000] TO BUS 90 [FURNAS 30.000] CKT 2
SINGLE 19	: OPEN LINE FROM BUS 31 [SEVF 30.000] TO BUS 91 [P. GARHA 30.000] CKT 1
SINGLE 20	: OPEN LINE FROM BUS 31 [SEVF 30.000] TO BUS 91 [P. GARHA 30.000] CKT 2
SINGLE 21	: OPEN LINE FROM BUS 33 [PSFU 30.000] TO BUS 79 [POVOAHГO 30.000] CKT 1
SINGLE 22	: OPEN LINE FROM BUS 33 [PSFU 30.000] TO BUS 79 [POVOAHГO 30.000] CKT 2
SINGLE 23	: OPEN LINE FROM BUS 33 [PSFU 30.000] TO BUS 80 [FURNAS 1 30.000] CKT 1
SINGLE 24	: OPEN LINE FROM BUS 33 [PSFU 30.000] TO BUS 80 [FURNAS 1 30.000] CKT 2
SINGLE 25	: OPEN LINE FROM BUS 33 [PSFU 30.000] TO BUS 81 [FURNAS 2 30.000] CKT 1
SINGLE 26	: OPEN LINE FROM BUS 44 [SEMF 30.000] TO BUS 83 [CAPELAS 30.000] CKT 1
SINGLE 27	: OPEN LINE FROM BUS 44 [SEMF 30.000] TO BUS 83 [CAPELAS 30.000] CKT 2
SINGLE 28	: OPEN LINE FROM BUS 44 [SEMF 30.000] TO BUS 84 [S. CIDADES 30.000] CKT 1
SINGLE 29	: OPEN LINE FROM BUS 44 [SEMF 30.000] TO BUS 84 [S. CIDADES 30.000] CKT 2
SINGLE 30	: OPEN LINE FROM BUS 44 [SEMF 30.000] TO BUS 85 [S.ROQUE 30.000] CKT 1
SINGLE 31	: OPEN LINE FROM BUS 44 [SEMF 30.000] TO BUS 85 [S.ROQUE 30.000] CKT 2
SINGLE 32	: OPEN LINE FROM BUS 44 [SEMF 30.000] TO BUS 86 [COVOADA 30.000] CKT 1
SINGLE 33	: OPEN LINE FROM BUS 44 [SEMF 30.000] TO BUS 86 [COVOADA 30.000] CKT 2
SINGLE 34	: OPEN LINE FROM BUS 45 [SECL 30.000] TO BUS 93 [LIVRAMENTO 30.000] CKT 1
SINGLE 35	: OPEN LINE FROM BUS 45 [SECL 30.000] TO BUS 93 [LIVRAMENTO 30.000] CKT 2
SINGLE 36	: OPEN LINE FROM BUS 45 [SECL 30.000] TO BUS 94 [RIBEIRA SECA 30.000] CKT 1
SINGLE 37	: OPEN LINE FROM BUS 45 [SECL 30.000] TO BUS 94 [RIBEIRA SECA 30.000] CKT 2

Fig. 4-10: Contingency analysis outcomes for the 30 kV lines, Scenario 1.

For Scenario 2, taking out the transmission lines of 60 kV one by one, all the single contingencies which are illustrated in the contingency agenda beneath (Fig. 4-11) have consequences on the system. The effects of this tripping are voltage drops under the minimum acceptable value of 0.95 pu and big overloads on branches. It is worth mentioning that the resulting violations are worse than the case scenario analyzed above, as these align with the system load profile and generation scattering. The worst branch overloading and voltage drops by 2-3% occur when considering the single contingencies 2, 3 and 4 (Fig. 4-11), namely disconnecting the transmission lines among the central fossil fuel plant (CTCL-CPP) and the substations of SELG or SEMF respectively. Simulation results are given beneath:

final results

<---------- MULTI-SECTION LINE ---------->		<---------- MONITORED BRANCH		
----------> CONTINGENCY	RATING	FLOW	%	
30.000 2 BASE CASE	14.8	19.4	136.7	3 CGPV-GPP 30.000 30*SEFO
30.000 2 SINGLE 1	14.8	19.3	136.5	3 CGPV-GPP 30.000 30*SEFO
30.000 2 SINGLE 2	14.8	19.4	137.1	3 CGPV-GPP 30.000 30*SEFO
30.000 2 SINGLE 3	14.8	19.4	137.1	3 CGPV-GPP 30.000 30*SEFO
60.000 1 SINGLE 4	37.4	42.3	114.9	1 CTCL-FPP 60.000 39*SESR
30.000 2 SINGLE 4	14.8	19.4	136.6	3 CGPV-GPP 30.000 30*SEFO
60.000 1 SINGLE 4	37.4	35.3	97.9	27*SEMF 60.000 39 SESR
30.000 2 SINGLE 5	14.8	19.4	136.6	3 CGPV-GPP 30.000 30*SEFO
30.000 2 SINGLE 6	14.8	19.4	136.6	3 CGPV-GPP 30.000 30*SEFO
30.000 2 SINGLE 7	14.8	19.7	138.9	3 CGPV-GPP 30.000 30*SEFO
30.000 2 SINGLE 8	14.8	19.2	135.3	3 CGPV-GPP 30.000 30*SEFO
30.000 2 SINGLE 9	14.8	19.4	136.6	3 CGPV-GPP 30.000 30*SEFO
30.000 2 SINGLE 10	14.8	19.4	136.6	3 CGPV-GPP 30.000 30*SEFO
30.000 2 SINGLE 11	14.8	19.4	136.6	3 CGPV-GPP 30.000 30*SEFO

MONITORED VOLTAGE REPORT:

SYSTEM	CONTINGENCY	<-------- B U S -------->		V-CONT	V-INIT	V-MAX	V-MIN
'ALL '	RANGE SINGLE 2	33	PSFU 30.000	0.94747	0.95187	1.05000	0.95000
'ALL '	RANGE SINGLE 2	79	POVOAHΓO 30.000	0.94748	0.95188	1.05000	0.95000
'ALL '	RANGE SINGLE 2	80	FURNAS 1 30.000	0.94747	0.95188	1.05000	0.95000
'ALL '	RANGE SINGLE 2	81	FURNAS 2 30.000	0.94747	0.95188	1.05000	0.95000
'ALL '	RANGE SINGLE 3	33	PSFU 30.000	0.94749	0.95187	1.05000	0.95000
'ALL '	RANGE SINGLE 3	79	POVOAHΓO 30.000	0.94750	0.95188	1.05000	0.95000
'ALL '	RANGE SINGLE 3	80	FURNAS 1 30.000	0.94750	0.95188	1.05000	0.95000
'ALL '	RANGE SINGLE 3	81	FURNAS 2 30.000	0.94750	0.95188	1.05000	0.95000
'ALL '	RANGE SINGLE 4	44	SEMF 30.000	0.94784	0.97487	1.05000	0.95000
'ALL '	RANGE SINGLE 4	83	CAPELAS 30.000	0.94792	0.97496	1.05000	0.95000
'ALL '	RANGE SINGLE 4	84	S. CIDADES 30.000	0.94792	0.97495	1.05000	0.95000
'ALL '	RANGE SINGLE 4	85	S.ROQUE 30.000	0.94786	0.97490	1.05000	0.95000
'ALL '	RANGE SINGLE 4	86	COVOADA 30.000	0.94790	0.97494	1.05000	0.95000

CONTINGENCY LEGEND:

LABEL	EVENTS
SINGLE 1	: OPEN LINE FROM BUS 1 [CTCL-FPP 60.000] TO BUS 4 [SEFO 60.000] CKT 1
SINGLE 2	: OPEN LINE FROM BUS 1 [CTCL-FPP 60.000] TO BUS 11 [SELG 60.000] CKT 1
SINGLE 3	: OPEN LINE FROM BUS 1 [CTCL-FPP 60.000] TO BUS 11 [SELG 60.000] CKT 2
SINGLE 4	: OPEN LINE FROM BUS 1 [CTCL-FPP 60.000] TO BUS 27 [SEMF 60.000] CKT 1
SINGLE 5	: OPEN LINE FROM BUS 1 [CTCL-FPP 60.000] TO BUS 37 [SEAR 60.000] CKT 1
SINGLE 6	: OPEN LINE FROM BUS 1 [CTCL-FPP 60.000] TO BUS 39 [SESR 60.000] CKT 1
SINGLE 7	: OPEN LINE FROM BUS 2 [CGRG-GPP 60.000] TO BUS 4 [SEFO 60.000] CKT 1
SINGLE 8	: OPEN LINE FROM BUS 4 [SEFO 60.000] TO BUS 11 [SELG 60.000] CKT 1
SINGLE 9	: OPEN LINE FROM BUS 27 [SEMF 60.000] TO BUS 35 [SEPD1 60.000] CKT 1
SINGLE 10	: OPEN LINE FROM BUS 27 [SEMF 60.000] TO BUS 36 [SEPD2 60.000] CKT 1
SINGLE 11	: OPEN LINE FROM BUS 27 [SEMF 60.000] TO BUS 39 [SESR 60.000] CKT 1

Fig. 4-11: Contingency analysis outcomes for the 60 kV lines, Scenario 2.

Tripping each one of the 30 kV are monitored the two branches between 3 CGPV-GPP and 30 SEFO rated at this voltage value being overloaded. The effect of this disconnection is violation on current rating by 174.5 % (Fig. 4-12). Voltages drop but do not surpass the rate of 1.5% (Fig. 4-13), which sag is a bit greater than in the corresponding high demand Scenario 1 of 2009 where the voltage reductions approached the figure of 1.3%. Beneath are illustrated the simulation solutions (Fig. 4-12 & 4-13).

<---------- MULTI-SECTION LINE ---------->					<---------- MONITORED BRANCH		
----------> CONTINGENCY		RATING	FLOW	%			
30.000 2	BASE CASE	14.8	19.4	136.7	3 CGPV-GPP	30.000	30*SEFO
30.000 2	SINGLE 1	14.8	21.1	149.1	3 CGPV-GPP	30.000	30*SEFO
30.000 1	SINGLE 2	12.5	21.0	174.5	3*CGPV-GPP	30.000	30 SEFO
30.000 2	SINGLE 3	14.8	19.4	136.6	3 CGPV-GPP	30.000	30*SEFO
30.000 2	SINGLE 4	14.8	19.4	136.8	3 CGPV-GPP	30.000	30*SEFO
30.000 2	SINGLE 5	14.8	19.4	136.6	3 CGPV-GPP	30.000	30*SEFO
30.000 2	SINGLE 6	14.8	19.4	136.6	3 CGPV-GPP	30.000	30*SEFO
30.000 2	SINGLE 7	14.8	19.4	136.6	3 CGPV-GPP	30.000	30*SEFO
30.000 2	SINGLE 8	14.8	19.4	136.6	3 CGPV-GPP	30.000	30*SEFO
30.000 2	SINGLE 9	14.8	19.4	137.3	3 CGPV-GPP	30.000	30*SEFO
30.000 2	SINGLE 10	14.8	19.4	136.8	3 CGPV-GPP	30.000	30*SEFO
30.000 2	SINGLE 11	14.8	19.8	139.5	3 CGPV-GPP	30.000	30*SEFO
30.000 2	SINGLE 12	14.8	19.4	136.7	3 CGPV-GPP	30.000	30*SEFO
30.000 2	SINGLE 13	14.8	19.4	137.1	3 CGPV-GPP	30.000	30*SEFO
30.000 2	SINGLE 14	14.8	19.4	136.7	3 CGPV-GPP	30.000	30*SEFO
30.000 2	SINGLE 15	14.8	19.3	136.4	3 CGPV-GPP	30.000	30*SEFO
30.000 2	SINGLE 16	14.8	19.4	136.6	3 CGPV-GPP	30.000	30*SEFO
30.000 2	SINGLE 17	14.8	19.4	136.7	3 CGPV-GPP	30.000	30*SEFO
30.000 2	SINGLE 18	14.8	19.4	136.6	3 CGPV-GPP	30.000	30*SEFO
30.000 2	SINGLE 19	14.8	19.4	136.7	3 CGPV-GPP	30.000	30*SEFO
30.000 2	SINGLE 20	14.8	19.4	136.6	3 CGPV-GPP	30.000	30*SEFO
30.000 2	SINGLE 21	14.8	19.4	136.6	3 CGPV-GPP	30.000	30*SEFO
30.000 2	SINGLE 22	14.8	19.4	136.7	3 CGPV-GPP	30.000	30*SEFO
30.000 2	SINGLE 23	14.8	19.4	136.6	3 CGPV-GPP	30.000	30*SEFO
30.000 2	SINGLE 24	14.8	19.4	136.7	3 CGPV-GPP	30.000	30*SEFO
30.000 2	SINGLE 25	14.8	19.4	136.6	3 CGPV-GPP	30.000	30*SEFO
30.000 2	SINGLE 26	14.8	19.4	136.6	3 CGPV-GPP	30.000	30*SEFO
30.000 2	SINGLE 27	14.8	19.4	136.6	3 CGPV-GPP	30.000	30*SEFO
30.000 2	SINGLE 28	14.8	19.4	136.6	3 CGPV-GPP	30.000	30*SEFO
30.000 2	SINGLE 29	14.8	19.4	136.6	3 CGPV-GPP	30.000	30*SEFO
30.000 2	SINGLE 30	14.8	19.4	136.6	3 CGPV-GPP	30.000	30*SEFO
30.000 2	SINGLE 31	14.8	19.4	136.6	3 CGPV-GPP	30.000	30*SEFO
30.000 2	SINGLE 32	14.8	19.4	136.6	3 CGPV-GPP	30.000	30*SEFO
30.000 2	SINGLE 33	14.8	19.4	136.6	3 CGPV-GPP	30.000	30*SEFO
30.000 2	SINGLE 34	14.8	19.4	136.6	3 CGPV-GPP	30.000	30*SEFO
30.000 2	SINGLE 35	14.8	19.4	136.6	3 CGPV-GPP	30.000	30*SEFO
30.000 2	SINGLE 36	14.8	19.4	136.6	3 CGPV-GPP	30.000	30*SEFO
30.000 2	SINGLE 37	14.8	19.4	136.6	3 CGPV-GPP	30.000	30*SEFO

Fig. 4-12: Contingency analysis outcomes for the 30 kV lines (branch overloading), Scenario 2.

```
MONITORED VOLTAGE REPORT:
SYSTEM                          CONTINGENCY  <-------- B U S --------->  V-CONT   V-INIT   V-MAX    V-MIN
'ALL         '             RANGE SINGLE 2          30 SEFO        30.000  0.94665  0.95749  1.05000  0.95000
'ALL         '             RANGE SINGLE 2          75 CALHETAS    30.000  0.94671  0.95755  1.05000  0.95000
'ALL         '             RANGE SINGLE 2          76 NORDESTE    30.000  0.94687  0.95771  1.05000  0.95000
'ALL         '             RANGE SINGLE 2          77 RIBEIRINHA  30.000  0.94668  0.95751  1.05000  0.95000
'ALL         '             RANGE SINGLE 3          33 PSFU        30.000  0.94985  0.95187  1.05000  0.95000
'ALL         '             RANGE SINGLE 3          79 POVOAHГO    30.000  0.94986  0.95188  1.05000  0.95000
'ALL         '             RANGE SINGLE 3          80 FURNAS 1    30.000  0.94986  0.95188  1.05000  0.95000
'ALL         '             RANGE SINGLE 3          81 FURNAS 2    30.000  0.94986  0.95188  1.05000  0.95000
'ALL         '             RANGE SINGLE 4          31 SEVF        30.000  0.94562  0.95885  1.05000  0.95000
'ALL         '             RANGE SINGLE 4          32 SEVF        10.000  0.94167  0.95492  1.05000  0.95000
'ALL         '             RANGE SINGLE 4          33 PSFU        30.000  0.93859  0.95187  1.05000  0.95000
'ALL         '             RANGE SINGLE 4          79 POVOAHГO    30.000  0.93860  0.95188  1.05000  0.95000
'ALL         '             RANGE SINGLE 4          80 FURNAS 1    30.000  0.93860  0.95188  1.05000  0.95000
'ALL         '             RANGE SINGLE 4          81 FURNAS 2    30.000  0.93860  0.95188  1.05000  0.95000
'ALL         '             RANGE SINGLE 4          88 V F II      10.000  0.94168  0.95492  1.05000  0.95000
'ALL         '             RANGE SINGLE 4          89 V F III     30.000  0.94562  0.95885  1.05000  0.95000
'ALL         '             RANGE SINGLE 4          90 FURNAS      30.000  0.94577  0.95907  1.05000  0.95000
'ALL         '             RANGE SINGLE 4          91 P. GARHA    30.000  0.94563  0.95886  1.05000  0.95000
'ALL         '             RANGE SINGLE 4          92 VF I        10.000  0.94168  0.95492  1.05000  0.95000
'ALL         '             RANGE SINGLE 17         33 PSFU        30.000  0.94796  0.95187  1.05000  0.95000
'ALL         '             RANGE SINGLE 17         79 POVOAHГO    30.000  0.94797  0.95188  1.05000  0.95000
'ALL         '             RANGE SINGLE 17         80 FURNAS 1    30.000  0.94797  0.95188  1.05000  0.95000
'ALL         '             RANGE SINGLE 17         81 FURNAS 2    30.000  0.94796  0.95188  1.05000  0.95000
'ALL         '             RANGE SINGLE 24         33 PSFU        30.000  0.94883  0.95187  1.05000  0.95000
'ALL         '             RANGE SINGLE 24         79 POVOAHГO    30.000  0.94884  0.95188  1.05000  0.95000
'ALL         '             RANGE SINGLE 24         80 FURNAS 1    30.000  0.94880  0.95188  1.05000  0.95000
'ALL         '             RANGE SINGLE 24         81 FURNAS 2    30.000  0.94884  0.95188  1.05000  0.95000

CONTINGENCY LEGEND:
LABEL          EVENTS
SINGLE 1    : OPEN LINE FROM BUS 3 [CGPV-GPP     30.000] TO BUS 30 [SEFO        30.000] CKT 1
SINGLE 2    : OPEN LINE FROM BUS 3 [CGPV-GPP     30.000] TO BUS 30 [SEFO        30.000] CKT 2
SINGLE 3    : OPEN LINE FROM BUS 13 [SELG         30.000] TO BUS 31 [SEVF        30.000] CKT 1
SINGLE 4    : OPEN LINE FROM BUS 13 [SELG         30.000] TO BUS 31 [SEVF        30.000] CKT 2
SINGLE 5    : OPEN LINE FROM BUS 13 [SELG         30.000] TO BUS 70 [LIVRAMENTO  30.000] CKT 1
SINGLE 6    : OPEN LINE FROM BUS 13 [SELG         30.000] TO BUS 70 [LIVRAMENTO  30.000] CKT 2
SINGLE 7    : OPEN LINE FROM BUS 13 [SELG         30.000] TO BUS 82 [RIBEIRA CHГ 30.000] CKT 1
SINGLE 8    : OPEN LINE FROM BUS 13 [SELG         30.000] TO BUS 82 [RIBEIRA CHГ 30.000] CKT 2
SINGLE 9    : OPEN LINE FROM BUS 30 [SEFO         30.000] TO BUS 75 [CALHETAS    30.000] CKT 1
SINGLE 10   : OPEN LINE FROM BUS 30 [SEFO         30.000] TO BUS 75 [CALHETAS    30.000] CKT 2
SINGLE 11   : OPEN LINE FROM BUS 30 [SEFO         30.000] TO BUS 76 [NORDESTE    30.000] CKT 1
SINGLE 12   : OPEN LINE FROM BUS 30 [SEFO         30.000] TO BUS 76 [NORDESTE    30.000] CKT 2
SINGLE 13   : OPEN LINE FROM BUS 30 [SEFO         30.000] TO BUS 77 [RIBEIRINHA  30.000] CKT 1
SINGLE 14   : OPEN LINE FROM BUS 30 [SEFO         30.000] TO BUS 77 [RIBEIRINHA  30.000] CKT 2
SINGLE 15   : OPEN LINE FROM BUS 31 [SEVF         30.000] TO BUS 33 [PSFU        30.000] CKT 1
SINGLE 16   : OPEN LINE FROM BUS 31 [SEVF         30.000] TO BUS 89 [V F III     30.000] CKT 1
```

Fig. 4-13: Contingency analysis outcomes for the 30 kV lines (voltage violations), Scenario 2.

4.4.2.3. Short Circuit Analysis Results

Short circuit analysis is a part of the static studies to define the potential distributed capacity that can be introduced into the grid. Principally, the main objective of such analysis is to check the short circuit power at every substation in order to evaluate the available space in terms of capacity to penetrate dispersed generation units. The Spanish grid code imposes that the short circuit power at a substation node has to be 20 times higher than the wind power installed. In addition, wind farms may stay connected under voltage dips caused by short circuits on the transmission network for 250 ms [101].

Throughout this thesis, three-phase short circuit analysis was implemented only for the high demand profile in both Scenarios 1 & 2 since this is the worst case scenario. Three-phase symmetrical faults are calculated for the system's substations nodes rated at voltages of 60, 30 and 10 kV. Simulation results of the three-phase short circuit current values are depicted in Fig. 4-14 to 4-16.

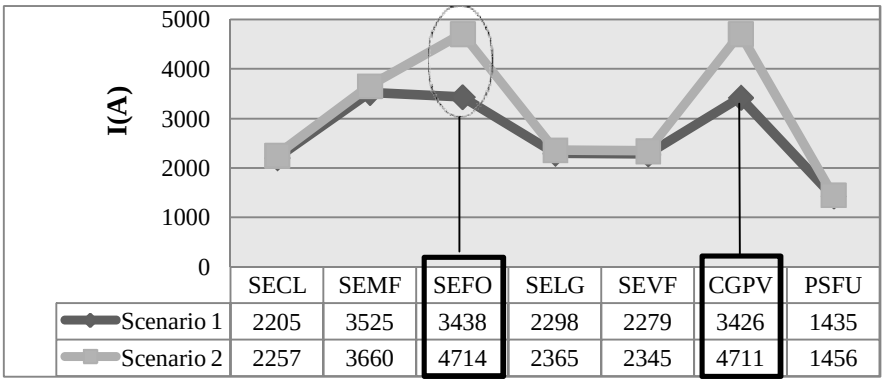

	SECL	SEMF	SEFO	SELG	SEVF	CGPV	PSFU
Scenario 1	2205	3525	3438	2298	2279	3426	1435
Scenario 2	2257	3660	4714	2365	2345	4711	1456

Fig. 4-14: Three-phase fault currents at 30 kV substation nodes.

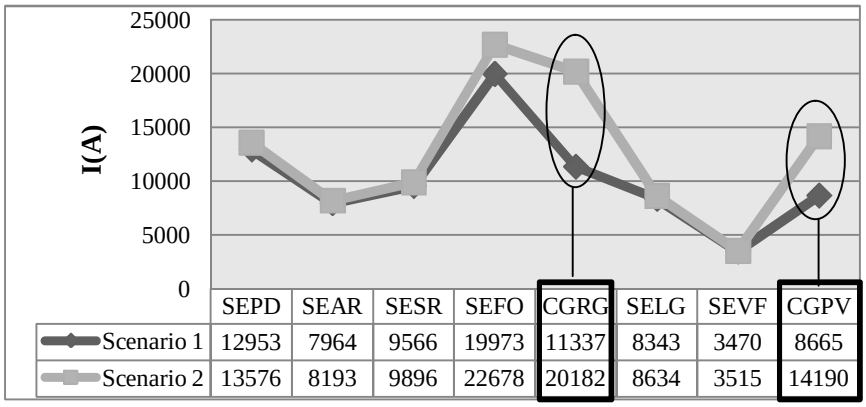

	SEPD	SEAR	SESR	SEFO	CGRG	SELG	SEVF	CGPV
Scenario 1	12953	7964	9566	19973	11337	8343	3470	8665
Scenario 2	13576	8193	9896	22678	20182	8634	3515	14190

Fig. 4-15: Three-phase fault currents at 10 kV substation nodes.

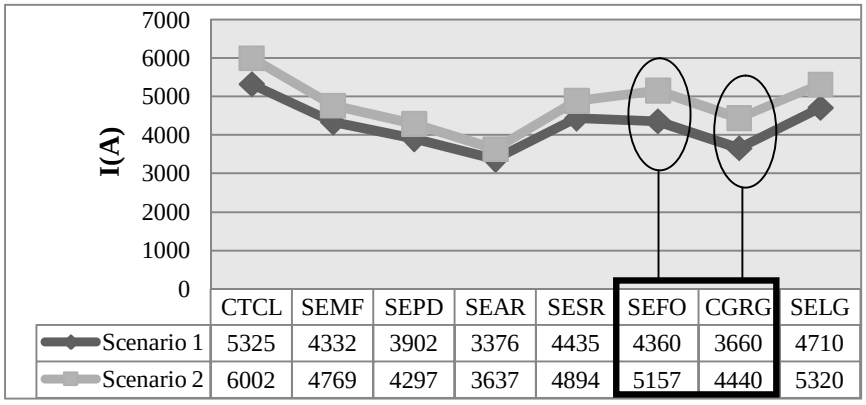

	CTCL	SEMF	SEPD	SEAR	SESR	SEFO	CGRG	SELG
Scenario 1	5325	4332	3902	3376	4435	4360	3660	4710
Scenario 2	6002	4769	4297	3637	4894	5157	4440	5320

Fig. 4-16: Three-phase fault currents at 60 kV substation nodes.

For both scenarios, the buses with the lowest short circuit level (SCL) are mainly at 30 kV and belong to the substations of SECL, SELG and SEVF. Moreover, the difference in fault values in the 30 kV are the smallest compared to the 60 and 10 kV except from the substation of SEFO and the power plant CGPV as indicated by the circles in Fig. 4-14. Generally, the distribution network of 10 kV suffers from very high short circuit values in comparison to the other voltage levels (Fig. 4-15). On the other hand, on the 60 kV network, there are not denoted extreme deviations in the short circuit values, except from those appeared in circle for both Scenarios 1 & 2 as it can be easily observed in Fig. 4-16.

Concluding, in Scenario 1, the total system losses amount for 0.8MW+7.2MVAr whereas these figures increase up to 1.1MW+8.9MVAr in Scenario 2. The soar in power losses and short circuit level is reasonable because DG units are added on the buses of CGRG and CGPV rated at 10 and 11 kV respectively and also the load profile is changed (almost 10%). Consequently, the most remarkable changes are denoted on the addition buses of CGRG and CGPV rated at 10 and 11 kV accordingly. The connection of additional distribution generators drives the fault level to unfavourably high values.

Appendix G concentrates the analytical short-circuit calculation results (Scenario 2) for some indicative buses, i.e. CGRG, CGPV and SEFO.

As aforementioned, Section 4.4.2, the low demand power flow and contingency analysis results for Scenarios 1 & 2 are presented in Appendices C to F.

4.4.3. Scenario 3- Wind Power Included

4.4.3.1. Power Flow Results

In this Scenario it is presumed a wind power installed potential of 14 MW by 2015, apart from the increased geothermal power by 25.77 MW at CGRG and CGPV nodes of 10 and 11 kV respectively (Table 4-7). Moreover, Table 4-10 beneath, illustrates the high load demand profile for the different system's substations as projected for 2015. All the simulation results that follow, regard solely the high demand case scenario.

The two main issues addressed before and will be considered in the present study were the power system losses and the fault level at the addition and nearby nodes. One more criterion to be considered is that the wind potential to be penetrated cannot surpass the 5% of the short circuit capacity at the connection point node (Spanish low voltage electrical regulations) [101].

Each individual wind turbine generates at 690 V and the wind turbine generators (WTGs) are connected to the distribution MV bus bars of 30 kV and 60 kV by dedicated lines through their 0.69/30 and 0.69/60 kV step-up transformers respectively. The wind generators aggregated operate for the 80% of their installed capacity. Power flow wind generators modeling data for steady-state analysis are shown in Tables 4-11 to 4-16 [103].

These DG units are normally penetrated into the buses with the highest short circuit capacity to induce the minor impacts on the system´s stability. Throughout this study, two rules of thumb were examined as where to add the wind energy generation. The former was to introduce these units at the lower voltage buses and the latter to try to add wind power to buses with denominator the higher short circuit capacity and the high load demanding to investigate the out-coming effects onto the electrical grid. In addition, among all the transmission and distribution substation nodes several of them were chosen to add the wind power to. These were some transmission and distribution substation buses rated at 60 kV and 30 kV respectively and they are analysed in the following section. Actually, the method being followed is a trial-error method, in order to define the most suitable nodes for wind energy penetration. Apart from power flow and short circuit analysis, also contingency simulations are employed where is appropriate. The analytical results are provided in Appendices H-P.

The central fossil fuel plant´s synchronous generators are once more chosen to be the slack nodes, thus their output cannot be controlled but is adjusted by the system automatically. Consequently, with the penetration of more renewable energy in terms of active and reactive power, and in order to keep the power balance, production has to be readjusted; otherwise there will be over excess and subsequent losses.

Table 4-10: High load demand at the substation nodes in 2015.

Substations	P (MW)	Q (MVAr)
SECL (30 kV)	4.7	1.861
SEMF (30 kV)	11.7	4.6
SEPD (10 kV)	21.9	7
SEAR (10 kV)	6.4	2.481
SESR (10 kV)	5.8	2.121
SEFO (30 kV)	25.4	5.201
SEFO (10 kV)	5.0	2.081
SELG (30 kV)	7.0	2.692
SELG (10 kV)	6.45	3.4
SEVF (30 kV)	5.8	2.2

Table 4-11: Wind Turbine Generator Data

Symbol	Value	Unit
S_n[5]	2	MVA
$Q_{max}(Q_{min})$	0.65(-0.65)	MVAr
$P_{max}(P_{min})$	2(0.1)	MW
Z_{source}	j0.8	pu
M_{base}	2.1	MVA

Table 4-12: Wind Turbine Transformer Data (A)

Symbol	Value	Unit
S_n	2.1	MVA
U_{np}/U_{ns}[6]	0.69/30	MW
Z_{tr}[7]	0.0073+j0.06	pu
M_{base}	2.1	MVA

[5] Sn: Rated power

[6] Unp/Uns: Step-down & step-up voltage

[7] Ztr: Transformer impedance

Table 4-13: Wind Turbine Transformer Data (B)

Symbol	Value	Unit
S_n	40	MVA
U_{np}/U_{ns}	0.69/60	MW
Z_{tr}	0.005+j0.05	pu
M_{base}	40	MVA

Table 4-14: 30/60 kV Network Lines

Voltage (kV)	Diameter (mm^2)	I (A)	R (Ohm/km)	X (Ohm/km)
30	95	360	0,207	0,363
60	185	540	0,101	0,389

Table 4-15 represents the losses encountered in the system within Scenarios 2 & 3. The total system losses with only geothermal generation added (Scenario 2) account for 1.1 MW+8.9 MVAr, whereas including wind generators addition at specific nodes the losses differentiate accordingly (Fig. 4-17 & 4-18).

Table 4-15: Total System Losses for Scenarios 2&3, year 2015.

Network buses	System losses (P, Q)	
	Scenario 2, geothermal power	Scenario 3, geothermal & wind
SEFO	1.1 MW+8.9 MVAr	1.5 MW+9.3 MVAr
SELG-60		1.1 MW+9.0 MVAr
SELG-30		1.1 MW+8.6 MVAr
SEMF-60		1.1 MW+8.8 MVAr
SEFO		1.5 MW+9.3 MVAr
SEVF		1.1 MW+8.6 MVAr
PSFU		1.5 MW+8.3 MVAr
SEPD1		1.0 MW+8.7 MVAr
SEPD		1.1 MW+8.8 MVAr
SEMF-30		1.1 MW+8.8 MVAr
SECL		1.1 MW+9.0 MVAr

It is clear that, the minimum reactive losses were obtained with DG penetration in bus-33 PSFU (Fig. 4-18).

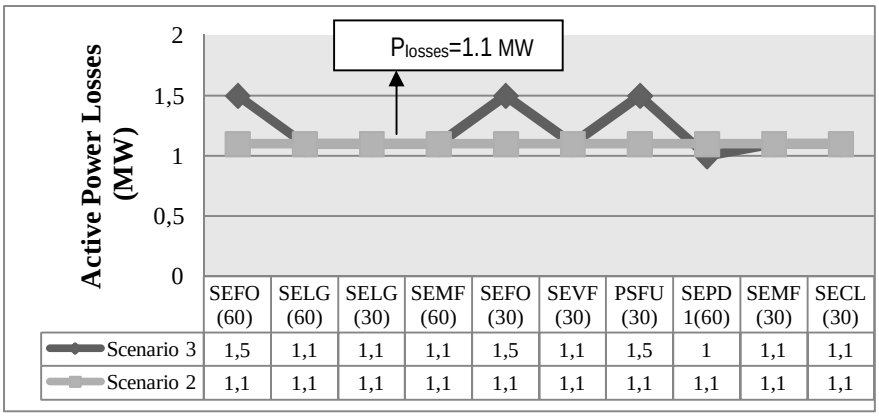

	SEFO (60)	SELG (60)	SELG (30)	SEMF (60)	SEFO (30)	SEVF (30)	PSFU (30)	SEPD 1(60)	SEMF (30)	SECL (30)
Scenario 3	1,5	1,1	1,1	1,1	1,5	1,1	1,5	1	1,1	1,1
Scenario 2	1,1	1,1	1,1	1,1	1,1	1,1	1,1	1,1	1,1	1,1

Fig. 4-17: Active power losses with different DG location.

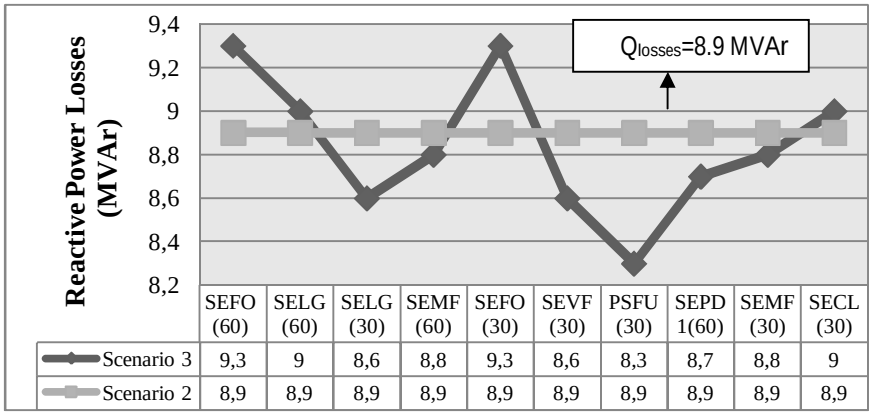

	SEFO (60)	SELG (60)	SELG (30)	SEMF (60)	SEFO (30)	SEVF (30)	PSFU (30)	SEPD 1(60)	SEMF (30)	SECL (30)
Scenario 3	9,3	9	8,6	8,8	9,3	8,6	8,3	8,7	8,8	9
Scenario 2	8,9	8,9	8,9	8,9	8,9	8,9	8,9	8,9	8,9	8,9

Fig. 4-18: Reactive power losses with different DG location.

4.4.3.2. Short Circuit Analysis Results

In Scenario 2, year 2015 a very slight voltage drop was detected at the distribution 30 kV bus of PSFU by 0.94997 pu. Thus, primarily the wind generator units were decided to be added to that node to finally reinforce the steady-state stability and at the meanwhile obtaining the minimum possible power losses; although this nodal penetration seems to converge to the best system´s voltage profile, the amount of wind power integration does not fit, but exceeds the 5% penetration restriction as mentioned above in Section 4.4.3.1.

Moreover, it is observed that the wind generation fires the short circuit level by 369.7 A (Table 4-16). However, the impact on power losses is minimal in all cases as the amount of power added was small compared to the total system handling capacity. Moreover, bus-33 has the lowest SCL figure for both Scenarios 2 & 3.

Figure 4-19 depicts the fault current values at the addition buses. The parenthesis denotes the voltage level in kV. The addition node that appears to have a low voltage and comes second in rising the fault current value unfavourably by 305 A is the SEFO bus rated at 30 kV.

The second criterion was to introduce the wind energy into the highest short circuit capacity nodes. As it was expected, if the substation addition buses were some of the ones with the highest short circuit level, numbered as, SELG 60 kV, SEMF 60 kV and SEPD1 60 kV there won't be induced any noticeable impacts on the system before and after the wind penetration regarding the power losses (Fig. 4-17 & 4-18), short circuit current rise (Fig. 4-19) and voltage levels.

Especially, bus SEPD1 60 kV seems to be the most suitable among the transmission nodes with power losses minimised to 1.0 MW + 8.7 MVAr and a 206 A increase in the three-phase fault current. In addition, implementing

the contingency analysis for this node, the results are smoother for a loss of one of its transport lines 60 /30 kV compared to the other buses (Appendix L).

For the same reasons, among the distribution nodes the most suitable to connect the wind generators to is the SEVF 30 kV. Here, the short circuit current rises 239 A and power losses are minimised to 1.1MW + 8.6MVAr. This could be abbreviated to the fact that wind generators added via transformers 0.69/30 kV to that node are behaved as swing generators to balance apparent power throughout the system. Voltage soars are observed at the nodes of 30 kV which are connected to the substation node SEVF and are fairly isolated from the power centres.

Buses- SELG and SEVF both rated at 30 kV appear to have equal rise by 239 A in fault current value. Considering the contingency agenda for the PSFU, SELG and SEVF nodes (Appendices J, M & O), the results are smoother for the loss of a 60/30 kV transmission line for bus PSFU instead of SELG and SEVF buses. Nevertheless, PSFU substation node has been excluded from being the addition bus due to the unfavourable increase in its fault level.

Table 4-16: Short Circuit Level at the addition buses: Scenarios 2&3, year 2015.

DG addition at bus	SCL (A)	
	Scenario 2, geothermal power	Scenario 3, geothermal & wind
SEFO	5156.7	5334.6
SELG-60	5320.1	5499.3
SELG-30	2364.7	2604.1
SEMF-60	4768.8	4953.1
SEFO	4714.3	5018.5
SEVF	2344.6	2584.3
PSFU	1455.8	1825.4
SEPD1	4297	4502.5
SEPD	13575.3	14208.3
SEMF-30	3660.4	3840
SECL	2257	2449.5

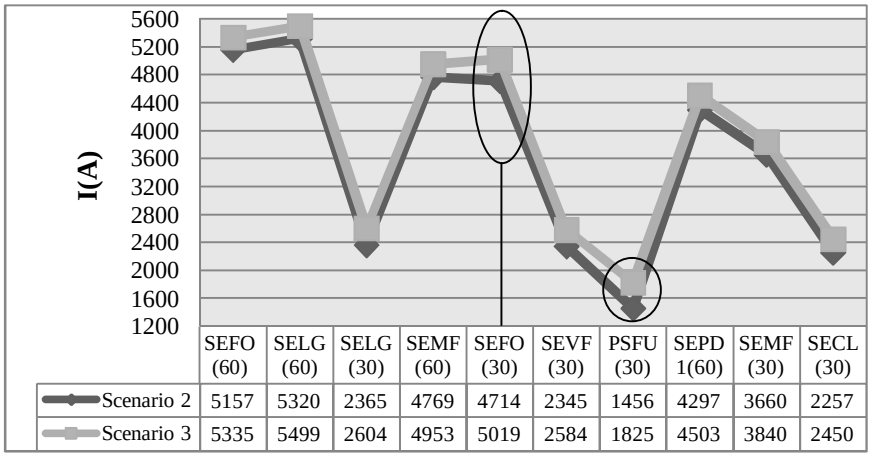

Fig. 4-19: Fault currents (A) at the addition buses, Scenarios 2 & 3.

4.4.4. Scenario 3- Wind Power Capacity Scattering

Instead of connecting all the wind generators at one solely substation node, it would be viable a generation scattering among different nodes with respect to load demanding and voltage profile. Several simulations were performed e.g. it was chosen to penetrate two wind turbines with generation of 2.0 MW at each of the 30/60 kV substation nodes of SEMF and SEVF and three machines at the 30 kV node of PSFU. The following conclusion was conducted; a generation scattering may induce less active and reactive losses, but raises up the short circuit value unfavourably. An explanation could be attributed to the three-phase fault calculation for the prescribed set of unbalances. The calculation process interconnects the three sequence networks to represent the unbalanced condition and solves for the sequence voltages. In addition, the calculation is based on the contributions from the series branch currents flowing in each branch (including any generator contributions) connected to the fault node. Therefore, when the wind power is connected to more than one substation nodes, the sum of fault current contributions from the power stations' generators is higher.

The respective results are given in Appendices Q & R.

4.5. Transient Stability Analysis

4.5.1. Performing Dynamic Simulations in PSS/E

The dynamic studies examine the impacts on the power system´s transient stability with the introduction of distributed generation into the grid. The fault ride through capability and frequency response of network elements, especially talking about generators are checked to see if they have adequate stability margin and that the voltage recovery following fault clearing is adequate.

The dynamic data file (.dyr) in PSS/E consists of parameter info for generators, turbines, exciters, governors etc. The version 31 provides with a dynamic model library for a DFIG variable speed wind turbine. The model includes generator, electrical control, wind turbine and pitch control. The most prevalent disturbance in order to check against the wind turbine generators' (WTGs) model response subjected to grid disturbances is a three-phase symmetrical fault on the interconnection bus.

PSS/E version 31 also contains the WT3 model that is commonly used and occupies a doubly fed induction generator. In addition, it has the following modules: a) Generator/converter module, b) electrical control module, c) turbine module, and d) pitch module. Dynamic simulations involve the generators and protection system modeling. It is considered that conventional generators can offer primary regulation whereas the wind generators cannot. In all the simulations executed throughout this thesis the speed controller value of conventional generators is adjusted, thus they can give 1.5% of their power potential if it is necessary. Moreover, the dynamic modeling of conventional generators concerns the definition of the standard generator model, the excitation limiter model (voltage regulation) and the governor model (speed control). According to the different generator types, within the current study the appropriate models were chosen which are included in the PSS/E library:

- Thermal power plants (for steam and/or gas turbines): GENROU round rotor generator, IEEG1 (IEEE-1981) governor model, EXST1 (IEEE-1981) excitation model.
- DFIG: In order to model this kind of technology is utilized the WT3 model of PSS/E that occupies doubly fed induction generator (Fig. 4-20). This technology allows inertia and speed control, because the blades are decoupled from the generator, whereas is connected to the grid via an AC/DC/AC converter.

The schematic figure (Fig. 4-21) beneath shows the interaction among the generic control modules in a wind turbine. The WT3 generic modules data for a DFIG are briefly given in the bibliography such as [13].

In more details, the WT3 generic model comprises of the modules as follows:

- WT3G: generator/converter module

- WT3E: electrical control module
- WT3T: mechanical control module
- WT3P: pitch control module

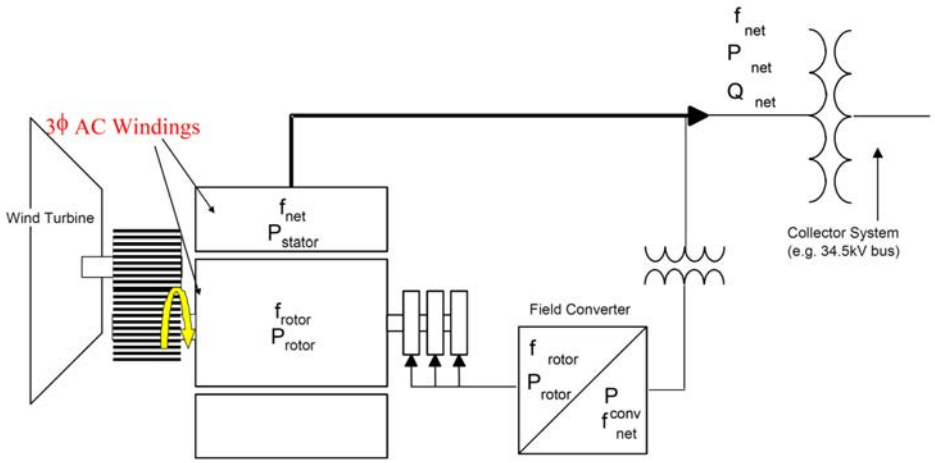

Fig. 4-20: Doubly Fed Induction Machine Technology [13].

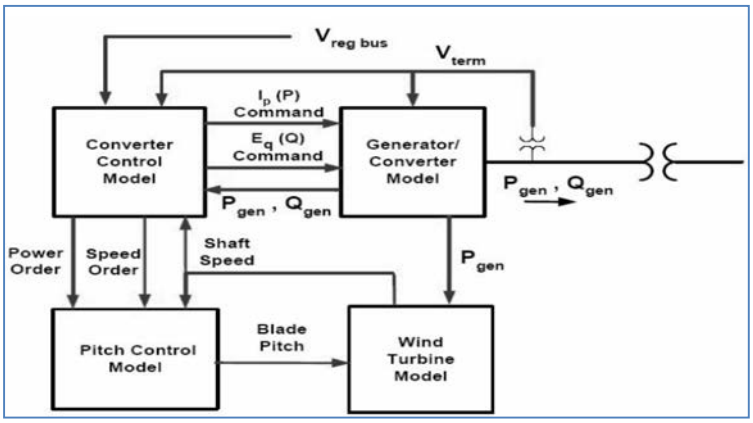

Fig. 4-21: PSS/E DFIG Generic Model [23].

The following Tables (Table 4-17 to 4-20) represent the WT3 generic modules data as entered in PSS/E simulation platform [13].

Table 4-17: Generator Module WT3G1

Symbol	Value	Unit
Xeq	0.8	pu
Pll gain	30	constant
Pll integrator gain	0	constant
Pll max	0.1	MW
MW rating	2	MW
No of lumped WTs	1	integer

Table 4-18: Mechanical Control Module WT3T1

Symbol	Value	Unit
Vw	1.25	pu of rated wind speed
H	4.95	sec
DAMP	0	pu P/pu speed
Kaero	0.007	constant
Theta2	21.98	degrees
Htfac	0.875	Hturb/H
Freq1	1.8	Hz
D_{SHAFT}	1.5	pu

Table 4-19: Electrical Module WT3E1

Symbol	Value	Unit
Tfv	0.15	sec
Kpv	18	pu
Kiv	5	pu
Tfp	0.05	sec
Kpp	3	pu
Kip	0.6	pu
PMX	1.12	pu
PMN	0.1	pu
QMX	0.309	pu
QMN	-0.309	pu
IPMAX	1.1	pu

Table 4-20: Pitch Control Module WT3P1

Symbol	Value	Unit
Tp	1.25	constant
Kpp	4.95	pu
Kip	0	pu
Kpc	0.007	pu
Kic	21.98	pu
TetaMin	0.875	degrees
TetaMax	1.8	degrees
RTetaMax	1.5	degrees/sec
P_{MX}	1	pu on Mbase

4.5.2. Voltage and Frequency Performance

Reactive power production capability defines the voltage control and inertia response for the frequency behaviour. Fixed speed generators (FSG) do not provide voltage regulation and consume reactive power, although DFIG provide local voltage control and the higher the penetration rate the higher will be the voltage figure.

A complete steady-state analysis required both of thermal and voltage magnitude violations. While, wind penetration levels are increased, existing thermal generation must be removed to accommodate it. Load flow analysis is affected by decommission via the elimination of a unit´s reactive supply. Dynamic analysis is affected by decommission via the elimination of a unit´s inertia. The system frequency depends on various penetration levels of wind energy by implementing generation displacement or /and load increase by the corresponding penetration level. Actually, the DFIGs do not provide any inertial support thus the total system inertia declines with the penetration level of DFIGs and the simultaneous removal of conventional generation results to the deterioration of the system´s frequency. Contradictorily, when load increases in order to reach the power balance, the total inertia of the system remains the same. As a result, the system would not suffer from a generation unit loss. Concluding, a DFIG can either positively or negatively affect the frequency nadir during a generation loss circumstance depending on how power balance is retrieved.

For instance, the Spanish System Operator (REE) has numbered various technical specifications, i.e. P.O.12.2 & P.O.12.3 [101] regarding the acceptable voltage dips in a wind farm after a short circuit fault in order to remain connected to the grid. The pre-mentioned voltage drop is characterized by a voltage decay followed by a voltage recovery in two ramps with different slope. As illustrated in Fig. 4-22 below, the voltage decay rises up to 20% of the nominal value for the first 0.5 seconds, followed by a voltage enhancement divided in two parts: firstly from 20% to 80% of the nominal value in the next 0.5 seconds and one from the 80% to the 95% of the nominal value in a total time of 14 seconds. Additionally, in case of a double-line-to-ground fault the voltage nadir does not drop beyond the 60% of the nominal value.

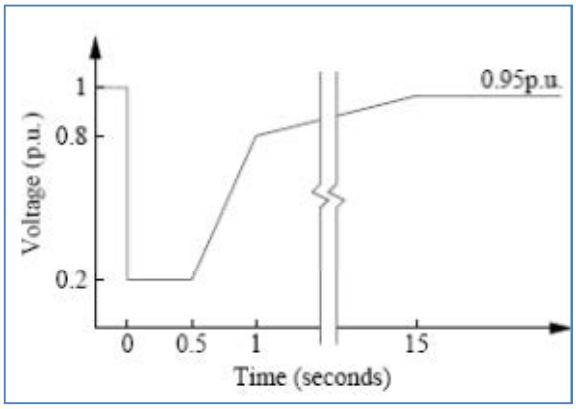

Fig. 4-22: Voltage behaviour after a short circuit incident [101].

The voltage in an electrical system is regulated by all generators. The high penetration level of wind energy into the network requires an active participation from the wind farms in the voltage control scheme at the connection point, complying also with the Transmission System Operators (TSOs) requirements. The generators control the voltage through the reactive power that consume/generate. The direct relationship among the voltage difference and the reactive power has already been demonstrated above with equations (2-5) & (4-1). As Reactance (X)>> Resistance (R), the variations in reactive power affect at a higher rate the voltage drop than any variations in the active power, P. This can lead to the disconnection of wind farms and may threat the system´s power stability.

4.5.3. Dynamic Simulations Outcomes

4.5.3.1. Testing the DFIG into the Island´s Power System

In order to test the wind turbine riding through capability over perturbations, a bolted three-phase symmetrical fault was applied on the distribution connection point of the wind farm, which was loosely selected to be the bus SEVF rated at 30 kV. The fault is applied one second after the initiation of the simulation lasting for 200 milliseconds. This time corresponds to 9 cycles for the 50 Hz system and the total simulation time was defined at 20 s. During the fault, the wind turbines and the system´s conventional generators performance was investigated under this circumstance as the figures illustrate beneath.

Figure 4-23, represents that during the fault on the 30 kV interconnection point, the voltage at addition bus drops to zero, whereas the terminal voltage of the wind turbine bus depresses by almost 90% reaching the value of 0.1 pu. It was expected that the voltage reduction in the WT terminal bus would follow the same pattern as for the faulted node; however the minimum terminal value for the former is higher. After fault, at 1.2 seconds, both sites gradually recover to 1 pu. The 90% voltage depression can be attributed to the fact that the wind turbine generators are directly connected to the faulted bus via transformers and are not stood off from it.

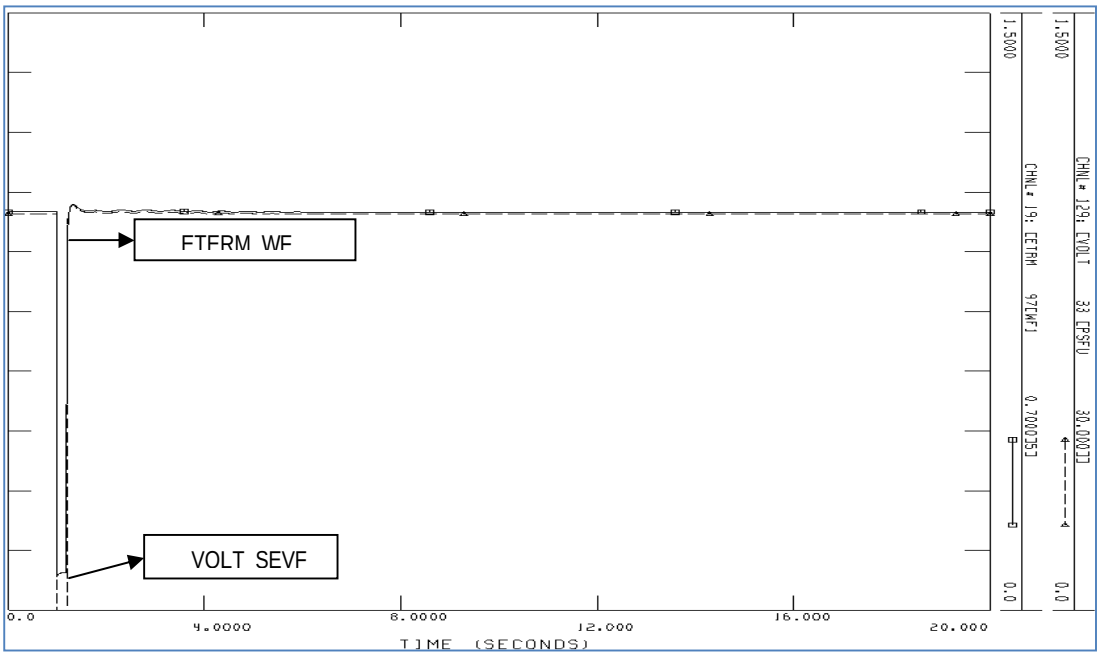

Fig. 4-23: Voltage response for WTG terminal & 30 kV Wind Farm bus bar after a 3-phase fault incident.

Figures 4-24 & 4-25 illustrate the mechanical, electrical and reactive power output (Fig. 4-25) of the wind turbine generators during the short circuit occurrence. The most critical for WTGs is when the fault occurs at the connection point of the transmission network. Examining the active power response, is observed that during the fault, the rotor speed increases giving a negative slip and starts to accelerate. Actually, there is a difference among the electrical and mechanical power, where the former tends to be zero (decrease). Mechanical power at the beginning remains the same and after the fault starts to oscillate causing mechanical stress in the drive train system. The pitch module responds by altering the blade pitch angle (increases) during the fault in order to reduce the mechanical power. Both, electrical and mechanical outputs are reduced during the fault event and their oscillations last about 5 s, where the generator tries to restore its pre-fault value. It is worth mentioning that a few milliseconds after fault, the generator operates as a motor thus absorbs a great amount of real and reactive power.

The wind farm generates active power (Fig. 4-25) immediately after fault clearance and helps to keep it in operation during the fault sequence. Furthermore, Fig. 4-25 shows that wind turbine generators during fault supply with reactive power the grid and comply with the Wind Grid Code. During the fault, reactive power injection to the grid increases to support voltage drop. After fault (for shortly), reactive power oscillates probably due to the magnetization of the rotor windings in the generator. Besides, the DFIG offers the capability of controlling the reactive power and thereby controlling the voltage on the grid.

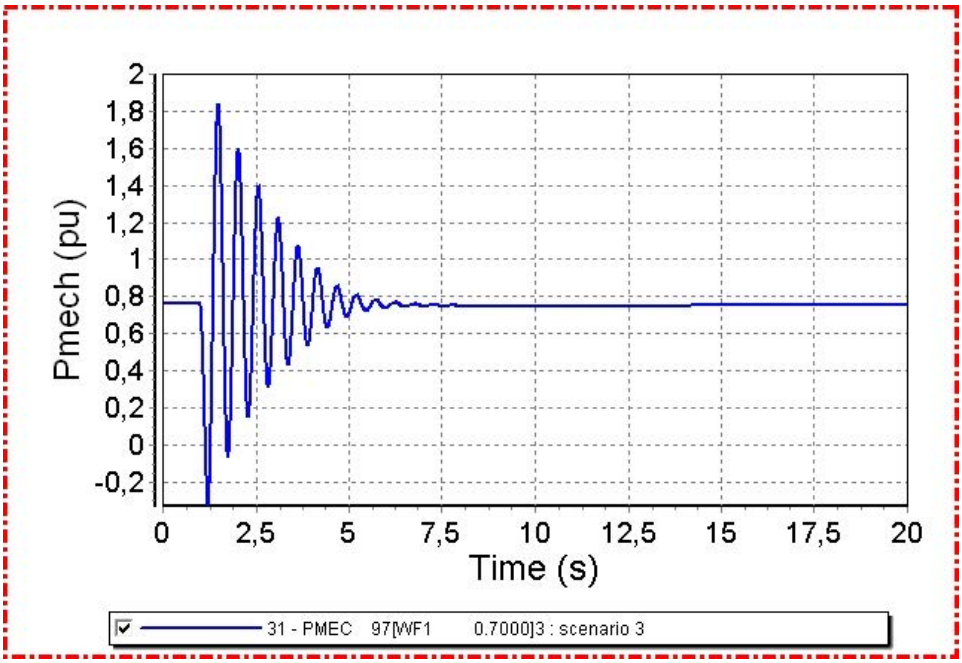

Fig. 4-24: Mechanical power of DFIG after the 3-phase fault incident.

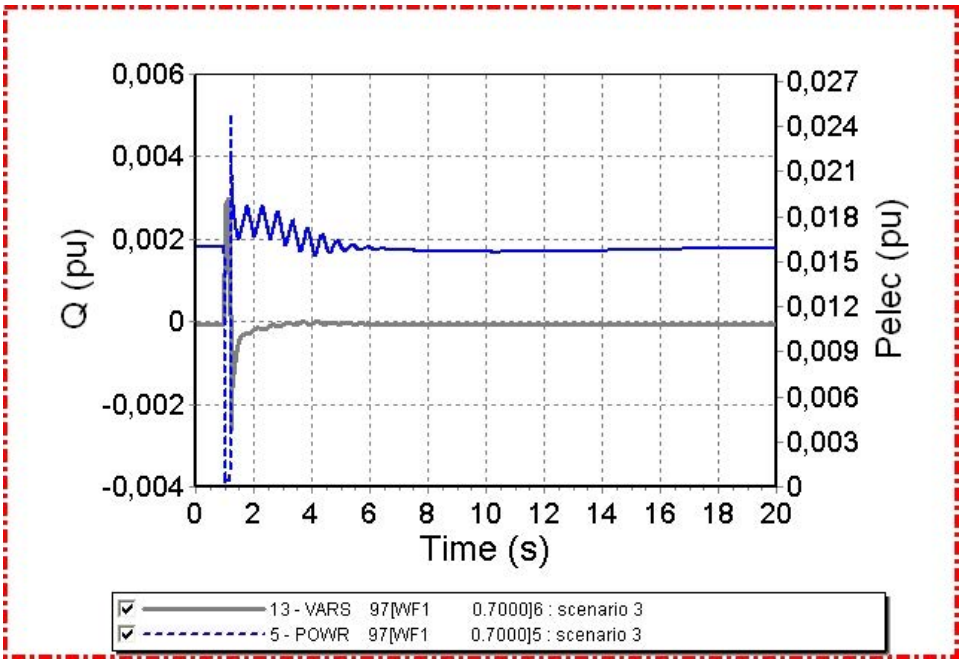

Fig. 4-25: Electrical and reactive power output of DFIG after the 3-phase fault incident.

Frequency increases (Fig. 4-26) during the fault time as rotor speed increases to minimize the drive-train loads due to mechanical stress. Oscillations last up to 5 seconds where both locations restore their initial value. In addition, variations in frequency figures do not overpass the 0.2 Hz with the minimum value being at 49.8 Hz.

Figure 4-27 justifies the explanation above for the mechanical power output (Fig. 4-24). Pitch angle increases during fault in order to minimize mechanical power and oscillates strongly following the same pattern with the latter.

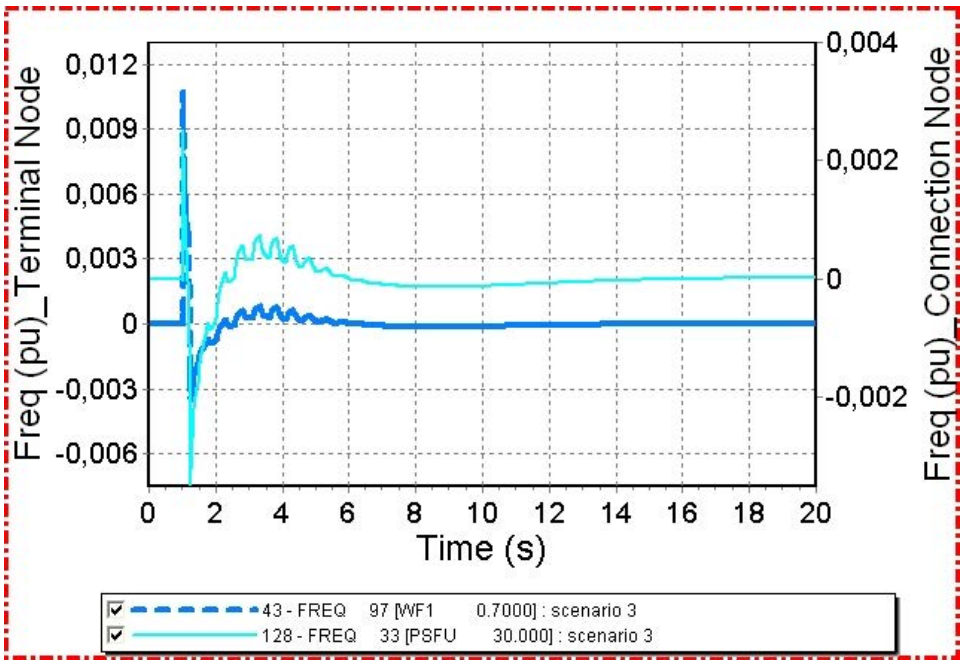

Fig. 4-26: Frequency deviation at the wind farm (WF) connection node & WT terminal bus.

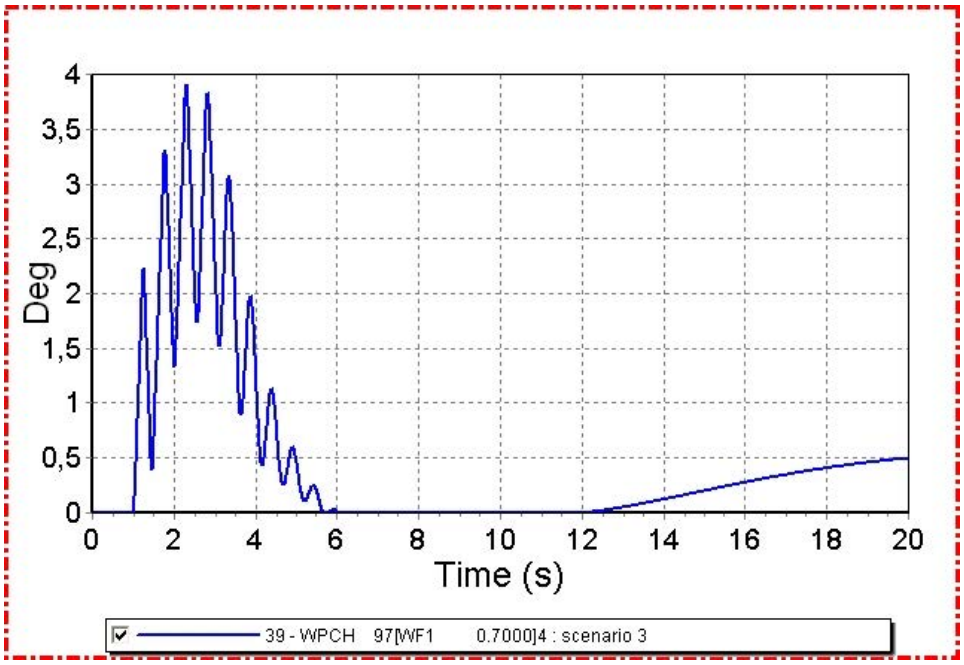

Fig. 4-27: Pitch angle response after a 3-phase fault incident.

Figure 4-28 represents the voltage dips of conventional generators during the fault event with the minimum value being at 0.84 pu. All of them reach the new steady-state condition in a few of seconds. The increased requirement in reactive power demand can justify the voltage drop at the terminal buses of the conventional generators, whereas recovery is obtained immediately after fault occurrence (Fig. 4-29).

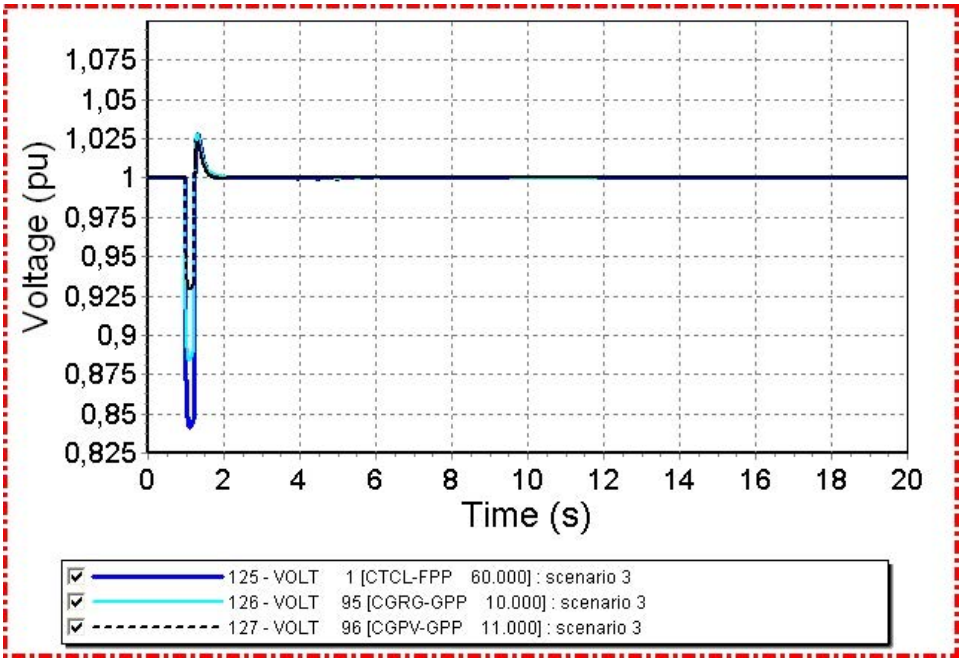

Fig. 4-28: Voltage response of the conventional generators after a 3-phase fault incident.

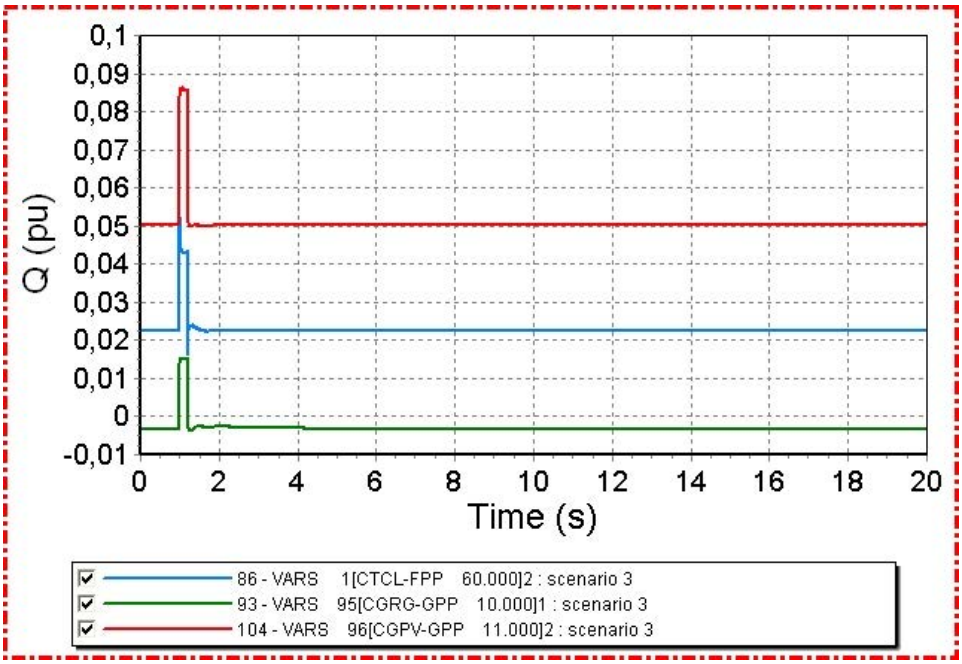

Fig. 4-29: Reactive power output of the conventional generators after a 3-phase fault incident.

Figure 4-30 shows that the machines are stabilizing together. Moreover, Fig. 4-31 justifies that the tripping behaviour of wind turbines during the fault incident- they produce almost zero electric active power, imposes the necessity to the conventional generators increase their active output. The new steady-state situation is achieved in about 5 seconds.

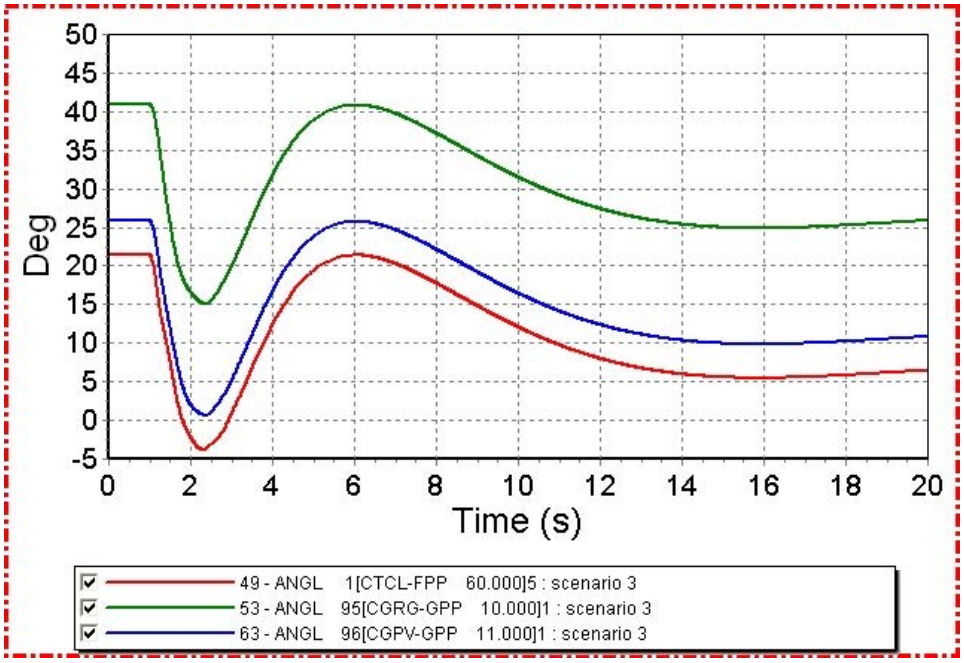

Fig. 4-30: Relative rotor angles of the conventional generators after a 3-phase fault incident.

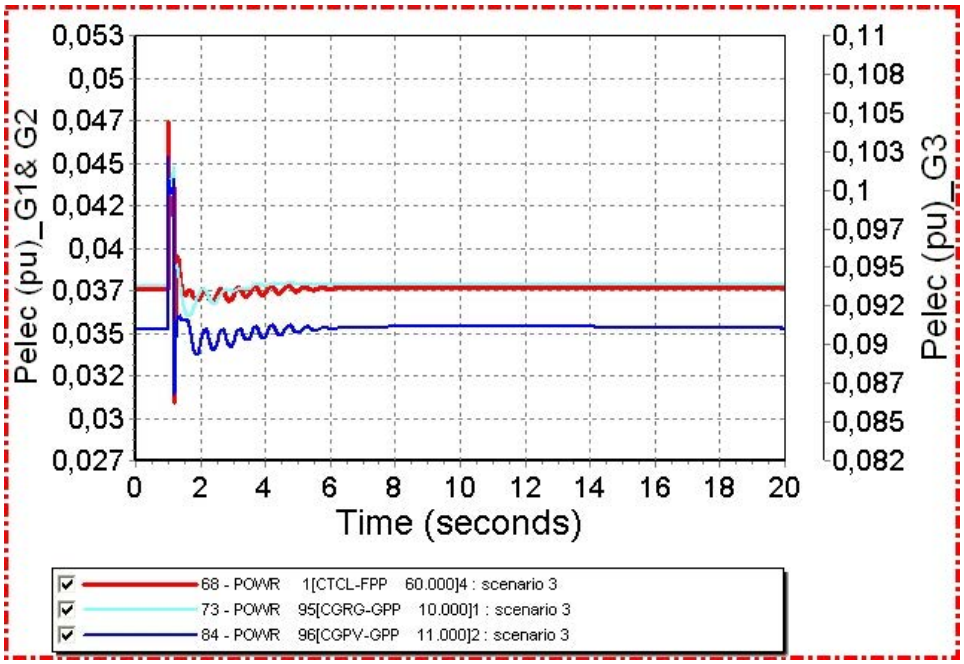

Fig. 4-31: Active power output of the conventional generators after a 3-phase fault incident.

4.5.4. Performing Various Dynamic Studies

In this part some additional dynamic analyses are realized which are typical to describe the stability behaviour of the system under different disturbances. Transient stability in terms of power, frequency and voltage behaviour is examined against a principal generator loss, an important transmission line disconnection and a three-phase fault at the swing bus.

4.5.4.1. Loss of one central thermal generator (CTCL-CPP swing bus, 60 kV)

The Figures beneath (Fig. 4-32 & 4-33) illustrate the system correspondence after such a loss. The generation that is taken out of operation is of 8.32 MW. The variations in frequency at the transmission substation nodes during transit oscillations are lower than 0.225 Hz, whereas the frequency reaches approximately the value 49.9 Hz in about in 20 seconds. Voltages during the perturbation time remain over the 98% (Fig. 4-33) of the nominal value (0.9875 pu) and after that period of time recover to a new steady-state condition. Fig. 4-34 shows these active power outputs of the remaining generation units during the fault occurrence. It was truly accepted that the remaining conventional and dispersed machines need to increase their output to compensate for the loss of a generator unit.

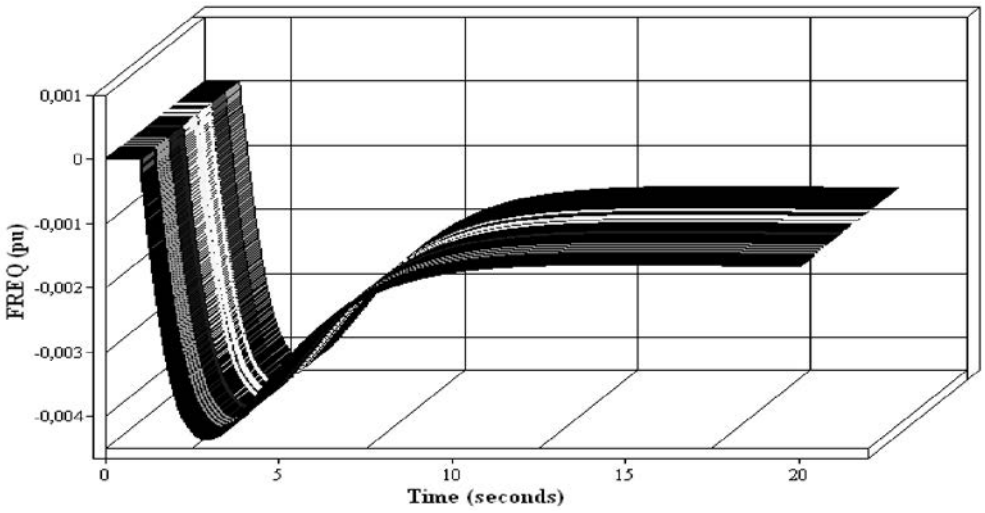

Fig. 4-32: Frequency deviation at the transmission substation nodes after a slack generator loss.

4.5.4.2. Loss of the transmission line CTCL-SEFO rated at 60 kV

As it can be easily seen from Fig. 4-35, the voltage drops slightly for all the substation nodes with the highest dip being noticed at the terminal bus of the tripped line, SEFO rated at 60 kV. Nevertheless, in all cases the reductions do not fall under impermissible values (±2%). Figure 4-36 depicts the frequency deviation at the transmission substation nodes during the fault incident. It fluctuates with peaks below zero during the line tripping and a new steady-state is also obtained under zero value, shortly after 9 seconds. The frequency drops, because a generator is lost and the others will supply to share the load. The remaining generators´ governor speeds will decrease due to lower droop contribution and set a new steady frequency below its nominal figure established at 49.999 Hz. The biggest frequency oscillation belongs to SEPD1 60 kV substation bus but all remain within the permissible limits.

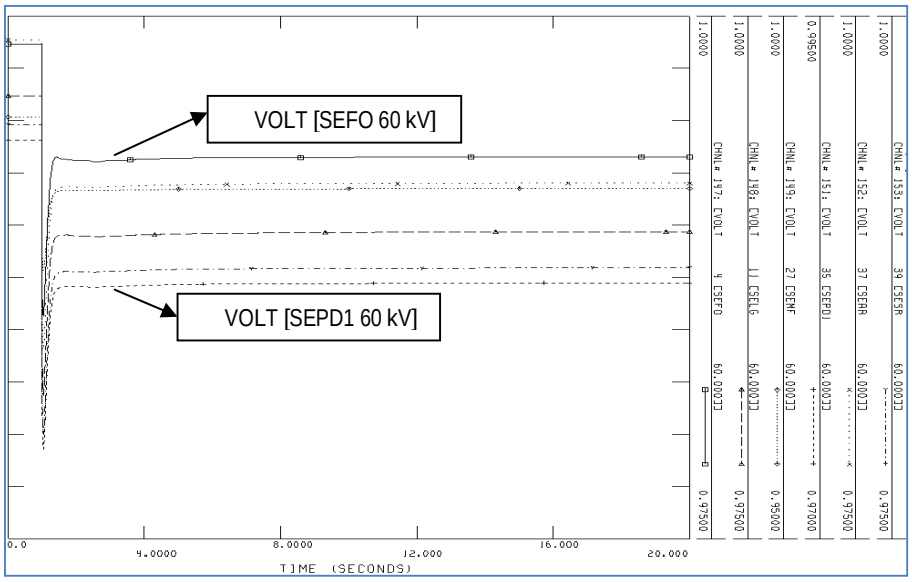

Fig. 4-33: Voltage deviation at the transport substations after a slack generator loss.

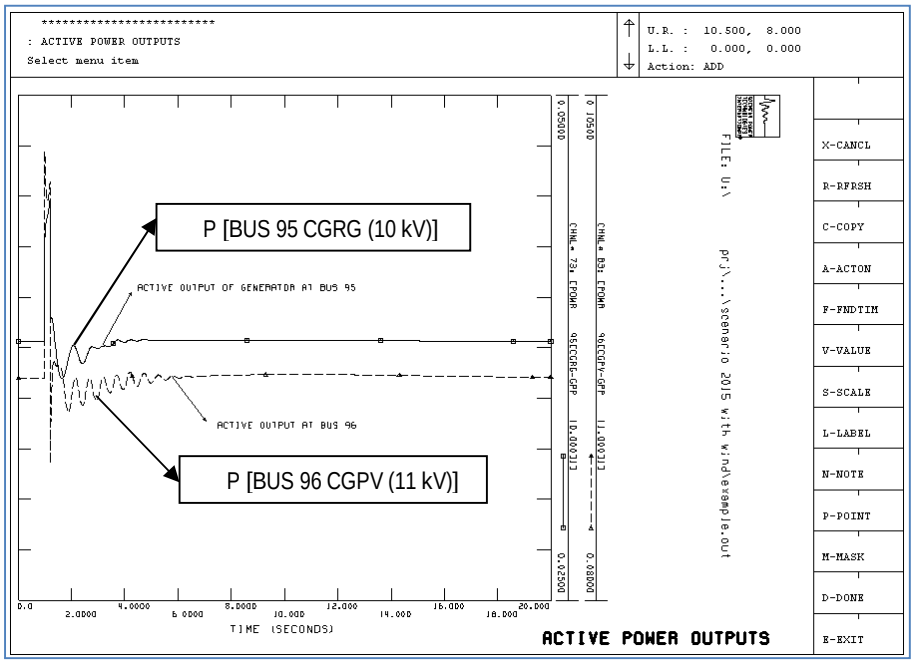

Fig. 4-34: Power outputs of the generation units in operation during the fault incident

4.5.4.3. Three- phase fault at swing bus 1 CTCL-CPP rated at 60 kV

Figures 4-37 to 4-40 represent the effects on transient stability may induce on the system a three-phase fault at the slack bus. During fault time, the WT generator terminal voltage (Fig. 4-37) and active power output (Fig. 4-38) are reduced with the former obtaining the 30% of its nominal value and producing about 450 kW (rated value 1.6 MW).

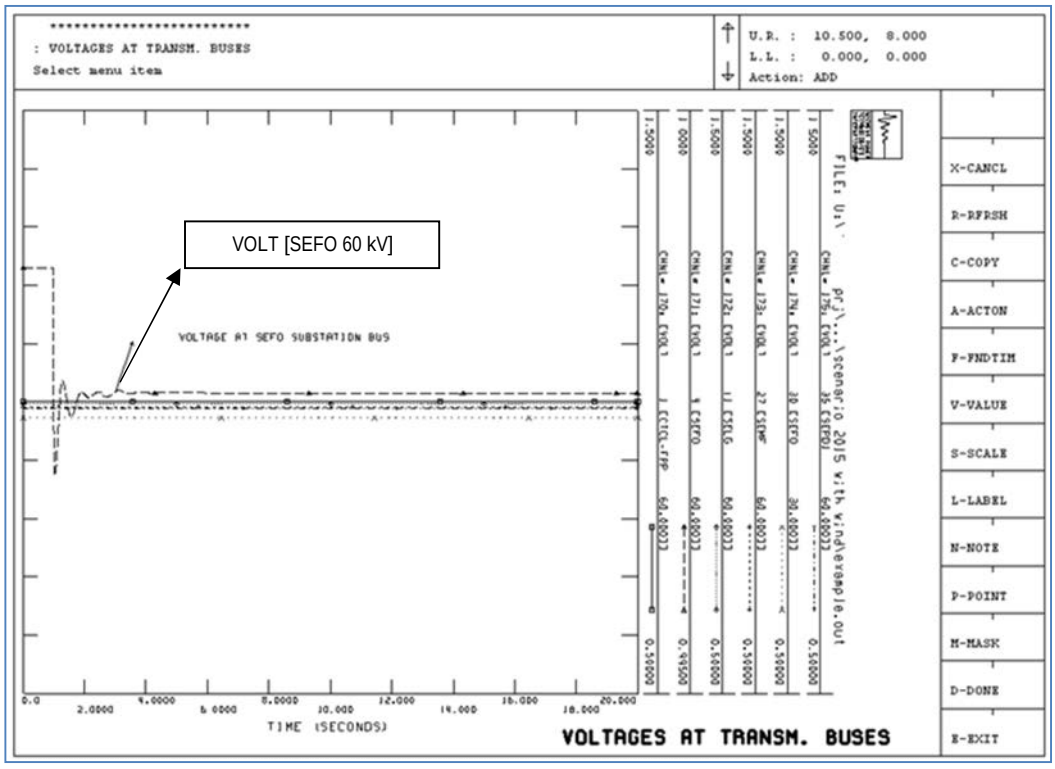

Fig. 4-35: Voltage deviation at the transport substations after a transmission line loss.

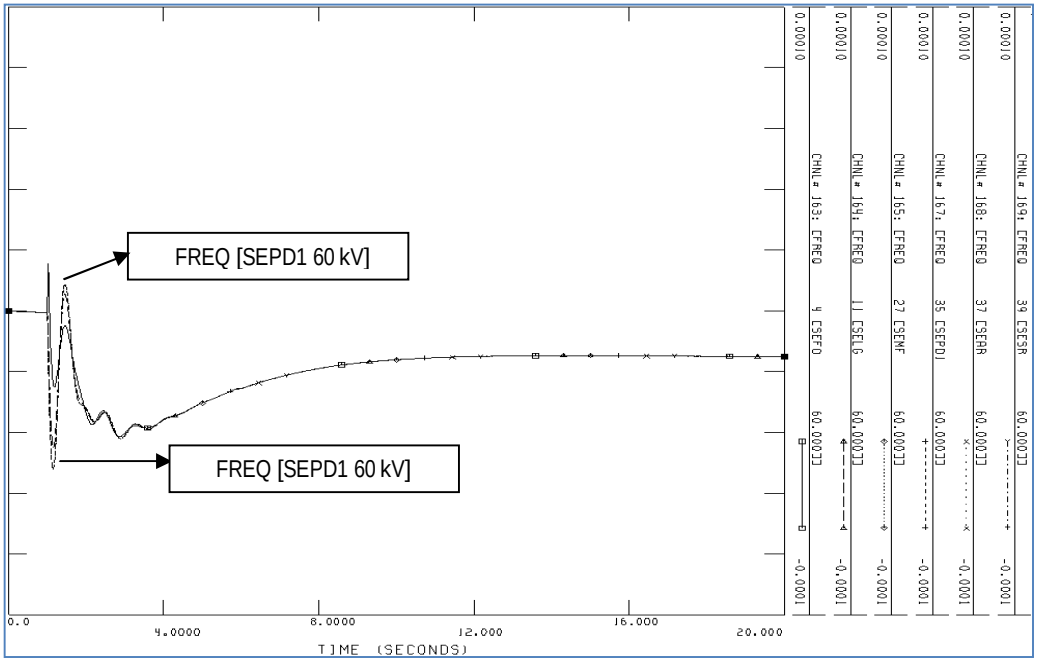

Fig. 4-36: Frequency deviation at the transport substations after a transmission line loss.

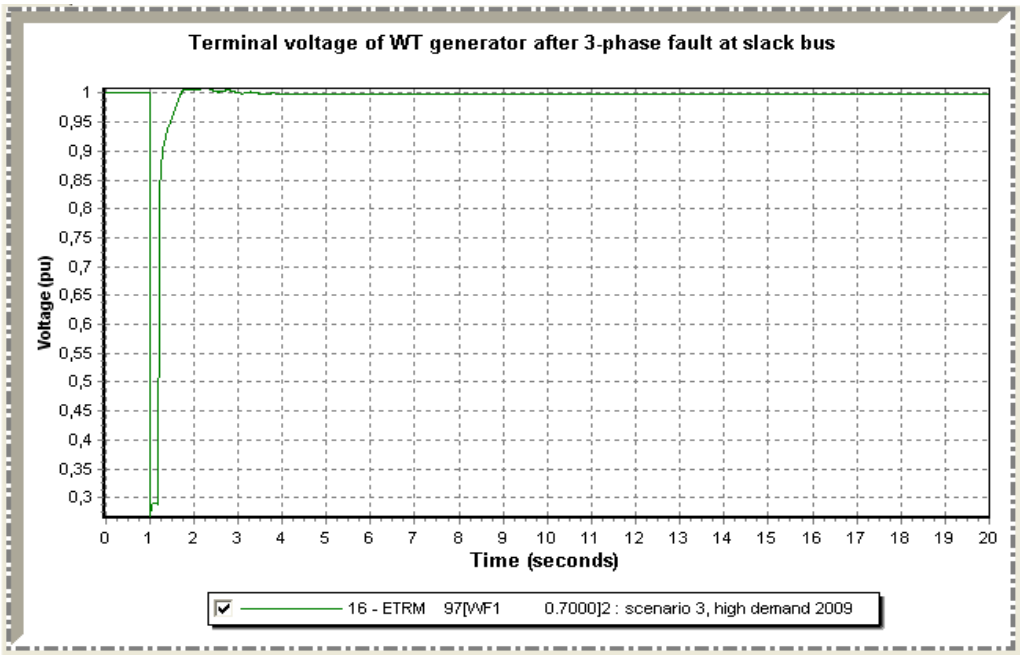

Fig. 4-37: Voltage terminal value of WT generator after 3-phase fault at slack bus.

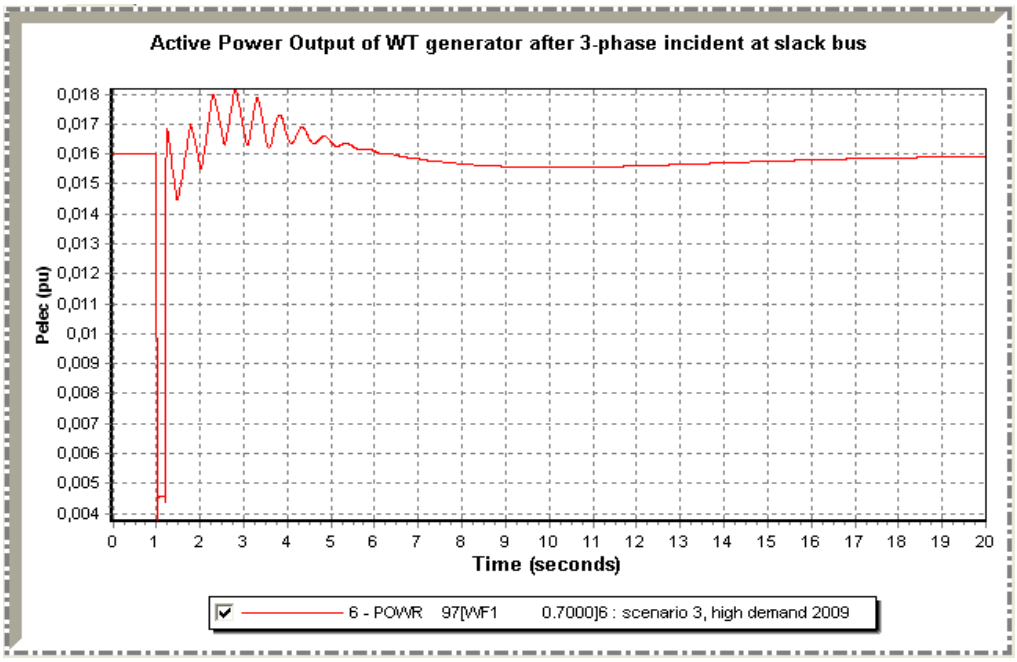

Fig. 4-38: Active power output of WT generator after 3-phase fault at slack bus.

Voltage values at the substation nodes all drop almost by 90% but soon after the fault recover to the pre-fault values (Fig. 4-39). Similarly, frequencies deviate sufficiently and increase no more than 0.4 Hz during fault period time (Fig. 4-40). In all cases a new steady-state condition is achieved.

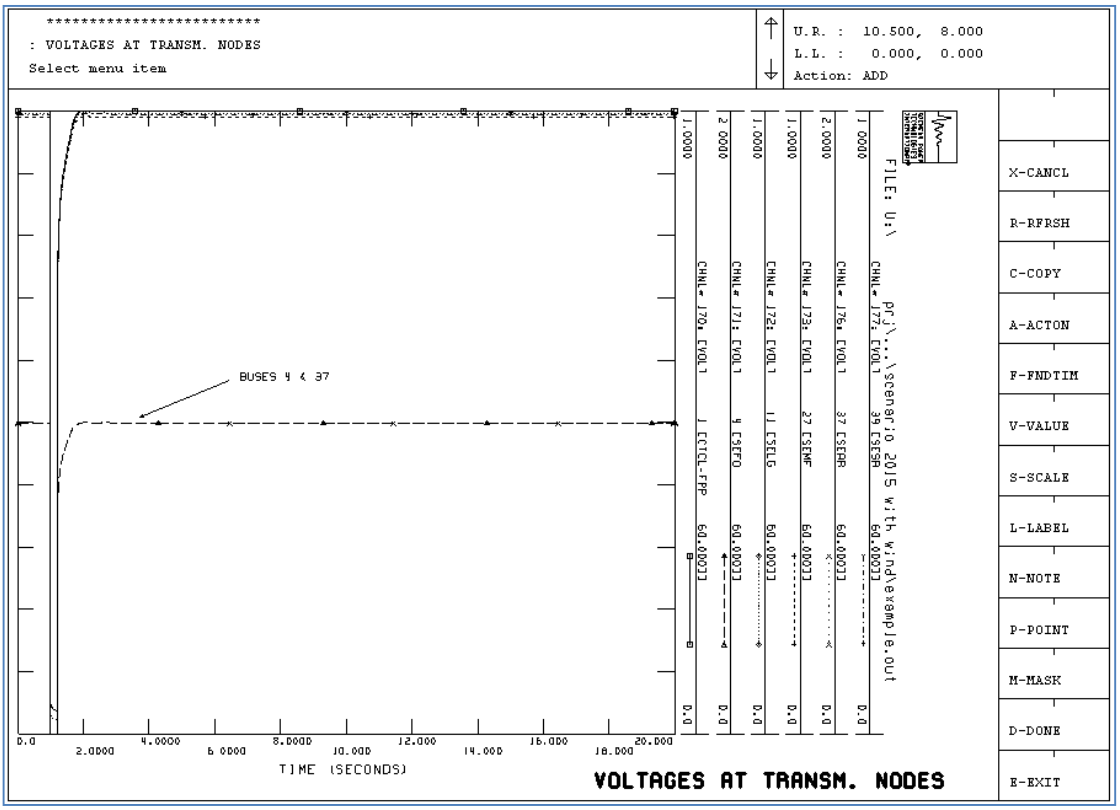

Fig. 4-39: Voltage values of transmission nodes after 3-phase fault at slack bus.

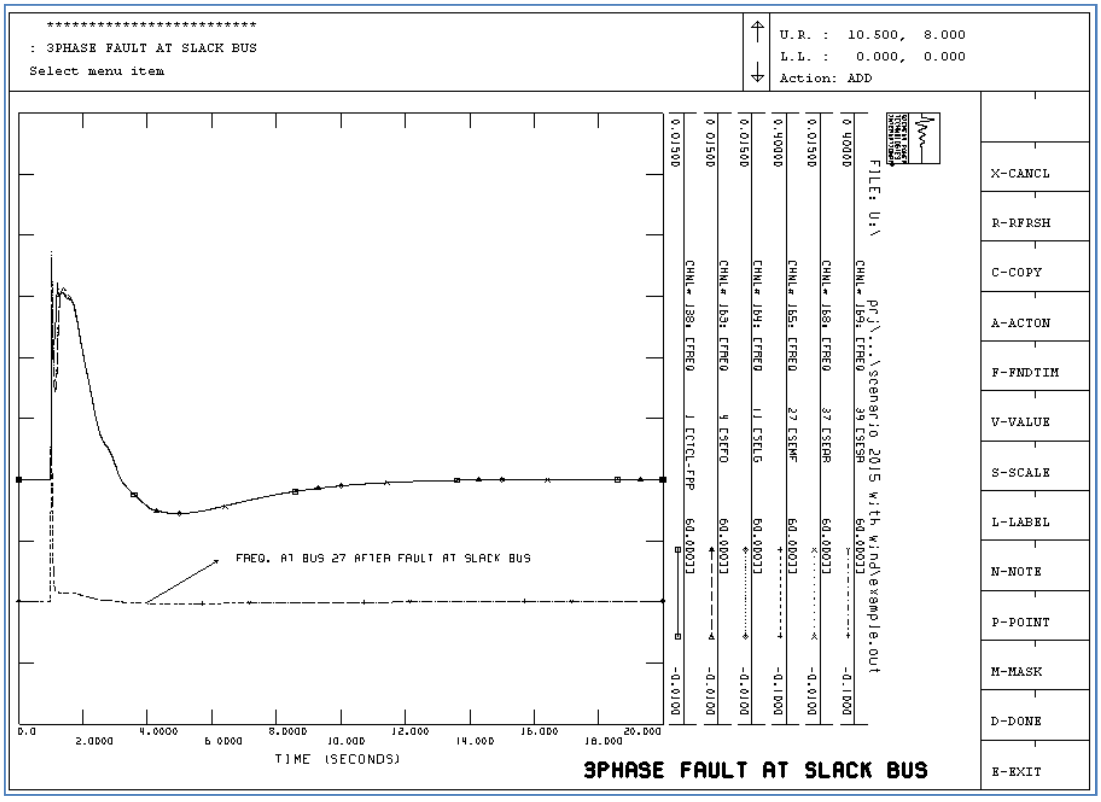

Fig. 4-40: Frequency deviations at transmission substation nodes after 3-phase fault at slack bus.

4.5.5. Open-Circuit Set Point Step Tests

In this research, there were performed open circuit set point step tests for two exciter models namely, EXST and IEET1 to identify the exciter that is not well-tuned. Throughout this simulation, each generator being tested is initialized to unity terminal voltage on open circuit. Furthermore, a simple step change of 5% (typically from 0.01 to 0.05) is applied to the voltage regulator references and the resulting responses of field voltage and generator terminal voltage are observed. The step magnitude should not exceed the 10% since the objective of this test is to examine small disturbance behavior.

The excitation system IEET1 at bus 1-CTCL (swing bus) is very oscillatory for K_F=0.02 compared to EXST model for the same synchronous machine (Fig. 4-41). The typical tuning gain parameters of a rate feedback type excitation system are T_F and, more particular K_F. Figures 4-41 to 4-43 illustrate the effects of exciter tuning on the field voltage and generator terminal voltages for the different excitation systems. A value of K_F=0.08 pu is observed to yield an acceptable open circuit response. IEET1 and EXST models are indicated as 1 and 2 respectively in the following graphs.

Figure 4-44 depicts the blocks of the EXST excitation system in PSS/E. The variable limiter has minimum and maximum values of V_TV_{RMIN}-K_CI_{FD} and V_TV_{RMAX}-K_CI_{FD} respectively. This limiter is operated as input of the generator terminal voltage (V_T) and field current (I_{FD}) including a constant parameter K_C.

From Fig. 4-41 & 4-42, it can be seen that the field (EFD) voltage response for the EXST exciter model is very exact during the step signal being applied to the exciter set point and the final steady-state profile has a good convergence characteristic.

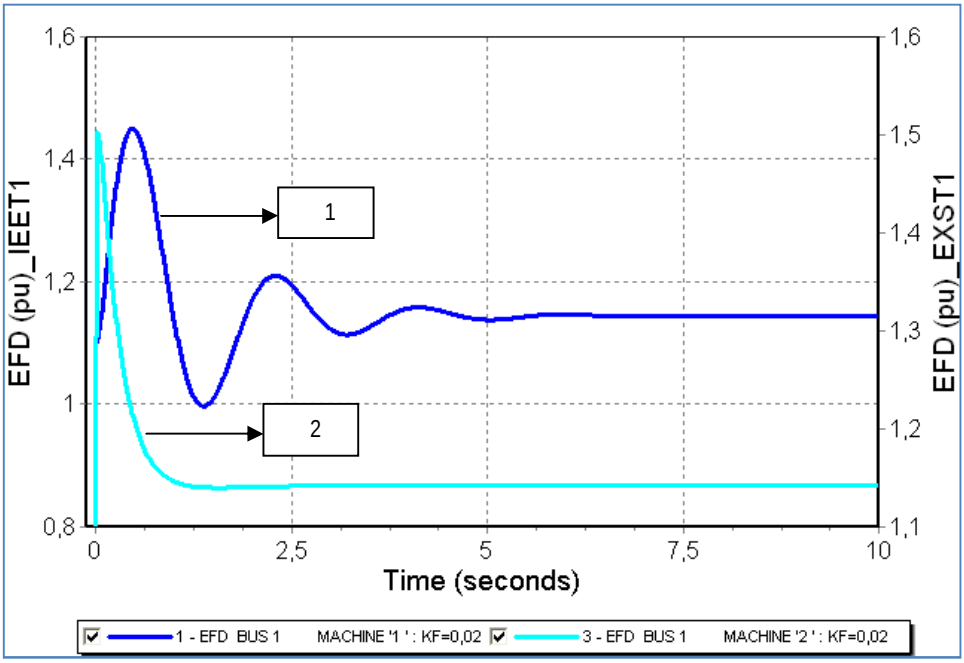

Fig. 4-41: Field voltages for IEET1 & EXST exciter models.

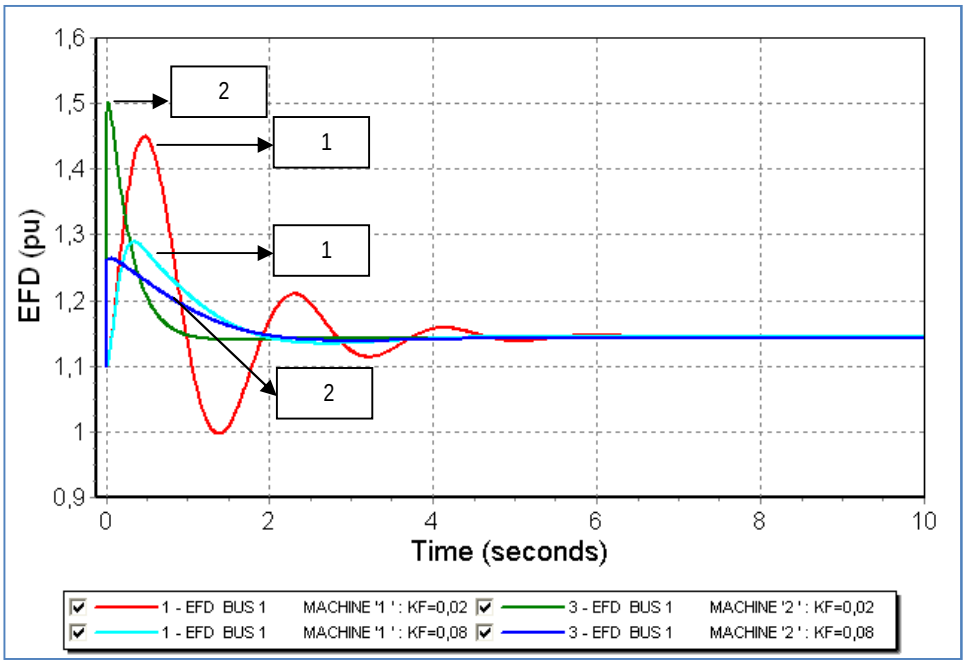

Fig. 4-42: Effect of exciter tuning for IEET1 & EXST excitation models.

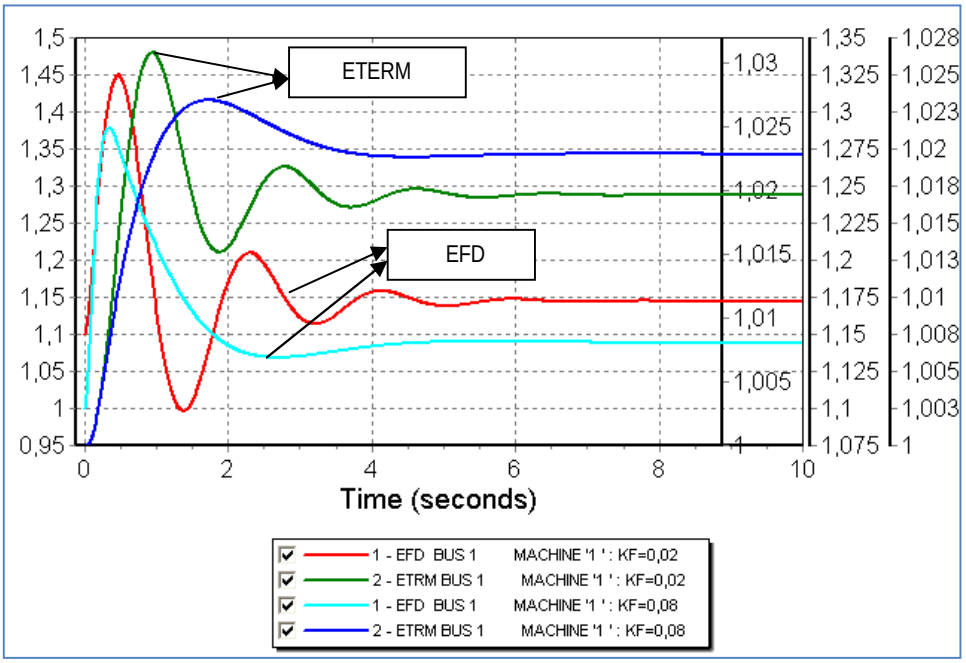

Fig. 4-43: Field and terminal voltage responses for IEET1 exciter model.

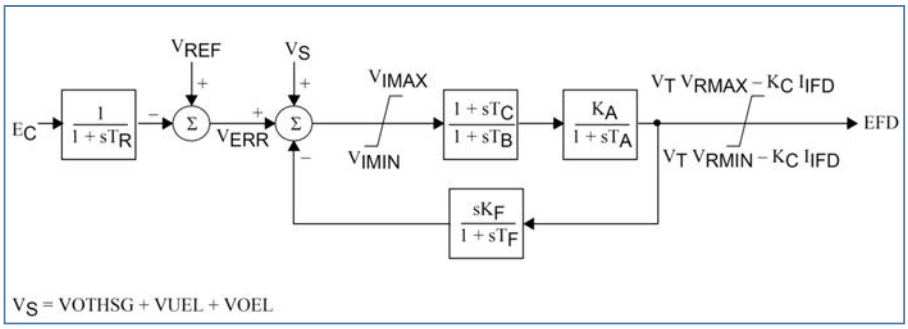

Fig. 4-44: EXST exciter model in PSS/E [11].

4.6. Summary

The main goal of the present work was to propose the potential areas for the introduction of renewable energies into an autonomous power grid. In this case hydroelectric power plants were not taken into consideration as their potential is very small compared to the total system handling. Focus was concentrated upon wind power and geothermal installations. To achieve this objective it was necessary to accomplish load flow, contingencies (N-1), short circuit and dynamic analyses. PSS/E version 31.0 software tool and its wind turbine model WT3 are used for the relevant simulations throughout this work.

4.6.1. Discussion on Steady-State Analysis

Within this thesis three case Scenarios were defined to check the system´s voltage and frequency stability with the addition of 25.77 (Scenario 2) and 14 MW (Scenario 3) of geothermal and wind power respectively. In each Scenario, high and low demand configurations were employed, except for Scenario 3 that only high load requirement was considered as it is the worst case scheme.

- Scenario 1, year 2009 base case
- Scenario 2 year 2015 additional geothermal power
- Scenario 3, year 2015 with wind energy and geothermal power.

The autonomous power system consists of a main thermal plant and two big geothermal power stations. The fossil fuel plant is not only at the centre of the transmission network but also is the only conventional source of the island. For that reason, the slack bus was chosen to be the high transmission voltage node of its substation (1 CTCL-CPP, 60 kV).

Throughout the Scenario 1 & 2 case studies, there were not observed voltage violations, but thermal line overloading rated between 124% and 128% against their power ratings for high and load demanding respectively. In Scenario 3, various substation nodes were examined to add wind power to, the ones selected as most suitable, voltage and thermal violations follow the same pattern. Wind power inclusion under specific scattering and connection topology cannot affect the electrical system and reduce the losses. Concretely, the total system losses with only geothermal generation added accounts for 1.1 MW+8.9 MVAr, whereas encountering wind generators addition at specific nodes the losses differentiate accordingly. Nevertheless, the impact on power losses is minimal in all cases as the amount of power added was small compared to the total system handling capacity. Moreover, it is important to note that power balance is kept as the conventional generators´ output is controlled and readjusted according to the system demand.

The results drawn from N-1 study showed that wind energy penetration improves the system security, especially when wind power is more distributed. The most critical results in terms of voltage and thermal violations were concluded when disconnecting the line between 1 CTCL and 27 SEMF substations rated at 60 kV. This can be attributed to the fact that SEMF substation has to satisfy a high load demand at its 30 kV node and at the nearby buses that is connected to via several distribution lines. The three main substations that connect the transmission to the distribution network are SEFO 60/30, SEMF 60/30 and SEPD 60/10 kV, where the power flow though transmission and subsequently through distribution branches depends on the transmission lines that initiate from 1 CTCL-CPP bus, the slack bus.

Short circuit analysis showed that the penetration of wind power and generally of distributed generation raises the short circuit level. Especially, a three-phase fault implemented at the addition bus increases the short circuit current at this bus and to the ones interconnected to it via branches. One solution to minimize the short circuit level could be to increase the impedance of the HV/MV transformer of the network or adding some fault current limiting devices such as reactors.

4.6.2. Discussion on Dynamic Analysis

A three-phase fault was implemented at the connection node of the wind farm whereas voltage, real, reactive power and frequency behaviour were examined not only for the wind turbine generators but also for the conventional generators. The short circuit current is increased at the addition bus and to the ones interconnected to it via branches. In all cases, a new steady-state is achieved according to the pre-fault value. Moreover, the wind farm as introduced to the Island´s electrical system remains connected under voltage dips caused during the fault on the transmission and/or distribution voltage connection node. The results proved to be more critical when power installation was scattered among different distribution nodes since the frequency and terminal voltages where the wind power is connected to, after a three-phase fault application, need more time to recover to their pre-fault values. Specifically, the terminal voltage of wind generators drops significantly and frequency´s long in duration oscillation depicts that system´s stability is disturbed.

Additional fault incidents were implemented such as the loss of a swing generator, the outage of an important transmission line and a three-phase fault application at the slack bus. The results showed that the voltage and frequency behaviour at the system's substations does not fall under impermissible values, while they are soon after the fault clearing reset to their initial conditions. In more details, when a symmetrical short circuit is applied to the slack bus, voltage and frequency values at the terminal bus of the wind generators and the substations recover adequately where the later ones do not vary more than 0.4 Hz.

Chapter 5. PHIL Experiments for DER Integration

5.1. Introduction

The structure and characteristics of LV distribution networks and particularly of Islands or autonomous grids may provoke problems and constraints which lead to limitations of the DG integration level into this type of power systems. In respect to these limitations, aspects like voltage deviations, reactive power control, power quality and reliability need to be considered. Therefore, the energy management and interaction of DG units penetrated into LV distributions networks has to be assessed.

Power quality measurements are of high concern, especially in diesel-powered Island or Microgrid systems, since the majority of most small Island power systems and off-grid remote areas are relied on diesel-fuelled generators to fulfil their energy necessities. Particularly, one important issue questioned in islanded networks is the transient behavior of diesel gensets during critical disturbances induced by intermittent power sources and load step changes and more than that, the degraded power quality caused by their inherit torque oscillations.

Voltage deviations induced by load changes and power delivery limitations are observed during reactive power unbalances. Reactive power control and subsequently voltage control are necessary for regulating the voltage levels across the distribution feeders. In more details, the nodal voltages which represent the connection points of distributed generation must be regulated in order to be maintained within specific limits that is a significant power quality criterion in electricity supply.

Switched capacitors, reactors and VAR compensating devices such as Static Synchronous Compensator (STATCOM), commonly advantageous for industrial applications, are used to control reactive power flow and thus maintaining voltage in electrical systems and have proved to be effective since they can reduce the energy transfer limitations mentioned above under normal and fault conditions. Besides, STATCOMs have already been applied to distribution systems, i.e. 400 V and medium voltages, namely 35 kV, 10 kV etc.

Apart from VAR compensating devices, distributed generators interfaced to power electronic converters are, usually, controllable reactive power sources. Additionally, the energy storage systems (i.e. DC Capacitors or Supercapacitors) which are introduced as backup sources are able to control the active power flow and can be key effective solutions to increase distributed generation in an Island power system or generally in a LV distribution network.

This research study discusses the performance of real time and PHIL simulations to emulate and verify the ‘‘smart’’ coexistence of central and decentralised generation very close to realistic conditions utilizing an impedance as hardware-under-test (HuT) in order to examine the generation plants integration into LV distribution networks. As mentioned above, in Section 1.4.2, this research work studies two sets of tests; The first case study elaborates the testing of an average model of STATCOM in real time simulation platform and the second case study involves two blocks of experiments; a) the implementation of a Microgrid model in RSCAD/RTDS environment and b) the execution of various experiments in a real Microgrid test site. In the end, PHIL tests are performed for both case studies.

The chapter starts with a review on the tests executed indicating their technical objectives. In continuation, the basic implementation aspects such as the reference standards, testing method and the used equipment throughout the experiments are also detailed. Then follows a more extensive description of the simulation modeling and tests. The first group of real time simulations and PHIL experiments is analysed, where an average model of STATCOM is designed in the RSCAD/RTDS environment to investigate its impact on voltage regulation within a LV network. In addition, the second group of RSCAD/RTDS and PHIL tests is outlined which demonstrates the energy management system of a LV distribution network including a diesel synchronous machine and inverter-based sources. Finally, the conducted Microgrid experiments are discussed.

The last part of this chapter is dedicated to the discussion on the respective results. Moreover, a detailed description of the inverter-based STATCOM’s controller design is given. The current and voltage control loops are studied in order to define the respective transfer functions and the affiliated Bode plots as data reference for

verification of the selected inverter model. The outcomes regarding the energy management within the distribution power system were, then, verified at a real Microgrid (MG) infrastructure through experiments during which various tests were performed concerning the dynamic operation of the diesel generator and the battery- inverters within the LV islanded power system.

5.2. Background and Objectives of the Tests Executed

Real time simulations and especially Power hardware-in-the-loop simulation (PHIL) allow testing and validating the electrical properties of power system devices such as converters, wind energy generators, hybrid and energy storage systems. The most considerable advantage of this type of simulation platform is that the system can be interfaced to real hardware components, generally called HuT.

This kind of experimenting gives the possibility to test repeatedly and analyze the behavior of the physical device, very close to realistic conditions [117, 135]. For instance, the hardware part can be subjected to several simulated fault incidents and its resulting response can be verified.

The objectives of the two case studies, namely Case Study 1 and Case Study 2 analysed and discussed throughout this thesis, are outlined beneath.

5.2.1. Case Study 1: PHIL Technique Applied to a LV network for Integrating an Average Model of STATCOM with a Capacitor

A converter based Static Synchronous Compensator (STATCOM) is a shunt device that hosts voltage stability and mitigates voltage sags at the point of common coupling by absorbing or generating reactive power [136]. An energy storage system (ESS) connected to the DC bus of a STATCOM in generally in low voltage distribution networks or a Microgrid infrastructure appears to be a very promising solution for power quality issues since they can control the active power flow in the point of common coupling. In that way, the STATCOM's traditional operating modes, namely, capacitive and inductive will not be limited to reactive power compensation but it may be also feasible to control the active power flow within the STATCOM and the point of common coupling through charging/discharging the energy storage system [21-24]. Besides, storage batteries, ultra capacitors, flywheels, comprise backup energy storage devices, which must be included in Microgrids to ensure uninterrupted power supply. They should be connected to the DC bus of the Microgrid and be provided with ride-through capabilities during system changes.

The execution of real time simulations of a STATCOM model in RTDS has been limited up to now. However, within the literature A. Sattar et al., [131] research work is reported as an implementation of this kind of simulations, where a grid connected wind farm with a two-level inverter based STATCOM model was simulated in the RTDS to analyze the dynamic and transient characteristics close to realistic conditions. Throughout the proposed study it was shown that the terminal voltage of the wind farm remained at the desired value under different wind conditions and network faults. The above work was performed in the real time RSCAD/RTDS environment; nevertheless PHIL experiments were not conducted.

The applicability of PHIL technique for integrating VAR compensating devices such as Static Synchronous Compensators with a DC Capacitor is rather restricted up to now; hence this effort will be reinforced throughout this study.

5.2.1.1. Technical Objectives of the Tests

Firstly, the controller design of a three-phase voltage source inverter is studied, where the current and voltage proportional-integral (PI) controllers are extrapolated and implemented in the inverter-based STATCOM model. The

main objective of the gain regulators´ calculation, the low pass filter and cut-off frequency determination in line with the affiliated Bode plots drawn in Matlab, is to verify the trade-off between the inverter's dynamic performance and stability.

Moreover, an average model of STATCOM integrated with a DC capacitor into a three-phase LV network is simulated in RSCAD/RTDS environment and PHIL experiments are executed utilizing a variable resistance as hardware part. These tests have various aims and are indicated beneath;

The real time and PHIL simulations aim at investigating: i) the effects of STATCOM on voltage regulation at the common coupling of this inverter-interfaced source, ii) the reactive power compensation during step load changes in the hardware impedance, and iii) the inverter's control in order to maintain the DC-side voltage equal to a reference value by charging/discharging the capacitor.

Additionally, this research work aimed at modeling the Bootstcap Maxwell Supercapacitor that the ICCS-NTUA Power Systems Lab owns by taking into consideration conducted experimental measurements. The test procedure included charging and discharging the Supercapacitor. In that way, an experimental complete cycle of charging and discharging on a real energy storage device was executed in the Lab environment. Appendix S concentrates these results.

5.2.2. Case Study 2: Implementation of a Microgrid Model for DER Integration in Real-Time Simulation Platform

Throughout this study two blocks of experiments were accomplished. PHIL and real time simulations are executed to emulate the energy management system of a real Microgrid including a diesel synchronous machine and inverter-based sources. Moreover, conventional frequency and voltage droops were incorporated into the respective inverters. The PHIL laboratory tets are conducted as a data reference for verification. In order to complete this study a set of specific objectives were defined and are given beneath.

Finally, for tests aiming at analyzing the energy transfer in an AC Microgrid, a set of experiments were conducted related to the diesel generator and the battery inverters that were available in CRES premises. Their respective objectives follow.

5.2.2.1. Technical Objectives of the Tests

RSCAD/RTDS tests have the following objectives: i) modeling of a three-phase LV network in RSCDA/RTDS software that includes a diesel generator, feeders, various resistive loads and a three-phase battery inverter, ii) calculation of battery inverter´s droop curves (droop f & V) and iii) load sharing for parallel operation of the system´s power devices.

The execution of the Microgrid experiments aim at: i) evaluating the diesel generator and battery inverters´ active power droop control, ii) calculating f/P droop for parallel operation of three inverters (master-slave) during step load changes for load asymmetries and during a 24-hr load profile, and iv) load sharing for parallel operation of two battery inverters connected both in one phase.

5.3. Implementation Aspects

5.3.1. Reference Standard Procedure

During the experimental procedure no specific standards or guidelines were followed since there are no specific ones for Power Hardware- in-the-Loop tests. However, a reference PHIL procedure was followed. For example, the protections in the RTDS had to be tested in order to ensure that in case of a possible error in the simulation layer no

damage will be done to the equipment. Moreover, before the closed loop tests were performed, it is essential to check that the signals will be inserted to the simulated system having the correct characteristics of amplitude and phase.

During the experiments in the CRES' Microgrid no specific standards or specified procedures were followed. The evaluation regarded mainly feasibility and overall performance of the DER devices under different operating conditions and configurations. Also, the evaluation process of the results was done empirically.

5.3.2. Testing Method

For the PHIL tests, the testing methodology included the following steps:

- The entire network under study was numerically simulated using the RTDS system. The results helped us to examine the expected values of the flowing currents and node voltages in the simulated network.
- As already mentioned in Section 3.3.5, the protection models were added in the RSCAD draft in order to ensure the safety of the equipment.
- The closed loop of the PHIL simulation was modelled in RSCAD/RTDS in order to verify whether the whole system is stable or not.
- The physical setup was prepared. The measurement equipment was installed. Using oscilloscopes in addition to the RTDS runtime environment helped monitoring all the relevant quantities such as currents and voltages.
- The simulation system run in open loop, and the results were evaluated.
- The system run in closed loop and the PHIL tests were performed.

The steps followed for experimental implementation and testing in CRES' Microgrid are summarized below:

- The battery inverters used in the tests are the SMA-Sunny Island (SI) 4500 inverters. By default, one of the inverters is connected to the appropriate grid phase and can operate in all possible modes such as grid-forming and grid-connected with droop characteristics. The other two inverters were reconfigured appropriately so that they operate under different modes.
- The DER units that were used for the tests include 3 battery inverters (13.5kWp), 1 diesel generator (12.5kVA), one load bank (13.5kW), 2 PV panels (1.1 and 2.5kW) . The loads used in the tests are 3 groups of resistors (2.5, 1.5 and 0.5kW), which are combined appropriately in order to obtain the maximum number of combinations. The selection is done by the supervisory control via a look-up table and historical data that define the consumption profile. Apart from that, a reactive consumer (capacitor) was also used in one of the tests. The specific capacitor is a 3-phase 2.5kVAr component.

For the data logging and supervisory control, various communication protocols like Interbus, and SMANet protocol (RS485) were used during the tests. All data were collected and stored to the SCADA personal computer that uses LabVIEW. The fast transients and waveforms were measured by using oscilloscope.

5.3.3. Implementation details and Used Equipment

5.3.3.1. PHIL Experimental Set-Up

For the PHIL tests the following equipment sets were used:

- The Real Time Digital Simulator (RTDS) where the simulated network was designed. A desktop computer is necessary for the design of the network and the control of the RTDS.
- A single phase (5 KVA) AC/DC/AC converter provided by Triphase was used in order to allow the low power output signal of the RTDS to be amplified and used as a higher voltage signal. The control of the Triphase amplifier is possible using a desktop computer with the Matlab/Simulink program installed.

- The hardware under test was a resistor whose value varied according to the experiments.

Figure 5-1 depicts the PHIL topology as implemented in NTUA research infrastructure.

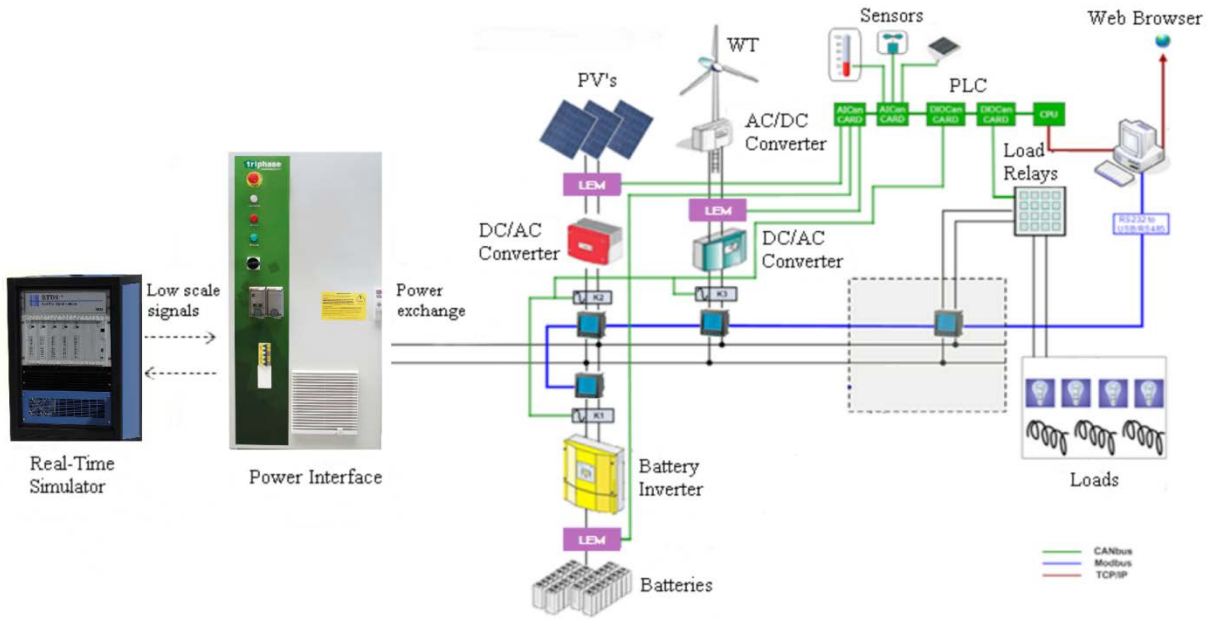

Fig. 5-1: PHIL environment in NTUA Lab for DER devices [127].

5.3.3.2. Microgrid Set-Up

Figure 5-2 illustrates the CRES Microgrid infrastructure [127]. The Microgrid was setup and used either in single or in three-phase configuration according to the specific test. Unbalanced loading was also examined. During the experimental part of the project the main equipment mentioned in Section 5.3.2 was used.

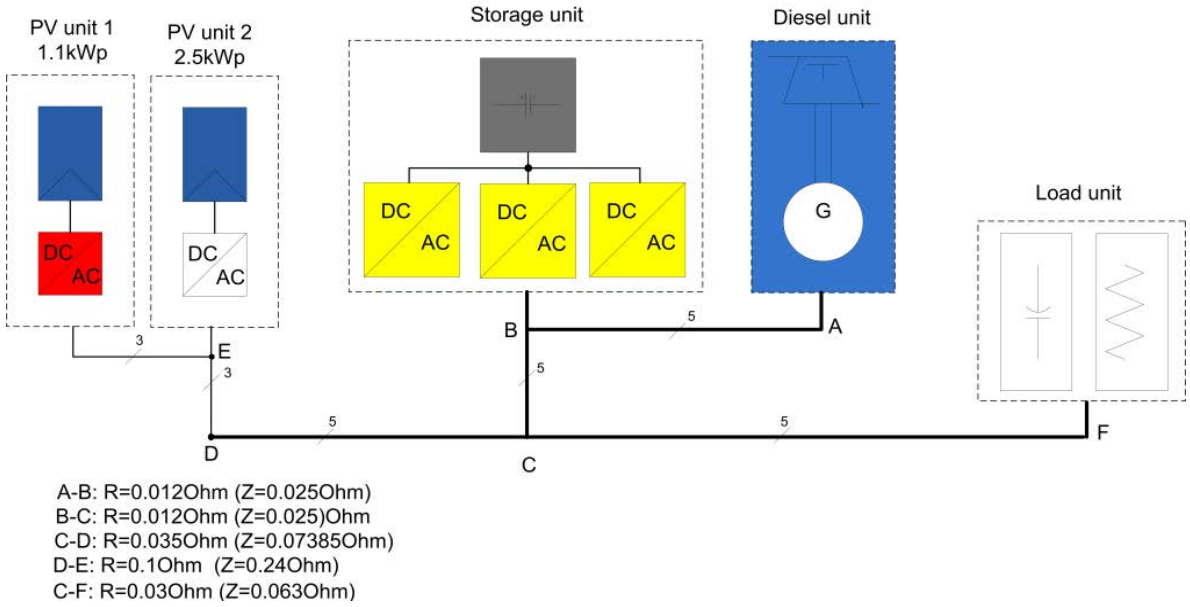

Fig. 5-2: CRES Microgrid topology.

Apart from these units other equipment like sensors and transducers were also used. In more details, the data logging included sensors and transducers (current transformers, active and reactive power transducers) but also for this purpose the data logging system built-in the battery inverters was used. Specifically, for the PVs and loads the used metering equipment included

- Current transformers, active and reactive power transducers for the electric power
- Voltage transducers for the RMS voltage measurement

The battery inverters were supervised and controlled in terms of frequency using their own system and via serial communication. Finally, the connection to the public grid point was monitored by using the existing three-phase power analyzer that is interfaced to the central SCADA by using serial communication and Modbus protocol.

The diesel unit´s droop for the Microgrid experiments is considered arbitrarily as -0.06Hz/kW according to its governor's settings. Moreover, it is defined by (5-1) where Δf is the absolute change in the frequency (Hz) and ΔP is the absolute difference in the output power (kW) that caused the subsequent change in the frequency.

$$R = -\frac{\Delta f}{\Delta P} \tag{5-1}$$

However, from (5-1) yields (5-2) that gives the frequency in Hz and power P in kW. A droop characteristic of f-P can be calculated by its droop (slope) and one more point as it may be easily seen by Fig. 5-3 beneath.

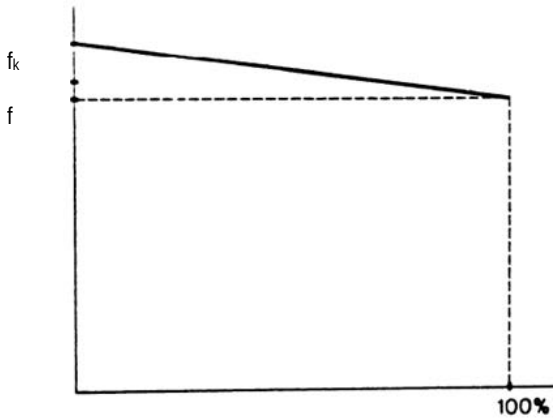

Fig. 5-3: Droop f-P.

$$f = f_k - \frac{Rf_{nom}}{P_{nom}} P \tag{5-2}$$

The diesel generator is studied in islanded mode under load variations where an increase in load demand imposes an increase in diesel power output and a subsequent reduction in speed.

In order to determine the frequency droop curve, one has to vary the active power exchanged by the generator with the Microgrid and measure the corresponding frequency at the output of the diesel genset. Thus, its f-P droop curve was experimentally derived under symmetric and asymmetric loads.

The f-P and V-Q droops of the SI inverter [137] are given by (5-3) and (5-4) respectively where the parameters are set to: i) Δf_{pu}=-2%, ii) ΔV_{pu}=-6%. Moreover, these droop curves were utilized for the RSCAD/RTDS simulations.

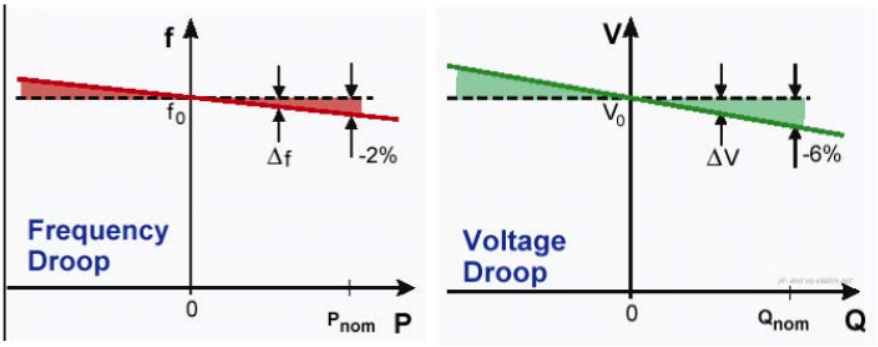

Fig. 5-4: Battery Inverter f-P & V-Q droop characteristics [137].

$$f=50-\frac{1}{3.3}P \Leftrightarrow P=3.3(50-f) \tag{5-3}$$

$$V=230-4.1818Q \Leftrightarrow Q=0.239(230-V) \tag{5-4}$$

The frequency droop curve was experimentally derived. In order to obtain each inverter's droop curve, data sets consisting of inverter's output frequency and active power have to be available. Not only the f-P droop calculation was evaluated but also the frequency, active and reactive power responses with static load changes.

5.4. Simulations Modeling for Case Study 1

Herein, the controller design of the inverter-based STATCOM model utilized throughout this research work is described. The analysis of the real time tests being conducted in RSCAD/RTDS software comes second and lastly, the performed PHIL tests are reviewed.

5.4.1. STATCOM Controller Design & Low Pass Filter Frequency Determination

5.4.1.1. DQ Reference Frame for Three-Phase Inverters

The definition of the control rationale and the calculation of the controller parameters are based on the following concepts; a) Average meaning, b) Mathematical description of the system: time and frequency domain, and c) The relationship between the temporary response and the Bode diagram [138].

In order to simulate the control of the Average Model of a three-phase inverter described throughout this study with its inherited control loops, well-established parameter values of DC/AC inverters were utilized concerning the PM (phase margin) and the cut-off frequency [139]. In continuation, the proportional gain values of the PI controllers for both, current and voltage loops in dq axes have been calculated and the corresponding Bode diagrams were plotted.

The dynamics for the AC side of the three-phase voltage source inverter (VSI) can be described by the differential equation beneath (5-5), where V_{inv} is the three-phase voltage output at the AC side of the inverter, V_L is the voltage applied to the low-pass filter (L) and V_{grid} is the grid three-phase voltages [126].

$$V_{inv} = V_L + V_{grid} = L_{filter} \frac{di_{grid}}{dt} + V_{grid} \tag{5-5}$$

Finally, the inverter's transformed three-phase voltage components into dq coordinates are given by (5-6).

$$\begin{cases} V_{inv\_d} = V_{grid\_d} - L_{filter}\omega i_q + L_{filter}\dfrac{di_d}{dt} \\ V_{inv\_q} = V_{grid\_q} + L_{filter}\omega i_d + L_{filter}\dfrac{di_q}{dt} \end{cases} \tag{5-6}$$

A more detailed analysis of the derived equations and the Park Transformation is given in Appendix T.

Fig. 5-5 illustrates the power stage of a VSI with its IGBT bridge schematic followed by a low-pass filter (L) connected to the grid.

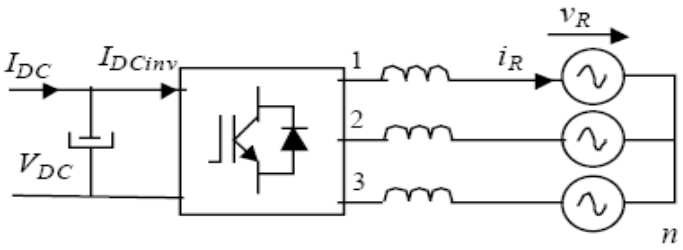

Fig. 5-5: Simplified grid-connected VSI with focus on L-filter [126].

The network topology including the STATCOM was first simulated in Simulink/Matlab as represented in Fig. 5-6, and then in RSCAD/RTDS. The system consists of an infinite bus, 2 LV lines and a load. The STATCOM is simulated like a VSI which consists of three controllable voltage sources generating and introducing the AC voltages into the network. The upper objective of the inverter's control is to try to maintain the STATCOM's DC voltage magnitude equal to a reference value by charging/discharging the capacitor. This control is deduced into two corresponding loops [126];

a) A current regulation loop (Fig. 5-7): This loop consists of two proportional-integral (PI) controllers that control the d-axis and q-axis currents. The controllers' outputs are the V_d and V_q voltages. The V_d and V_q voltages are converted into phase voltages V_a, V_b, V_c which are used to feed the controllable voltage sources. The i_d reference (in our case i_{d^*}) comes from the DC-link voltage regulator. The i_q reference (in our case i_{q^*}) comes from the q coordinate of the load current. This value is generated by the transformation of the three phase sinusoidal load currents I_a, I_b, I_c to i_d and i_q variables.

b) A voltage regulation loop (Fig. 5-8): A DC voltage controller which keeps the DC link voltage constant to its nominal value using a PI controller maintaining. On the DC side, the inverter is modeled by a current source charging the DC capacitor. The DC reference current $I_{DC\_inv^*}$ is computed so that the instantaneous power at the AC input of the

inverter remains equal to instantaneous power at the DC output (P_{AC}=P_{DC}). This is depicted in (5-7). In addition, the Simulink blocks of the Inverter and Capacitor control models depicted in Fig. 5-6 are further analyzed in Appendix U.

$$V_a I_a + V_b I_b + V_c I_c = V_{DC} I_{DC} \tag{5-7}$$

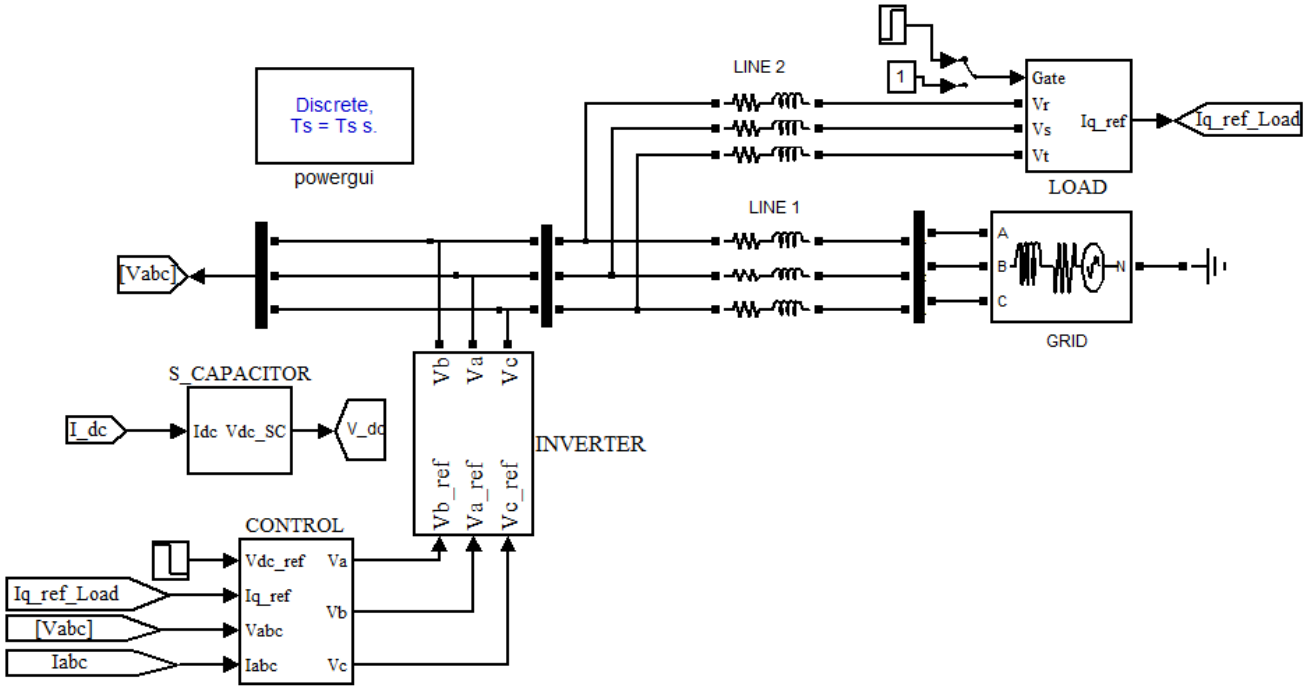

Fig. 5-6: Simulated network with STATCOM integration [126].

5.4.1.2. Current Control Loop

Fig. (5-7) illustrates the regulation of i_d and i_q current coordinates utilizing two conventional PI feedback inner control loops, one for each respectively. The values assigned with an * are the reference values whereas the ones assigned with sub-index fil are the filtered ones being measured [126].

The open loop transfer function for both current control structures is similar and is drawn by (5-8).

$$TF(s) = \overbrace{Kp_i \frac{T_{ni}s+1}{T_{ni}s}}^{\text{PI controller}} \cdot \overbrace{\frac{1}{L_{filter}s}}^{\text{Inverter}} \cdot \overbrace{\frac{k_{si}}{\tau_{fil}s+1}}^{\text{Feedback filter}} \tag{5-8}$$

The parameters to be determined concerning the design of the PI controller in the inner current loop are the following;

- The Phase Margin in degrees; here a value of PM=50^0 is decided.

- The cut-off (f_c) frequency of the current control loop. Evaluating (5-9) at f_c = 500 Hz yields ω_c and the corresponding time constant τ_c

$$\omega_c = 2\pi f_c = 3141.6 \ rad/s$$
$$\tau_c = \frac{1}{\omega_c} = 3.18 \ \ s \tag{5-9}$$

- The cut-off frequency of the low-pass filter (f_{fil}) of the open loop system. Selecting a value of f_{fil} = 1000 Hz, the angular frequency ω_{c_fil}= 6283.18 rad/s and the time constant τ_{fil}=1.59E-4 s are derived.
- The low-pass filter inductance (L_{filter}); here a value of 0.001 henries is chosen.

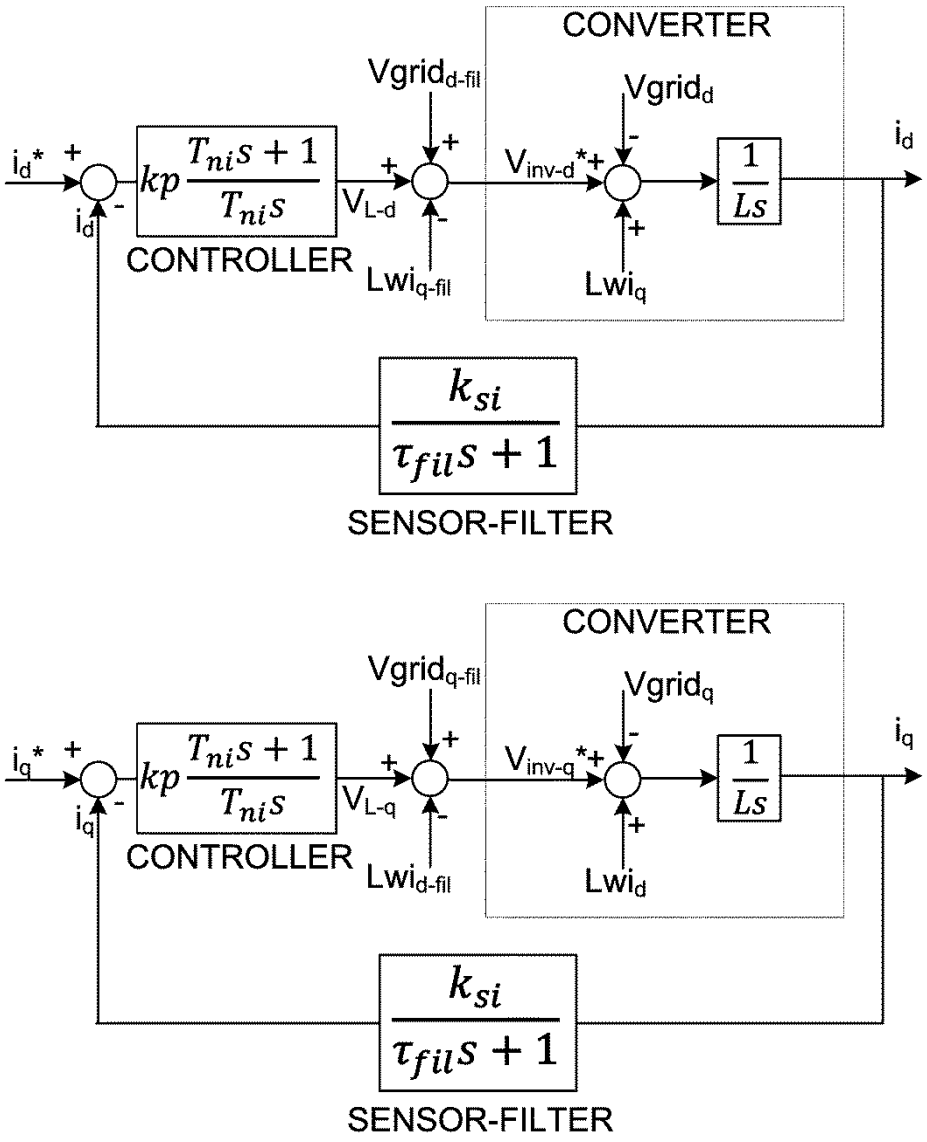

Fig. 5-7: Current control structures in d,q axes respectively.

For the sake of simplicity, it was assumed that the current measurement filter has a unity gain, such as k_{fil} =1. In addition, from the Phase Margin (PM) equation, described in (5-10), the T_{ni} that is a time constant value can be obtained:

$$PM = a\tan(T_{ni}\omega_c) - a\tan(\tau_{fil}\omega_c) \Rightarrow T_{ni} = 1.3\cdot 10^{-3}\ \text{s} \tag{5-10}$$

The proportional gain of the PI regulator K_{pi} is calculated via the expression given in (5-11), where the quantity in the absolute is the transfer function of the open current loop as being already demonstrated above, in (5-8).

$$\left| K_{p_i}\frac{T_{ni}s+1}{T_{ni}s}\cdot\frac{1}{L_{filter}s}\cdot\frac{1}{\tau_{fil}s+1}\right| = 1 \tag{5-11}$$

Taking the Laplace Transformation and substituting $s=j\omega_c$ into (5-11), and carrying out some mathematical calculations yields from (5-12) that K_{pi}=3.41.

$$K_{p_i} = L_{filter}(\omega_c)^2\frac{\sqrt{1+(\omega_c\tau_{fil})^2}}{\sqrt{(\omega_c)^2+\left(\frac{1}{T_{ni}}\right)^2}} \tag{5-12}$$

The controller transfer function lies in (5-13),

$$PI_I(s) = 3.41\frac{s+769.23}{s} \tag{5-13}$$

Finally, the following open current loop transfer function (5-14) is acquired,

$$G_I(s) = \frac{3.41s+26.23}{1.59\cdot 10^{-7}s^3+10^{-3}s^2} \tag{5-14}$$

5.4.1.3. Voltage Control Loop

Considering an efficiency n=1, the instantaneous power at the DC input of the inverter remains equal to the instantaneous power at the AC output (P_{AC}=P_{DC}). Consequently, the i_d reference current is computed as shown in Fig. 5-8.

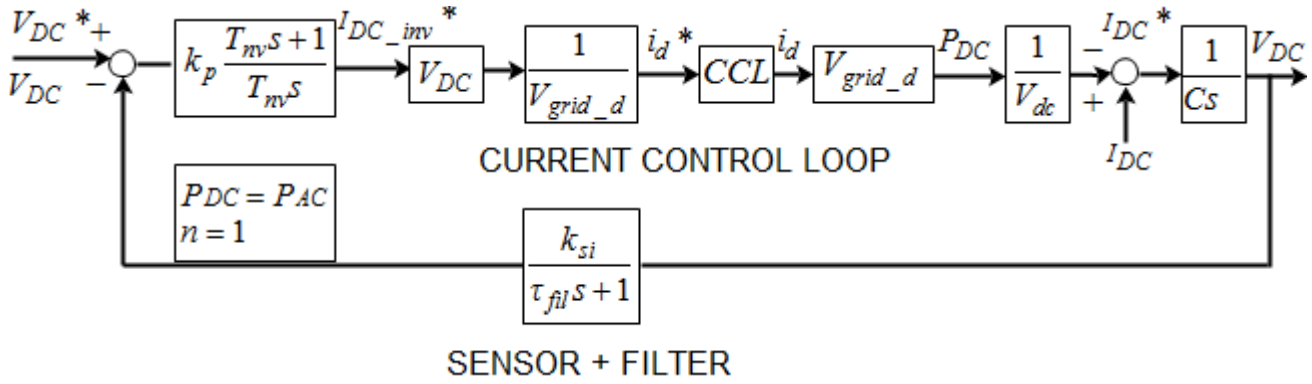

Fig. 5-8: Block diagram of outer voltage control loop. CCL: Current Control Loop

Similarly to the current open loop control, the next step is to define the parameters of the voltage feedback loop for the inverter-based STATCOM model studied throughout this thesis. These are the ones indicated beneath:

- The Phase Margin in degrees; here a value of PM=60^0 is decided.
- The cut-off (f_c) frequency of the voltage control loop. Evaluating equation (5-15) at f_c = 5 Hz yields ω_c and the corresponding time constant τ_c.

$$\omega_c = 2\pi f_c = 31.416 \ \ rad/s$$
$$\tau_c = \frac{1}{\omega_c} = 3.18 \cdot 10^{-2} \ \ s \tag{5-15}$$

- The cut-off frequency of the low-pass filter (f_{fil}) of the outer voltage loop scheme. Thus, selecting a value of f_{fil} =50 Hz, the angular frequency ω_c = 314.16 rad/s and the time period τ_{fil}=0.003183 s are derived.
- The capacitance, C; here a value of 0.5 Farads is chosen. This large value of capacitance at the inverter's DC-side could be loosely represented by a very simplistic Supercapacitor model.

Again for convenience issues, it was assumed that the voltage measurement filter has a unity gain, such as k_{fil} =1. In addition, from the Phase Margin (PM) equation, described in (5-16), we can obtain the time constant T_{nv} value as,

$$PM = a\tan(T_{nv}\omega_{c\_v}) - a\tan(\tau_{fil}\omega_{c\_v}) \Rightarrow$$
$$\Rightarrow T_{nv} = 7.05 \cdot 10^{-2} \ \ s \tag{5-16}$$

The proportional gain of the PI regulator K_{pv} is calculated via the expression given by (5-17), where the quantity in the absolute is the transfer function of the voltage feedback loop.

$$\left| K_{pv} \frac{s + \frac{1}{T_{nv}}}{s} \cdot \frac{1}{Cs} \cdot \frac{1}{\tau_{fil}s+1} \right| = 1 \tag{5-17}$$

Implementing the Laplace Transformation and substituting $s=jw_c$ into (5-17), and performing some mathematical simplifications yields from (5-18) that $K_{pv}=14.38$.

$$K_{pv} = C(\omega_c)^2 \frac{\sqrt{1+(\omega_c \tau_{fil})^2}}{\sqrt{(\omega_c)^2 + \left(\frac{1}{T_{nv}}\right)^2}} \tag{5-18}$$

The PI controller transfer function lies in (5-19),

$$PI_v(s) = 14.38 \frac{s+14.18}{s} \tag{5-19}$$

Concluding, the following voltage control loop transfer function is achieved,

$$G_v(s) = \frac{14.38s + 189.52}{15.91 \cdot 10^{-4} s^3 + 0.5 s^2} \tag{5-20}$$

5.4.2. RSCAD/RTDS Simulations

The next step was to simulate the Average Model of a STATCOM in RTDS/RSCAD. Similarly to the Simulink/Matlab model, the IGBT Voltage-Source Converter is represented by equivalent controlled voltage sources generating the set of three phase AC voltages, whereas pulse-width modulation (PWM) switching frequencies are neglected.

In addition, the integration and control concept of a capacitor model is represented which consists of an equivalent series resistance ESR=0.1 Ohms and an equivalent series DC capacitor with large value of C=0.5 F. The objective of the STATCOM controller is to regulate the voltage of common coupling of this inverter-interfaced source, in addition to match the DC voltage requirement and enhance the distribution system reliability by maintaining the STATCOM's DC voltage constant under different load profiles.

Numerous simulations were performed in pure simulation environment.The first simulation task was implemented on a three-phase LV distribution network with and without the integration of the STATCOM model connected to a DC capacitor. Two sets of simulations were performed under different load profiles, one for P=1 kW, Q=2 kVAr and the second one for P=0 kW, Q=0.5 kVAr respectively.

Table 5-1 summarizes the network parameter values used for the real time simulations. Figures 5-9 and 5-10 represent the network topology in RSCAD and its inherited blocks with and without the STATCOM penetration. Va, Vb, Vc are the three-phase voltages at the STATCOM terminals. N1, N2, N3 and N7, N8, N9 are the three-phase voltages at the load terminals and at its point of common connection (PCC) respectively. N4, N5, N6 are the three-phase voltage sources. For our convenience, the voltages were grouped into their three phase RMS values as indicated beneath (Fig. 5-11).

Figure 5-12 illustrates the DC capacitor model built in RTDS. Moreover, Fig. 5-13 & 5-14 represent snapshots of the Average Model Computation block and the STATCOM's controller built in RSCAD.

Table 5-1: System Parameters [126]

Network Parameters	Values
V_{grid_ms}	400 V
$RL_{line1,2}$	0.2+j0.924 Ohm
C	0.5 F
ESR	0.1 Ohm
L_{filter}	1 mH
R_{HuT}	78 Ohm
L_{HuT}	140 mH

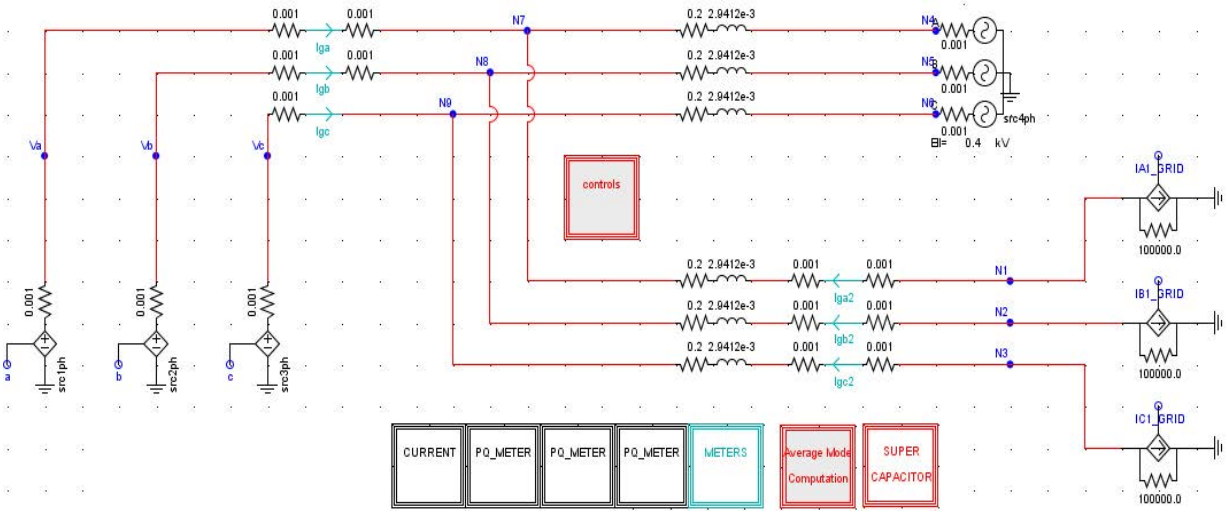

Fig. 5-9: RSCAD/RTDS model for the simulated network including STATCOM.

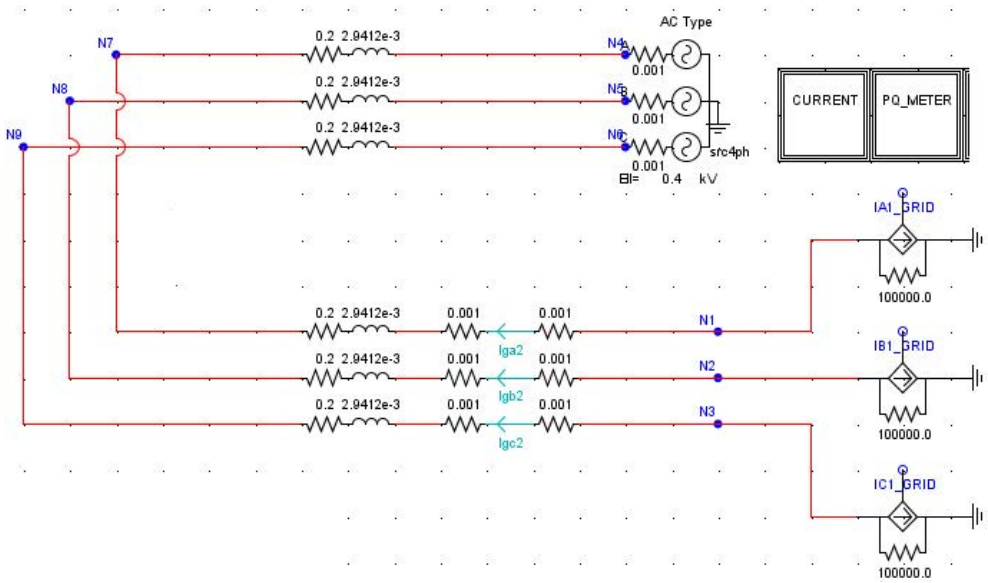

Fig. 5-10: RSCAD/RTDS model for the simulated network without STATCOM.

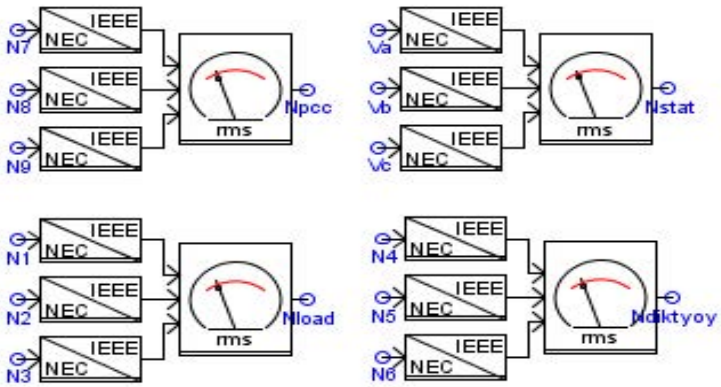

Fig. 5-11: RSCAD/RTDS blocks that attribute the rms values.

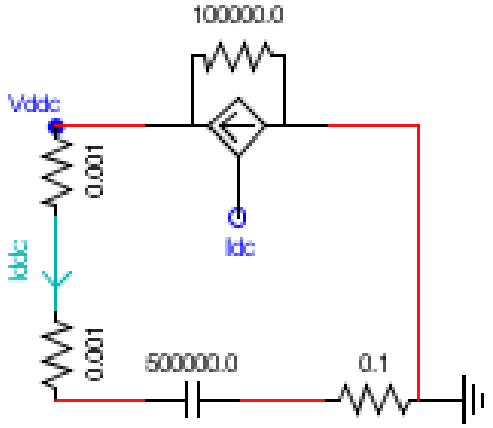

Fig. 5-12: DC capacitor model in RSCAD/RTDS.

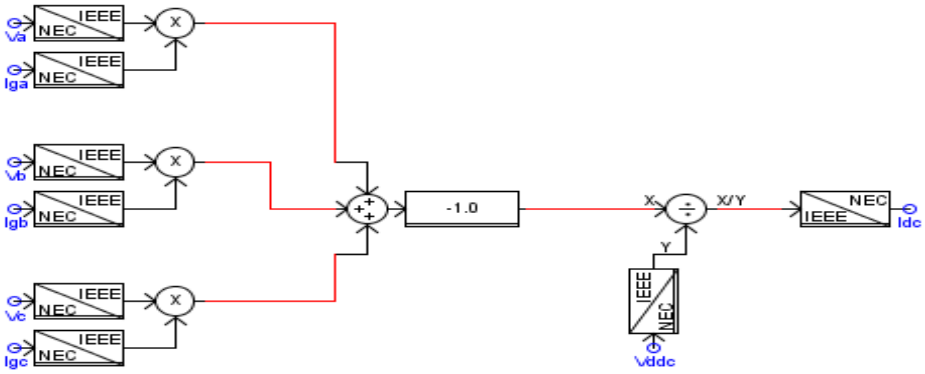

Fig. 5-13: Average Model Computation block in RSCAD/RTDS interface.

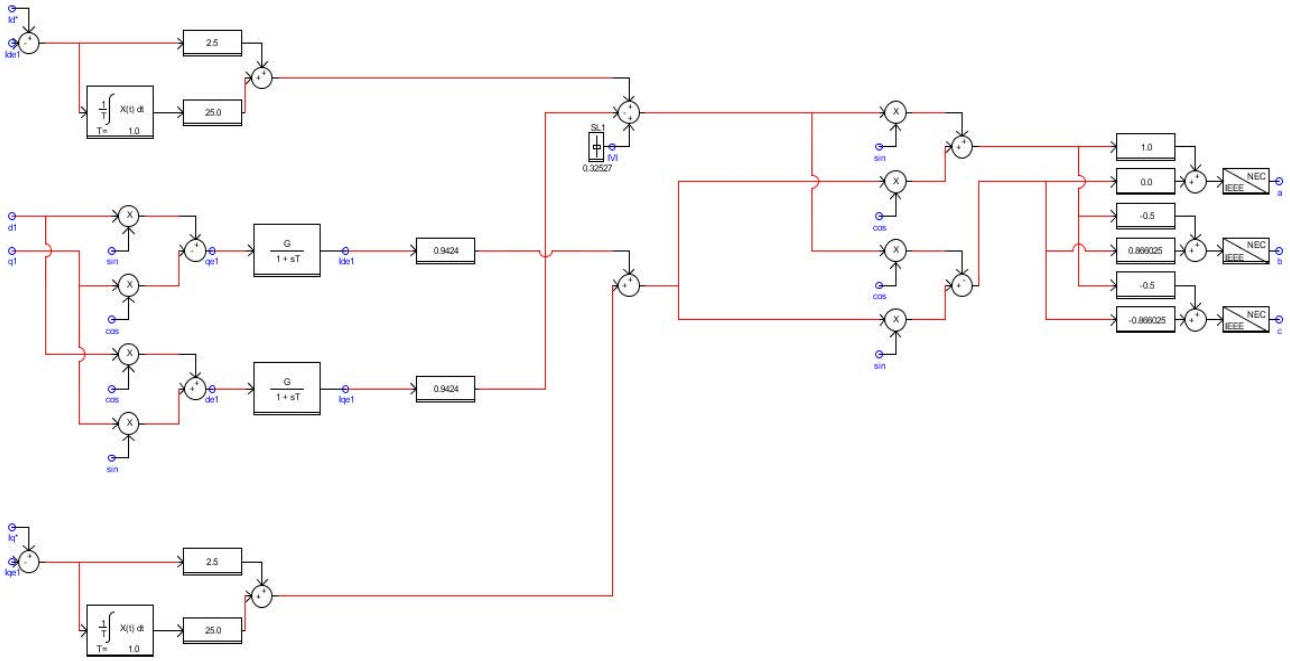

Fig. 5-14: Control structure of the STATCOM in RSCAD/RTDS interface.

5.4.3. Power Hardware-in-the-Loop Simulations

As explained in Section 3.3.4, PHIL simulations occupy a closed-loop interaction that can reduce the accuracy of the simulation and may evoke instability. For these reasons, and before running the PHIL experiments, the system's stability needed to be checked in Simulink for the two test cases; with and without the integration of the STATCOM. Due to stability issues that were arisen, three inductances of 0.05 H were added, one for every phase, in series with the three controlled current sources (Fig. 5-15 & 5-16). The appropriate protections are added as well as the time delay of the feedback current signals was considered. Furthermore, the DC capacitor´s nominal voltage was reduced to 200 V (the system was initially tested for a Vdc rated at 400 and 600 V), nevertheless its capacitance was kept at C=0.5 F.

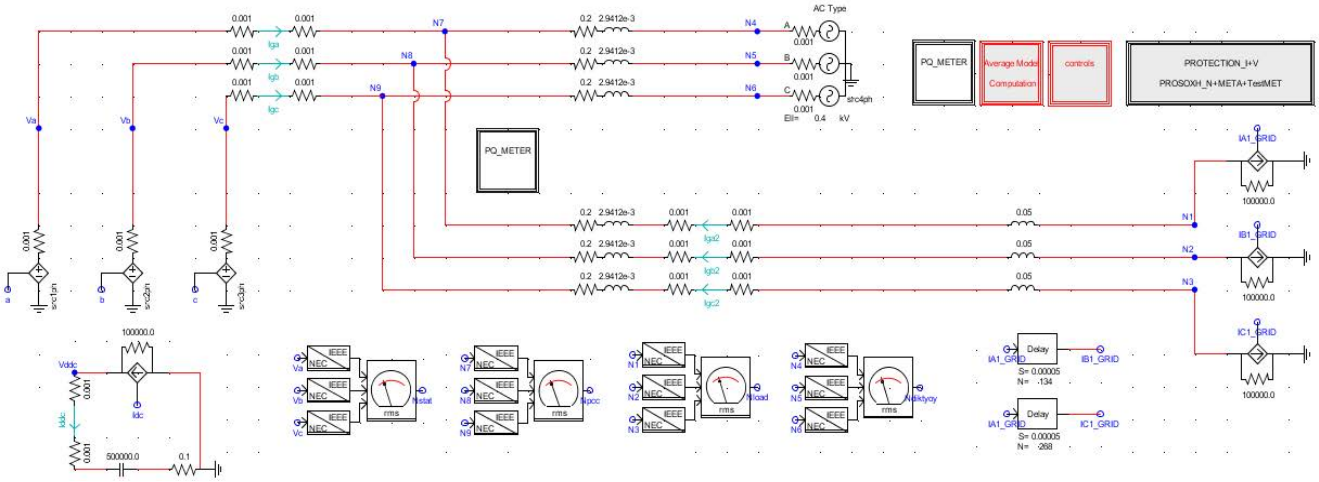

Fig. 5-15: RSCAD/RTDS model with STATCOM during the PHIL test.

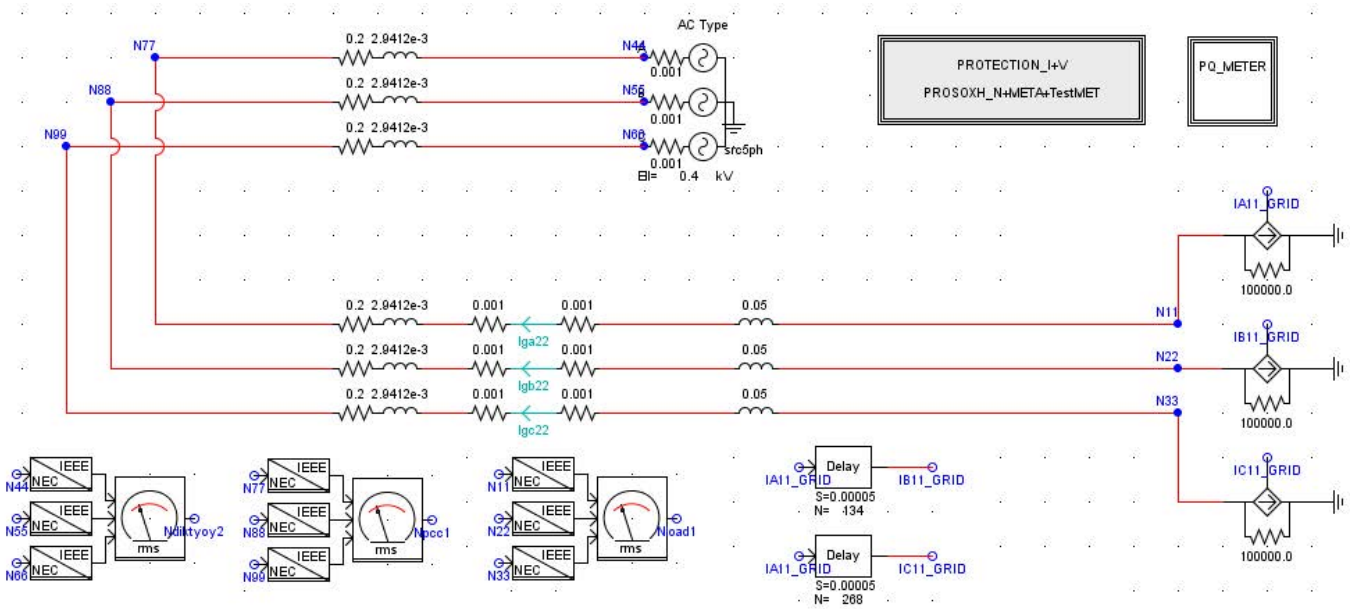

Fig. 5-16: RSCAD/RTDS model without STATCOM during the PHIL test.

In continuation, Power Hardware-in-the-Loop experiments are executed utilizing a variable resistor and inductor of 78 Ohms and 140mH respectively as HuT. In order to demonstrate the effectiveness of the STATCOM for voltage sag mitigation and reactive power compensation, a step decrease from 140 to 103 mH of the hardware inductive load was implemented.

Figure 5-17 gives an overview of the laboratory PHIL set-up. At the output of the RTDS, the impedance load is connected where the current is measured at one phase by the Thriphase sensor and is fed back to the system to close the loop. This low output signal is amplified to a higher scale by the power amplifier and will feed the system's three controlled current sources (phase difference by 120^0) in RSCAD/RTDS where the HuT is connected to.

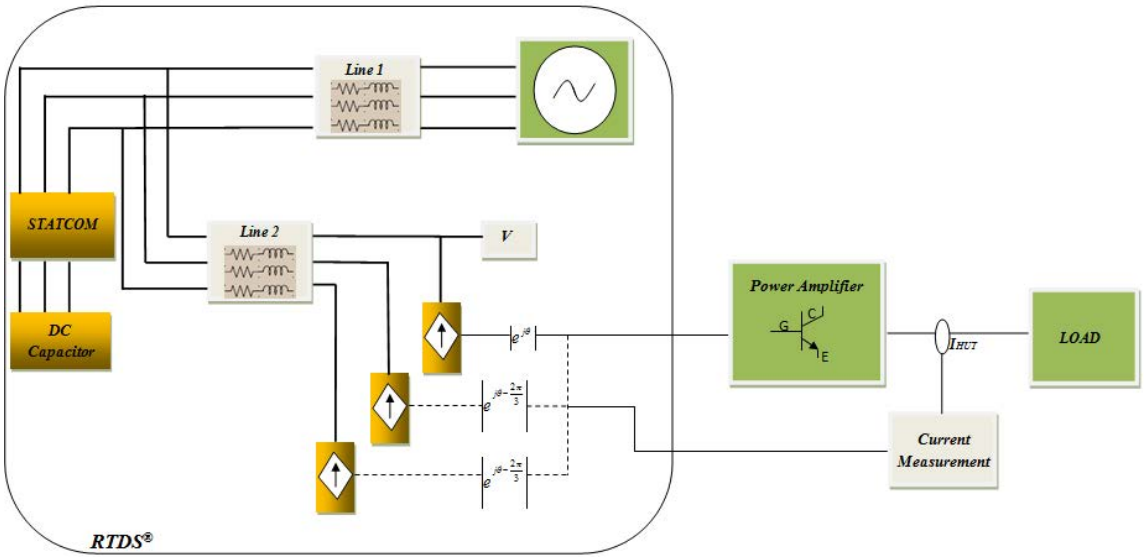

Fig. 5-17: PHIL experimental topology.

Figure 5-18 illustrates the Simulink stability model for the PHIL test.

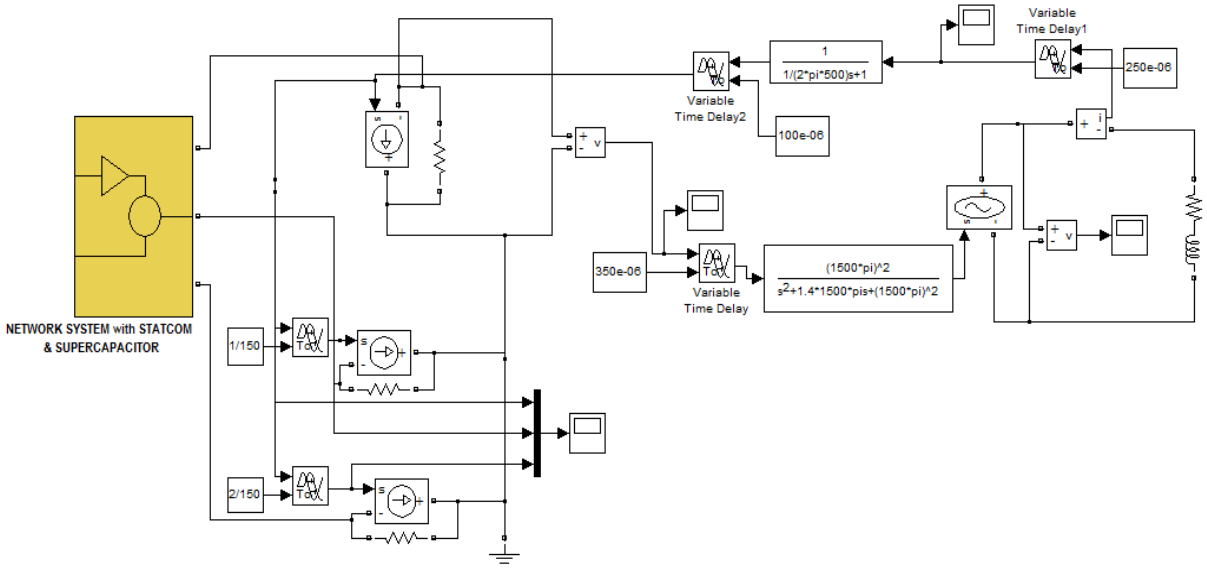

Fig. 5-18: Simulink/Matlab model for the PHIL test.

5.5. Description of Simulations and Test Experiments for Case Study 2

5.5.1. RSCAD/RTDS Simulations

The network topology includes a diesel generator, 2 LV lines, a bank of restive loads and a three-phase inverter. Table 5-2, 5-3 and 5-4 summarize the network parameter values and the diesel generator internal characteristics necessary for the execution of the real time simulations [127],[135]. The used equipment included different parts of the laboratory Microgrid, thus the selected network values are based on the parameters of the Microgrid devices.

The first simulation task was implemented on a three-phase LV distribution network with and without the integration of the battery inverter. Subsequently, the system´s frequency was checked upon load changes with and without the storage penetration. In order to verify the frequency and power responses at the diesel generator´s terminals, a static load change is pursued at each phase with the utilization of a breaker.

Figure 5-19 represents the network topology without the SI introduction, whereas Fig. 5-20 illustrates the power system with the storage included.

Table 5-2: System Parameters

Network Parameters	Values
$Vg_{\_rms}$	400 V
RL_{line1}	0.012+j6.88E-4 Ohm
RL_{line2}	0.042+j2.428E-4 Ohm
Diesel genset	13.164 kVA
Battery S_{nom}	3.3 kVA
R_{load}	12.6 kW
R_{HuT}	105.8 Ohm

Table 5-3: Diesel Generator Parameters (A)

Ratings		
3-phase Output	Sn	13.164 kVA
Voltage	Un	230.94 V
Current	In	19 A
Frequency	f	50 Hz
Speed	n	1500 rpm
Pair poles	p	4
Inertia Constant	H	1.7 MWs/MVA

Table 5-4: Diesel Generator Parameters (B)

Resistances		
Stator Winding	Ra	0.009626 Ohm
Reactances		
Stator leakage reactance	Xa	0.0576 pu
Synchronous - Direct Axis	Xd	2.9619 pu
Synchronous - Quadrature Axis	Xq	1.2067 pu
Transient - Direct Axis	X'd	0.23037 pu
Transient - Quadrature Axis	X'q	0.228 pu
Subtransient - Direct Axis	X''d	0.093245 pu
Subtransient - Quadrature Axis	X''q	0.1097 pu
Time Constants		
D: Open Circuit-Transient	T'do	4.3 s
D: Open Circuit-Subtransient	T''do	0.032 s
Q: Open Circuit-Transient	T'qo	0.85 s
Q: Open Circuit-Sub transient	T''qo	0.05 s

5.5.2. Power Hardware-in-the-Loop Simulations

The hardware part utilized throughout these experiments was a variable resistive load of 105.8 Ohm. Figure 5-21 shows the network model during the PHIL experiment. Furthermore, in order to validate the accuracy of the results, virtual simulations were performed in RSCAD/RTDS. The entire closed loop system was simulated including the real resistive load of 105.8 Ohm and the results were then compared with the results from the PHIL tests. In more details, the resulting rms values (current, voltage) were compared with the values expected according to the off-line simulations (Fig. 5-22) [127],[135].

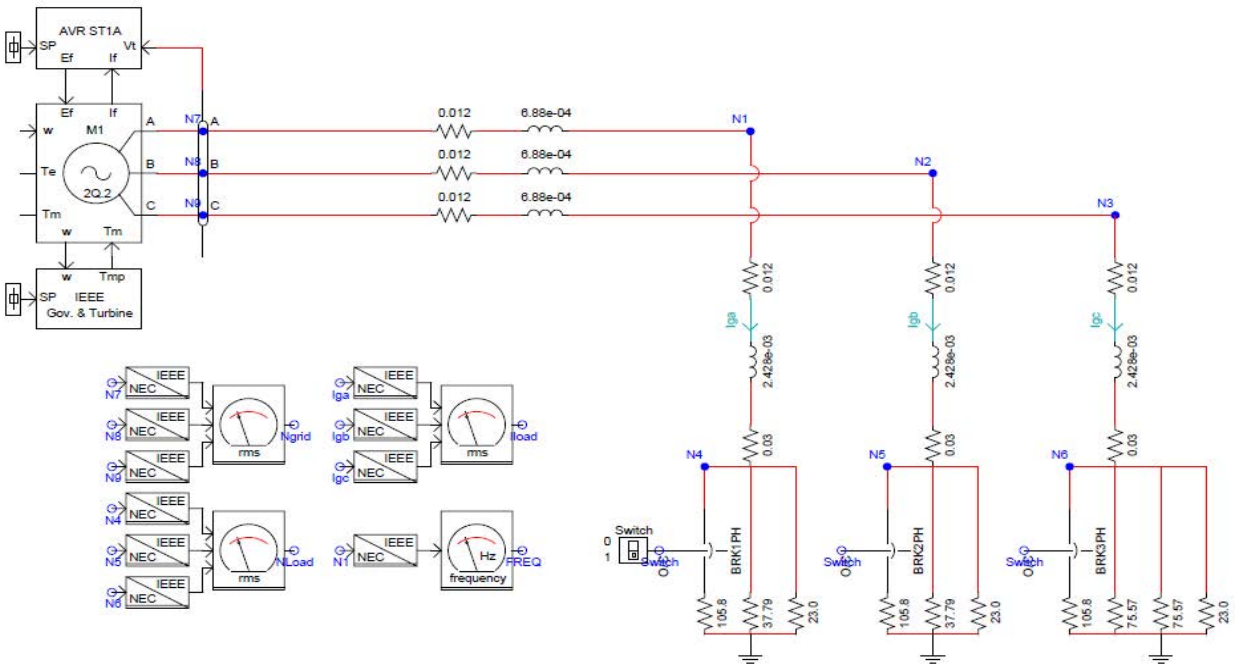

Fig. 5-19: RSCAD/RTDS model for the simulated network without storage.

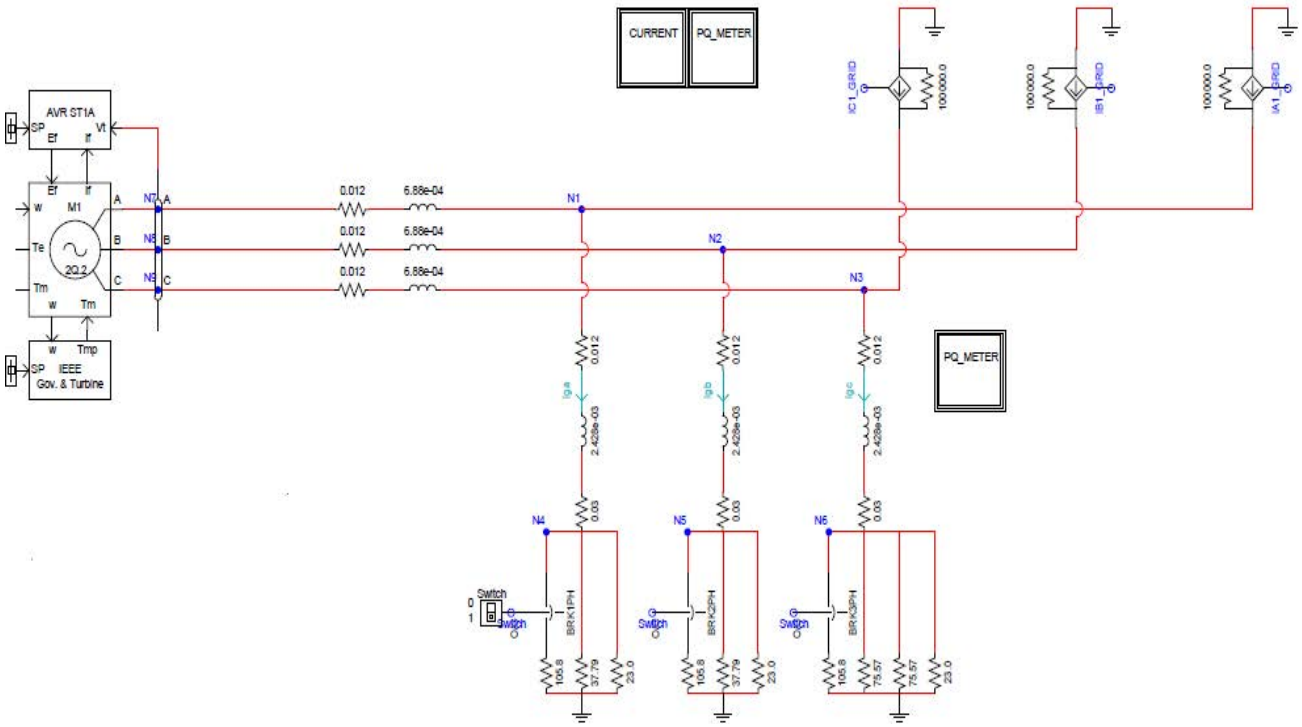

Fig. 5-20: RSCAD/RTDS interface of the simulated network model without storage.

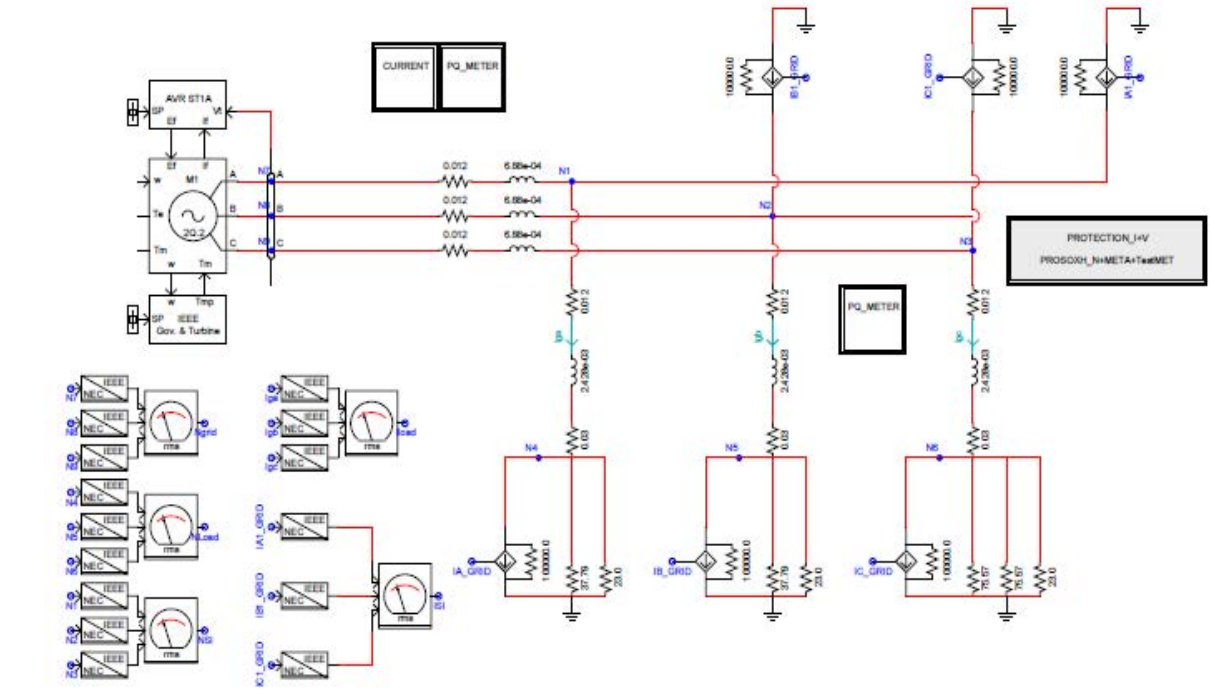

Fig. 5-21: RSCAD/RTDS model during the PHIL test.

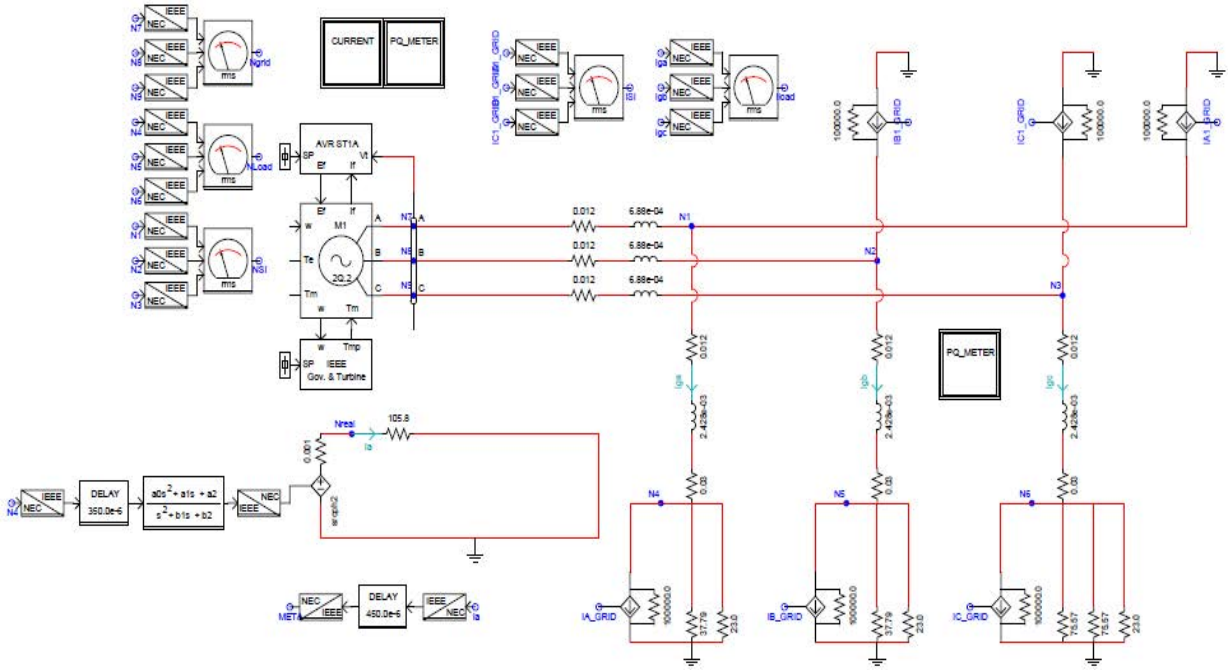

Fig. 5-22: RSCAD/RTDS model during the VPHIL test.

5.5.3. Microgrid Experiments

For tests aiming at analyzing the energy transfer in an AC Microgrid, several experiments were conducted related to the diesel generator and the battery inverters that were available in CRES premises and are analyzed beneath.

5.5.3.1. Diesel Generator Tests

The diesel generator is studied in islanded mode since there was not disposable a synchronization unit to be connected to the main grid. Moreover it suffers from frequency and voltage fluctuations due to harmonics distortion. These variations were examined upon step load changes. An increase in load demand induces also an increase in diesel loading and a subsequent reduction in torque, resulting in frequency deterioration.

In order to determine the frequency droop curve, one has to vary the active power exchanged by the generator with the Microgrid and measure the corresponding frequency at the output of the diesel genset. Thus, its *f-P droop* curve was experimentally derived under symmetric, asymmetric loads and a 2-hr load profile (Fig. 5-23). Frequency and active power being exchanged in the system are acquired with a one second sampling rate. However, a mean average is drafted every minute for the symmetric and asymmetric loads, whereas instantaneous frequency values are considered for the load profile.

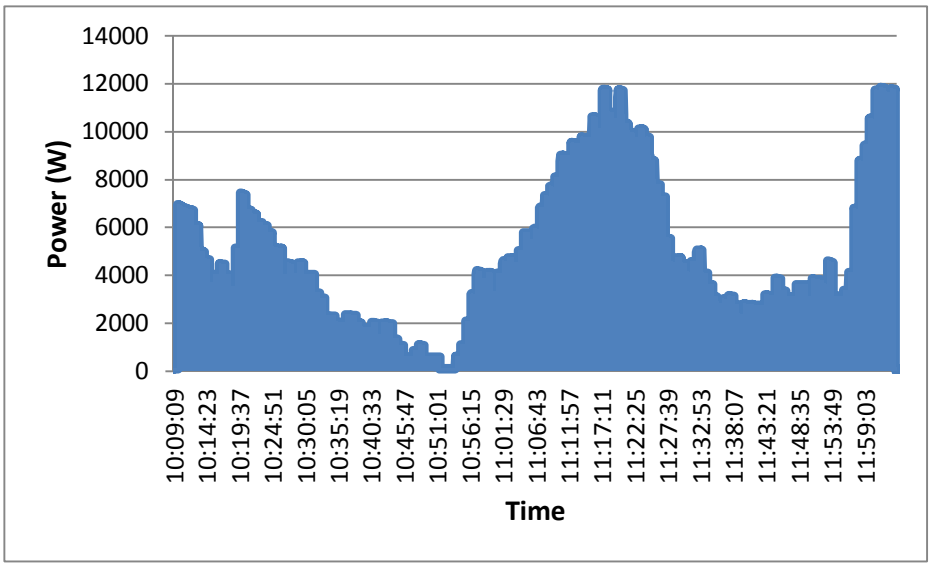

Fig. 5-23: A 2-hr load profile for the diesel genset.

5.5.3.2. Battery Inverters Tests

In droop mode, the inverter was impossible to run in parallel with the diesel generator since the latter suffers from serious oscillations of a period rated roughly at 0.08 s. Consequently, this fluctuation in frequency will influence the diesel genset´s and in extension the inverter´s power output.

A) Measurement of battery inverters' f-P droop curve

The purpose of this experiment is to determine the CRES battery inverters´ (Sunny Island 4500) droop curves. The frequency droop curve has to be experimentally derived. In order to obtain the inverter's droop curve, data sets consisting of inverter's output frequency and active power have to be available.

In more details, the f-P droop calculation was evaluated with static load changes and only one inverter being in use. The PV inverter is also included. Moreover, the f-P droop was measured for master-slave operation of the three inverters with static load variation, asymmetries and a 2-hr Load profile. Master-slave concept means that one of the system´s inverters is nominated as the master which is responsible to control the slaves and therefore for managing the system.

B) Grid connected to disconnected mode

During this experiment two measurements have been conducted under transition of the Microgrid from grid connected to isolated mode; the difference between the two tests is the operation mode of the master battery inverter. In each test, when the Microgrid is grid connected, the battery inverter by default intakes power to charge its battery. Principally, the inverter consumes about 2.7 kW depending on the battery´s state-of-charge (SOC), whereas the two connected PV inverters produce roughly 2 kW and the load demand is about 1.5 kW. The data logging of each test includes: Phase Voltage of the battery inverter and frequency.

It is worth mentioning that when the battery inverter operates in droop mode, the second PV unit is unable to operate in parallel with the system due to high sensitivity of its anti-islanding protection.

C) Battery inverter active power droop control

The purpose of this experiment is to examine the load sharing for parallel operation of two SI inverters 4500 being both connected in one phase and demonstrate the concept of the battery inverters' active power control by changing the frequency droop (*droop f*) curve. For all the following cases, the output power is measured: i) different droops (-2Hz/P_{nom}, -1Hz/P_{nom}) [8] and f_{idle} (intersection of the *droop f* curve with the *f* axis) is equal to 50 Hz, ii) same droop (-1Hz/P_{nom}) and f_{idle}=50 Hz and iii) same droop (-1Hz/P_{nom}) but the idle frequency is changed to 50.3 Hz.

5.6. Results & Discussion

5.6.1. Test Results for Case Study 1

The affiliated Bode plots for the current open loop transfer function described in Section 5.4.1 are given in Fig. 5-24. As it can be easily observed in these diagrams, the cut-off frequency value obtained is 3140 rad/s, i.e. 499.74 Hz, which is a very approximate value to the one originally specified (500 Hz). Moreover and as it was anticipated, the PM approximately reaches the figure of 50^0 (49.7^0).

The corresponding Bode diagrams for the voltage control loop transfer function described in the same section are given in Fig. 5-25. As it can be seen in these diagrams, the cut-off frequency obtained is of 31.10 rad/s, i.e. 4.995 Hz, which is also a very approximate value to the one originally specified (5 Hz). Moreover and as it was expected, the PM reaches almost the rate of 60^0 (61.4^0).

Apart from the Bode diagrams, Fig. 5-26 and 5-27 compare the V_{DC} and I_q reference (V_{DC^*}, I_{q^*}) and simulation result values according to the parameters that were chosen for the corresponding control loops. Initially, it was assumed a voltage step decrease from 600 to 550 V at the time of 1.5 s (Fig. 5-26). Secondly, by implementing solely various step changes on the I_q reference value, it was shown that the resulting measured values follow the reference one and tailors the system stability. Figure 5-27 depicts a paradigmatic step increase from 0 to 10 A for the I_q reference at 0.2 s. The approach results in a good trade-off between the dynamic performance and stabilization.

[8] Nom: nominal

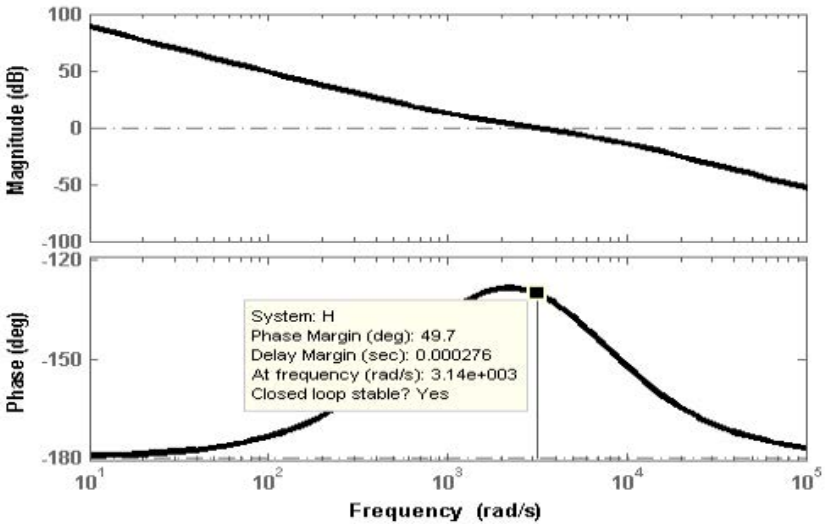

Fig. 5-24: Bode diagrams of $G_I(s)$ in inner current control loop [126].

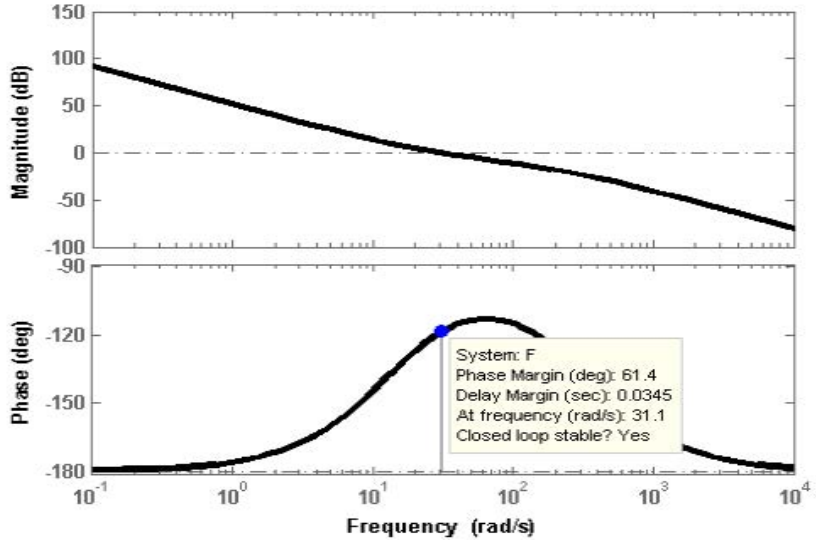

Fig. 5-25: Bode diagrams of $G_V(s)$ in outer voltage control loop [126].

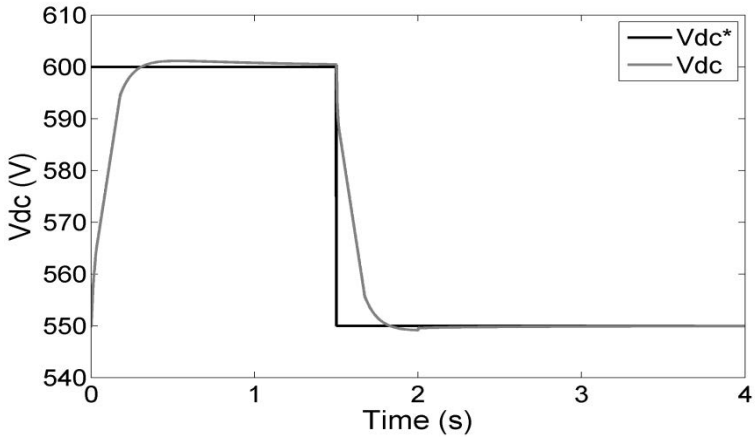

Fig. 5-26: Reference vs Simulated V_{DC} bus voltage values [126].

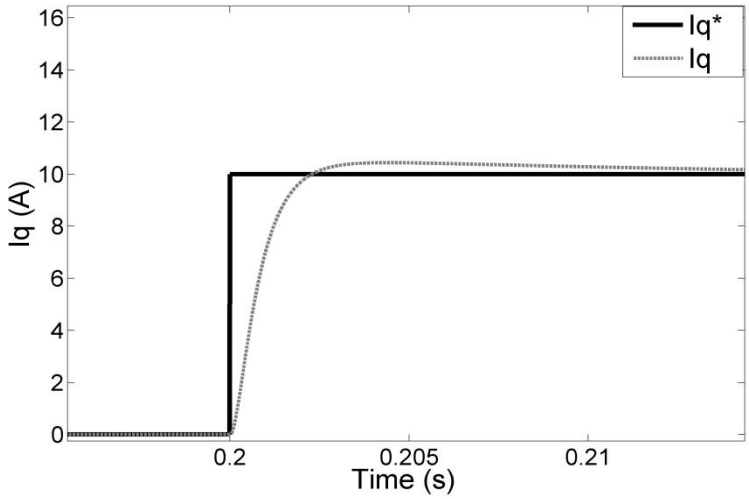

Fig. 5-27: Step response of the I_q reference current coordinate [126].

The effects of the STATCOM on voltage stability were more severe for higher reactive demand, thus only some indicative results will be presented for reactive power demand rated at 2 kVAr.

Fig. 5-28 depicts the DC link voltage of the STATCOM. We can observe that the voltage is kept constant to the selected reference value (i.e. Vdc=0.4 kV) and the PI controller maintained the primary voltage to be equal to the reference value defined in the control system dialog box by achieving an error of almost zero value.

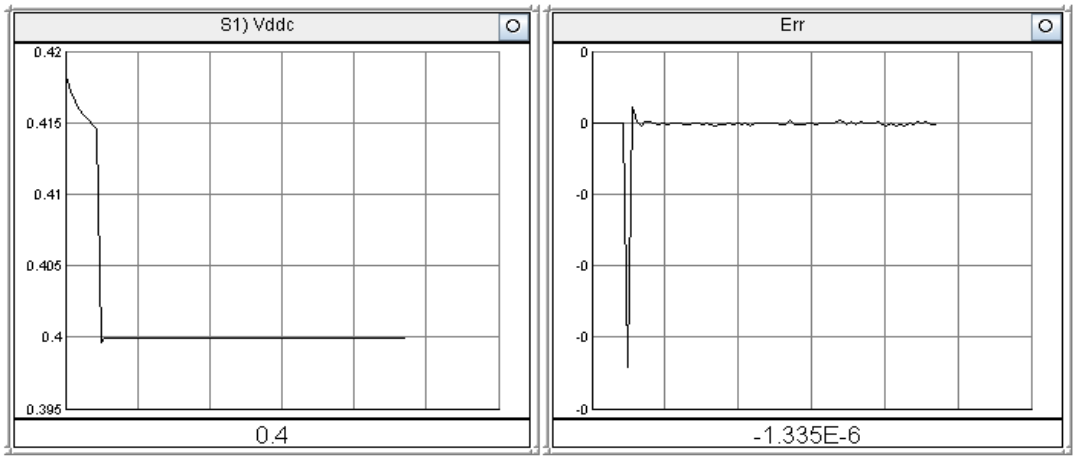

Fig. 5-28: Outer voltage regulation of the STATCOM's DC link voltage in RSCAD/RTDS.

Table 5-5 concentrates the RSCAD/RTDS numerically (off-line simulations) derived voltage profiles at different locations throughout the network system, namely at the PCC and load terminals, with and without (sub-index 1) the STATCOM model integration respectively. It is clearly proven that the STATCOM improves the system's voltage by comparing the N_{ppc}, N_{ppc1}, N_{load} and N_{load1}. Moreover, the reactive power generated by the STATCOM inverter model is rated at 2.093 kVAr and fully compensates the load demand which is of 2 kVAr.

Table 5-5: Numerically derived steady-state voltage values (Off-line simulations)

Nodal Voltages	RMS Values (V)
N_{pcc} (with STATCOM)	230.7
N_{pcc1} (without STATCOM)	227.9
N_{load} (with STATCOM)	227.7
N_{load1} (without STATCOM)	224.8

In addition, Fig. 5-29 depicts the two anti-diametric phase currents; one that feeds the load (I_{load}) and the other that feeds the controllable currents sources where the HuT is supposed to be connected to.

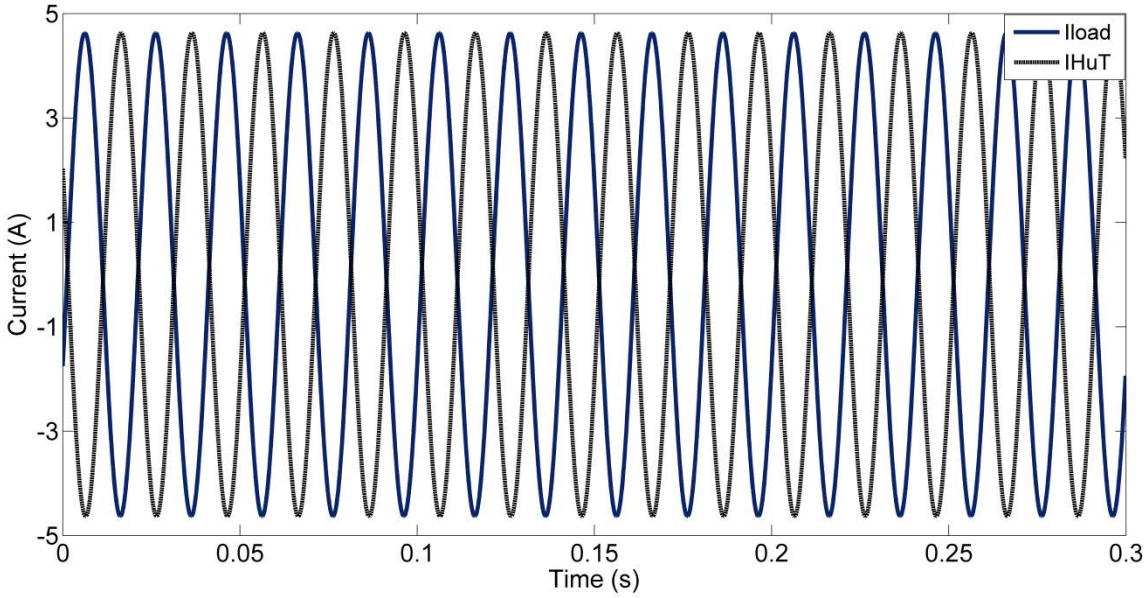

Fig. 5-29: Single-phase load current and I_{HuT} phase current of the controllable current sources.

Initially, during the PHIL experiments, a resistive and inductive load of 78 Ohms and 140 mH respectively comprised the hardware part. In order to demonstrate the effectiveness of the STATCOM for voltage sag mitigation and reactive power compensation, a step decrease from 140 to 103 mH of the hardware inductive load was implemented. The following graphs (Fig. 5-30 & Fig. 5-31) show the results from the PHIL tests. In more details, Fig. 5-30 and 5-31 illustrate the transient responses of the STATCOM's active and reactive power respectively during the voltage sag.

The results in both figures show the transient behaviour of the STATCOM since it increases its reactive power in order to mitigate the voltage drop and a new steady-state operation is achieved, i.e. 1.307 kVAr for the reactive and 0.01984 kW for the active power accordingly.

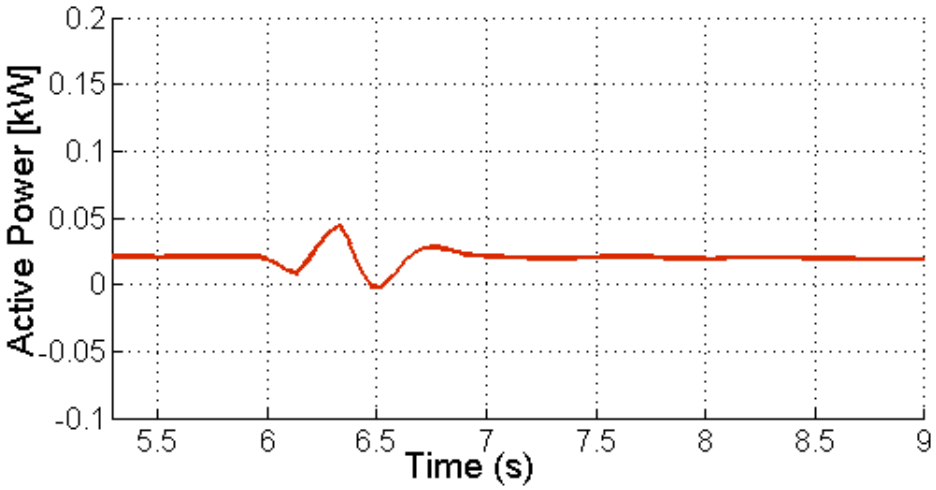

Fig. 5-30: Active Power Transient response with STATCOM (load change).

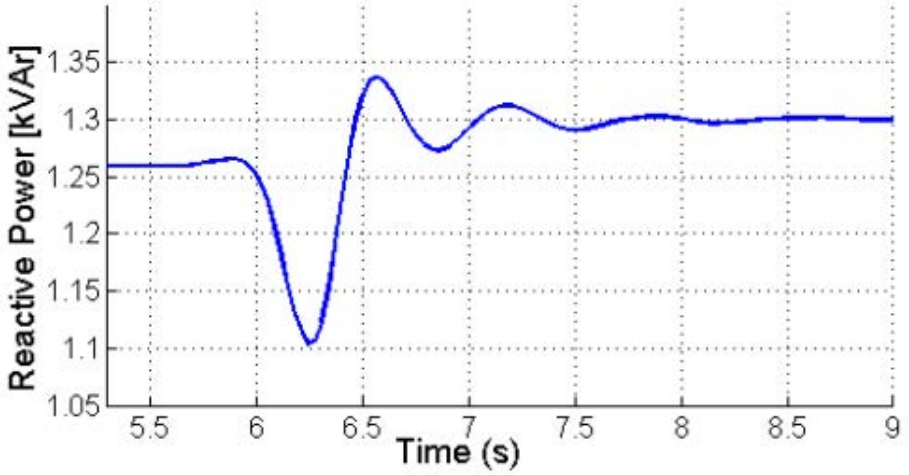

Fig. 5-31: Reactive Power Transient response with STATCOM (load change).

Table 5-6 summarizes the PHIL voltage profiles measured at different locations throughout the LV network with and without (indicated with sub-index 1) the STATCOM model integration. These are the steady-state values after the dynamic change in the inductive load, i.e. from 140 mH to 103 mH. Specifically, N_{load} and N_{pcc} indicate the three-phase voltages at the load's and STATCOM's terminals respectively. As it was anticipated, the STATCOM compensates and thus regulates the voltage at the load side since it feeds the system with reactive current (Table 5-5 & 5-6), as well as the voltage values during the PHIL tests coincide with the ones from the off-line simulations.

Table 5-6: PHIL numerically derived steady-state voltage profiles

Nodal Voltages	RMS Values (V)
N_{pcc} (with STATCOM)	230.7
N_{pcc1} (without STATCOM)	227.9
N_{load} (with STATCOM)	227.7
N_{load1} (without STATCOM)	224.8

5.6.2. Test Results for Case Study 2

Tables 5-7 and 5-8 summarize the real time simulation results without and with the storage inclusion respectively during step load change (from base to full load).

Table 5-7: Numerical Results without Storage

Basic Load	Full Load
P_{diesel}= 10.92 kW	P_{diesel}=12.33 kW
f=50 Hz	f=49.68 Hz
Q_{diesel}= 0.689 kVAr	Q_{diesel}= 0.8933 kVAr
P_{load}= 10.88 kW	P_{load}=12.3 kW

Table 5-8: Numerical Results with Storage

Basic Load	Full Load
P_{diesel}= 10.93 kW	P_{diesel}=11.74 kW
f=50 Hz	f=49.81 Hz
Q_{diesel}= 0.6898 kVAr	Q_{diesel}= 0.8601kVAr
P_{inv}= -0.05 kW	P_{inv}= 0.6173 kW
Q_{inv}= 0.3035 kVAr	Q_{inv}= 0.374 kVAr
P_{load}= 10.88 kW	P_{load}=12.3 kW

From equation (5-1) and considering that the diesel active power output is rated at P_{diesel}= 10.92 kW, the diesel droop characteristic is given by equation (5-21). Moreover, it is confirmed at 6%. The three-phase output power of diesel totals to 13.164 KVA.

$$P_{diesel} = 10.92 + \frac{13.164 \cdot (50 - f)}{3} \tag{5-21}$$

Table 5-9 concentrates the PHIL numerical results under step load change (from base to full load).

Table 5-9: PHIL Numerical Results

Basic Load	Full Load
P_{diesel}= 10.93 kW	P_{diesel}=11.78 kW
f=50 Hz	f=49.84 Hz
P_{inv}= -0.004233 kW	P_{inv}= 0.5168 kW
Q_{inv}= 0.2164 kVAr	Q_{inv}= 0.2935 kVAr
P_{load}= 10.88 kW	P_{load}=12.3 kW

Figures 5-32 & 5-33 illustrate the step load change from basic load, 10.88 kW to full load, 12.3 kW. The reactive power demand is of 0.656 kVAr. The battery inverter is not included.

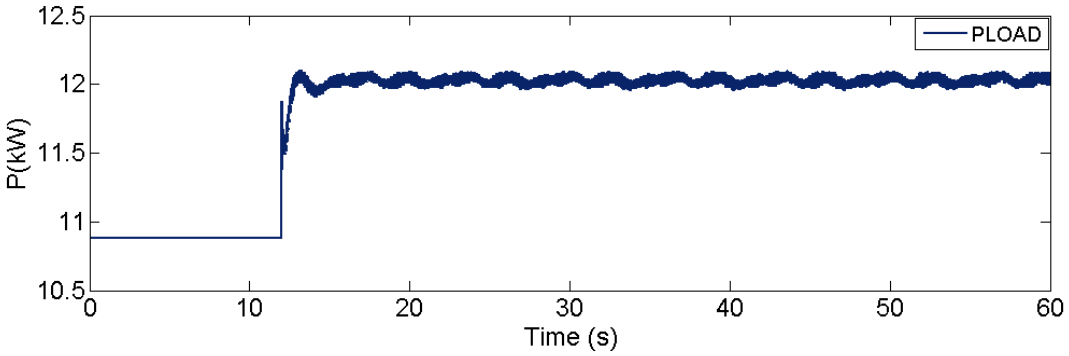

Fig. 5-32: Active power load demand.

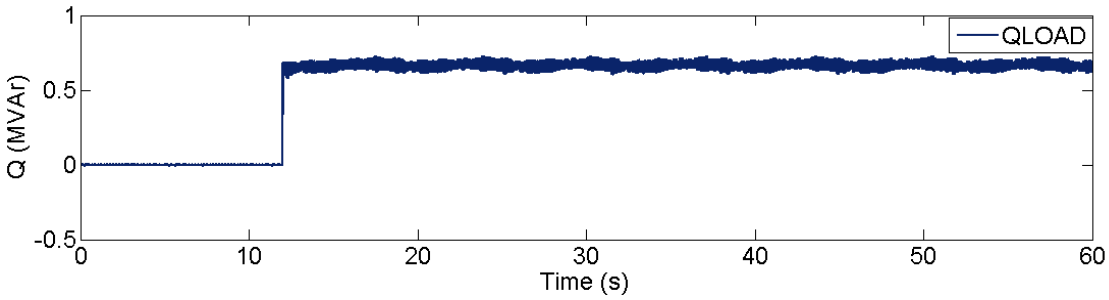

Fig. 5-33: Reactive power load demand.

Figures 5-34 to 5-36 show the RSCAD/RTDS transient responses with and without the battery inverter penetration respectively during a load change from 10.88 kW to 12.3 kW.

Figures 5-37 & 5-38 show the RSCAD/RTDS transient responses with load change from 10.93 kW to 11.78 kW during the PHIL tests.

As it can be easily seen from Fig. 5-34 beneath, the battery inverter enhances the frequency stability by covering part of the load change, whereas frequency oscillations are reduced. Moreover, the steady-state frequency is higher (49.81 Hz) when storage is included than when it is not included (49.68 Hz).

The diesel generator has to fully satisfy the power demand thus its output during the off-line simulations is higher without the energy storage penetration ranging between 10.92 kW and 12.33 kW under load change. However, when the battery inverter is participating, the load demand is satisfied by both the inverter and diesel, thus the diesel generator's output is less, ranging between 10.93 kW and 11.74 kW under the load change. In this case, the inverter injects to the system active and reactive power of 0.6173 kW and 0.374 kVAr respectively (Fig. 5-37).

Figure 5-38 shows the frequency transient response under load change during PHIL tests. In more details, frequency drops to 49.84 Hz, a touch lower than the drop detected (49.81 Hz) during off-line simulations. Moreover, the diesel's and inverter's power outputs slightly differ during the PHIL tests with the ones derived from the off-line simulations.

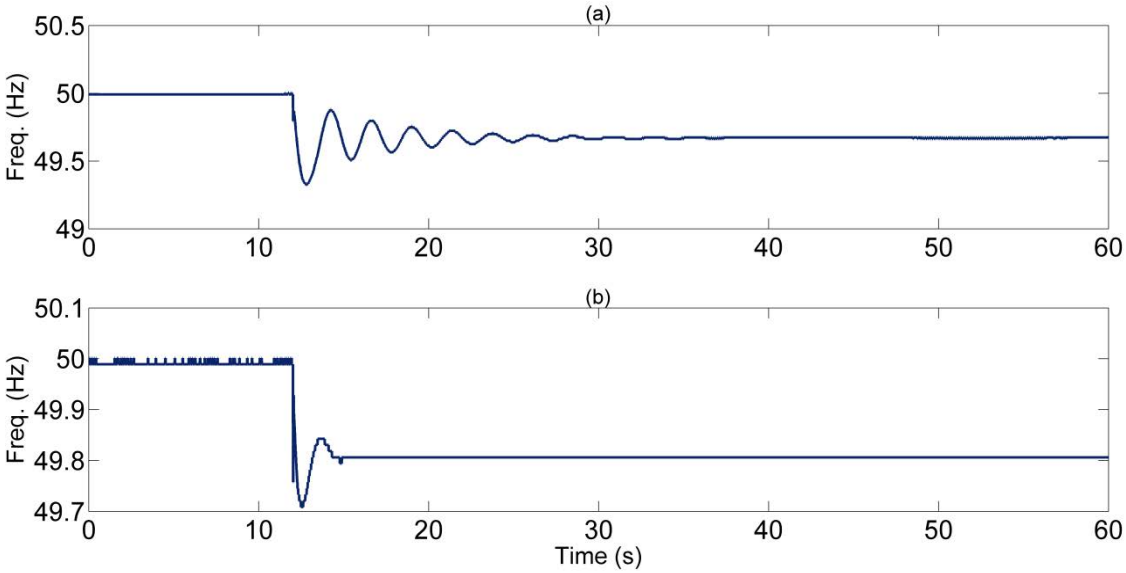

Fig. 5-34: Frequency response (load change) a) without & b) with storage.

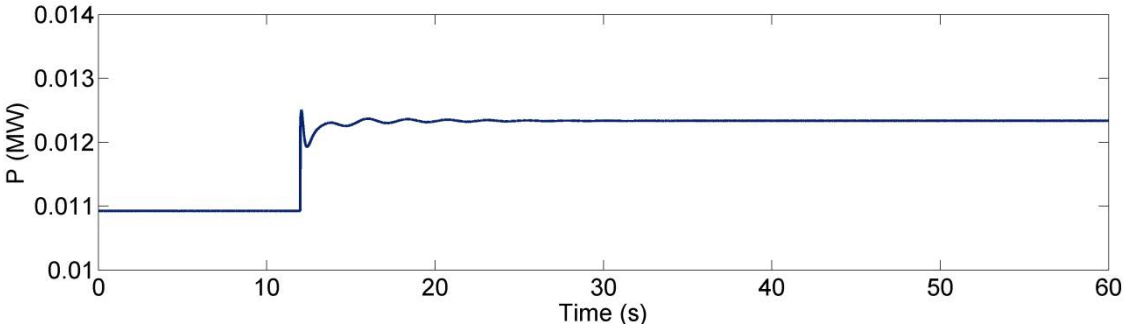

Fig. 5-35: Diesel´s active power output without storage during load change.

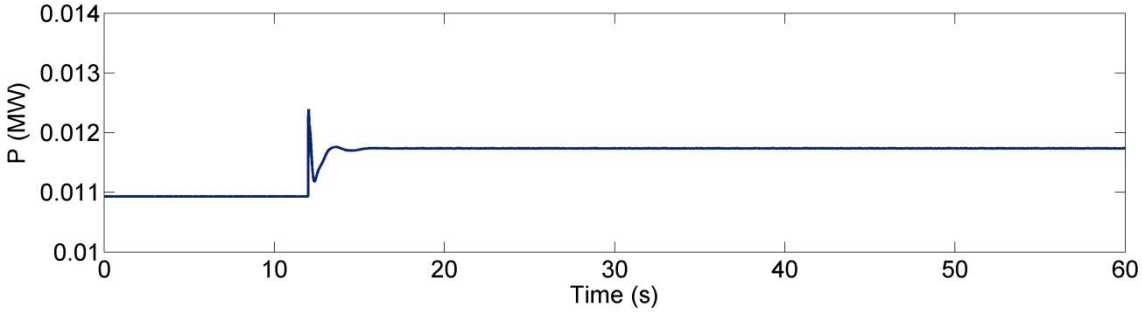

Fig. 5-36: Diesel´s active power output with storage during load change.

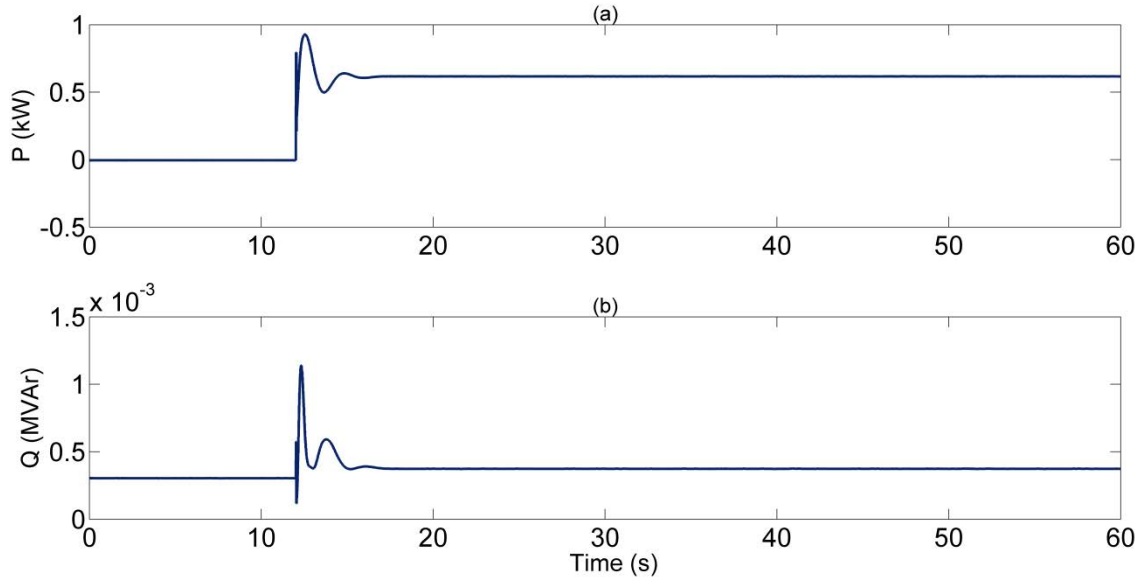

Fig. 5-37: Battery Inverter a) active & b) reactive power responses with load change.

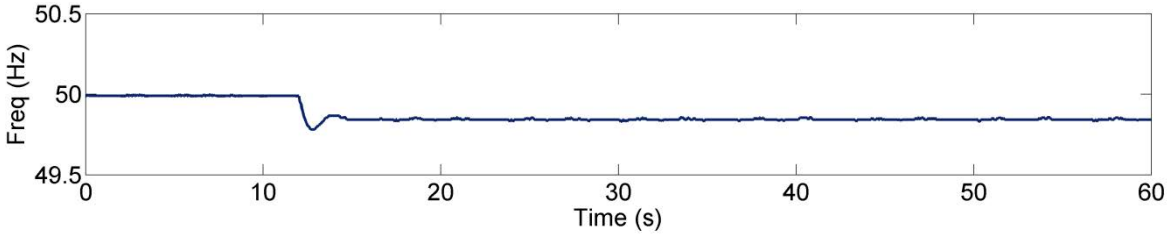

Fig. 5-38: Frequency response (load change) during PHIL tests.

5.6.3. Microgrid Experimental Results

5.6.3.1. Diesel Genset Tests

The diesel generator suffers from frequency and voltage fluctuations due to harmonics distortion in the pulsating torque. Figures 5-39 and 5-40 depict these variations upon different load demands and step changes. The diesel generator's torque pulsations oscillate at a frequency of 0.08 s (Fig. 5-39). In more details, Fig. 5-39 shows that when the load is heavier, i.e. in b and c, the amplitude of the frequency oscillations is larger. However, the frequency´s drop/rise depends on the amount of load change. For instance, when there is a change of no-load to partial load (i.e. from 0 kW to 7 kW), frequency drops from 50.3 to 49.84 Hz. Considering a change from 6 kW to 12 kW, the drop in frequency is even less at the rate of 0.3 Hz (i.e. from 49.8 Hz to 49.5 Hz). In addition, the lowest decrease in frequency is observed when the diesel generator's loading varies from 11 kW to 12 kW. This decrease is of 0.06 Hz (49.5 Hz to 49.44 Hz).

Figure 5-40 illustrates the harmonic content of the diesel generator's voltage fluctuations during a step change from no-load to full load operation. The peak-to-peak voltage is of 660 kV. In no-load operation, the first harmonic of 50 Hz has an rms value of 210 V, whereas the second harmonic can be found at 250 Hz with an rms value of almost 10 V. In full load operation, the second harmonic is found at 220 Hz. Evidently, the diesel generator suffers from inherent frequency and voltage flickering.

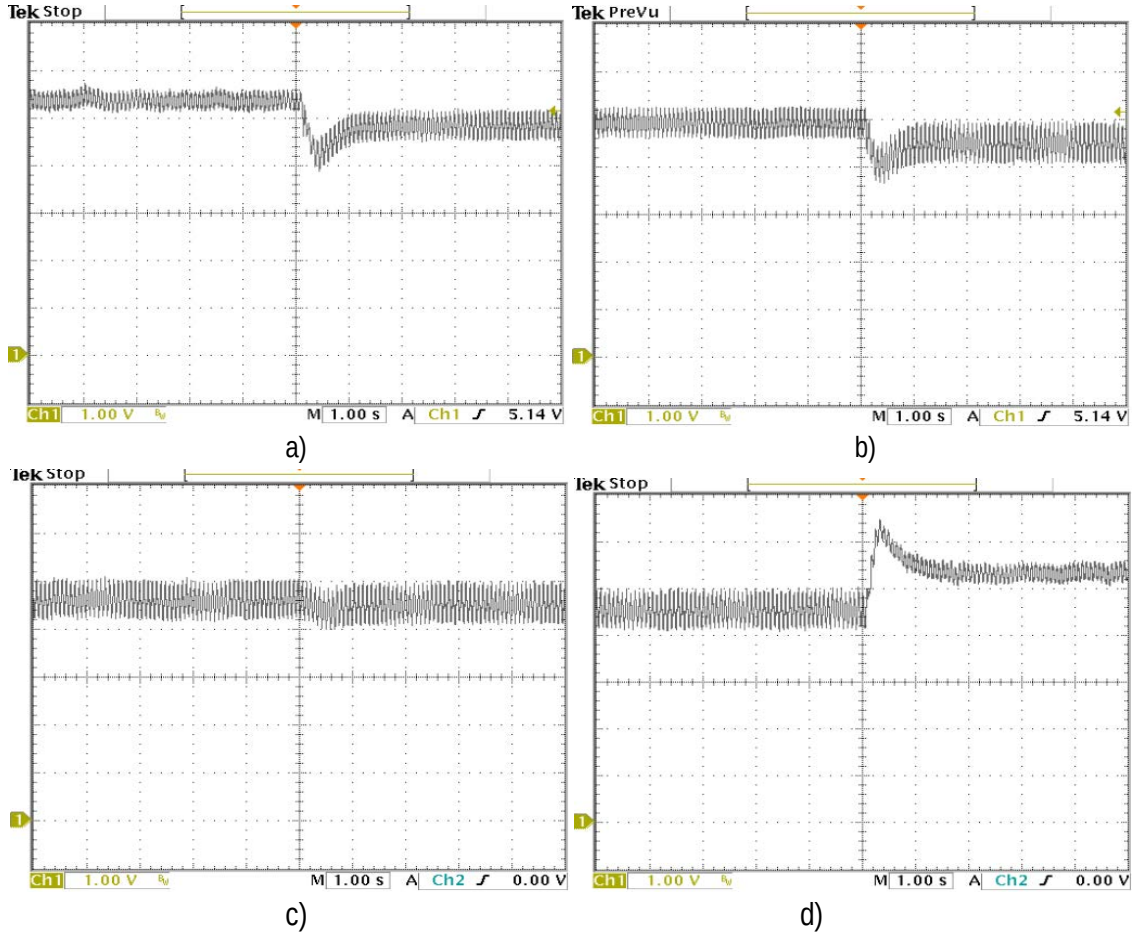

Fig. 5-39: Frequency oscillations under load changes, a) 0 to 7 kW, b) 6 to 12 kW, c) 11 to 12 kW & d) 12 to 0 kW.

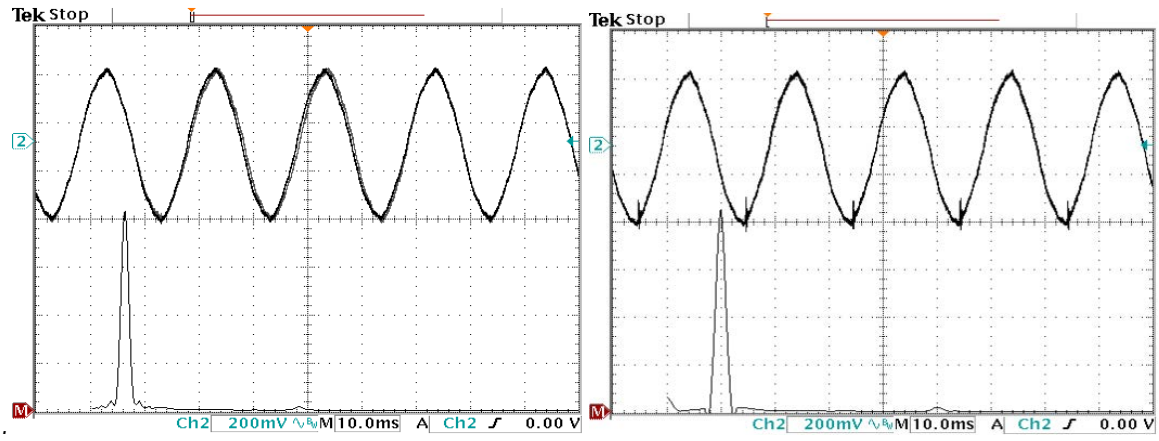

Fig. 5-40: Voltage fluctuations: a) full-load, b) no-load.

Furthermore, the diesel frequency/power (f-P) droop curve was experimentally derived under asymmetric and symmetric loads. The following diagrams (Fig. 5-41 & 5-42) illustrate these results respectively. It is worth mentioning that under asymmetric loading the droop and idle frequency (f_{idle}) differs from phase to phase where the biggest difference is detected on phase A (Slope:-0.044 Hz/kW).

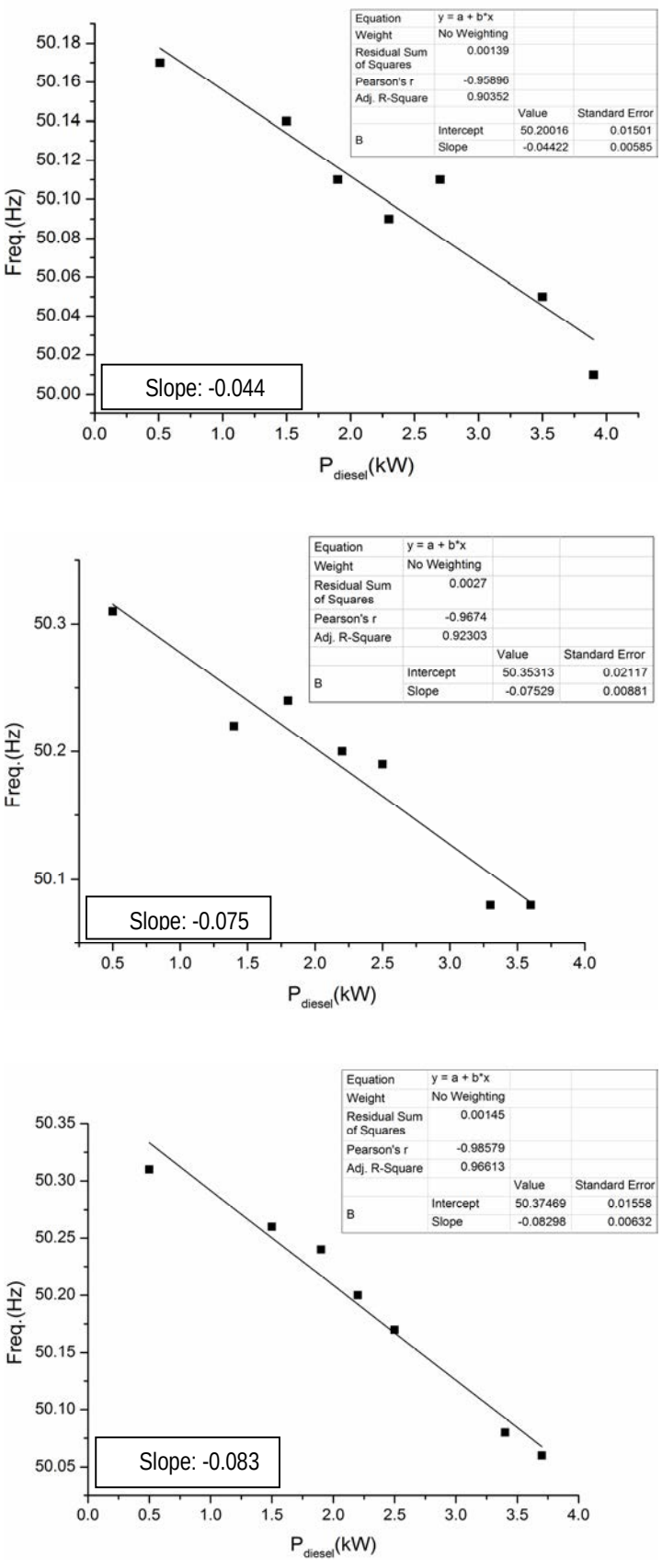

Fig. 5-41: The measured f-P droop curve of the diesel genset for asymmetric loads.

Table 5-10 summarizes the idle frequency deviation in values. It is hypothesized that this deviation is due to possible errors in data logging of the diesel genset´s droop and idle frequency potentiometers resulting in a slight change in the governor´s gains. This change can be attributed to environmental conditions, and especially temperature due to heat at the test site that can affect the results of the experiments.

However, for a three-phase symmetric load the droop characteristic was confirmed at -0.06Hz/kW (Fig. 5-42).

Table 5-10: Asymmetric Loads

Phase	Droop (Hz/kW)	Fidle (Hz)
A	-0.044	50.2
B	-0.075	50.35
C	-0.083	50.38

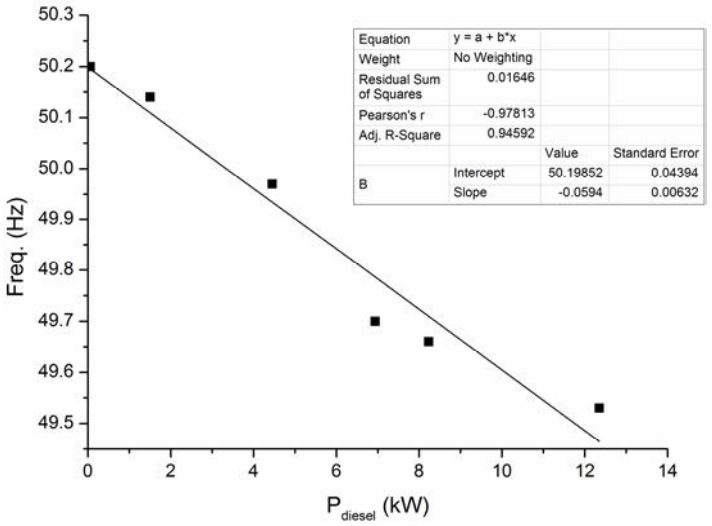

Fig. 5-42: The measured f-P droop curve of the diesel genset for 3-phase symmetric loading.

Moreover, the diesel f-P *droop* curve was experimentally derived for a 2-hr load profile.

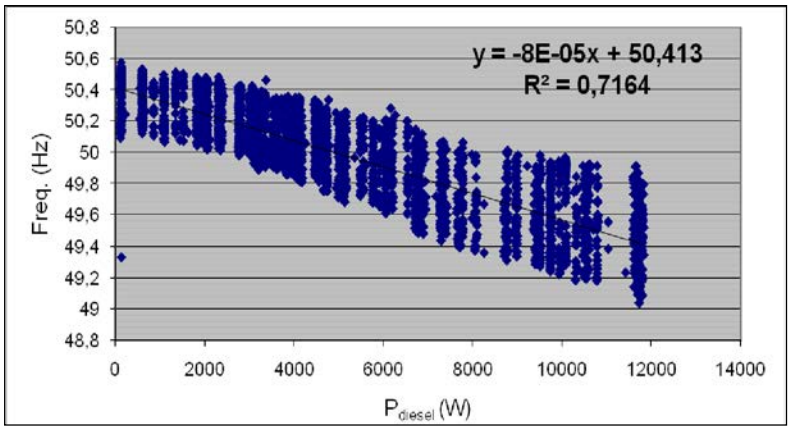

Fig. 5-43: The f-P droop curve of the diesel generator for a 2-hr load profile.

5.6.3.2. Battery Inverter Tests

The following figures (Fig. 5-44 to 5-46) illustrate the experimental results from the battery inverters' tests. In order to obtain each inverter's droop curve, data sets consisting of inverter's output frequency and active power have to be available. The f-P droop calculation was evaluated with static load changes and only one inverter being in use. The one PV inverter is also included. Moreover, the f-P droop was measured for operation of the three inverters (master-slave) with static load variation and asymmetries.

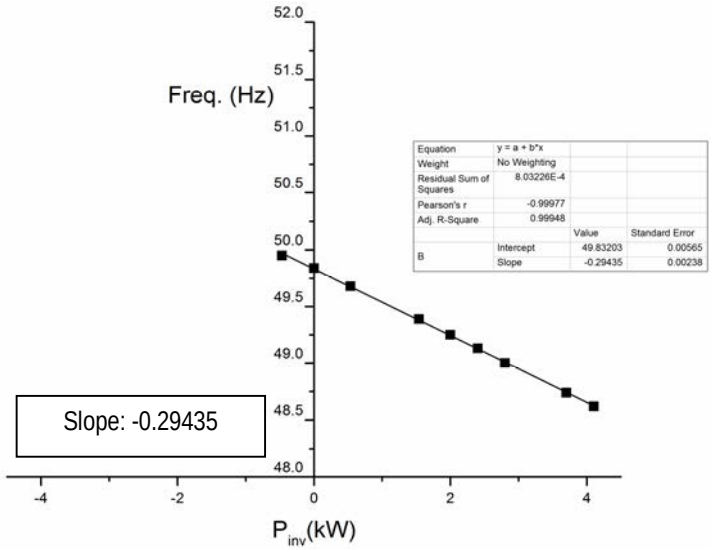

Fig. 5-44: The f-P droop curve of one battery inverter (phase A).

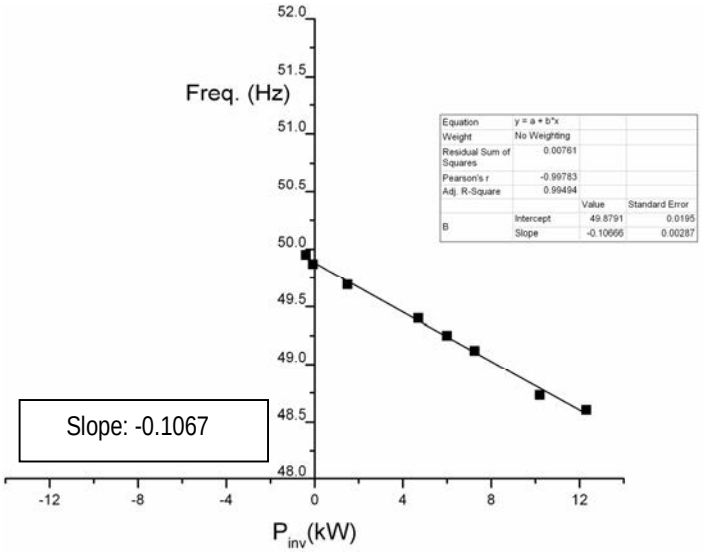

Fig. 5-45: The f-P droop calculation for three-phase operation.

Generally, the Master Inverter defines the frequency in both cases: Either when it is connected to one phase or when the three inverters are connected to the three phases (master-slave operation); i.e. at 4.1 kW (single-phase operation) and 12.3 kW (three-phase operation) load demand, the frequency is the same at the figure of 48.6 Hz. In addition, under asymmetric loads any variation in the master inverter´s power output will once again define the change

in the frequency. For instance, in our case the master inverter is connected to phase A, thus any changes in load demand at this phase and only in this phase will dominantly affect the frequency behavior. This result is evident in Fig. 5-46.

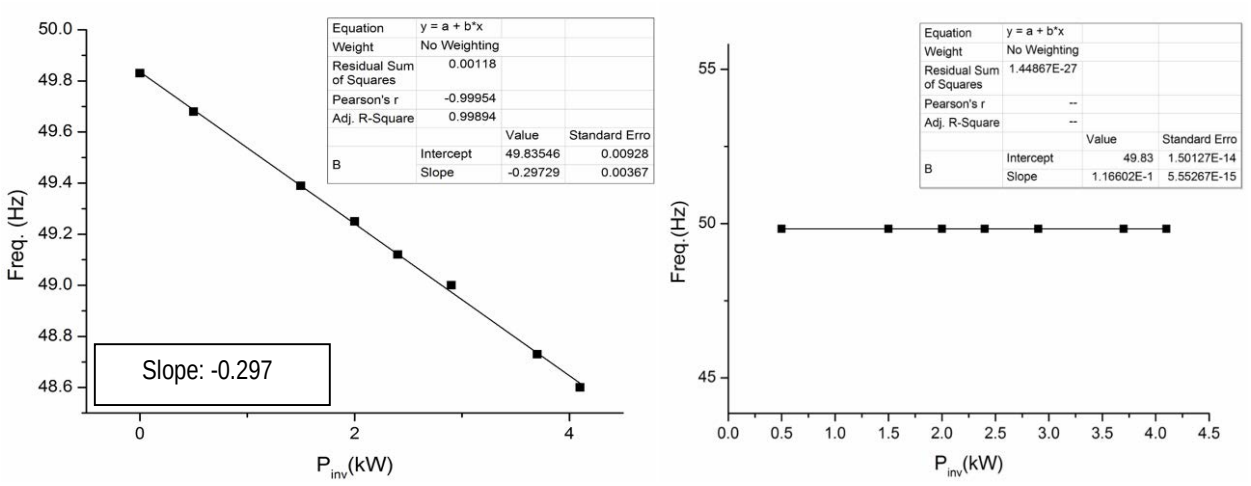

a) b)

Fig. 5-46: The f-P droop curve for asymmetric load variation: a) phase A (master inverter), b) phases B, C (slave inverters).

Figure 5-47 shows the f-P droop curve for the three inverters with a 2-hr load profile.

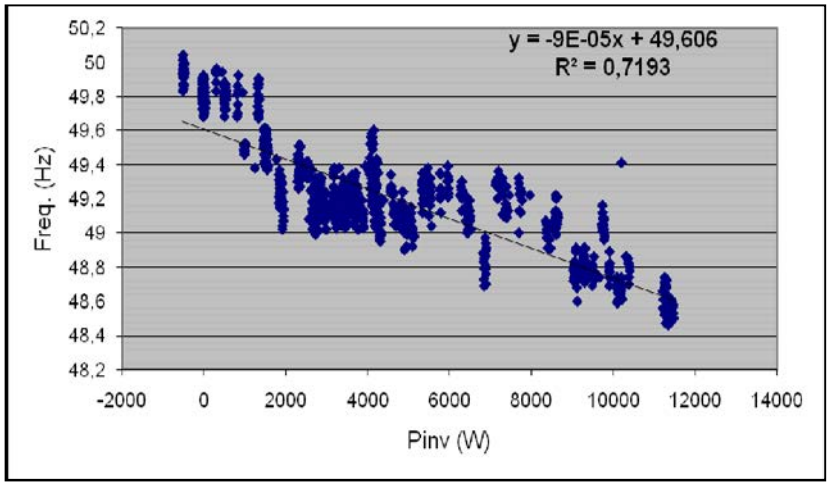

Fig. 5-47: The battery inverters´ f-P droop curve for a 2-hr load profile.

One additional experiment involved the load sharing for parallel operation of two battery inverters being both connected in one phase and demonstrate the concept of the battery inverters' active power control by changing the frequency droop (droop f) curve. For all the following cases, the output power is measured: a) different droops (-2Hz/P_{nom}, -1Hz/P_{nom}) and f_{idle} (intersection of the droop f curve with the y-axis) is of 50 Hz, b) same droop (-1Hz/P_{nom}) and f_{idle}=50 Hz and c) same droop (-1Hz/P_{nom}) but the idle frequency is changed to 50.3 Hz. Figure 5-48 illustrates these results.

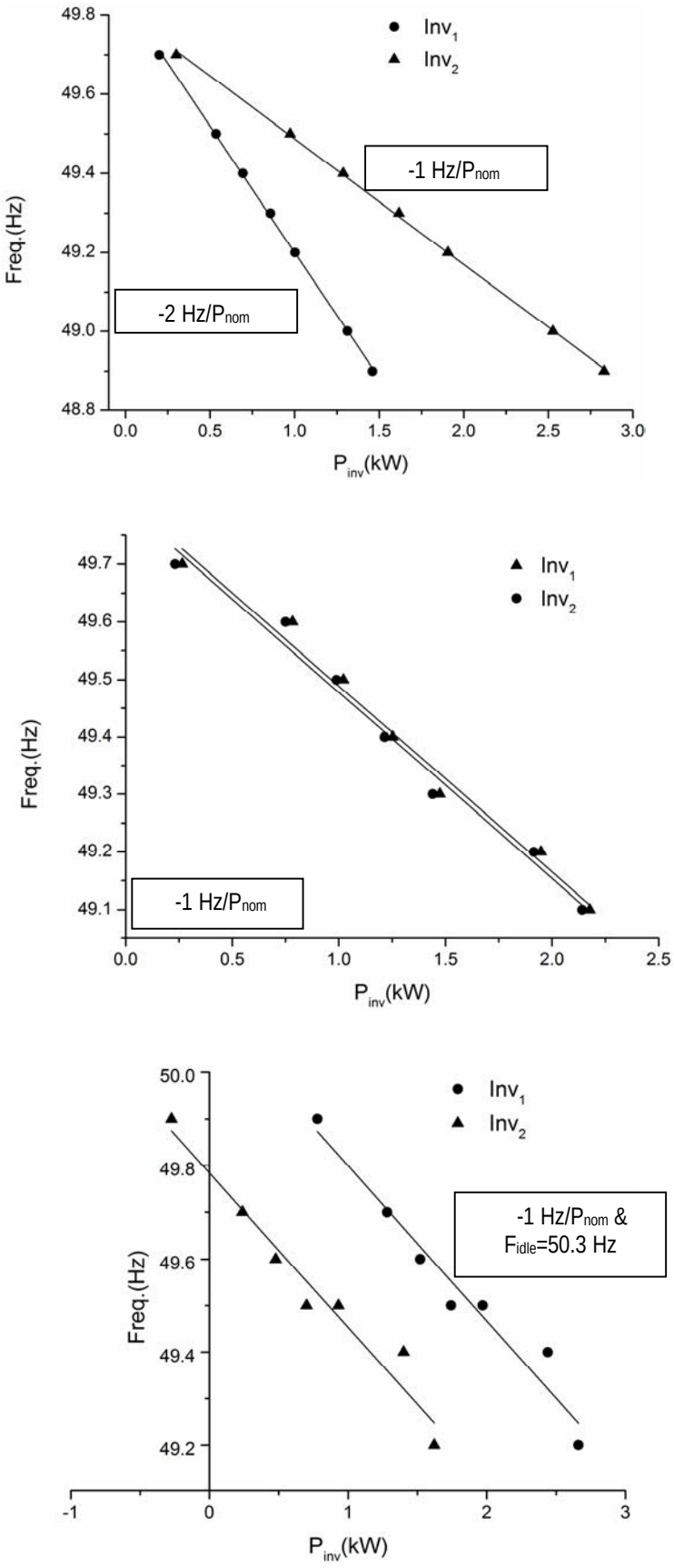

Fig. 5-48: Load sharing for parallel operation of two battery inverters.

The last experiment included the investigation on the frequency and voltage behavior of the battery inverter by changing the load demand and switching the mode operation (grid connected to islanded transition). Figures 5-49 to 5-51 depict these outcomes. First of all, in Fig. 5-49 only the master inverter is connected to phase A while the Microgrid is islanded. The frequency and voltage fluctuations are derived from no-load to full load step change, i.e. from 0 kW to 4.1 kW.

Regarding the disconnection tests, the inverter´s voltage waveform does not substantially change (Fig. 5-49) because the load is purely restive and not reactive, whereas its frequency suffers from a drop of 1.22 Hz, namely from 49.84 Hz to 48.62 Hz.

When the inverter's operation mode is changed (DroopMains operation), namely it is operated together with the utility in droop mode and in case a transition from grid connected to island mode occurs, the voltage remains uninfluenced as it presents no interruption (Fig. 5-50) and the frequency falls to 49.6 Hz.

Considering a specific operation mode of the battery inverter (Fast Mains operation), the voltage falls to zero (Fig. 5-51) when switching from grid connected to disconnected operation and the battery inverter is behaved as grid former with, however, an interruption of about 1.2sec in the voltage waveform.

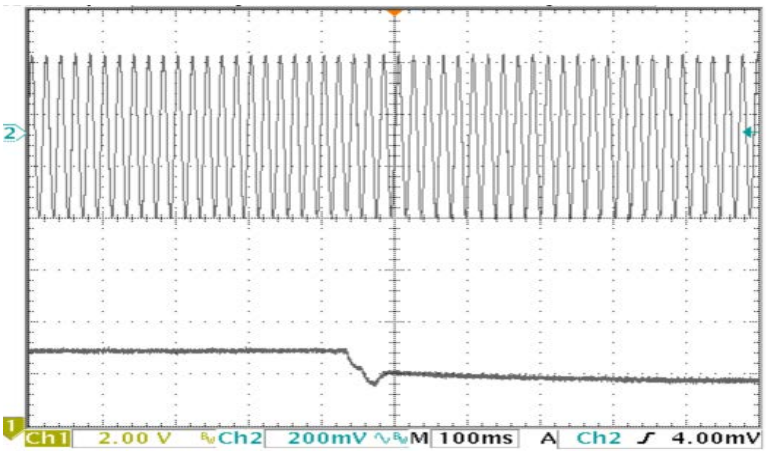

Fig. 5-49: Battery Inverter´s voltage and frequency response under step change in the load.

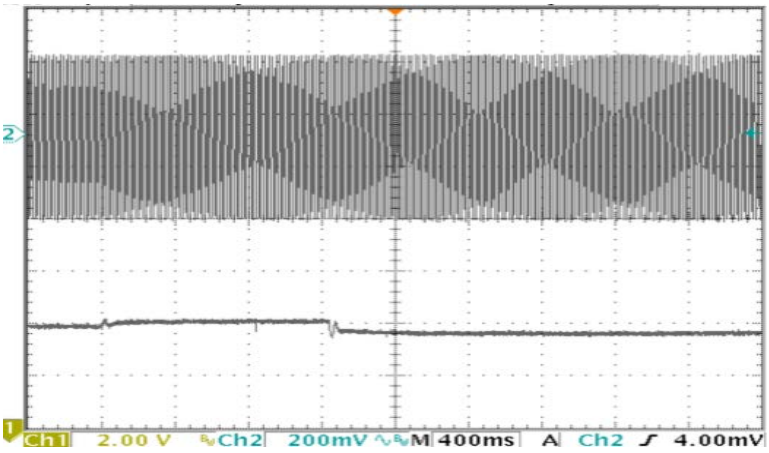

Fig. 5-50: Master Inverter´s voltage disturbance (DroopMains mode).

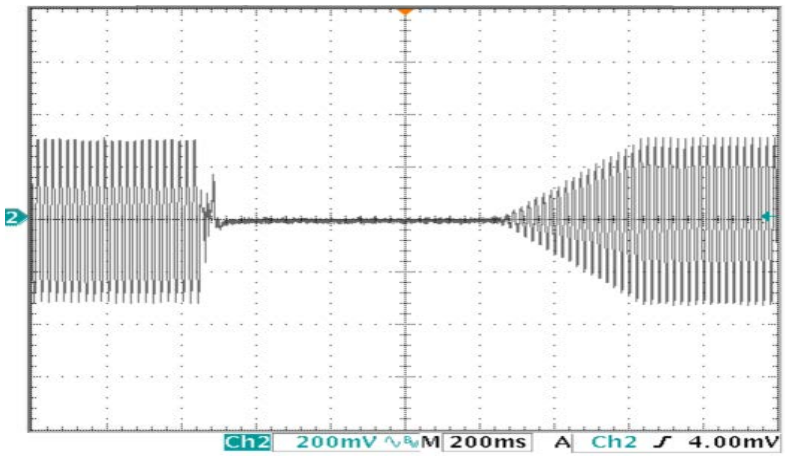

Fig. 5-51: Master Inverter´s voltage disturbance (Fast Mains mode).

5.7. Summary

This Chapter resumes the results of PHIL and Microgrid tests in support of the studies on the DER integration within the DERri European project. The current research work is divided into two test case studies;

The first one demonstrated a detailed description of switching inverters' controller design and investigated the effects of an inverter-based STATCOM on voltage regulation of a low voltage distribution network using RSCAD/RTDS environment. The Average Model of a STATCOM interfaced to DC capacitor was simulated, where the IGBT Voltage-Source Converter was represented by equivalent controlled voltage sources. The STATCOM was modeled in the Real-Time Digital Simulator's (RTDS) dedicated software RSCAD. Subsequently, PHIL tests were executed with the Hardware under Test (HuT) being a passive single phase load of varying inductance and resistance.

PHIL simulation results confirmed that the STATCOM model studied throughout this work is suited for voltage sag mitigation, since it compensated the reactive power required during a step decrease in the hardware inductance and led to improved steady-state voltages. Additionally, the implemented control strategy of the ESS maintained the VSI's DC bus voltage constant.

The second case study demonstrated an implementation of a Microgrid model in RSCAD/RTDS simulation platform for DER device integration. PHIL simulations were executed to emulate the energy management of a real Microgrid system including a diesel synchronous machine and inverter-based sources. Moreover, their dynamic behaviour was examined within the LV islanded power system and more than that the adequate performance of the laboratory set-up is verified through tests on a real experimental site.

Concluding, RSCAD/RTDS is an effective tool suitable for transient analysis due to its fast computation in real time and the laboratory hardware interfacing capability it offers. Furthermore, PHIL experiments provide high flexibility in the research of complex problems which concern the penetration of various energy systems with respect to network stability and security.

However, there still exist uncertainties when performing PHIL tests. For instance, in real life there is no ideal Power Interface. As a result, imperfections that are mainly inserted by the power interface can reduce the accuracy of the simulation. Examples of these imperfections are the time-delay and the low pass filter of the amplifier, the time-delay of the sensor and the sensor's noise. Therefore, an accuracy analysis of the PHIL tests is recommended. There are different techniques on this matter. The one that we followed during the experiments was that we run the off-line simulations on RSCAD/RTDS software and compare the results with those obtained by the real PHIL tests.

Additionally, throughout this research work virtual hardware-in-the-loop experiments (off-line simulations) were performed in Matlab/Simulink to check the system's stability for the different test scenarios. There is also the uncertainty related to measurement devices (e.g. current measurement of the power interface) that has to be taken into consideration.

PART III. The Operation *of* a Diesel Genset in an Autonomous Network

Part three, documents the operation of a diesel-powered autonomous grid which takes into account the power quality measurements with focus on frequency and voltage flickering. A new control scheme is proposed in order to eliminate the amplitude range of these inherit electrical oscillations.

Chapter 6. A Diesel-Powered Island Grid

6.1. Introduction

Autonomous power grids, like small and medium sized islands, are ordinarily medium/low voltage networks fed by central power stations, such as diesel power plants. The main concern in weak Island grids is the power quality issues including the effects from the connection and integration of renewable energy sources due to the islanded operation of these units. Besides, autonomous power systems appear to have different characteristics from interconnected grids of relatively fixed frequency and high short-circuit capacity, where the renewable energy sources are ordinarily connected.

Diesel engine generating units have customarily been introduced as backup sources in autonomous power grids whereas lately, have been used in hybrid power systems to assist the penetration of renewable energies, such as wind and solar energy sources [140-147]. A diesel genset converts the chemical energy (fuel ignition) into mechanical energy via a combustion engine, and in continuation into electrical energy via a synchronous machine operating as a generator.

However, one important issue questioned in islanded networks is the transient behavior of diesel gensets during critical disturbances induced by intermittent power sources and load step changes and more than that, the degraded power quality induced by their inherit torque oscillations [148-153]. The flicker concern is higher when firing asymmetries take place among the cylinders, namely fuel/air compression ratios, ignition imbalances etc, affecting seriously the frequency oscillations in the shaft torque.

The majority of the literature reports related to this topic, analyze the pulsed nature of diesel generating units and state that flickering is an inherit problem a diesel induces itself [67, 154-159]. Although the bibliography reviews formulate the problem, study the dynamic response of a diesel genset, and analyze quantitatively the phenomenon but without attending an answer to sort out or even improve this permanent frequency and voltage fluctuations occurrence [67, 154, 160, 161]. Such an effort will be reinforced throughout this thesis.

In more details, [67, 154] present the outcomes of power quality measurements with emphasis on voltage flickering in a medium-voltage network containing diesel generating units. The results mainly recorded the coupling between the engine shaft torque pulsations and so voltage fluctuations due to cylinder misfiring. In [148], a control strategy is proposed that eliminates the electrical fluctuations within a multi-unit diesel power plant. This control scheme is relied upon controlling the phase of the rotor angles of each one generator during the synchronization process.

The main objective of this research study is the analysis of the operation of a diesel-powered autonomous grid that takes into account the power quality measurements with focus on frequency flickering. Broadly speaking, this is an inherit problem of the diesel generators and internal combustion engines induced by the pulsed variation of the diesel genset´s torque [67, 154] and it was also detected during the onsite Microgrid experiments described in Chapter 5.

The current work demonstrates and analyses the steady-state electrical fluctuations that are evident in diesel-driven generators for two different medium-speed diesel powered plants rated at 16 and 8.1 kVA respectively. The presence of low-frequency oscillations, mainly rated at 50 Hz is highly linked to the pressure imbalance during firing process, in addition to the torque pulsations among the cylinders. A control scheme is proposed in order to eliminate the amplitude range of these inherit frequency oscillations, and could be very useful for rural and Island power network configurations. For instance, this control structure is implemented on the 8.1 kVA diesel genset model.

The chapter starts with a description of the test power system which is a low voltage network rated at 400 V that consists of an isolated diesel genset system connected to a resistive constant load. In continuation, the diesel genset modeling in Simulink is detailed. A background on the inherit torque oscillations met in diesel-driven generators is given and the Simulink blocks of the model, namely throttle, intake manifold, mass flow rate, compression stroke, torque generation and acceleration are analytically described. Finally, the power quality simulation results are outlined for all the test case scenarios employed.

6.2. Case study: Description of the System

The test power system is a low voltage network rated at 400 V that consists of an isolated diesel genset connected to a constant resistive load and a controllable power source. The controllable source is nothing more than a dynamic power source which corresponds to frequency's changes by varying it output according to a characteristic droop curve (w/P). An energy storage system, such as a battery inverter could represent this dynamic power source.

The operation of the diesel genset with the presence and absence of the dynamic power source in the LV distribution network is studied by performing a number of simulation tests. Fig. 6-1 & 6-2 illustrate the test set-up configurations for both groups of simulations for analysing the interaction between the genset and the dynamic power source. In addition, the Simulink blocks for the complete model configuration are given in Fig. 6-3.

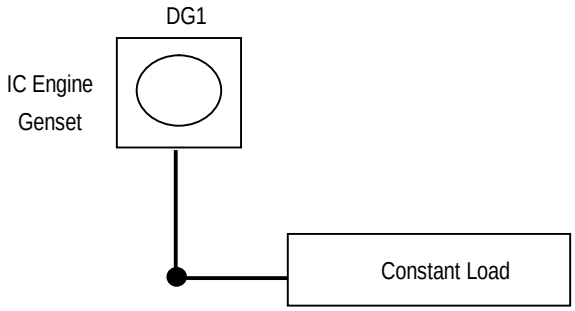

Fig. 6-1: Single-line diagram of the synchronous source connected to a resistive load.

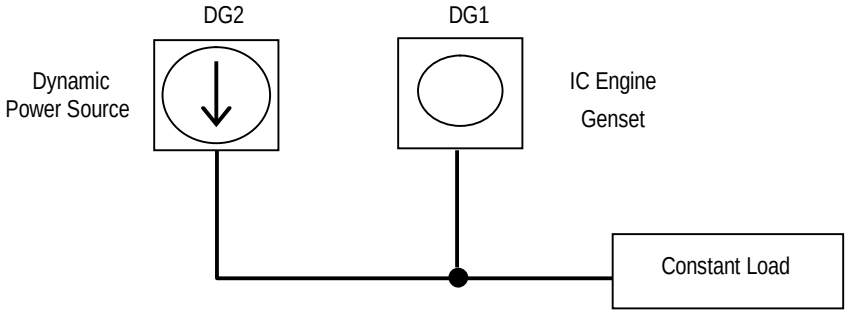

Fig. 6-2: One-line diagram of the power system with a synchronous source and a dynamic power source.

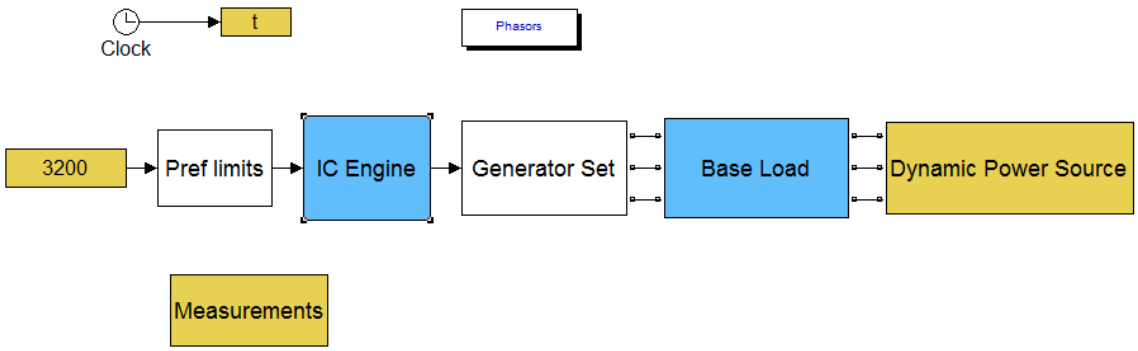

Fig. 6-3: Matlab/Simulink system model including the dynamic power source.

In more details, two set of tests were performed throughout this research work; firstly, the steady-state operation of an isolated diesel genset system is examined for two generator preset models from the Simulnk Library, which are rated at 16 kVA (Model 1) and 8.1 kVA (Model 2) respectively. The resistive load is of 3 kW.

Secondly, a couple of simulation results are given for the above distribution network that now consists of a diesel engine coupled to a standard synchronous machine model of 8.1 kVA running in parallel with a dynamic power source both satisfying a resistor. The load sharing capability of the sources is monitored during changes in the base load, i.e. from 4 to 7 kW.

The diesel genset's engine utilized within this study is a four-stroke four-cylinder engine operating at a rated speed of 1500 rpm. The tables below (Table 6-1 & 6-2) concentrate their data.

The steady-state electrical frequency fluctuations that are evident in diesel-driven generators in addition to the torque pulsations among the cylinders are analyzed and discussed throughout the two sets of tests.

Table 6-1: Diesel Generator Parameters (A)

Ratings		Model 1	Model 2
3-phase Output	Sn	16 kVA	8.1 kVA
Rated Voltage	Un	400 V	400 V
Frequency	f	50 Hz	50 Hz
Speed	n	1500 rpm	1500 rpm
Pole pairs	p	2	2

Table 6-2: Diesel Generator Parameters (B)

		Model 1	Model 2
Stator Winding	Rs	0.0645 pu	0.0820125 pu
Reactances			
Synchronous - Direct Axis	Xd	1.734 pu	1.8 pu
Synchronous - Quadrature Axis	Xq	0.861 pu	0.895 pu
Transient - Direct Axis	X'd	0.177 pu	0.184 pu
Transient - Quadrature Axis	X'q	0.228 pu	0.072 pu
Subtransient - Direct Axis	X''d	0.111 pu	0.115 pu
Subtransient - Quadrature Axis	X''q	0.199 pu	0.207 pu
Time Constants			
d: Transient	T'd	0.018 s	0.012 s
d: Sub-transient	T''d	0.0045 s	0.003 s
q: Transient	T''q	0.0045 s	0.003 s

6.3. Diesel Genset Modeling

This section gives a detailed description of the Simulink model of the diesel genset system that includes an internal combustion engine driving a synchronous generator.

6.3.1. Torque oscillations in diesel engine gensets

The resulting mean output torque of an internal combustion engine is the sum of the instantaneous torques produced by the subsequent momentary fuel pressures within each cylinder [162] and oscillates periodically at different frequencies [148]. The gas pressures performed on each piston vary against crank angle throughout a cycle and this takes place every 360 crank degrees for a two-stroke engine and every 720 crank degrees (two crankshaft revolutions) for a four-cycle engine. This occurs because in a two-stroke engine, the power stroke cycle coincides with one shaft revolution.

Contradictorily, in a four-stroke engine, the power stroke cycle coincides with two shaft revolutions. In overall, the power imbalance due to varying pressure pulses results to torque periodic fluctuations of several frequencies over crank angles depending on the number of cylinders, engine speed and firing asymmetries [161, 163]. In a prototypical balanced operation, the torque produced will be the same for each one cylinder and the pulsation frequency will be equal to the firing frequency. However, even the latest diesel engines models are not characterized by a perfectly balanced operation since the engine cylinders do not produce equal torques.

The main goal of this research study is to appraise the function of a four-cycle engine driving a synchronous generator connected to a grid in order to comprehend the origin of the output power fluctuations resulting from engine torque oscillations which influence voltage and frequency, especially when referring to islanded power grids.

The instantaneous shaft torque profile utilised throughout this study, against crank angle values discretized at 30^0 intervals of a total of 720^0 degrees is illustrated in the following graph (Fig. 6-4). This curve depicts the negative and positive torque needed for compression and power stroke and then normalised to its peak value of 1 pu. Moreover, the torque profile given beneath corresponds to solely one cylinder and the mean of the total torque is calculated by summing the four momentary torque components with an 180^0 angular displacement between the consecutive cylinders of the engine.

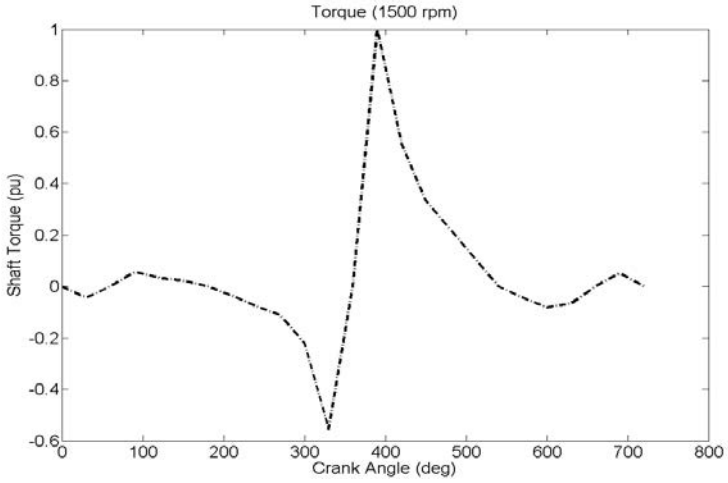

Fig. 6-4: Torque output curve for certain crank angles.

The angular displacement between successive firings in a four-cycle engine is 180^0 [164]. In addition, the firing process of a specific cylinder in this kind of engines takes place every two shaft revolutions with a period given by (6-1) below for a diesel generator of p poles and electrical frequency f [67, 154].

$$T_{REV} = \frac{p}{2f} \tag{6-1}$$

Consequently, the time needed for two consecutive firings is given by (6-2), where k_c=2 for a 2-stroke machine and k_c=4 for a 4-stroke one respectively.

$$T_{PS} = \frac{k_c}{2} T_{REV} \tag{6-2}$$

6.3.2. The Simulink Model

The Simulink Model (Fig. 6-3) consists of four elementary blocks, i.e. the internal combustion engine, the generator set, the base/constant load and the dynamic power source block, where the later entails the proposed control scheme to eliminate flickering at the output of the synchronous generator. The internal combustion engine, synchronous generator and dynamic power source blocks described beneath.

6.3.2.1. IC engine- based genset systems

The Simulink IC engine model described throughout this research work is grounded on the results disseminated by Crossley and Cook (1991) and portrays the simulation of a four-cylinder spark ignition internal combustion engine. The core parts of the engine model as described by [165] are indexed beneath:

- Throttle
- Intake manifold
- Mass flow rate
- Compression stroke
- Torque generation and acceleration

A) <u>Throttle</u>

The throttle body is the key element of the model's simulation and the constrained input is the angle of the throttle plate [165]. Two functions may depict the ratio of air introduction into the manifold and these are; a) an empirical function of the throttle plate angle solely and b) a function containing the atmospheric and manifold pressures. These two equations are described by (6-3) - (6-5) respectively.

$$\frac{dm_{ai}}{dt} = f(\theta) g(P_m) \tag{6-3}$$

Equation (6-3) expresses the mass flow rate into manifold (g/s) where,

$$f(\theta) = 2.821 - 0.05231\theta + 0.10299\theta^2 \tag{6-4}$$

θ is the throttle angle in degrees. Moreover, (6-5) includes the atmospheric and manifold pressure functions, where P_m is the manifold pressure (bar) and P_{amb} is the ambient pressure (bar).

$$g(P_m)=\begin{cases} 1, & P_m \le \frac{P_{amb}}{2} \\ \frac{2}{P_{amb}}\sqrt{P_m P_{amb} - P_m^{\,2}}, & \frac{P_{amb}}{2} \le P_m \le P_{amb} \\ -\frac{2}{P_m}\sqrt{P_m P_{amb} - P_m^{\,2}}, & P_{amb} \le P_m \le 2P_{amb} \\ -1, & P_m \ge 2P_{amb} \end{cases} \tag{6-5}$$

B) Intake Manifold

The difference between the time derivatives of the inward and outward mass flow rates illustrates the net change of air mass over time. This amount is in proportion analogous to the time derivative of the manifold pressure [165]. The following equation (6-6) illustrates this result,

$$\frac{dP_m}{dt} = \frac{RT}{V_m}(\dot{m}_{ai} - \dot{m}_{ao}) \tag{6-6}$$

Where:

R	specific gas constant,
T	temperature (°K)
V_m	manifold volume (m^3)
$d(m_{ao})/dt$	outgoing mass flow rates of air (g/s)
$d(m_{ai})/dt$	ingoing mass flow rates of air (g/s)
dP_m/dt	time derivative of the manifold pressure (bar/s).

C) Incoming mass flow rate

The output of the manifold plate is the mass air flow rate that is induced onto the engine's cylinders and is given empirically [165] by (6-7), where N is the engine speed in rad/s.

$$\dot{m}_{ao} = -0.366 + 0.08979\,NP_m - 0.0337\,NP_m^{\,2} + 0.0001N^2P_m \tag{6-7}$$

In order to find the total air charge drawn up to the cylinders, it is necessary to integrate the incoming mass flow rate into the manifold and display it at the end of each one intake stroke event. Besides, for an inline four-stroke engine, the fuel is injected every one-fourth of revolution cycle. This procedure defines the whole air mass that is introduced in every cylinder successively to the intake stroke and antecedent to compression.

Figures 6-5 to 6-7 show the Throttle and Intake Manifold subsystems. The throttle valve operates in a nonlinear way and is simulated as a subsystem with three inputs, i.e. the theta angle, the manifold and the atmospheric pressures. The variables of (6-3) to (6-5) equations are represented in Simulink as function blocks. Thus, it is possible to describe efficiently the nonlinear behavior of the throttle valve. By comparing the pressure ratio to its switch threshold via a switch block, which is fixed at one half in (6-5), we can determine whether the mass air flow is sonic or not. If the flow is sonic, then its rate depends exclusively on the throttle angle. Moreover, the flow direction if from the higher to the lower pressures, so the ´´min´´ block warrants that the pressure ratio (pratio) is unity or less (Fig. 6.6). The intake manifold subsystem is modeled according to the differential equation (6-6).

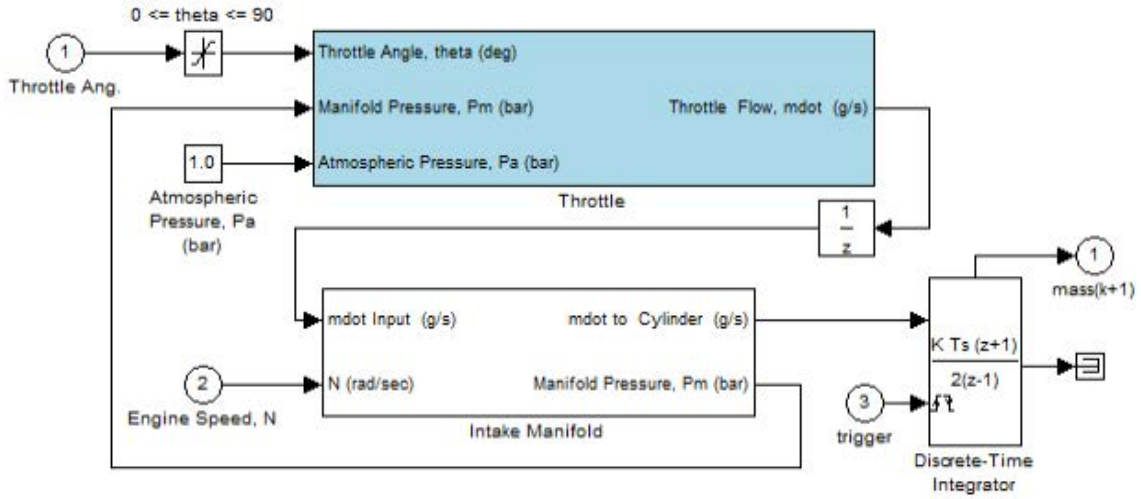

Fig. 6-5: Throttle Manifold Dynamics [165].

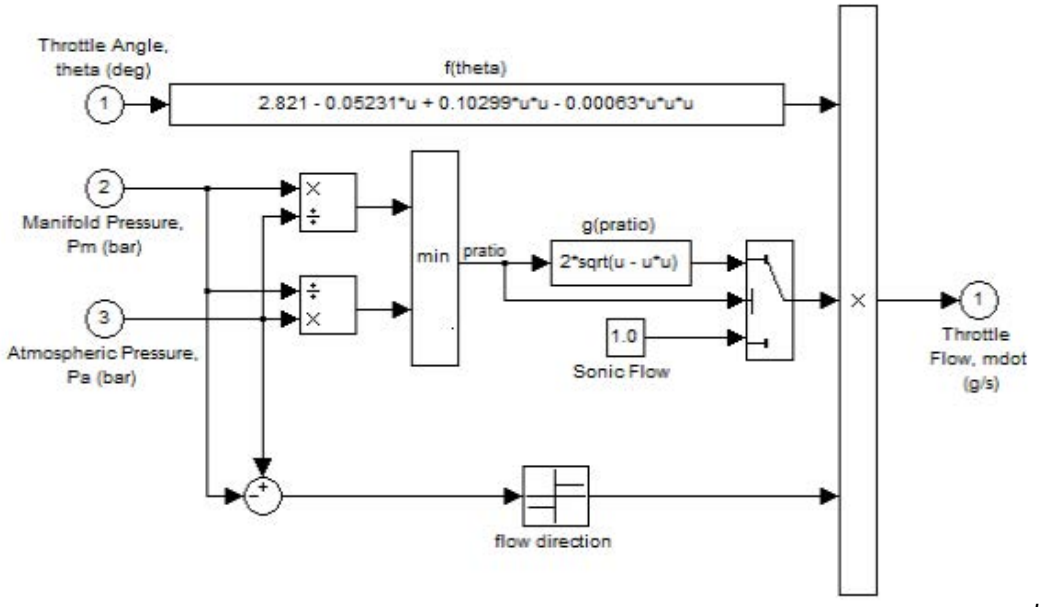

Fig. 6-6: Throttle Flow vs. Valve Angle and Pressure [165].

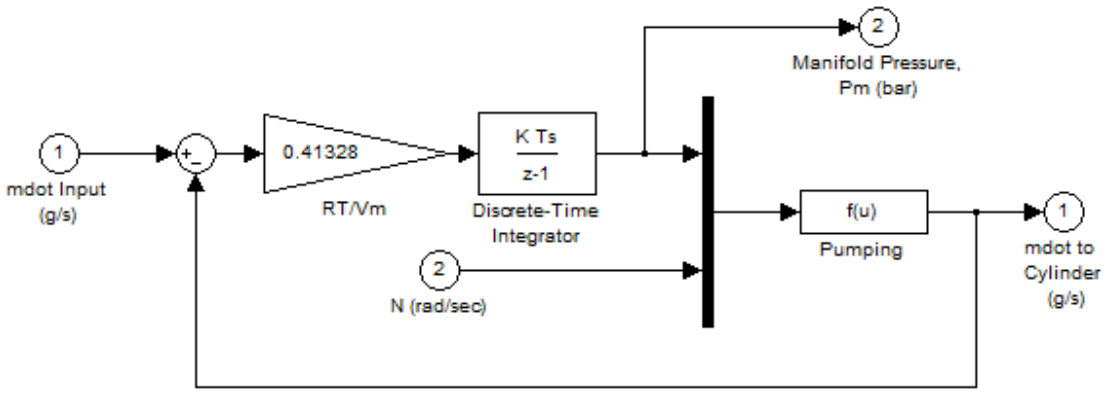

Fig. 6-7: Intake Manifold Subsystem [165].

D) Torque generation and acceleration

The last step is the combustion process which entails the torque produced by the engine and is described by an empirical equation given by (6-8).

$$T_m = -181.3 + 379.36 m_a + 21.91(A/F) - 0.85(A/F)^2 + 0.26\sigma - 0.0028\sigma^2 + 0.027N - 0.000107N^2 + 0.00048N\sigma + 2.55\sigma m_a - 0.05\sigma^2 m_a \quad (6\text{-}8)$$

Where:

T_m	torque produced by the engine (Nm)
m_a	mass of air for combustion (g)
A/F	air to fuel ratio
σ	spark advance

Figure 6-8 illustrates the function block parameters for the computation of the engine torque. As it can be easily seen, the latter is a relationship of four variables (air charge, air to fuel ratio, spark advance and speed).

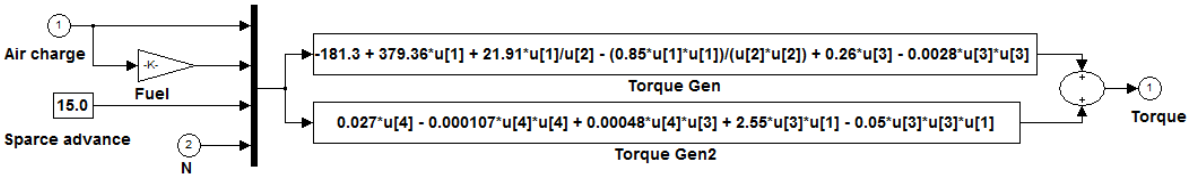

Fig. 6-8: Combustion process and torque generation.

The torque that loads the engine subtracted by the engine torque results in acceleration and this net difference is described by equation (6-9).

$$J\dot{N} = T_m - T_{load} \quad (6\text{-}9)$$

Where:

J Engine rotational moment of inertia (kg-m^2)

d(N)/dt Engine acceleration (rad/s^2)

In our case, the torque produced will drive a synchronous machine which loads the engine.

E) Compression Stroke

Since the engine model utilised within this thesis is a four-cylinder and four-stroke engine, the firing event of each consecutive cylinder takes place every 180^0 of crankshaft revolution, resulting in each cylinder experiencing ignition on successive crank rotations. Fig. 6-9 illustrates the Throttle & Manifold Intake, Compression and Combustion Systems. The combustion of every intake charge is delayed by 180^0 of crankshaft revolution from the completion of the intake stroke (Fig. 6-10).

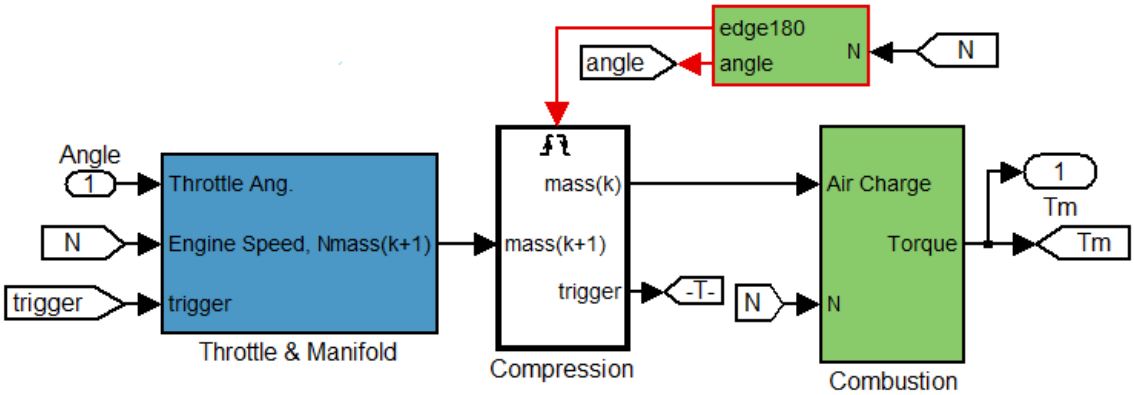

Fig. 6-9: Intake Manifold Subsystem.

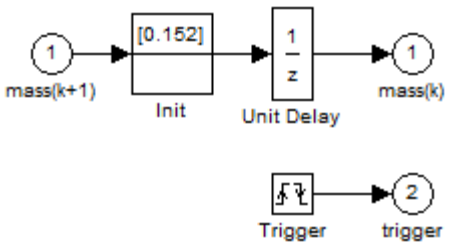

Fig. 6-10: Unit Delay Block in the Compression Subsystem.

Here, a power stroke cycle corresponds to two shaft revolutions, thus the mass air charge for the combustion process is calculated over half stroke cycle. During the intake stroke in the manifold, an integrator in the Intake block integrates the mass flow rate. At the one-fourth of crank rotation (180^0), the intake valve closes and the output of the compression subsystem is the accumulated mass charge, which is available for use 180^0 after due to the unit delay during the combustion process. All along the combustion stroke, the crankshaft speeds up because of the generated torque. Moreover, during the last 180^0 shaft rotation, the intake integrator is rest for the next complete cycle of the cylinder.

It is worth mentioning that the valve events happen with a frequency of four times of crankshaft rotation. Each one incident triggers a single execution of the compression block (Fig. 6-11), whereas this event induces pulses analogous to concrete rotational positions in order to manage the intake and compression timing. Considering that the mean torque (T_m) is calculated over 180^0 angular displacement, we included an extra intake integrator to calculate the shaft position displacement throughout the entire cycle of 720^0 (Fig. 6-12 & 6-13).

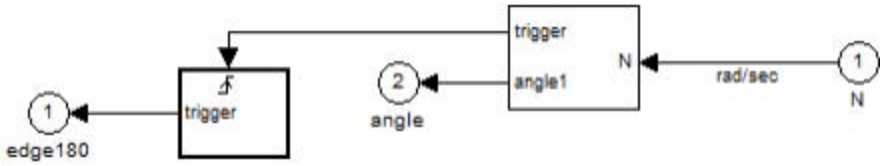

Fig. 6-11: Rotational velocity to synchronized discrete event conversion.

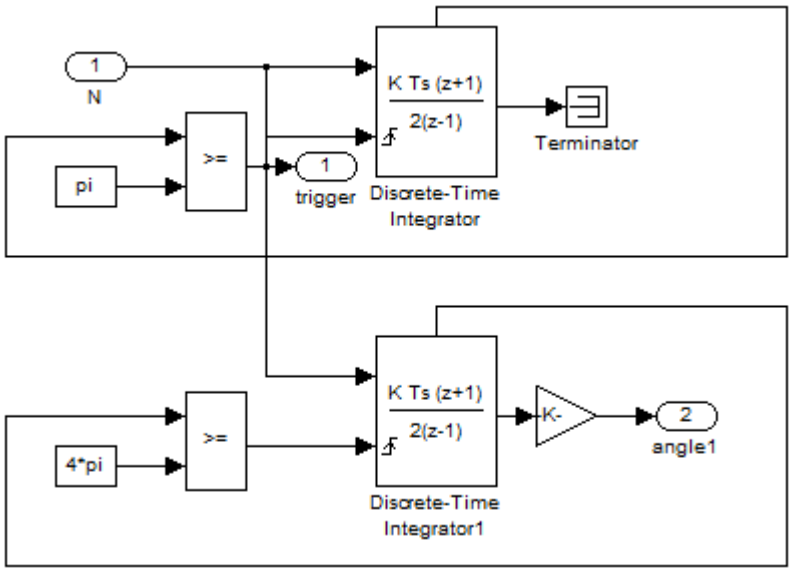

Fig. 6-12: Calculation of angular position over 720 crank degrees.

In addition, the model provided by [165] accounts for a complete four-stroke cycle of only one cylinder. Therefore, throughout the current thesis, we went a step further; the momentary position of the crankshaft for all the four cylinders was evaluated in order to define the relation between the instantaneous torque profile to the one of the mean values (Fig. 6-13).

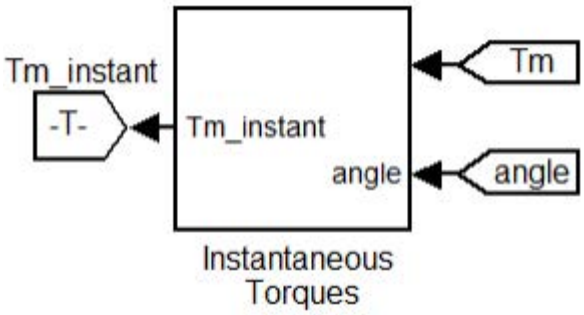

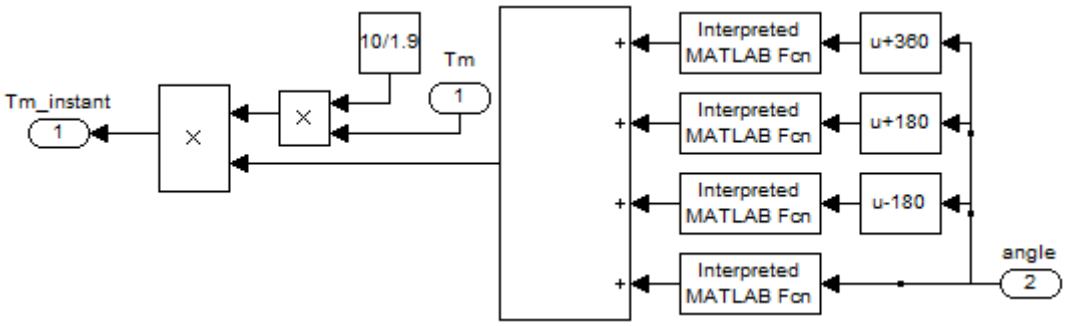

Fig. 6-13: Mean vs. instantaneous torque values including angular displacement during firing events.

6.3.2.2. Generator Set

The Simulink model of the synchronous generator used in this study consists of two inputs, the mechanical power input P_m and the field voltage V_f, whereas one of the obtained outputs is the machine's rotational speed, ω.

The corresponding mechanical input power of the machine is computed as in (6-10), where T is the mechanical torque and ω is the angular velocity in rad/s.

$$P_m = \mathrm{T} \times \omega \tag{6-10}$$

The second input, V_f supplies the DC-side of the main field winding of the synchronous machine and is given by the voltage regulator model to (Fig. 6.14) used in this thesis in conjunction with the engine model.

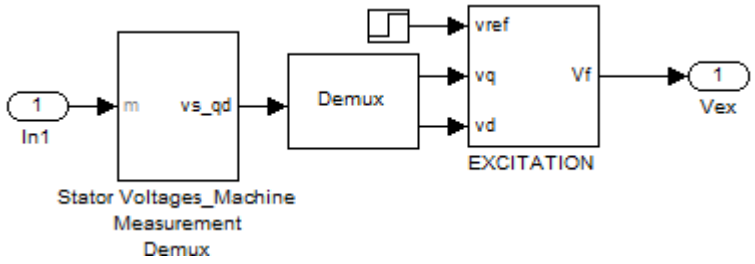

Fig. 6-14: AVR Excitation System Block.

The generator set block consists of the synchronous machine (Fig. 6-15) with inputs the mechanical power (P_m) and the field voltage (V_f), as well as output the generator's synchronous speed (ω). The synchronous machine is connected to a constant load which is a simple resistor.

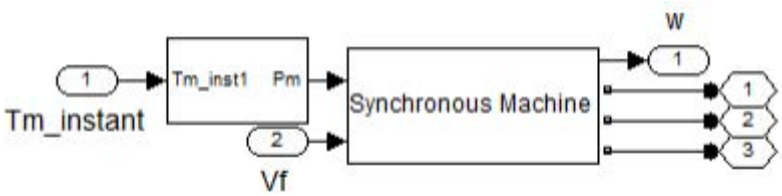

Fig. 6-15: Simulink block of synchronous machine.

6.3.2.3. *Dynamic Power Source Block*

The dynamic power source is a controlled three-phase source which is used to supply a given active and reactive power set-point in order to reduce the frequency flickering and trying to keep the frequency stable under load step changes. In our study, the active power flow is controlled via f/P droop control (Fig. 6-16).

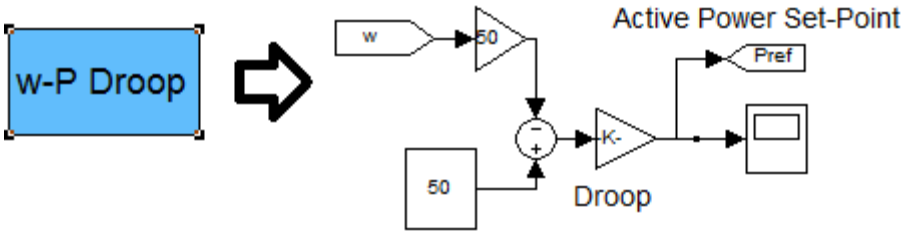

Fig. 6-16: Simulink block of dynamic power source control scheme.

6.4. Power Quality Simulation Measurements

As aforementioned, three set of tests are employed within this work in order to study and analyze the steady-state electrical fluctuations that are evident in diesel-driven generators. The first two are implemented for two different diesel powered plants with a speed of 1500 rpm and being rated at 16 kVA (Model 1) and 8.1 kVA (Model 2) respectively. These simulations, actually served to verify the theoretical approach used to describe the power quality problem which highly correlates the amplitude of the electrical oscillations to the pressure imbalance between the diesel engines' cylinders.

The last set of tests concerns the diesel powered plant rated at 8.1 kVA. Here, a control scheme is proposed in order to eliminate the amplitude range of the inherit frequency oscillations. The case study considered different scenarios for load demand ranging between 4 and 7 kW. Moreover, all these scenarios were combined with and without the control scheme integration into the system to verify its contribution on the steady-state electrical fluctuations.

6.4.1. Results for Diesel Genset, Model 1

Model 1 is the diesel genset rated at 16 kVA connected to a resistive load of 3 kW. The pulsating characteristic of the engine torque produced by the four engine's cylinders is evaluated and is apparent in Fig. 6-17. The periodic frequency of the pulsations is 50 Hz for the instantaneous torque values, Tinst.

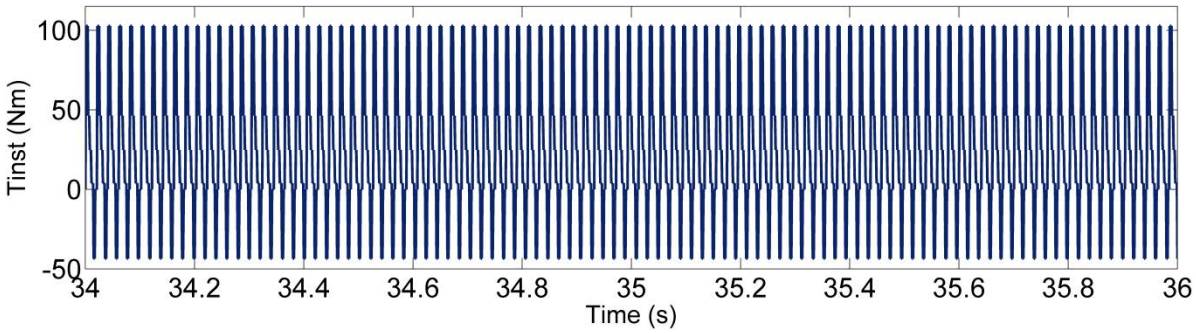

Fig. 6-17: a) Average values of torque, b) Engine torque instantaneous profile.

When a fault incident takes place like an ignition asymmetry or when an active cylinder is out of operation, the output instant torque is increased as it can be easily seen in Fig. 6-18 & 6-19, because the synchronous generator needs to produce more power to satisfy the demand. The instantaneous torque profiles depicted in Fig. 6-18 are the contributions of the remaining three cylinders in operation. The net torque of the misfiring cylinder is supposed to be zero.

The following graph (Fig. 6-18) depicts the instantaneous torque values after taking one cylinder out. The frequency of the pulsations is 36 Hz.

Fig. 6-19 illustrates the instantaneous torque profile after taking out two of the four in total cylinders. The frequency of the pulsations is 25 Hz.

The problem becomes exacerbated when asymmetry resides between two individual cylinders.

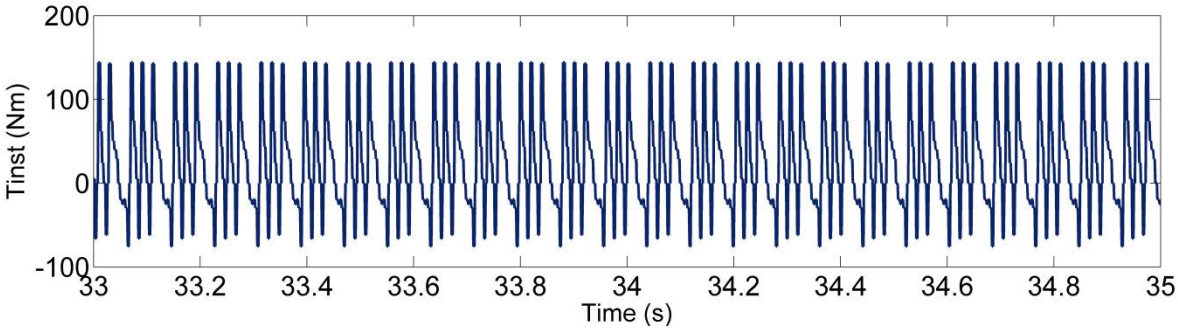

Fig. 6-18: One cylinder out of operation: Engine torque instantaneous profile.

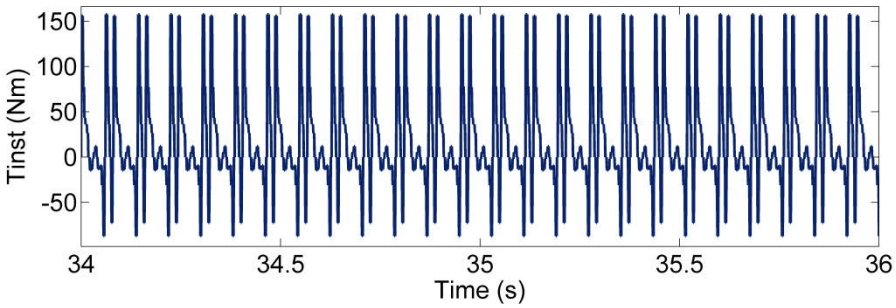

Fig. 6-19: Fault incident at two alternate cylinders: Engine torque instantaneous profile.

6.4.2. Outcomes for Diesel Genset, Model 2

Model 2 is the diesel genset rated at 8.1 kVA connected to a resistive load of 3 kW. Once again the pulsating characteristic of the engine torque is evaluated and is apparent in the following figures.

Fig. 6-20 shows the pulsating nature of the instantaneous torque values of the 8.1 kVA diesel generator. The oscillation frequency is rated at 50 Hz. When one cylinder is misfiring the frequency of the instantaneous torque pulsations falls to 37 Hz (Fig. 6-21).

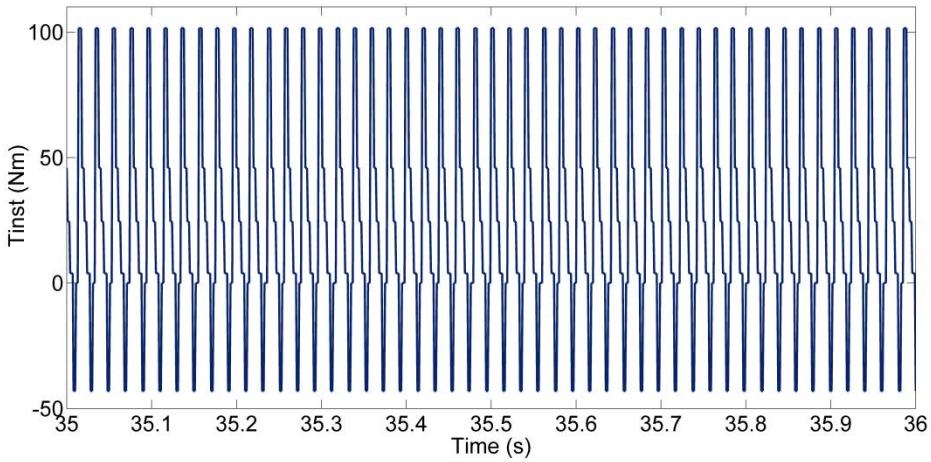

Fig. 6-20: Diesel generator 8.1 kVA: Engine torque instantaneous profile.

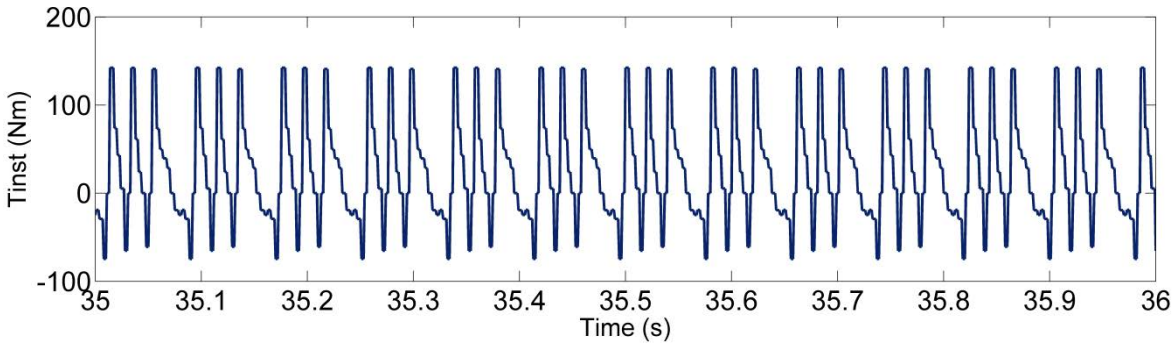

Fig. 6-21: One cylinder out of operation: Engine torque instantaneous values.

6.4.3. A method to eliminate frequency flickering

Throughout this case study various potential scenarios were considered for the diesel power plant of 8.1 kVA under different load demands. The system is investigated with and without the addition of the dynamic power source for all case scenarios.

All the graphs that follow depict the effect of a power source when running in parallel to the diesel's generator set (Fig. 6-2) which are both connected to a resistive load. In more details, the figures beneath illustrate the time variation of generator set quantities during the steady-state regime before and after applying the proposed control scheme. These are the generator's speed, the active power set-point for the dynamic source, the active and mechanical power outputs of the diesel generator, the voltage amplitude, the instantaneous torque waveforms etc.

1) Scenario 1: Diesel power plant rated at 8.1 kVA, resistive load of 4 kW and a dynamic power source.
2) Scenario 2: Diesel power plant rated at 8.1 kVA, resistive load of 7 kW and a dynamic power source.
3) Scenario 3: Considering Asymmetry in Torque Pulsations.

6.4.3.1. Simulation Results for Scenario 1

The droop gain for the dynamic power source is defined as -6 kW/Hz (Fig. 6-16), i.e. the dynamic power source supplies the system with 6 kW of power when the frequency changes by 1 Hz.

Tables 6-3 and 6-4 depict the amplitude range of the frequency and voltage oscillations for the diesel genset set without and with the integration of the controlled power source into the system during the steady-state regime. The dynamic power source generates the active power being set by the droop control scheme. It is obvious that with the dynamic power source inclusion, a reduction of almost five times in the amplitude range of the frequency oscillations

is observed; whereas the amplitude of the voltage oscillations increases roughly three times. This could be attributed to the fact that the controlled source supplies the system with uninterrupted active power as it can be observed in Fig. 6-22.

Table 6-3: Electrical Quantities & Fluctuations without the Dynamic Power Source

Ratings		Model 2
3-phase Output	Sn	8.1 kVA
Load	P_{load}	4 kW
Amplitude range of frequency oscillations	$\Delta\boldsymbol{\omega}$	40 rpm
Amplitude range of voltage oscillations	ΔV	14 V

Table 6-4: Electrical Quantities & Fluctuations with the Dynamic Power Source

Ratings		Model 2
3-phase Output	Sn	8.1 kVA
Load	P_{load}	4 kW
Power set-point (dynamic source)	Pref	-6 kW
Amplitude range of frequency oscillations	$\Delta\boldsymbol{\omega}$	8 rpm
Amplitude range of voltage oscillations	ΔV	35 V

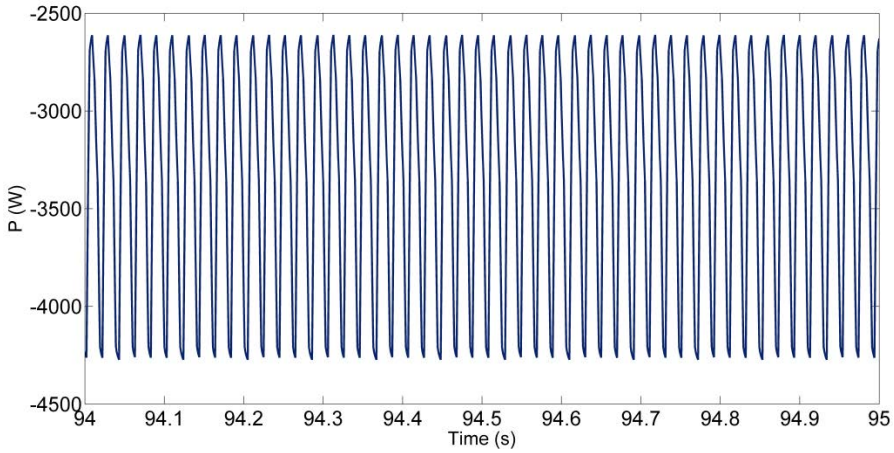

Fig. 6-22: Active power delivered by the dynamic source.

Figures 6-23 to 6-26 include the results of diesel genset's steady-state electrical variations with and without the presence of the dynamic power source into the system.

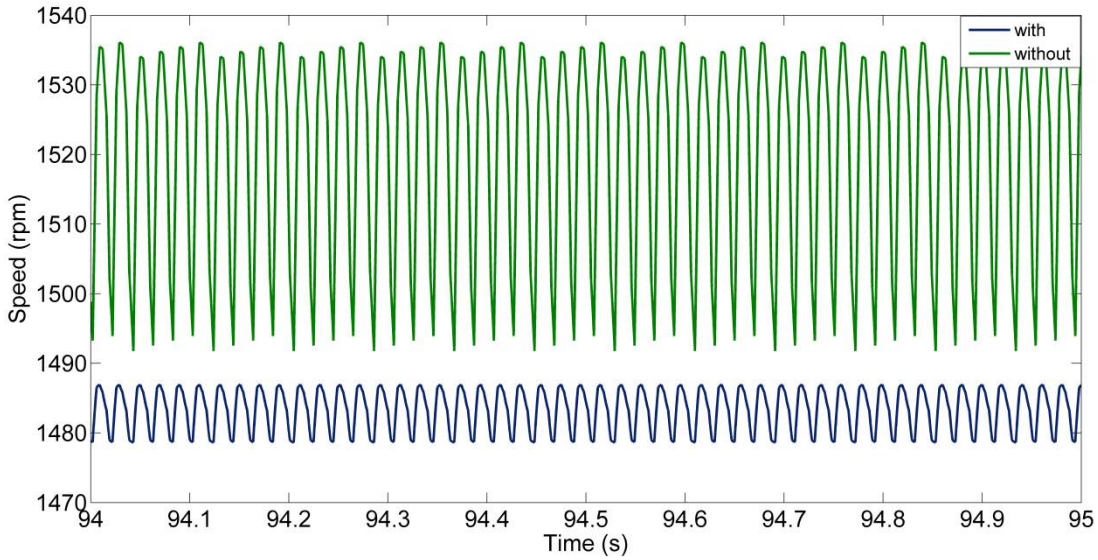

Fig. 6-23: Generator speed without and with the dynamic power source.

Penetrating or not the dynamic power source, the oscillations frequency is of 50 Hz. Moreover, from Fig. 6-23 the effect of the dynamic power source integration is obvious since the amplitude range of the rotational speed pulsations is approximately reduced from 40 to approximately 8 rpm, and consequently the best steady-state regime is attained when the controlled power source is added to the system.

The voltage variation is enclosed in Fig. 6-24. Considering the penetration of the dynamic power source, the stability of the voltage fluctuations is better although the peak-to-peak values shift to higher amplitude range, i.e. between 545 and 580 V. Nevertheless, this range remains among the acceptable limits for distribution levels (±5% of nominal voltage).

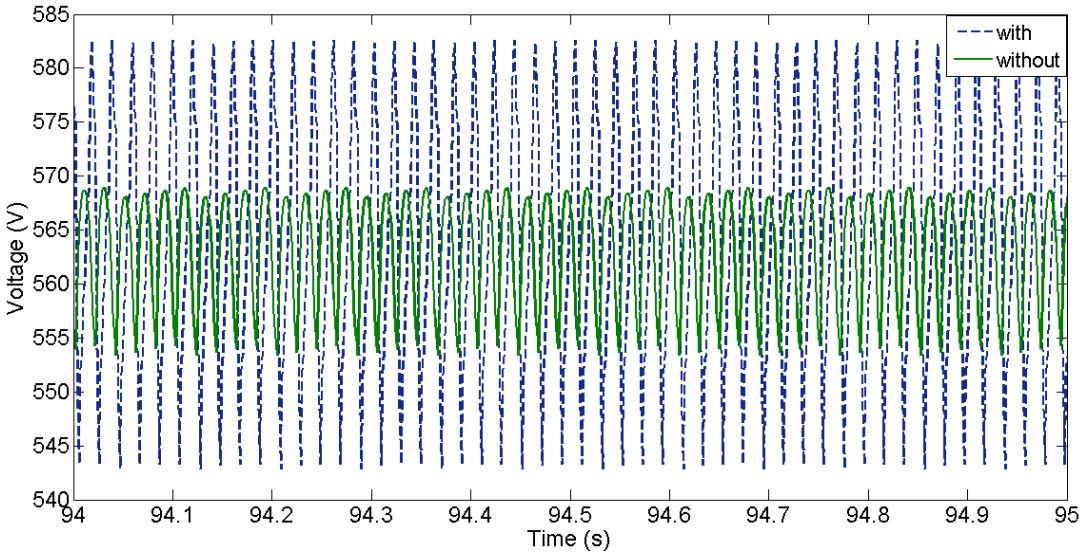

Fig. 6-24: Generator's output voltage a) without, b) with the dynamic power source.

Figures 6-25 & 6-26 show the generator's instantaneous torque profile, its mechanical power (Fig. 6-25) and electrical power outputs (Fig. 6-26) with and without the dynamic power source integration. Another expected conclusion is that we can observe a reduction in the mechanical and torque outputs of the diesel engine generator

when the dynamic power source is present. Moreover, the electrical power output of the generator suffers from more severe fluctuations when the dynamic power source is absent, however when the droop controller is incorporated into the system, its profile reaches a steady-state regime similarly to the generator's synchronous speed pattern.

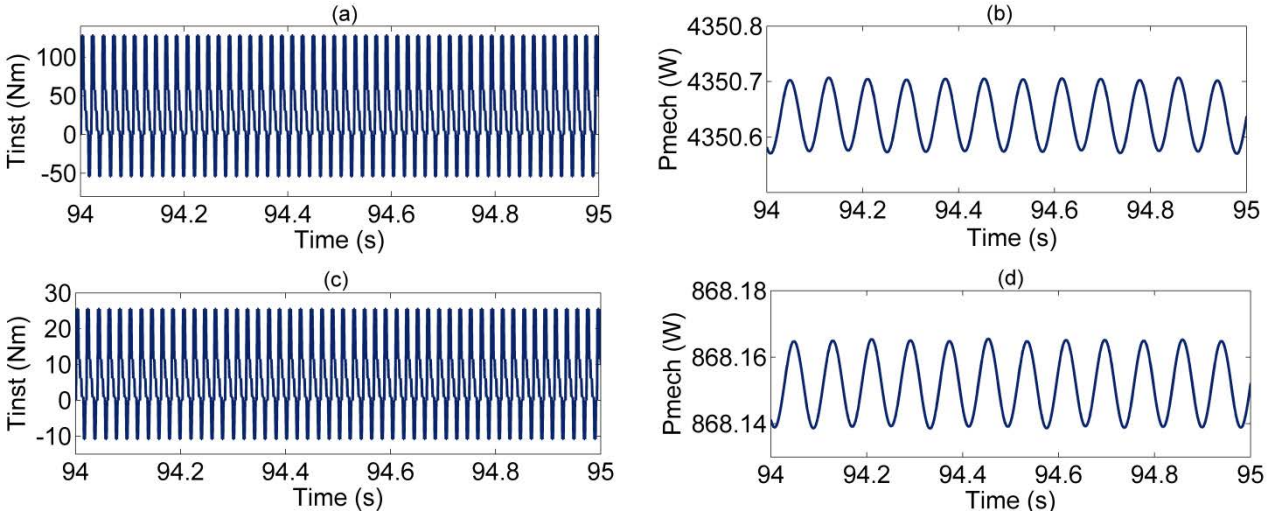

Fig. 6-25: Instantaneous torque and mechanical outputs without (a, b) and with (c, d) the dynamic power source integration.

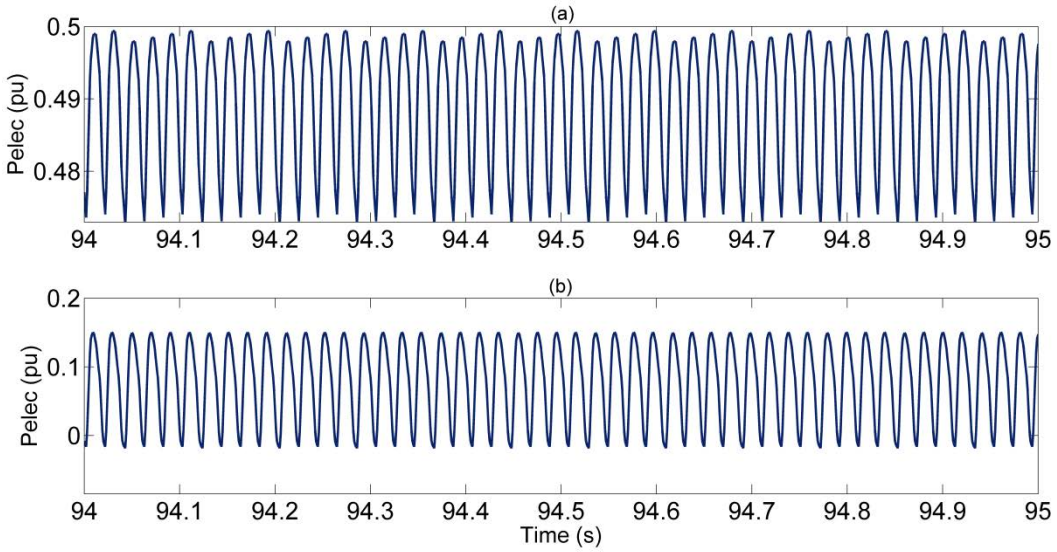

Fig. 6-26: Electrical power output a) without, b) with the dynamic power source integration.

6.4.3.2. Simulation Results for Scenario 2

In this case, we consider the extreme scenario of maximum loading for the diesel generator. Thus, the load is increased to 7 kW and the dynamic power source is set like previously to inject 6 kW into the system. Figures 6-27 & 6-28 illustrate the speed and the voltage amplitude of the generator, respectively with and without the integration of the dynamic power source.

Initially, the amplitude range of the pulsations accounts for almost 75 rpm, whereas with the droop controller this amplitude is once again eliminated to approximately 8 rpm. Tables 6-5 and 6-6 concentrate a brief summary of the diesel genset quantity parameters and the range of fluctuations resulting from the simulations without and with the dynamic power source integration.

Table 6-5: Electrical Quantities & Fluctuations without the Dynamic Power Source

Ratings		Model 2
3-phase Output	Sn	8.1 kVA
Load	P_{load}	7 kW
Amplitude range of frequency oscillations	$\Delta\omega$	75 rpm
Amplitude range of voltage oscillations	ΔV	25 V

Table 6-6: Electrical Quantities & Fluctuations with the Dynamic Power Source

Ratings		Model 2
3-phase Output	Sn	8.1 kVA
Load	P_{load}	7 kW
Power set-point	Pref	-6 kW
Amplitude range of frequency oscillations	Δw	8 rpm
Amplitude range of voltage oscillations	ΔV	35 rpm

The results, here, are more severe for both the frequency and voltage fluctuations amplitude, since the former is reduced nine times and the later is increased only by 10 V compared to 21 V for a load of 4 kW. As it was mentioned before, this rise in voltage amplitude is acceptable due to the continuous active power injection resulting from the droop controller (Fig. 6-29).

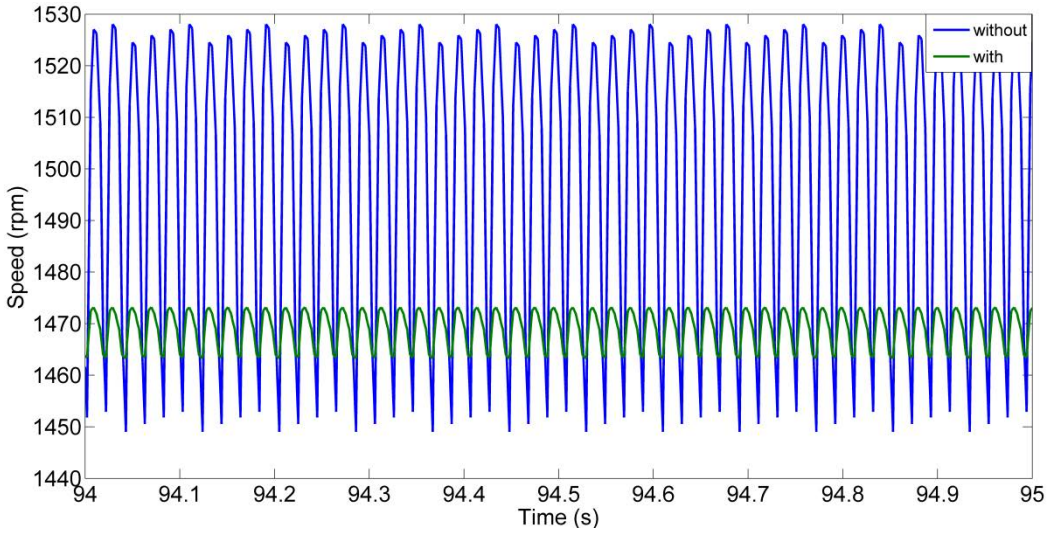

Fig. 6-27: Generator speed without and with the dynamic source.

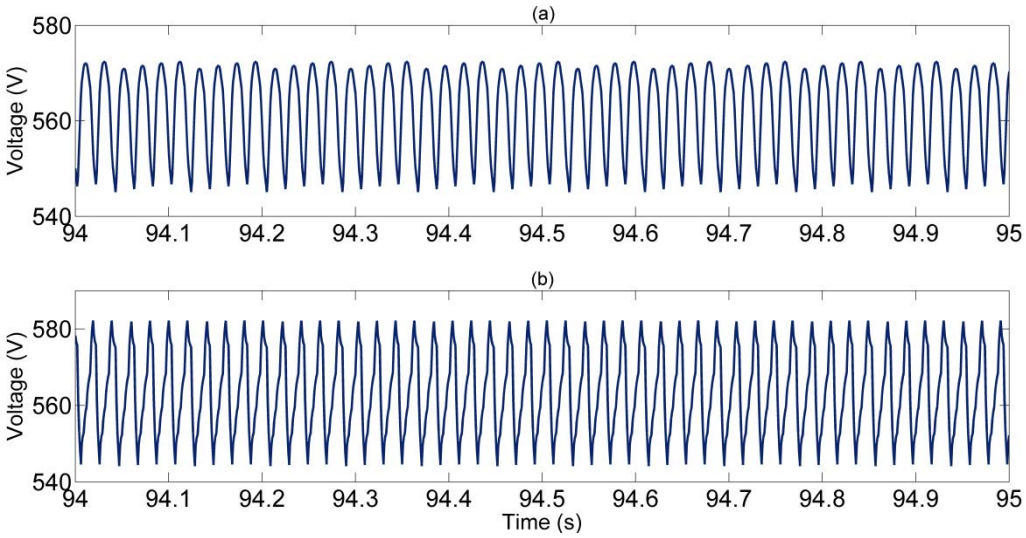

Fig. 6-28: Generator's output voltage a) without, b) with the dynamic power source.

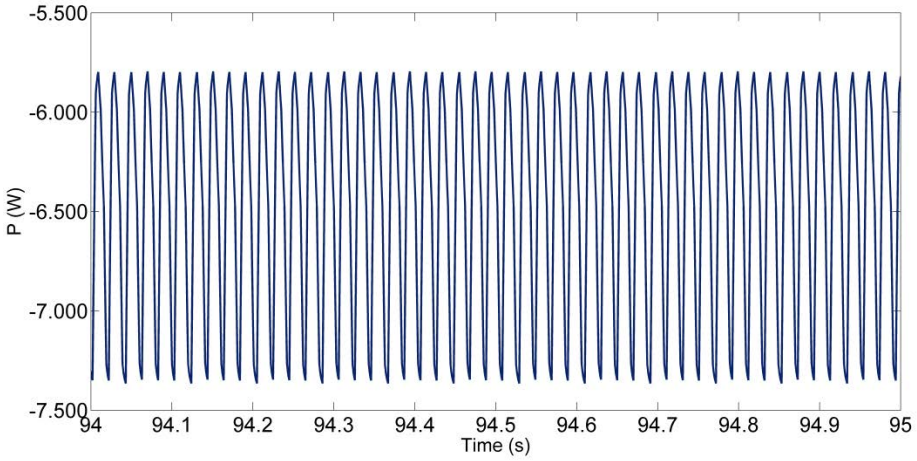

Fig. 6-29: Active power delivered by the dynamic source.

Figures 6-30 & 6-31 show the generator's instantaneous torque profile, its mechanical power (Fig. 6-30) and electrical power outputs (Fig. 6-31) with and without the dynamic power source inclusion, respectively. A great reduction in mechanical and torque quantities of the diesel engine generator is observed when the dynamic power source is present. Moreover, the electrical power output of the generator once again suffers from more severe fluctuations when the dynamic power source is absent, however when the droop controller is incorporated into the system, its profile reaches a steady-state regime similarly to the generator's synchronous speed pattern.

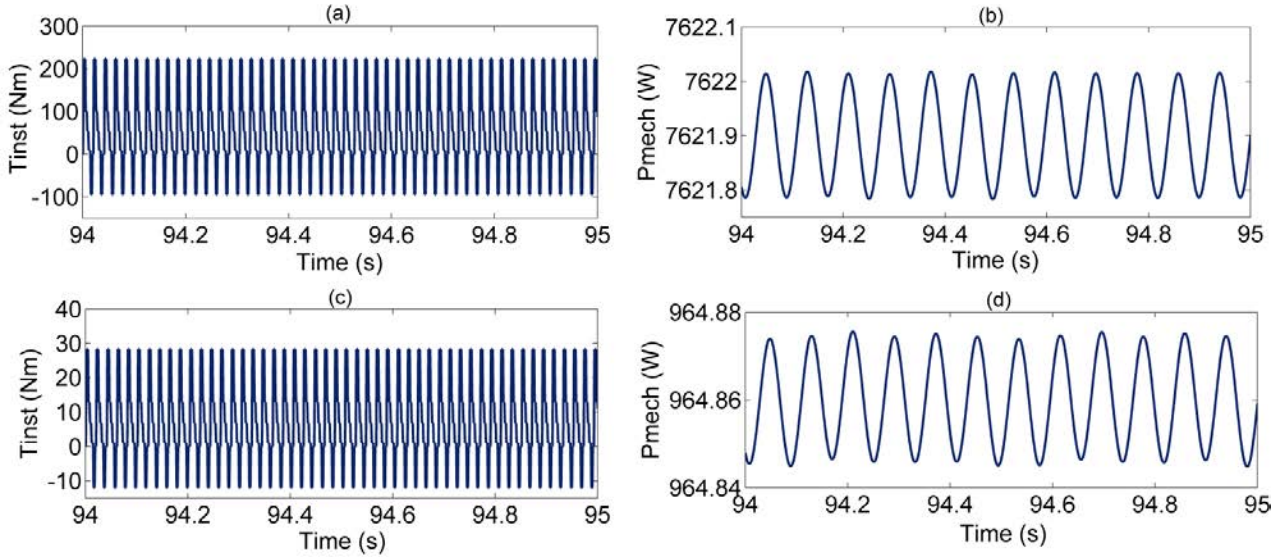

Fig. 6-30: Instantaneous torque and Mechanical outputs without (a, b) and with (c, d) the dynamic power source integration.

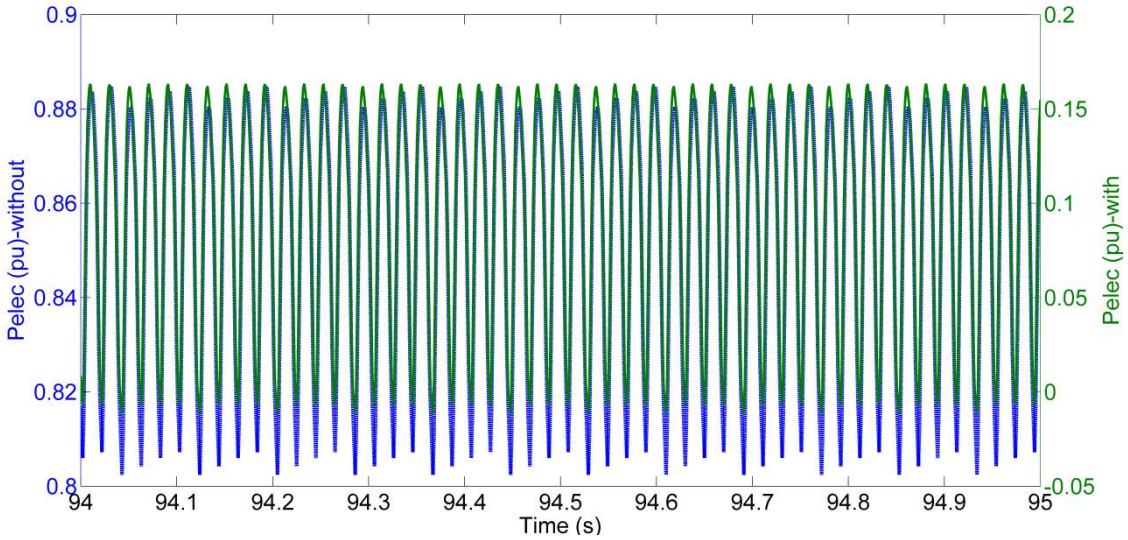

Fig. 6-31: Electrical power output without and with the dynamic power source integration.

6.4.3.3. Simulation Results for Scenario 3

The last scenario proposes to conduct simulations considering asymmetries in torque pulsations, while keeping the same model of the diesel genset (Model 2) and using a load of 5.5 kW. For instance, the electrical fluctuations are studied upon the misfiring of one cylinder.

For all the employed scenarios and magnitudes discussed, these simulation outcomes seem to be the most critical and severe when the dynamic power source is absent. The best compensation is gained if the droop control is implemented since the system's torque and, thus generated power is reduced. Additionally, in this case not only the frequency oscillations but also the voltage amplitude variation is evidently improved (Fig. 6-32 & 6-33).

Initially and without the dynamic power source inclusion, the amplitude range of the speed pulsations accounts for almost 170 rpm, whereas with the droop controller contribution this amplitude is reduced to the peak-to-peak value of 13 rpm (Fig. 6-32). Tables 6-7 and 6-8 concentrate a brief summary of the diesel genset quantity parameters and the relevant fluctuations range resulting from the simulations without and with the dynamic power source integration.

It is evident that with the implementation of the droop control when an asymmetry incident occurs, the peak-to peak-oscillations of the frequency and voltage magnitudes (Fig. 6-33) are greatly compensated.

Table 6-7: Electrical Quantities & Fluctuations without the Dynamic Power Source

Ratings		Model 2
3-phase Output	Sn	8.1 kVA
Load	P_{load}	5.5 kW
Amplitude range of frequency oscillations	$\Delta\boldsymbol{\omega}$	170 rpm
Amplitude range of voltage oscillations	ΔV	60 V

Table 6-8: Electrical Quantities & Fluctuations with the Dynamic Power Source

Ratings		Model 2
3-phase Output	Sn	8.1 kVA
Load	P_{load}	5.5 kW
Power set-point (dynamic source)	Pref	-6 kW
Amplitude range of frequency oscillations	$\Delta\boldsymbol{\omega}$	13 rpm
Amplitude range of voltage oscillations	ΔV	40 V

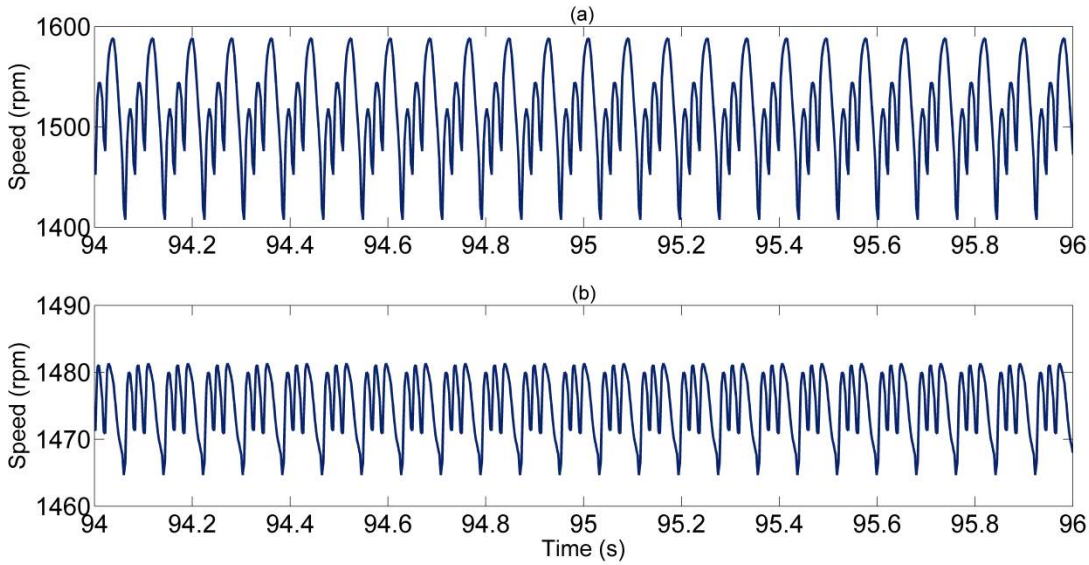

Fig. 6-32: Generator speed a) without, b) with the dynamic source.

Figure 6-34 & 6-35 show the generator's instantaneous torque profile, its mechanical power (Fig. 6-34) and the dynamic source's electrical outputs (Fig. 6-35) with and without the dynamic power source inclusion, respectively. The diesel genset generates reduced torque and mechanical outputs. We can notice an approximately five times reduction in these values when the dynamic power source is included in the system compared to the values obtained when it is not present.

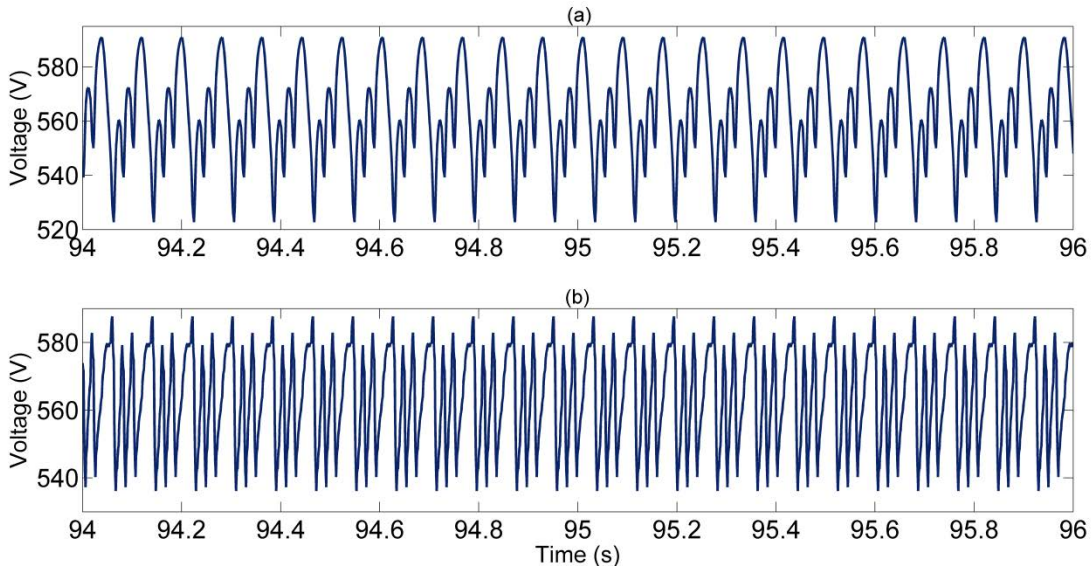

Fig. 6-33: Generator's output voltage a) without, b) with the dynamic power source.

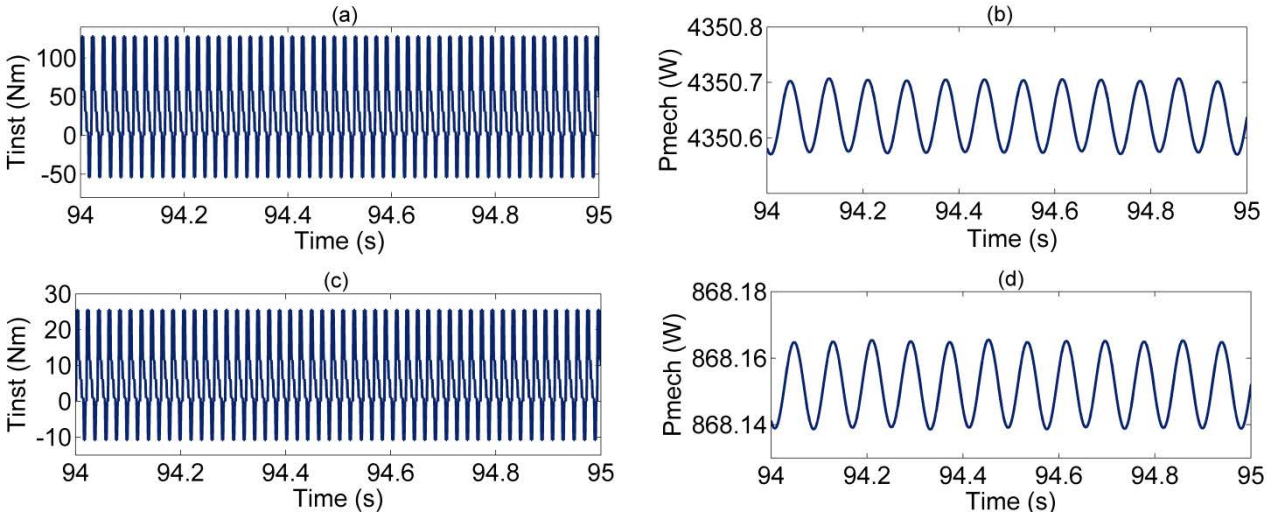

Fig. 6-34: Instantaneous torque and Mechanical outputs without (a, b) and with (c, d) the dynamic power source integration.

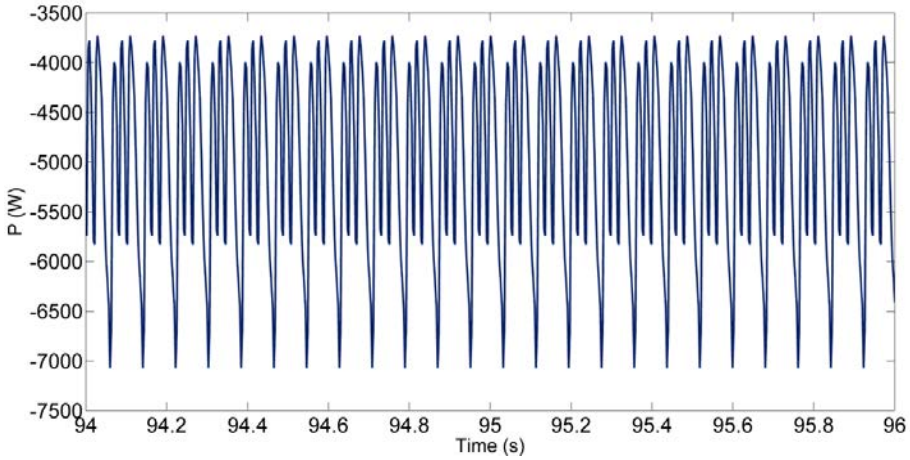

Fig. 6-35: Active power delivered by the dynamic source.

6.5. Summary

This chapter presents the outcomes for the operation of a diesel-powered island grid system. The simulations were focused on power quality measurements with emphasis placed on frequency flickering. The spectral analysis of the recorded voltage and frequency variations certified that diesel generators are the main source of flicker in the system. This was also shown during the onsite Microgrid experiments described in Chapter 5.

The steady-state electrical fluctuations that are evident in diesel-driven generators were evaluated for two different diesel powered plants with a speed of 1500 rpm rated at 16 kVA and 8.1 kVA respectively. The presence of low-frequency oscillations, mainly rated at 50 Hz is highly linked to the pressure imbalance during firing process, in addition to the torque pulsations among the cylinders. Moreover, the flicker concern was higher when firing asymmetries take place among the cylinders, e.g. taking out of operation one cylinder, affects seriously the frequency oscillations and torque profile in the shaft torque.

A new control scheme is proposed that allows enhancing the power quality of a diesel genset power plant by compensating for the generator electrical fluctuation. This control strategy is based on the ω/P droop control which defines a given active power set-point to be supplied by a dynamic power source. In order to define the effect of the controlled dynamic power source, three different case scenarios were studied with and without its integration into the power system.

In more details, the time variation of the generator's set quantities is investigated during the steady-state regime before and after applying the proposed control scheme. These are the generator's speed, the active power set-point for the dynamic source, the active and mechanical power outputs of the diesel generator, the voltage amplitude and the instantaneous torque waveforms etc.

The three scenarios employed are outlined below:

a) Scenario 1: Diesel power plant rated at 8.1 kVA, resistive load of 4 kW and a dynamic power source.
b) Scenario 2: Diesel power plant rated at 8.1 kVA, resistive load of 7 kW and a dynamic power source.
c) Scenario 3: Considering Asymmetry in Torque Pulsations.

The simulations results showed that the best compensation in frequency flickering is obtained with the presence of the dynamic power source. In addition, the torque produced by the diesel generator is higher without the droop controller, whereas the amplitude range of frequency oscillations is reduced and this drop depends on the droop control scheme implemented in line with the load demand. Furthermore, the results are more severe and critical when considering torque pulsations asymmetries.

Concluding, this methodology could be very useful for rural and isolated power networks. This was a preliminary effort and at a later time the extended analysis of the proposed control could be implemented to improve the voltage steady-state behaviour so as the dynamic source absorbs/injects the necessary power amount only during frequency changes.

PART IV. Conclusions & Outlook

Part four concentrates the main conclusions and gives recommendations for future work.

Chapter 7. Final Conclusions

7.1. Thesis Summary

With renewable electricity generation increasing, there will be some important changes in the electric power systems, notably through smaller generators embedded in the distribution network. The introduction of this type of units in medium and low voltage (MV/LV) networks, which may loosely represent an Island or autonomous power network since MV/LV levels are of high interest as most of distributed energy sources (DER) will be connected there, allows a better management of the resources, and an optimum planning of the power generation system.

The employment of large amounts of distributed generation within the distribution networks can affect significantly the system´s stability since this kind of generators may have less ability to control the voltage and frequency than conventional generation units. However, the changes induced by the amount and sitting of distributed generation penetration mainly in Island or autonomous electrical grids require steady-state and transient stability analyses of the distribution network.

Grid analysis studies concerning the potential integration of distributed generation are commonly attained by public power utilities and distributed system operators since the detailed data of the distribution networks is not always available.

The principal objective of the current thesis was to investigate on distributed generation integration into MV/LV electrical grids and this survey tried to answer some specific aims questioned such as, defining the best planning and fitting of DER units within distribution networks, applying recommendations and solutions to advance their penetration level, studying the effect of FACT devices on voltage stability and the impact of diesel gensets on frequency steady-state oscillations within autonomous power systems.

Hence, the greatest part of this thesis is dedicated to a simulation-based methodology to analyse MV/LV distribution networks from an electrical point of view and test their dynamic stability as well as the location of additional DER, either they operate in connected or isolated mode. For this type of analyses, tools that provide computational power and flexibility are necessary.

Generally, the main conclusions derived show a good fitting of the applied methodology. A spell of the targeted outcomes depicted that the penetration level and location of distributed generation within the studied MV off-grid power system did not have had serious impacts on voltage and frequency stability. However, the application of a three-phase fault at the connection node of the wind farm proved the severity of its consequent impacts on the system. Moreover, the used control of an integrated inverter-based STATCOM device showed its suitability for reactive power compensation and voltage stability.

In more details, throughout this research work, a case study has been accomplished in PSS/E based on a real Island grid model with a total potential installed of about 133 MW. Embedded generation with a specific penetration level has been added to the distribution network model.

Steady-state and Dynamic Analysis configurations were proposed in order to determine upon the allocation and the maximum capacity of distributed generation (geothermal and wind power) that may be inhabited within the studied islanded electrical grid. In that way, it was possible to check the off-grid system's behaviour under normal operation and against several disturbances onto the grid.

The static and dynamic studies employed three different time-frame and potential scenarios, namely Scenario 1, 2 & 3 to check the system´s voltage and frequency stability with the addition of 25.77 MW and 14 MW of geothermal and wind power respectively.

There are about seven substations where the voltage is stepped down from 60 kV to 30 kV or 10 kV and two substations which bring the voltage down from 30 kV to 10 kV. Each substation has one to four power transformer banks with a capacity of between 0.5 MVA and 20 MVA. A group of substations were proposed to introduce this embedded generation with the extension in mind to suggest the voltage level to connect these units. The main issues addressed were the nodal voltages, the line active and reactive power losses, in addition to the three-phase faults

located at different places throughout the transmission and distribution network of the Island power system. Concretely, two rules of thumb have been considered to specify the correctness of the trial-error method used within this research work. The former was to introduce the embedded generation units at the lower voltage buses and the latter to try to add them to buses with denominator the higher short circuit capacity and the high load demanding and at the meanwhile obtaining the minimum possible power losses. One more criterion taken into account was that the wind potential to be penetrated cannot surpass the 5% of the short circuit capacity at the connection point node.

Geothermal plants using basic machine model such as synchronous generator, exciter and governor and a Wind farm employing Doubly-fed Induction Generator (DFIG) technology were chosen throughout this research work. The adequate stability margin of the system was investigated upon the fault ride through capability and frequency response of the network elements, whereas a three-phase fault application at the connection point of the wind farm was proved to be the most critical perturbation. Moreover, two different exciter models (IEET1 & EXST1) were chosen to perform open-circuit set-point step tests and record their field voltage and terminal voltage responses after tuning application.

The power flow results showed that when only geothermal power is added to the system there were not voltage violations observed, but thermal line overloading rated between 124% and 128% against their power ratings. Furthermore, various substation nodes were examined to add wind power and at the ones selected as most suitable, voltage and thermal violations follow the same pattern. Wind power inclusion under specific scattering and connection topology cannot affect the electrical system and reduces power losses. Concretely, the total system losses with only geothermal generation added accounts for 1.1 MW+8.9 MVAr, whereas encountering wind generators addition at specific nodes the losses differentiate accordingly (decrease or increase depending on the connecting bus). Nevertheless, the impact on power losses is minimal in all cases as the amount of power added was small compared to the total system handling capacity. Additionally, it is important to note that power balance is kept while the conventional generators´ output is controlled and readjusted according to the system demand.

The results drawn from contingency (N-1) study showed that wind energy penetration improves the system security, especially when wind power is more distributed. The most critical results in terms of voltage and thermal violations were concluded when disconnecting transmission lines that interconnect central generation plants and big substations. This can be attributed to the fact that central substation feed and serve high load demands.

Short circuit analysis demonstrated that the penetration of wind power and generally of distributed generation raises the short circuit level. Especially, a three-phase fault implemented at the addition bus increases the short circuit current at this bus and to the ones interconnected to it via branches. One solution to minimize the short circuit level could be to increase the impedance of the HV/MV transformer of the network or adding some fault current limiting devices such as reactors.

Some conclusions are offered on the dynamic simulations, where in all cases a new steady-state is achieved according to the pre-fault value. First of all, simulation results indicated that the wind farm as introduced to the Island´s electrical system remains connected under voltage dips caused during the three-phase fault occurrence on the connection node.

Moreover, the results proved to be more critical when additional power was scattered among different distribution nodes since the frequency and terminal voltages where the wind power is connected to, after the three-phase fault application, need more time to recover to their pre-fault values. Dynamic simulations suggested that a short circuit fault is a good choice since it causes relatively large voltage oscillations at the connecting node. Specifically, the terminal voltage of wind generators drops significantly and frequency´s long in duration oscillation depicts that system´s stability is disturbed.

Additional fault incidents were implemented such as the loss of a swing generator, the outage of an important transmission line and a three-phase fault application at the system's slack bus. The simulation outcomes depicted that the voltage and frequency behaviour at the system's substations do not fall under impermissible values, while they are soon after the fault clearing reset to their initial conditions. In more details, when a symmetrical short circuit is applied

to the slack bus, voltage and frequency values at the terminal bus of the wind generators and the substations recover adequately where the later ones do not vary more than 0.4 Hz.

Apart from the static and dynamic simulations accomplished in PSS/E software tool, it was important to research on the control performance and interaction of the devices such as power converters connected to distribution grids since they may induce significant impacts on the power quality parameters. Power stability, namely voltage drop/rise and frequency disturbances due to the high rates of DER integration into distribution grids increases the demand for network support by means of provision and control of reactive and active power exchanges respectively.

Consequently, and according to the EU grid codes, each generating unit penetrated into MV/LV networks needs to be tested and to be awarded a so-called ´´type-specific unit certificate´´ that refers to its electrical characteristics like the connecting voltage, the power capacity, type of generator etc. Generally, two options for performing system experiments exist; a) testing real devices or b) running a simulation.

Hence, real time simulations in RSCAD/RTDS environment and Power Hardware-in-the-loop (PHIL) experiments were reinforced throughout this thesis and this will not only allow us to size and locate the distributed generation systems, but will also let us optimize MV/LV and generally Island power networks. In more details, this work tries to combine laboratory or field tests in line with system level simulations of distributed generation devices to demonstrate their conformity with the technical issues related to grid penetration into MV/LV networks.

Real time simulations and PHIL experiments were grouped into two sets of tests. The first set discussed the performance of VAR compensating devices, i.e. a STATCOM interfaced to a DC-capacitor, for reactive power compensation and voltage control. The second case study demonstrated an implementation of a Microgrid model in RSCAD/RTDS simulation platform for DER device integration. For both case studies, PHIL tests were performed with the Hardware under Test (HuT) being a passive single phase load of varying inductance and resistance.

Real time simulations of the first group of tests demonstrated a detailed description of switching inverters' controller design and investigated the effects of an inverter-based STATCOM on voltage regulation of a low voltage distribution network using RSCAD/RTDS environment. The Average Model of a STATCOM interfaced to a DC-capacitor was simulated, where the IGBT Voltage-Source Converter was represented by equivalent controlled voltage sources.

The conclusions offered on the PHIL simulation results confirmed that the STATCOM model studied throughout this work is suited for voltage sag mitigation, since it compensated the reactive power required during a step decrease in the hardware inductance (from 140 mH to 103 mH) and led to improved steady-state voltages. Additionally, the implemented control strategy of the capacitor maintained the VSI's DC bus voltage constant.

Regarding the second set of tests, PHIL simulations were executed to emulate the energy management of a real Microgrid system including a diesel synchronous machine and inverter-based sources. Moreover, their dynamic behaviour was examined within the LV islanded power system and more than that the adequate performance of the laboratory set-up was verified through tests on a real experimental site.

Simulation results for both group of tests indicated that RSCAD/RTDS is an effective tool suitable for transient analysis due to its fast computation in real time and the laboratory hardware interfacing capability it offers. Furthermore, it is worth mentioning that PHIL experiments provide high flexibility in the research of the complex problems which concern the penetration of various energy systems with respect to network stability and security.

However, there still exist uncertainties when performing PHIL tests. For instance, in real life there is no ideal Power Interface. As a result, imperfections that are mainly inserted by the power interface can reduce the accuracy of the simulation. Examples of these imperfections are the time-delay and the low pass filter of the amplifier, the time-delay of the sensor and the sensor's noise. The total time delay in the current PHIL experiments was about 750μsec.

Therefore, an accuracy analysis of the PHIL tests was recommended. There are different techniques on this matter. The one that we followed during the experiments was that we ran the off-line simulations on RSCAD/RTDS software and compare the results with those of the real PHIL tests. Additionally, throughout this research work virtual hardware-in-the-loop experiments (off-line simulations) were performed in Matlab/Simulink to check the system's

stability for the different test scenarios. There is also the uncertainty related to measurement devices (e.g. current measurement of the power interface) that has to be taken into consideration.

One additional issue questioned in islanded networks is the transient behavior of diesel gensets during critical disturbances caused by intermittent power sources and load step changes and more than that, the degraded power quality induced by their inherit torque oscillations.

This thesis also presented the outcomes for the operation of a diesel-powered Island grid system. The system was modelled in Simulink/Matlab. The simulations were focused on power quality measurements with emphasis placed on frequency flickering. The spectral analysis of the recorded voltage and frequency variations verified that the diesel generators are the main source of flicker in the system. This was also shown during the onsite Microgrid experiments described in Chapter 5.

The steady-state electrical fluctuations that are evident in diesel-driven generators were evaluated for two different diesel powered plants rated at 16 and 8.1 kVA and a nominal speed of 1500 rpm respectively. The presence of low-frequency oscillations, mainly rated at 50 Hz is highly linked to the pressure imbalance during firing process, in addition to the torque pulsations among the cylinders. Moreover, the flicker concern was higher when firing asymmetries take place among the cylinders, e.g. taking out of operation one cylinder, affecting seriously the frequency oscillations and torque profile in the shaft torque.

A new control scheme was proposed that allows enhancing the power quality of a diesel genset power plant by compensating for the generator's electrical fluctuations. This control strategy was based on the frequency droop (w/P) control which defines a given active power set-point to be supplied by a dynamic power source. The simulation results demonstrated the effect of the controlled dynamic power source considering different load demand scenarios with and without its integration into the power system.

In more details, the time variation of the generator's set quantities was investigated during the steady-state regime before and after applying the proposed control scheme. These are the generator's speed, the active power set-point for the dynamic source, the active and mechanical power outputs of the diesel generator, the voltage amplitude, the instantaneous torque waveforms etc.

The simulations results suggested that the best compensation in frequency flickering was obtained with the presence of the dynamic power source. In addition, the torque produced by the diesel generator was higher without the droop controller, whereas the amplitude range of frequency oscillations was reduced and this drop depends on the droop control scheme implemented in line with the load demand. Finally, the results were more severe and critical when considering torque pulsations asymmetries.

7.2. Future Research Work

This thesis is mainly focused on investigating and deriving a methodology for distributed generation integration into MV/LV electrical grids, which aims at defining the suitable areas and zones for an optimal penetration of distributed generation into these voltages, in addition to examining its dynamic and transient impacts on system level. Furthermore, Part II gives an example for integration in a real Island power system with PSS/E software tool and more than that, a typical MV/LV voltage distribution network is selected for additional simulations in RSCAD environment that may loosely represent an Island or autonomous power system since MV/LV levels are of high interest as most of distributed energy resources will be connected there.

Therefore, future work could possibly concentrate on the application of the used methodology in additional real networks that represent autonomous power systems, Islands or even connected grid configurations.

The principal advantage of this methodology is that up to now, the existent literature reviews are very limited and do not analyze an autonomous power grid system as a whole from an electrical point of view by employing static and

dynamic simulations within PSS/E software to define the quantity (how much) and the allocation (where to add the distributed generation). However, the current incentives and proposals are more qualitative and theoretical than quantitative. This effort is reinforced throughout this thesis.

Hence, recommendations for future work could be to extend the model by employing various scenarios for distributed generation integration in order to check over the autonomous power system's dynamic limit for a 100% RES penetration. Moreover, a next step could be the improvement of the dynamic model where all units may have simple exciter (i.e. SEXS), stabilizer (i.e. PSS2) and governor models (i.e. TGOV) with the same common parameters, especially for RES.

Studies including the development of Pumped Storage Hydro (PSH) units employing Doubly-Fed induction machine or the simulation of various energy storage systems in PSS/E to evaluate their impacts on transient stability, voltage and reactive power control, fast frequency regulation (i.e. response to sudden generation/load imbalances) would be particularly valuable. Another consideration, similarly to the previous recommendations which could be in line with H2020 targets, is to investigate on the contribution of distributed generation and generally of Microgrid configurations to ancillary services.

On the other hand, the deployment of RSCAD/RTDS simulations and PHIL laboratory tests as a data reference for verification in the domain of DER integration is at its early stage of development. Specifically, the existent literature is very limited regarding this kind of tests that study the control strategy of MV/LV islanded power networks with the integration of inverter-based devices and even energy storage systems. The prevalent advantage of this kind of experimenting is that in the end the implementation and development of a methodology that characterizes the energy supply devices and system analysis for decentralised grid services is viable.

Nevertheless, the limitation of these tests is that the accuracy is not perfect. It is a common problem that stability and accuracy issues arise in PHIL simulations due to errors mainly caused by the Power Interface, namely the time delay of the amplifier and the sensor, the sensor noise etc. Thus, improved Interface Algorithms and Interface Compensation approaches could be considered as future work.

Ultimately, this research study proposes an innovative control scheme to eliminate the inherit frequency and voltage oscillations of a diesel genset, and this methodology could be very useful for rural and isolated power networks. This was a preliminary effort and at a later time the extended analysis of the proposed control could be implemented to improve the voltage steady-state behaviour so as the dynamic source absorbs/inject power only during frequency step changes.

Clearly, forthcoming works could be built upon this thesis' results and propose more effective methods which can come in especially handy for real power plants. Additionally, the expected outcomes drawn through this thesis' field tests and simulations could be the basis for analysis and comparison of the dynamic performance among different energy sources and thus, finally choose which best fits in our grid studies. In that way, the developed scheme (s) is postulated to be a useful solution for distributed generation planners with the potential to become a tool for fostering DER integration into MV/LV or Island power systems and a provisional step towards smart distribution networks.

As a closing remark, I would like to underline that long term government leadership is the key point to establish a clear vision towards distributed generation integration since the power system architecture is bound for change. In addition, initiatives and decision making on site selection is needed to "flip the distributed generation equation''. The primary mandate of the utility industries is and always has been to ''keep the lights on''. This attitude is based on risk avoidance over innovation. The energy market has grown and the necessity to switch to alternative and more competitive solutions merges. Consequently, we have to endure a new power world that brings distributed generation from *Cinderella to Centre Stage!*

References

[1] N. Jenkins, R. Allan , P. Crossley , D. Kirschen, and G. Strbac, "Embedded generation," in *Power and Energy Series 31*, IEE, Ed., 2000.

[2] European Commission, "Durban climate conference 2011 http://ec.europa.eu/clima/policies/international/negotiations/un/durban/index_en.htm, July, 2014.

[3] The Parliament of the United Kingdom, "Climate Change," 2008.

[4] Low Carbon team, "The UK low carbon transition plan ", 2009.

[5] REE, "El sistema eléctrico español 2005," June 2006.

[6] T. Tuerkucar and D. Gailey, "Survey Study of Status and Penetration Levels of Distributed Generation (DG) in Europe and the US (Stage One)," DTI, UK: http://www.distributedgeneration.gov.uk/documents/27_10_2003_06_05_2003_kel_00306-partone.pdf, 2003.

[7] P. Dondi, D. Bayoumi, C. Haederli, D. Julian, and M. Suter, "Network integration of distributed power generation," *Journal of Power Sources* vol. 106, pp. 1–9, 2002.

[8] M. Stefan and I. Darul´a, "Large scale integration of renewable electricity production into the grids," *Journal of Electrical Engineering,* vol. 58, pp. 58-60, 2007.

[9] PPC, "Technical requirements for the interconnection of independent generation to the grid," 2001.

[10] J. M. Rodriguez, O. Alonso, M. Duvison, and T. Domingez, "The integration of renewable energy and the system operation: The Special Regime Control Centre (CECRE) in Spain," in *Power and Energy Society General Meeting - Conversion and Delivery of Electrical Energy in the 21st Century, 2008 IEEE*, 2008, pp. 1-6.

[11] M. A. Kashem and G. Ledwich, "Multiple Distributed Generators for Distribution Feeder Voltage Support," *Energy Conversion, IEEE Transactions on,* vol. 20, pp. 676-684, 2005.

[12] P. Kundur and N. Balu, *Pwer System Stability and Control*.

[13] M. K. Donnelly, J. E. Dagle, D. J. Trudnowski, and G. J. Rogers, "Impacts of the distributed utility on transmission system stability," *Power Systems, IEEE Transactions on,* vol. 11, pp. 741-746, 1996.

[14] L. F. Ochoa, A. Padilha-Feltrin, and G. P. Harrison, "Evaluating distributed generation impacts with a multiobjective index," *Power Delivery, IEEE Transactions on,* vol. 21, pp. 1452-1458, 2006.

[15] L. F. Ochoa, A. Padilha-Feltrin, and G. P. Harrison, "Evaluating Distributed Time-Varying Generation Through a Multiobjective Index," *Power Delivery, IEEE Transactions on,* vol. 23, pp. 1132-1138, 2008.

[16] ENTSOE, https://www.entsoe.eu/publications/system-operations-reports/operation-handbook/Pages/default.aspx.

[17] ENTSOE, https://www.entsoe.eu/major-projects/network-code-development/Pages/default.aspx.

[18] R. B. Alderfer, M. M. Eldridge, and T. J. Starrs, "Making Connections: Case Studies of Interconnection Barriers and their Impact on Distributed Power Projects," NREL Report SR-200-28053, July 2000.

[19] P. Bousseau, F. Fesquet, and et al., "Solutions for the grid integration of wind farms-a Survey," in *Wind energy* vol. 9: Wiley Interscience, December 2005, pp. 13-25.

[20] V. Van Thong, E. Vandenbrande, J. Soens, D. Van Dommelen, J. Driesen, and R. Belmans, "Influences of large penetration of distributed generation on N-1 safety operation," in *Power Engineering Society General Meeting, 2004. IEEE*, 2004, pp. 2177-2181 Vol.2.

[21] S. Eckroad, "FACTS with energy storage: conceptual design study," in *EPRI Report TR-111093, EPRI,*, P. A. The Technical Writer's Handbook. Mill Valley, Calif, USA, M. Young,, Ed., 1999.

[22] A. Arulampalam, J. B. Ekanayake, and N. Jenkins, "Application study of a STATCOM with energy storage," in *IEE Proceedings*, 2003, pp. 373-384.

[23] A. Nazarloo, S. Hosseini, E. Babaei, and M. Sharifian, "Integrated DSTATCOM with Supercapacitor used in IEEE industrial distribution system," *ECTI Trans. on Electrical Eng., Electronics and Communications,* vol. 10, 2012.

[24] Agbedahunsi et al., "Frequency control improvement within a microgrid, using enhanced STATCOM with energy storage," in *6th IET International Conference on PEMD*, 2012.

[25] S. Ropenus and K. Skytte, "Regulatory review and barriers for the electricity supply system for distributed generation in EU-15," in *Future Power Systems, 2005 International Conference on*. vol. 16-18, 2005.

[26] R. Villafáfila, A. Sumper, and e. al, "On wind power integration into electrical power system: Spain vs. Denmark," Institute of Energy Technology (IET) and Aalborg University (AAU).

[27] J. Machowski, J. W. Bialek, and J. R. Bumby, "Power System Dynamics, Stability and Control," Second Edition ed: John Wiley & Sons, Ltd, 2008.

[28] J. D. Glover, M. S. Sarma, and T. J. Overbye, "Power System Analysis and Design," Fifth ed USA: Global Engineering, 2011.

[29] E. Communities, "Directive 2009/72/EC concerning common rules for the internal market in electricity and repealing directive 2003/54/EC," 2009b.

[30] European Wind Energy Association (EWEA).

[31] J. McDonald, "Adaptive intelligent power systems: Active distribution networks," *Energy Policy,* vol. 36, 2008.

[32] Eurelectric 2009, "Statistics and Prospects for the European Electricity Sector, 37th edition," 2009.

[33] L. M. Cipcigan and P. C. Taylor, "Investigation of the reverse power flow requirements of high penetrations of small-scale embedded generation," *Renewable Power Generation, IET,* vol. 1, pp. 160-166, 2007.

[34] F. Bignucolo, R. Caldon, and V. Prandoni, "Radial MV networks voltage regulation with distribution management system coordinated controller," *Electric Power Systems Research,* vol. 78, pp. 634-645, 2008.

[35] R. Cossent and e. al, "Large-scale integration of renewable and distributed generation of electricity in Spain: Current situation and future needs," *Energy Policy* vol. 39, pp. 8078-8087, 2011.

[36] BOE, "Law 54/1997, November 27th, of the Electricity Sector-in Spanish," 1997.

[37] S. Chowdhury, S. P. Chowdhury, and P. Crossley, *Microgrids and Active Distribution Networks*, 2009.

[38] CIRED, "Dispersed Generation. Preliminary Report of CIRED Working Group WG04," 1999.

[39] IEA, "Distributed Generation in Liberalised Electricity Markets," http://www.iea.org/textbase/nppdf/free/2000/distributed2002.pdf, 2006.

[40] Purchala and R. Belmas, "Distributed generation and the grid integration issues," KU Leuven and Imperial College London.

[41] E. Lakervi and E. J. Holmes, *Electric distribution network design*, Second ed.: IEE power engineering, 2003.

[42] N. Jenkins, B. Awad, and J. B. Ekanayake, "Intelligent Load Control for Frequency Regulation in MicroGrids," 2008.

[43] E. Dialynas and N. D. Hatziargyriou, "Impact of Microgrids on Service Quality," in *Power Engineering Society General Meeting, 2007. IEEE*, 2007, pp. 1-5.

[44] Y. Zhu and K. Tomsovic, "Optimal Distribution Power Flow for Systems with Distributed Energy Resources," *Electric Power and Energy Systems,* vol. 29, pp. 260-267, 2007.

[45] S. P. Chowdhury, S. Chowdhury, and P.A.Crossley, "Islanding Protection of Distributed Systems with Distributed Generators-A Comprehensive Survey Report," in *IEEE Power Engineering Society General Meeting*, Pittsburgh, PA, 2008.

[46] C. L. Moreira and J. A. Peas Lopes, "MicroGrids Dynamic Security Assessment," in *Clean Electrical Power, 2007. ICCEP '07. International Conference on*, 2007, pp. 26-32.

[47] S. P. Chowdhury, S. Chowdhury, C. F. Ten, and P. A. Crossley, "Islanding Operation of Distributed Generators in Active Distribution Networks," in *43rd International Universities Power Engineering Conference*, Padova, Italy, 2008.

[48] Ministry of Industry, Tourism, and Trade, "National Action Plan on Renewable Energies in Spain (PANER) 2011-2020-in Spanish," 2010b.

[49] N. Khayat, J. Tayie, and R. Seliga, "Stand alone adjustable speed power generating set," in *Proc. Intl conf. on harmonics and power quality*, 2002, pp. 639-643.

[50] Muhamad Reza, "Stability analysis of transmission systems with high penetration of distributed generation," Ph.D. thesis: Delft University of Technology, 2006.

[51] Henk Polinder and e. al., "Basic operation principles and electrical conversion systems of WTs.," 2004.

[52] E. Vittal, "A static analysis of the maximum wind penetration level in Iowa and a dynamic assessment of frequency response in wind turbine types." vol. Master: University of Iowa, 2008.

[53] V. Akhmatov, H. Knudsen, and A. H. Nielsen, "Advanced Simulation of Windmills in the Electric Power Supply," *Electrical Power and Energy Systems* vol. 22, 2000.

[54] H. Knudsen and J. N. Nielsen, "Introduction to the Modeling of Wind Turbines," in *Wind Power in Power Systems*, T.Ackermann, Ed., 2005.

[55] E. Vittal, A. Keane, and M. O'Malley, "Varying penetration ratios of wind turbine technologies for voltage and frequency stability," in *Power and Energy Society General Meeting - Conversion and Delivery of Electrical Energy in the 21st Century, 2008 IEEE*, 2008, pp. 1-6.

[56] A. Buckspan, L. Pao, J. Aho, and P. Fleming, "Stability analysis of a wind turbine active power control system," in *American Control Conference (ACC), 2013*, pp. 1418-1423.

[57] G. Lalor, A. Mullane, and M. O'Malley, "Frequency Control and Wind Turbine Technologies," *IEEE Transactions on Power Systems,* vol. 20, 2005.

[58] M. A. Yurdusev, R. Ata, and N. S. Cetin, "Assessment of Optimum Tip Speed Ratio in Wind Turbines Using Artificial Neural Networks," *Energy,* vol. 31, 2006.

[59] Y. Lei and e. al., "Modeling of the Wind Turbine With a Doubly Fed Induction Generator for Grid Integration Studies," *IEEE Transactions on Energy Conversion,* vol. 21, 2006.

[60] G. Ramtharan, J. B. Ekanayake, and N. Jenkins, "Frequency support from doubly fed induction generator wind turbines," *IET Renewable Power Generation,* vol. 1, 2007.

[61] J. Morren, J. Pierik, and S. W. H. d. Haan, "Inertial response of variable speed wind turbines," *Electric Power Systems Research,* vol. 76, pp. 980-987, 2006.

[62] M. Kayikci and J. V. Milanovic, "Reactive Power Control Strategies for DFIG-Based Plants," *Energy Conversion, IEEE Transactions on,* vol. 22, pp. 389-396, 2007.

[63] X. Lie and P. Cartwright, "Direct active and reactive power control of DFIG for wind energy generation," *Energy Conversion, IEEE Transactions on,* vol. 21, pp. 750-758, 2006.

[64] F. Schwartz, R. Pegallapati, and M. Shahidehpour, "Small hydro as green power," in *IEEE Power Engineering Society General Meeting*, 12-16 June 2005, pp. 1883–1890.

[65] G. Pepermans, J. Driesen, D. Haeseldonckx, R. Belmans, and W. Dâ€™haeseleer, "Distributed generation: definition, benefits and issues," *Energy Policy,* vol. 33, pp. 787-798, 2005.

[66] S. A. Papathanassiou, "A technical evaluation framework for the connection of DG to the distribution network," *Electric Power Systems Research,* vol. 77, pp. 24-34, 2007.

[67] S. A. Papathanassiou and F. Santjer, "Power-quality measurements in an autonomous island grid with high wind penetration," *Power Delivery, IEEE Transactions on,* vol. 21, pp. 218-224, 2006.

[68] T. Boutsika, S. Papathanassiou, and N. Drossos, "Calculation of the fault level contribution of distributed generation according to IEC Standard 60909," in *Proceedings of CIGRE Symposium Power Systems with Dispersed Generation*, Athens, April 2005.

[69] K. Jarrett, J. Hedgecock, R. Gregory, and T. Warham, "Technical guide to the connexion of generation to the distribution network," Distributed Generation Co-coordinating Group and Technical Steering Group, Department of Trade and Industry, UK, http://www.distributedgeneration.gov.uk/documents/05_01_2004_kel00318.pdf, 2004.

[70] DCode, "The distribution code and the guide to the distribution code of licensed distribution network operators of Great Britain," www.dcode.org.uk, 2011.

[71] Q. Kejun, Z. Chengke, Y. Yue, S. Xiaodan, and M. Allan, "Analysis of the environmental benefits of Distributed Generation,," in *Power and Energy Society General Meeting - Conversion and Delivery of Electrical Energy in the 21st Century*, IEEE, Ed., 2008, pp. 1-5.

[72] S. Papathanassiou and N. Hatziargyriou, "Technical requirements for the connection of dispersed generation to the grid," *Electric Power Systems Research* vol. 77, pp. 24-34, 2007.

[73] T. Boutsika, S. Papathanassiou, and N. Drossos, "Calculation of the fault level contribution of distributed generation according to IEC Standard 60909," in *Proceedings of CIGRE Symposium Power Systems with Dispersed Generation*, Athens, 2005.

[74] "Voltage characteristics of electricity supplied by public distribution systems," European Normative 50160 CENELEC, 1999.

[75] S. Chondrogiannis, M. Barnes, and M. Aten, "Technologies for Integrating Wind Farms to the Grid," DIT (Now BIS), AREVA T&D Technology Centre, 2006.

[76] P. Chiradeja, "Benefit of Distributed Generation: A Line Loss Reduction Analysis," in *Transmission and Distribution Conference and Exhibition: Asia and Pacific, 2005 IEEE/PES*, 2005, pp. 1-5.

[77] R.H.Lasseter and P.Paigi, "Microgrid: a conceptual solution," in *Proc. of Power Electronics Specialists Conference(PESC)*, Aachen, Germany, 2004, pp. 4285- 4290.

[78] N. Hadjsaid, J. F. Canard, and F. Dumas, "Dispersed Generation Impact on Distribution Networks," *IEEE Computer Applications in Power,* 1999.

[79] CIGRE, "Impact of increasing contribution of dispersed generation on the power system," in *Final Report, Study Committee no. 37*, 1998.

[80] L.Kumpulainen and K.Kauhaniemi, "Distributed Generation and Reclosing Coordination," in *Proc. of Nordic Distribution and Asset Management Conference,NORDAC 2004, Espoo*, 2004.

[81] J. A. P. Lopes, N. Hatziargyriou, J. Mutale, P.Djapic, and N. Jenkins, "Integrating distributed generation into electric power systems: A review of drivers, challenges and opportunities," *Electric Power System Research,* vol. 77, pp. 1189-1203, 2007.

[82] S.P.Chowdhury, C.F.Ten, and P.A.Crossley, "Operation and control of DG based power island in smart grid environment," in *20th International Conference on Electricity Distribution*, Prague, 2009.

[83] F. M. Gatta, F. Iliceto, S. Lauria, and P. Masato, "Modeling and Computer Simulation of in Dispersed Generation in Distribution Networks. Measures to prevent disconnection during system disturbances," in *Proc. of IEEE Power Tech Conference*, Bologna, Italy., 2003.

[84] F.A.Viawan, D.Karlsson, A.Sannino, and J.Daalder, "Protection Scheme for Meshed Distribution Systems with High Penetration of Distributed Generation," in *Proc. of Power System Conference 2006: Advance Metering, Protection, Control, Communication and Distributed Resources*, 2006.

[85] M.A.Redfern, J.I.Barrett, and O.Usta, "A New Microprocessor Based Islanding Protection Algorithm for Dispersed Storage and Generation Units," *IEEE Transactions on Power Delivery,* vol. 10, pp. 1249-1254, 1995.

[86] M.Robitaille, K.Agbossou, and M.L.Doumbia, "Modeling of an Islanding Protection Method for a Hybrid Renewable Distributed Generator," in *Proc. of Electrical and Computer Engineering*, Canada, 2005, pp. 1477-1481.

[87] C.G.Bright, "Comparison of Rate of Change of Frequency Protection: A Solution to the Detection of Loss of Mains" in *IEE, Developments in Power System Protection*, 2001.

[88] IEC White Paper, "Microgrids for disaster preparedness and recovery," 2014.

[89] Ofgem, "Office of the Gas and Electricity Markets," http://www.ofgem.gov.uk.

[90] A. M. Mohamad, N. Hashim, N. Hamzah, N. F. N. Ismail, and M. F. A. Latip, "Transient stability analysis on Sarawak's Grid using Power System Simulator for Engineering (PSS/E)," in *Industrial Electronics and Applications (ISIEA), 2011 IEEE Symposium on*, pp. 521-526.

[91] I. D. Margaris, J. C. Mantzaris, M. E. Karystianos, A. I. Tsouchnikas, C. D. Vournas, N. D. Hatziargyriou, and I. C. Vitellas, "Methods for evaluating penetration levels of wind generation in autonomous systems," in *PowerTech, 2009 IEEE Bucharest*, 2009, pp. 1-7.

[92] N. Hemdan and M. kurrat, "Influence of distributed generation on different loadability aspects of electric distributions systems," in *20th International Conference on Electricity Distribution, CIRED,*, Prague, 2009.

[93] L. Yazhou, A. Mullane, G. Lightbody, and R. Yacamini, "Modeling of the wind turbine with a doubly fed induction generator for grid integration studies," *Energy Conversion, IEEE Transactions on,* vol. 21, pp. 257-264, 2006.

[94] M. Emranjeet and I. Syed, "Stability Considerations of Distributed Power Systems with Low Inertia Generators," in *International Conference on Communication, Conference & Power (ICCCP´07)*, Muscat, 2007.

[95] PSSE Siemens PTI, "High -Performance Transmission Planning Application for the Power Industry," in *https://www.pti-us.com/pti/software/psse/university/index.htm*.

[96] C. Grande-Moran and "Modeling of Three-winding Voltage Regulating Transformers for Posiive Sequence Load Flow Analysis in PSS/E," in *Siemens PTI eNewsletter*, 2010.

[97] J. D. Glover, M. S. Sarma, and T. J. Overbye, *Power System Analysis and Design*, Fourth (International Student Edition) ed.: Thomson, 2008.

[98] P. Schavemaker and L. V. Sluis, *Electrical Power System Essentials*: Wiley, 2009.

[99] PowerWorld Corporation, "Contingency Analysis," http://www.powerworld.com/WebTraining/I10ContingencyAnalysis.pdf., 2008.

[100] P. Scott and R. Dahman, "N-1-1 Contingency Analysis using PowerWorld Simulator," 2010.

[101] REE, "Procedimientos de operación de Red Eléctrica de España (REE)," http://www.ree.es/operacion/procedimientos operacion.asp.

[102] European Std., "Voltage Characteristics of Electricity Supplied by Public Distrubution Systems," in *EN 50160*, 1999.

[103] G. Kabashi et.al., "Wind Farm Modeling for Steady-state and Dynamic Analysis," *Wind Farm Modeling for Steady-state and Dynamic Analysis,* vol. 74, 2011.

[104] V. Akhmatov, "Analysis of dynamic behaviour of electric power systems with large amount of wind power," in *Ph.D. Thesis*: Technical University of Denmark, 2003, pp. 9-64.

[105] Q. M. Alias and W. A. Jaafar, "Distributed Generation Embedded in the Iraki Power Grid," *Engineering & Technology Journal,* vol. 28, 2010.

[106] J. Soens et.al., "Equivalent Transfer Function for a Variable Speed Wind Turbine in Power System Dynamic Simulations," *International Journal of Distributed Energy Resources,* vol. 1, pp. 111-131, 2005.

[107] T. Alquthami et. al., "Study of Photovoltaic Integration Impact on System Stability using Custom Model on PV Arrays Integrated with PSS/E," in *North American Power Symposium (NAPS)*: IEEE Conference Publications, 2010, pp. 1-8.

[108] J. G. Slootweg, "Wind Power: Modeling and Impact on Power System Dynamics," in *Ph.D. Thesis*: Technische Universiteit Delft, 2003.

[109] E. Vittal et.al., "A Steady-State Voltage Stability Analysis of Power Systems with High Penetrations of Wind," *IEEE Transactions on Power Systems,* vol. 25, 2010.

[110] Konstantina Mentesidi and M. Aguado, "The Potential Integration of Electrical Distributed Generation in an Island Power System," *International Journal of Distributed Energy Resources and Smart Grids,* vol. 9, pp. 341-366, 2013.

[111] K. Mentesidi and M. Aguado, "Dynamic behavior analysis of distributed generation in an off-grid network with power system simulator for engineering (PSS/E)," in *IEEE International Energy Conference, ENERGYCON 2014* Cavtat, Croatia, 2014, pp. 1042-1049.

[112] CENELEC, "EN 50160 Voltage characteristics of electricity supplied by public distribution networks," 2010.

[113] BDEW, "Technical guideline - Generating plants connected to the medium-voltage network,"

in http://www.bdew.de/internet.nsf/id/-A2A0475F2FAE8F44C12578300047C92F/%24file/BDEW%5FRL%5FEA-am-MSNetz%5Fengl.pdf, 2008.

[114] F. e.V., "Technical guidelines for power generating units - Part 3 - Determination of electrical characteristics of power generating units connected to MV, HV and EHV grids," 2010.

[115] DERlab, "European White Book on Real time Powerhardware-in-the-Loop testing," 2011-2012.

[116] F. Lehfuss, G. Lauss, P. Kotsampopoulos, N. Hatziargyriou, P. Crolla, and A.Roscoe, "Comparison of multiple power amplification types for Power Hardware-in-the-Loop applications," in *IEEE Workshop on Complexity in Engineering (COMPENG 2012)* Aachen, Germany., 2012.

[117] A. Roscoe, A. Mackay, G. Burt, and J. McDonald, "Architecture of a network-in-the-loop environment for characterizing AC power- system behavior," *IEEE Trans. Industrial Electronics,* vol. 57, pp. 1245-1253, 2010.

[118] M. Steurer, F. Bogdan, W. Ren, M. Sloderbeck, and S. Woodruff, "Controller and power hardware-in-loop methods for accelerating renewable energy integration," in *Power Engineering Society General Meeting, IEEE* 2007, pp. 1-4.

[119] K. Mentesidi, "PHIL Tests in support of the studies on the DER Integration," in *Experimental research and DER integration in the EU Energy System*, Milan, Italy, October, 2013.

[120] P. Kotsampopoulos, V. Kleftakis, G. Messinis, and N. Hatziargyriou, "Design, development and operation of a PHIL environment for distributed energy resources," in *the 38th Annual Conference of the IEEE Industrial Electronics Society IECON* 2012.

[121] P. Kotsampopoulos, A. Kapetanaki, G. Messinis, V. Kleftakis, and N.Hatziargyriou, "A PHIL facility for microgrids," *International Journal of Distributed Energy Resources,* vol. 9, pp. 71-86, 2013.

[122] F. Lehfuß, "Real time simulation with power hardware-in-the-loop of low voltage grids with photovoltaic generation," Master thesis: Carinthia University of Applied Sciences, System Design, 2010.

[123] RTDS Technologies, http://www.rtds.com.

[124] C. B. Jacobina, T. M. Oliveira, and d. S. E.R.C., "Control of the Single-Phase Three-Leg AC/AC Converter," *IEEE Transactions on Industrial Electronics,* vol. 53, pp. 467-476, 2006.

[125] H. W. Park, S. J. Paark, and C. U. Kim, "A Novel High-Performance Voltage Regulator for Single-Phase AC Sources," *IEEE Transactions on Industrial Electronics,* vol. 48, pp. 554-562, 2001.

[126] K. Mentesidi, M. Santamaria, A. Vassilakis, A. Rigas, V. Kleftakis, P. Kotsampopoulos, and M. Aguado, "Power Hardware-In-The-Loop technique applied to a LV Network for integrating a Supercapacitor with an Average Model of STATCOM," in *The IEEE International Workshop on Intelligent Energy Systems (IWIES 2013)* Vienna, Austria, November, 2013, pp. 167-172.

[127] K. Mentesidi, E. Rikos, V. Kleftakis, P. Kotsampopoulos, M. Santamaria, and M. Aguado, "Implementation of a Microgrid model for DER Integration in Real time Simulation Platform," in *International Symposium on Industrial Electronics (ISIE 2014)* Istanbul, Turkey, June, 2014.

[128] V. Karapanos, S. d. Haan, and K. Zwetsloot, "Real Time Simulation of a Power System with VSG Hardware in the Loop," in *Proc. IEEE Industrial Electronics Society IECON'2011*, Australia, 2011.

[129] M. Dargahi, A. Ghosh, G. Ledwich, and F. Zare, "Studies in power hardware in the loop (PHIL) simulation using real time digital simulator (RTDS)," in *IEEE International Conference on Power Electronics, Drives and Energy Systems*, December 16-19, 2012.

[130] P. McLaren, R. Kuffel, R. Wierckx, J. Giesbrecht, and L.Arendt, "A real time digital simulator for testing relays," *Power Delivery, IEEE Trans. on,* vol. 7, pp. 207-213, 1992.

[131] A. Sattar, A. Al-Durra, and S. Muyeen, "Real time implementation of STATCOM to analyze transient and dynamic characteristics of wind farm," in *37th Annual Conference on IEEE Industrial Electronics Society, IECON 2011*, 2011, pp. 3742-3747,.

[132] Carlos Bicudo da Ponte, "Geothermal Resources at the Azores," in *Geothermal programs under EEA Grants and cooperation within Europe*, Harpa, 2013.

[133] S. A. ELECTRICIDADE DOS AÇORES – EDA, "CARACTERIZAÇÃO DAS REDES DE TRANSPORTE E DISTRIBUIÇÃO DE ENERGIA ELÉCTRICA DA REGIÃO AUTÓNOMA DOS AÇORES," 2010.

[134] ENTSO-E, 2011.

[135] K. Mentesidi, E. Rikos, V. Kleftakis, P. Kotsampopoulos, and M. Aguado, "Real time Simulation Technique of a Microgrid Model for DER Penetration," *EAI Endorsed Transactions on Energy Web,* 2014.

[136] A. Chakraborty, S. Musunuri, A. Srivastava, and A. Kondabathini, "Integrating STATCOM and battery energy storage system for power system transient stability. ," *A review and application, Advances in Power Electronics Journal,* vol. 2012, pp. 1-12, 2012.

[137] Sunny Island, "4500 manual," http://files.sma.de/dl/5614/SI4500-FEAT-11-EE4405.pdf.

[138] M. Kazmierkowski, F. Blaabjerg, and R. Krishnan, "Control in Power Electronics, Selected Problems, Chapter 4," Academic Press USA, Ed., 2002, pp. 89-142.

[139] S. Shah, "Design & Implementation of Parallel Operation of Inverters with Instataneous Current Sharing Scheme Using Multiloop Control Strategy on FPGAPlatform," in *Electrical Engineering Department* Kanpur: Indian Institute of Technology, 2008, pp. 12-20.

[140] K. Cheong, P.Y. Li, and J. Xia, "Control Oriented Modeling and System Identification of a Diesel Generator Set (Genset)," in *American Control Conference* Marriott Waterfront, Baltimore, MD, USA, 2010.

[141] S. Krishnamurthy, T. M. Jahns, and R. H. Lasseter, "The operation of diesel gensets in a CERTS microgrid," in *Power and Energy Society General Meeting - Conversion and Delivery of Electrical Energy in the 21st Century, 2008 IEEE*, 2008, pp. 1-8.

[142] E. Alegria, T. Brown, E. Minear, and R. H. Lasseter, "CERTS Microgrid Demonstration With Large-Scale Energy Storage and Renewable Generation," *Smart Grid, IEEE Transactions on,* vol. 5, pp. 937-943, 2014.

[143] M. Datta, T. Senjyu, A. Yona, T. Funabashi, and K. Chul-Hwan, "A coordinated control method for leveling PV output power fluctuations of PV–Diesel hybrid systems connected to isolated power utility," *IEEE Transactions on Energy Conversion,* vol. 24, pp. 153-162, 2009.

[144] T. A. Theubou, R. Wamkeue, and I. Kamwa, "Reactive power management modeling of an autonomous Wind-Diesel Power plant," in *IECON 2012 - 38th Annual Conference on IEEE Industrial Electronics Society*, pp. 4326-4331.

[145] R. Ruther, D. C. Martins, and E. Bazzo, "Hybrid diesel/photovoltaic systems without storage for isolated mini-grids in Northern Brazil," in *Photovoltaic Specialists Conference, 2000. Conference Record of the Twenty-Eighth IEEE*, 2000, pp. 1567-1570.

[146] C. Kai Loon, P. Y. Li, and X. Jicheng, "Control oriented modeling and system identification of a diesel generator set (genset)," in *American Control Conference (ACC), 2010*, pp. 950-955.

[147] P. Bauer, L. E. Weldemariam, and E. Raijen, "Stand-alone microgrids," in *Telecommunications Energy Conference (INTELEC), 2011 IEEE 33rd International*, pp. 1-10.

[148] C. A. Platero, Bla, x, F. zquez, Fri, P. as, and A. J. Casado, "Coordinated Power Quality Improvement in Multiunit Diesel Power Plants," *Energy Conversion, IEEE Transactions on,* vol. 25, pp. 1102-1111.

[149] R. Pena, R. Cardenas, J. Proboste, J. Clare, and G. Asher, "Wind–diesel generation using doubly fed induction machines," *IEEE Transactions on Energy Conversion,* vol. 23, pp. 202-214, 2008.

[150] S. M. Islam, M. T. Iqbal, and J. E. Quaicoe, "Voltage fluctuations in a remote wind-diesel hybrid power system," in *Proc. 5th Int. Conf. Electr. Comput. Eng.-ICECE*, 2008, pp. 699-705.

[151] R. Fadaeinedjad, G.Moschopulos, and M. Moallem, "Flicker contribution of a wind turbine in a stand-alone wind diesel system," in *Can. Conf. Electr. Comput. Eng., Niagara Falls*, Canada, 2008.

[152] R. J. Best, D. J. Morrow, D. J. McGowan, and P. A. Crossley, "Synchronous Islanded Operation of a Diesel Generator," *Power Systems, IEEE Transactions on,* vol. 22, pp. 2170-2176, 2007.

[153] R.H. Lassater and et.al., "CERTS Microgrid Laboratory Test Bed," *IEEE Transactions on Power Delivery,* vol. 26, 2011.

[154] P. M. Anderson and M. Mirheydar, "Analysis of a diesel-engine driven generating unit and the possibility for voltage flicker," *Energy Conversion, IEEE Transactions on,* vol. 10, pp. 37-47, 1995.

[155] I. Haskara and W. Yue-Yun, "Cylinder Pressure-Based Combustion Controls for Advanced Diesel Combustion With Multiple-Pulse Fuel Injection," *Control Systems Technology, IEEE Transactions on,* vol. 21, pp. 2143-2155.

[156] M. Sivertsson and L. Eriksson, "Generator Effects on the Optimal Control of a Power Assisted Diesel-Electric Powertrain," in *Vehicle Power and Propulsion Conference (VPPC), 2013 IEEE*, pp. 1-6.

[157] T. Xisheng, D. Wei, and Q. Zhiping, "Investigation of the Dynamic Stability of Microgrid," *Power Systems, IEEE Transactions on,* vol. 29, pp. 698-706, 2014.

[158] L. Luo, L. Gao, and H. Fu, "The Control and Modeling of Diesel Generator Set in Electric Propulsion Ship," in *I.J. Information Technology and Computer Science, MECS*. vol. 2, 2011, pp. 31-37.

[159] T. Tudorache and C. Roman, "The Numerical Modeling of Transient Regimes of Diesel Generator Sets," *Acta Polytechnica Hungarica,* vol. 7, pp. 39-53, 2010.

[160] M. Dereszewski, A. Charchalis and S. Polanowski . "Analysis of Diagnostic Utility of Instantaneous Angular Speed Fluctuation of Diesel Engine Crankshaft," *KONES Powertrain and Transport,* vol. 18, p. 7, 2011.

[161] S. H. Gawande, L. G. Navale, M. R. Nandgaonkar, L. S. Butala, and S. Kunamala, "Cylinder Imbalance Detection of Six Cylinder DI Diesel Engine Using Pressure variation," *International Journal of Engineering Science and Technology,* vol. 2, 2010.

[162] A. C. M. Dereszewski, "analysis of diagnostic utility of instantanous angular speed fluctuation of diesel engine crankshaft," *KONES Powertrain and Transport,* vol. 18, p. 7, 2011.

[163] M. Desbazeille, R. B. Randall, F. Guillet, M. El Badaoui, and C. Hoisnard, "Model-based diagnosis of large diesel engines based on angular speed variations of the crankshaft," *Mechanical Systems and Signal Processing,* vol. 24, pp. 1529-1541, 2010

[164] P. Kučera and V. Píštěk, "VIRTUAL DIESEL ENGINE IN SIMULINK," in *Brno University of Technology,* 2013 http://pernerscontacts.upce.cz/30_2013/Kucera.pdf.

[165] P. R. Crossley and J. A. Cook, "Control 91," in *IEE International Conference*. vol. 2 Edinburgh, U.K., 1991, pp. 921-925.

[166] C. Laughman, S. B. Leeb, L. K. Norford, S. R. Shaw, and P. R. Armstrong, "A park transform-based method for condition monitoring of three-phase electromechanical systems " in *Power Electronics, Machines and Drives (PEMD 2010), 5th IET International Conference on* Brighton, UK, 2010.

[167] J. M. Aller, A. Bueno, and T. Pagá, "Power System Analysis Using Space–Vector Transformation," *IEEE Transactions on Power Systems* vol. 17, 2002.

Appendices

Appendix A: Network Data-Power Plants

Fossil Fuel Plant_CTCL

Generators		GEN I,II,III,IV	GEN V,VI,VII,VIII
Ratings			
Output	Sn	9.620 kVA	21.282 kVA
Power Factor	cosj	0,8	0,8
Voltage	Un	6.300 V	11.000 V
Current	In	882 A	1.117 A
Frequency	f	50 Hz	50 Hz
Speed	n	428 rpm	500 rpm
Resistances			
Stator Winding	Ra	0,016 Ω	0,019 Ω
Field Winding	Rf	0,131 Ω	0,178 Ω
Zero Sequence	Ro		
Reactances			
Synchronous - Direct Axis	Xd	2,300 pu	1,860 pu
Synchronous - Quadrature Axis	Xq	1,320 pu	0,930 pu
Transient - Direct Axis	X'd	0,430 pu	0,310 pu
Transient - Quadrature Axis	X'q		
Subtransient - Direct Axis	X"d	0,215 pu	0,207 pu
Subtransient - Quadrature Axis	X"q		0,251 pu
Negative Sequence (Inverse)	X2	0,225 pu	0,229 pu
Zero Sequence	Xo	0,126 pu	0,099 pu
Short-Circuit Ratio	Kcc	1,600	0,610
Time Constants			
Short-Circuit - Transient - Direct Axis	T'd	1,070 sec	1,250 sec
Short-Circuit - Subtransient - Direct Axis	T"d	0,035 sec	0,016 sec
Short-Circuit - Subtransient - Quadrature Axis	T"q		0,027 sec
Armature (Short-Circuit)	Ta		0,144 sec
Open Circuit - Transient - Direct Axis	T'do	5,800 sec	5,900 sec
Open Circuit - Subtransient - Direct Axis	T"do		0,033 sec
Open Circuit - Subtransient - Quadrature Axis	T"qo		0,132 sec

Transformers		TRF Gen. I,II,III,IV		TRF Gen. V,VI,VII,VIII	
Rated Power	Sn	10	MVA	23	MVA
Nominal Voltage (Primary - HV)	U1n	63.000	V	63.000	V
Nominal Voltage (Secondary - LV)	U2n	6.300	V	11.000	V
Short-circuit Voltage	Usc	8,35%		8,00%	
Load Losses (Pcu - cooper losses)	Pcc	50.000	W	98.790	W
No-load Losses (Pfe - iron losses)	Po	10.000	W	12.942	W
Excitation Current	I2o	2,995	A	0,770	A
Resistance (Primary - HV)	R1	2,041	W	0,688	W
Resistance (Secondary - LV)	R2	0,018	W	0,019	W
		Voltages (V)	Tap Pos.	Voltages (V)	Tap Pos.
Maximum	Umax	71.400	1	69.300	1
Nominal	Un	63.000	15	63.000	11
Minimum	Umin	58.200	23	56.700	21
Vector Group		YNd5		YNd5	

Geothermal Power Plant_CGRG

Generators		GEN I,II		GEN III,IV	
Ratings					
Output	Sn	6.750	kVA	3.625	kVA
Power Factor	cosj	0,8		0,8	
Voltage	Un	10.000	V	10.000	V
Current	In	389,7	A	209,3	A
Frequency	f	50	Hz	50	Hz
Speed	n	1.500	rpm	1.500	rpm
Resistances					
Stator Winding	Ra	0,068	Ω	0,252	Ω
Field Winding	Rf	0,796	Ω	0,481	Ω
Zero Sequence	Ro				
Reactances					
Synchronous - Direct Axis	Xd	2,160	pu	2,774	pu
Synchronous - Quadrature Axis	Xq	1,170	pu	1,646	pu
Transient - Direct Axis	X'd	0,329	pu	0,388	pu

Transient - Quadrature Axis	X'q	1,170 pu	1,646 pu
Subtransient - Direct Axis	X"d	0,265 pu	0,341 pu
Subtransient - Quadrature Axis	X"q	0,295 pu	0,315 pu
Negative Sequence (Inverse)	X2	0,280 pu	0,328 pu
Zero Sequence	Xo	0,029 pu	0,094 pu
Time Constants			
Short-Circuit - Transient - Direct Axis	T'd	1,493 sec	0,949 seg
Short-Circuit - Subtransient - Direct Axis	T"d	0,063 sec	0,047 seg
Short-Circuit - Subtransient - Quadrature Axis	T"q		
Armature (Short-Circuit)	Ta	0,115 sec	0,069 seg
Open Circuit - Transient - Direct Axis	T'do	8,045 sec	5,593 seg
Open Circuit - Subtransient - Direct Axis	T"do	0,080 sec	0,056 seg
Open Circuit - Subtransient - Quadrature Axis	T"qo		

Transformers		TRF 1		TRF 2	
Rated Power	Sn	8 MVA		8 MVA	
Nominal Voltage (Primary - HV)	U1n	62.980 V		62.980 V	
Nominal Voltage (Secondary - LV)	U2n	10.000 V		10.000 V	
Short-circuit Voltage	Usc	7,98%		7,94%	
Load Losses (Pcu - cooper losses)	Pcc	54.800 W		55.300 W	
No-load Losses (Pfe - iron losses)	Po	7.530 W		7.670 W	
Excitation Current	I2o	2,620 A		2,840 A	
Resistance (Primary - HV)	R1	1,500 W		1,500 W	
Resistance (Secondary - LV)	R2	0,053 W		0,053 W	
		Voltages (V)	Tap Pos.	Voltages (V)	Tap Pos.
Maximum	Umax	69.580	1	69.580	1
Nominal	Un	62.980	12	62.980	12
Minimum	Umin	59.980	17	59.980	17
Vector Group		YNd11		YNd11	

Geothermal Power Plant_CGPV

Generators		GEN I	
Ratings			
Output	Sn	16.250	kVA
Power Factor	cosj	0,8	
Voltage	Un	11.000	V
Current	In	853	A
Frequency	f	50	Hz
Speed	n	1.500	rpm
Resistances			
Stator Winding	Ra	0,023	Ω
Field Winding	Rf	0,052	Ω
Zero Sequence	Ro		
Reactances			
Synchronous - Direct Axis	Xd	2,150	pu
Synchronous - Quadrature Axis	Xq	1,090	pu
Transient - Direct Axis	X'd	0,290	pu
Transient - Quadrature Axis	X'q		
Subtransient - Direct Axis	X"d	0,190	pu
Subtransient - Quadrature Axis	X"q	0,550	pu
Negative Sequence (Inverse)	X2	0,370	pu
Zero Sequence	Xo	0,100	pu
Short-Circuit Ratio	Kcc	0,500	
Time Constants			
Short-Circuit - Transient - Direct Axis	T'd	0,800	sec
Short-Circuit - Subtransient - Direct Axis	T"d	0,040	sec
Short-Circuit - Subtransient - Quadrature Axis	T"q	0,040	sec
Armature (Short-Circuit)	Ta	0,200	sec
Open Circuit - Transient - Direct Axis	T'do	6,000	sec
Open Circuit - Subtransient - Direct Axis	T"do	0,060	sec
Open Circuit - Subtransient - Quadrature Axis	T"qo	0,080	sec

Transformers		TRF Gen. I	
Rated Power	Sn	17	MVA
Nominal Voltage (Primary - HV)	U1n	30.000	V
Nominal Voltage (Secondary - LV)	U2n	11.000	V
Short-circuit Voltage	Usc	7,74%	
Load Losses (Pcu - cooper losses)	Pcc	107.800	W
No-load Losses (Pfe - iron losses)	Po	12.300	W
Excitation Current	I2o	1,610	A
Resistance (Primary - HV)	R1	0,135	W
Resistance (Secondary - LV)	R2	0,030	W
		Voltages (V)	Tap Pos.
Maximum	Umax	31.500	1
Nominal	Un	30.000	3
Minimum	Umin	29.250	5
Vector Group		YNd5	

Appendix B: Network Data- Branches

Lines / Cables							
Type	Designation	Un [kV]	R [Ω/km]	X [Ω/km]	B [S/km]	Max. Load Capacity [A]	[MVA]
Line	Cu 185mm2	60	0,101	0,389	0,00000278	540	56,12
Line	Cu 95mm2	60	0,202	0,407	0,00000277	360	37,41
Line	Cu 95mm2	30	0,207	0,363	0,00000315	360	18,71
Line	Cu 70mm2	30	0,273	0,372	0,00000308	305	15,85
Line	Cu 50mm2	30	0,401	0,383	0,00000298	240	12,47
Line	Cu 35mm2	30	0,561	0,394	0,00000289	195	10,13
Cable	LX1HIE 120mm2	30	0,253	0,122	0,00006280	275	14,29
Cable	LXHIOV 240mm2	30	0,159	0,103	0,00005556	420	21,82
Cable	LXHIOV 120mm2	30	0,323	0,116	0,00003333	285	14,81
Cable	LXHIOV 70mm2	30	0,567	0,126	0,00003333	210	10,91
Cable	LXHIOV 50mm2	30	0,822	0,135	0,00002222	170	8,83
Cable	LXHIV 70mm2	30	0,567	0,126	0,00003333	210	10,91
Cable	LEHIV 70mm2	30	0,531	0,112	0,00003333	195	10,13
Cable	LEHIV 35mm2	30	1,041	0,141	0,00002222	135	7,01
Line	Cu 50mm2	10	0,402	0,384	0,00000298	240	4,16
Line	Cu 35mm2	10	0,561	0,395	0,00000289	195	3,38
Line	Cu 25mm2	10	0,733	0,404	0,00000282	165	2,86
Line	Cu 16mm2	10	1,219	0,420	0,00000271	120	2,08
Cable	LXHIOV 240mm2	10	0,160	0,091	0,00010000	420	7,27
Cable	LXHIOV 120mm2	10	0,401	0,101	0,00010000	285	4,94
Cable	LXHIOV 70mm2	10	0,568	0,110	0,00008401	210	3,64
Cable	LXHIOV 50mm2	10	0,822	0,118	0,00007375	170	2,94
Cable	LXHIAV 120mm2	10	0,401	0,101	0,00010000	285	4,94
Cable	LXHIAV 50mm2	10	0,822	0,118	0,00007375	170	2,94
Cable	LXHIAV 35mm2	10	1,113	0,122	0,00006586	145	2,51
Cable	LXHIV 185mm2	10	0,401	0,101	0,00010000	360	6,24
Cable	LXHIV 120mm2	10	0,401	0,101	0,00010000	285	4,94
Cable	LXHIV 70mm2	10	0,568	0,110	0,00008401	210	3,64
Cable	XHIOE 240mm2	10	0,075	0,094	0,00010000	523	9,06
Cable	PCAJ 95mm2	10	0,231	0,094	0,00010000	274	4,75
Cable	PCAJ 35mm2	10	0,627	0,110	0,00008482	155	2,68
Cable	PCAJ 25mm2	10	0,870	0,113	0,00007540	129	2,23
Cable	PCAJ 16mm2	10	1,376	0,122	0,00006911	100	1,73

Appendix C: Scenario 1-Power Flow Results (Low Demand)

Table C-1 concentrates the power flow results for Scenario 1. The total generation produced is at 64.4 MW where 43.7 MW come from the slack generators operation and 20.7 MW from the geothermal plants, whereas its reactive power delivery amounts for 16.2 MVAr. Charging is at 5.7MVAr. Low load demand arises to 63.5 MW and 19.4 MVAr, while shunts equal to 0.4MW and (-1.8 MVAr). Thus the active and reactive power losses are 0.5 MW and 4.4 MVar respectively. Additionally, the numerical difference among the high and low demand cases (in low demand the losses are smaller) in both reactive and active power losses was prospective as losses have to do with the total system handling capacity and the load demand.

The voltage profile of the transmission and distribution network needs to reside within the acceptable limits of ±5% of the nominal voltage value (0.95-1.05 pu). Moreover, is loosely accepted that are applied the same voltage limits for the transport and distribution network. There are no any voltage violations observed as it can be seen in Figure C-1. The bus with the lowest voltage figure of 0.963 pu is bus number 30 at the substation SEFO. The transformer branch of SEFO 60/30 experience active and reactive losses of 0.10 MW and 1.47 MVAR respectively and coincide with the high loading demand case of this scenario. Additionally, there are no any violations in branches.

ATable C-1: Case summary power flow outcomes, Scenario 1

Total	Generation	PQLoad	Shunts	Charging	Losses	Swing
MW	64.4	63.5	0.4	0	0.5	43.7
MVAr	16.2	19.4	-1.8	5.7	4.4	22.3

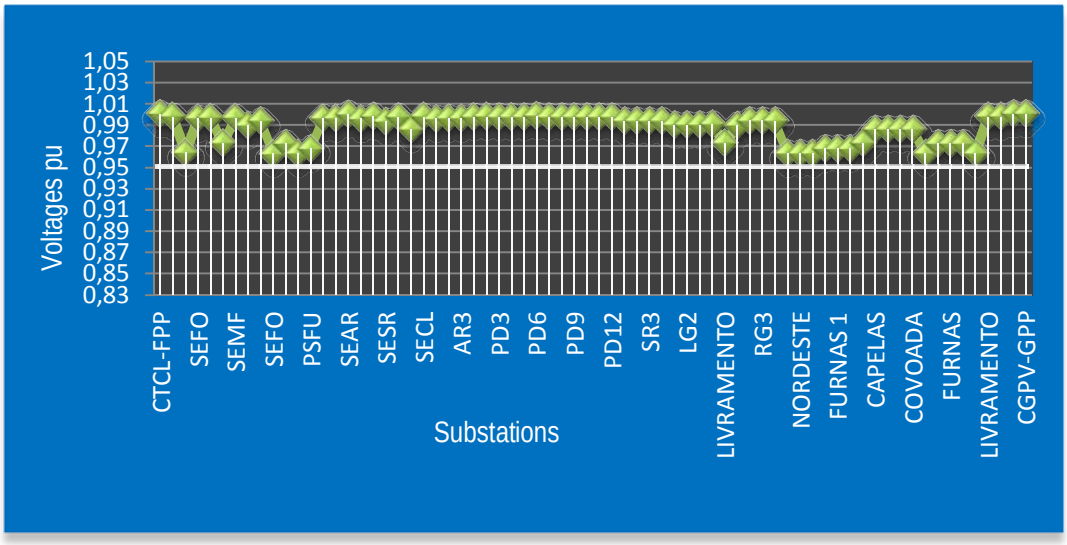

Figure C-1: *Voltage profile of the transmission and distribution network, Scenario 1.*

Appendix D: Scenario 2-Power Flow Results (Low Demand)

Regarding Scenario 2, load has increased by 10%, from 63.5 MW to 69.85 MW. This rise of 6.35 MW is allocated among the distribution substations accordingly to their load demand requirements. For instance, the nodes of 11.7 and 11.35 MW (Table 4-5) will suffer from an increase of 1.135 MW. Nodes that their power demand arises to 8.84 MW will have an increase of 0.884 MW and buses of 6.99 MW will reach up to 7.689 MW (0.699 MW increase). All the remaining substation nodes will increase their power demand by 0.208 MW. Reactive load demand also increases by 10%, from 19.4 MVAr to nearly 21.34 MVAr. This increase of 1.94 MVAr is distributed among the total number of nodes with each one suffering by a rise of 0.18 MVAr. The PSFU 30 kV bus and the nodes connected to it are very sensitive to power demand status. Thus, for a slightly higher demand at this node, voltage drops below 0.95 pu.

The geothermal power is regulated to be at 66.4 MW in 2015. This soar in power production in combination to the load demand rate will affect the conventional generators´ output (in our case the slack ones).

Table D-1 concentrates the case summary results. Total generation produced is at 71.1 MW where 25.6 MW come from the slack generators operation and 45.5 MW from the geothermal plants, whereas its reactive power delivery amounts for 20.9 MVAr. Charging is at 5.7MVAr. Low load demand arises to 69.7 MW and 21.4 MVAr, while shunts equal to 0.7MW and (-0.5 MVAr). Thus, the losses are 0.8 MW and 5.7 MVar for the real and reactive power respectively. Similarly, this scenario case does not experience any voltage violations (Fig. D-1). The bus with the lowest voltage figure of 0.959 pu is bus number 32 in the substation of SEVF. At the substation of SEFO rated at 30 kV there is again dictated a voltage instability around 0.976 pu.

ATable D-1: Case summary power flow outcomes, Scenario 2

Total	Generation	PQLoad	Shunts	Charging	Losses	Swing
MW	71.1	69.7	0.7	0	0.8	25.6
MVAr	20.9	21.4	-0.5	5.7	5.7	22.3

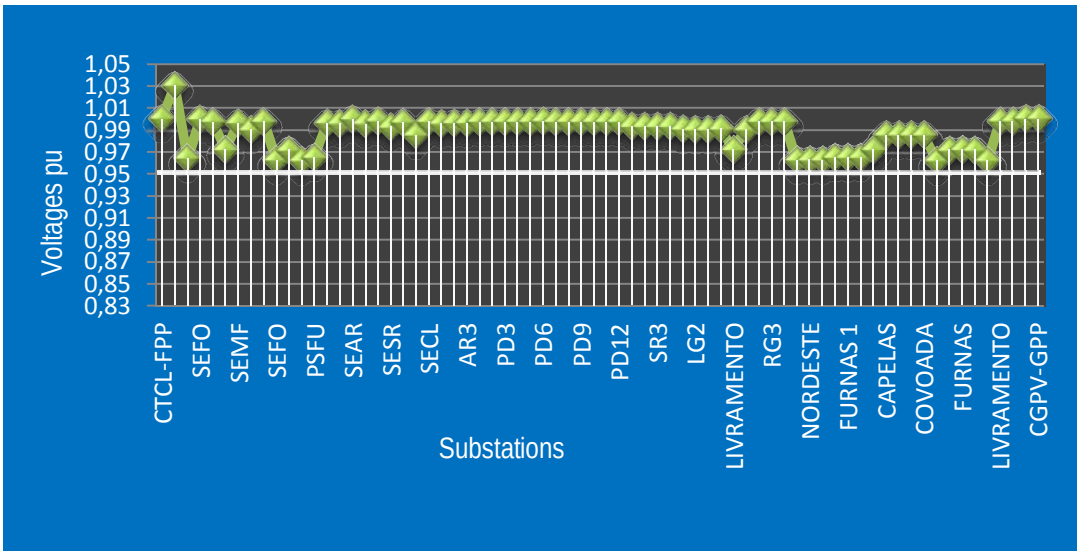

Figure D-1: *Voltage profile of the transmission and distribution network, Scenario 2.*

Appendix E: Scenario 1-Contingency Results (Low Demand)

For Scenario 1, tripping the system lines of 60 kV one by one, are observed the branches with over loadings and buses with violations in voltage rates. Here, there were not monitored such kind of violations.

Tripping the lines of 30 kV one by one, is monitored only one transmission branch between 3 CGPV-GPP and 30 SEFO rated at this voltage value being overloaded. In more details, the contingency with the worst consequences on the system is to take out the connection line among bus 3 CGPV-GPP and bus 30. The effect of this tripping is violation on current rating by 91.6%. The reason that this rating is smaller than the one in the high demand scenario can be attributed to the lower figure of demand requirement. Figure E-1 depicts the relative results.

```
                                                    final results
ACCC OVERLOAD REPORT: MONITORED BRANCHES AND INTERFACES LOADED ABOVE  80.0 % OF RATING SET A
                      % LOADING VALUES ARE % MVA FOR TRANSFORMERS AND % CURRENT FOR NON-TRANSFORMER BRANCHES
INCLUDES VOLTAGE REPORT

AC CONTINGENCY RESULTS FILE:  C:\Documents and Settings\kmentesidi\Desktop\results.acc
DISTRIBUTION FACTOR FILE:     C:\Documents and Settings\kmentesidi\Desktop\data.dfx
SUBSYSTEM DESCRIPTION FILE:   C:\Documents and Settings\kmentesidi\Desktop\sub.sub
MONITORED ELEMENT FILE:       C:\Documents and Settings\kmentesidi\Desktop\monitored.mon
CONTINGENCY DESCRIPTION FILE: C:\Documents and Settings\kmentesidi\Desktop\con 30.con

**PERCENT LOADING UNITS**
%MVA FOR TRANSFORMERS
% I  FOR NON-TRANSFORMER BRANCHES

**OPTIONS USED IN CONTINGENCY ANALYSIS**
Solution engine:              Fixed slope decoupled Newton-Raphson (FDNS)
Solution options
  Tap adjustment:             Lock taps
  Area interchange control:   Disable
  Phase shift adjustment:     Disable
  Dc tap adjustment:          Enable
  Switch shunt adjustment:    Enable all
  Non diverge:                Disable
Mismatch tolerance (MW ):     0.5
Dispatch mode:                Disable

<---------------- MULTI-SECTION LINE ----------------> <------------------ MONITORED BRANCH ------------------> CONTINGENCY
   RATING     FLOW      %
                                                      3 CGPV-GPP    30.000     30*SEFO        30.000 1  SINGLE 2
     12.5     10.9     91.6

MONITORED VOLTAGE REPORT:
SYSTEM                        CONTINGENCY  <-------- B U S --------->   V-CONT   V-INIT   V-MAX    V-MIN

CONTINGENCY LEGEND:
LABEL          EVENTS
SINGLE 1    : OPEN LINE FROM BUS 3 [CGPV-GPP    30.000] TO BUS 30 [SEFO        30.000] CKT 1
SINGLE 2    : OPEN LINE FROM BUS 3 [CGPV-GPP    30.000] TO BUS 30 [SEFO        30.000] CKT 2
SINGLE 3    : OPEN LINE FROM BUS 13 [SELG        30.000] TO BUS 31 [SEVF        30.000] CKT 1
SINGLE 4    : OPEN LINE FROM BUS 13 [SELG        30.000] TO BUS 31 [SEVF        30.000] CKT 2
SINGLE 5    : OPEN LINE FROM BUS 13 [SELG        30.000] TO BUS 70 [LIVRAMENTO  30.000] CKT 1
SINGLE 6    : OPEN LINE FROM BUS 13 [SELG        30.000] TO BUS 70 [LIVRAMENTO  30.000] CKT 2
SINGLE 7    : OPEN LINE FROM BUS 13 [SELG        30.000] TO BUS 82 [RIBEIRA CHÃ 30.000] CKT 1
SINGLE 8    : OPEN LINE FROM BUS 13 [SELG        30.000] TO BUS 82 [RIBEIRA CHÃ 30.000] CKT 2
SINGLE 9    : OPEN LINE FROM BUS 30 [SEFO        30.000] TO BUS 75 [CALHETAS    30.000] CKT 1
SINGLE 10   : OPEN LINE FROM BUS 30 [SEFO        30.000] TO BUS 75 [CALHETAS    30.000] CKT 2
SINGLE 11   : OPEN LINE FROM BUS 30 [SEFO        30.000] TO BUS 76 [NORDESTE    30.000] CKT 1
SINGLE 12   : OPEN LINE FROM BUS 30 [SEFO        30.000] TO BUS 76 [NORDESTE    30.000] CKT 2
SINGLE 13   : OPEN LINE FROM BUS 30 [SEFO        30.000] TO BUS 77 [RIBEIRINHA  30.000] CKT 1
SINGLE 14   : OPEN LINE FROM BUS 30 [SEFO        30.000] TO BUS 77 [RIBEIRINHA  30.000] CKT 2
SINGLE 15   : OPEN LINE FROM BUS 31 [SEVF        30.000] TO BUS 33 [PSFU        30.000] CKT 1
SINGLE 16   : OPEN LINE FROM BUS 31 [SEVF        30.000] TO BUS 89 [V F III     30.000] CKT 1
SINGLE 17   : OPEN LINE FROM BUS 31 [SEVF        30.000] TO BUS 90 [FURNAS      30.000] CKT 1
SINGLE 18   : OPEN LINE FROM BUS 31 [SEVF        30.000] TO BUS 90 [FURNAS      30.000] CKT 2
SINGLE 19   : OPEN LINE FROM BUS 31 [SEVF        30.000] TO BUS 91 [P. GARÇA    30.000] CKT 1
SINGLE 20   : OPEN LINE FROM BUS 31 [SEVF        30.000] TO BUS 91 [P. GARÇA    30.000] CKT 2
SINGLE 21   : OPEN LINE FROM BUS 33 [PSFU        30.000] TO BUS 79 [POVOAÇÃO    30.000] CKT 1
SINGLE 22   : OPEN LINE FROM BUS 33 [PSFU        30.000] TO BUS 79 [POVOAÇÃO    30.000] CKT 2
SINGLE 23   : OPEN LINE FROM BUS 33 [PSFU        30.000] TO BUS 80 [FURNAS 1    30.000] CKT 1
SINGLE 24   : OPEN LINE FROM BUS 33 [PSFU        30.000] TO BUS 80 [FURNAS 1    30.000] CKT 2
SINGLE 25   : OPEN LINE FROM BUS 33 [PSFU        30.000] TO BUS 81 [FURNAS 2    30.000] CKT 1
SINGLE 26   : OPEN LINE FROM BUS 44 [SEMF        30.000] TO BUS 83 [CAPELAS     30.000] CKT 1
SINGLE 27   : OPEN LINE FROM BUS 44 [SEMF        30.000] TO BUS 83 [CAPELAS     30.000] CKT 2
SINGLE 28   : OPEN LINE FROM BUS 44 [SEMF        30.000] TO BUS 84 [S. CIDADES  30.000] CKT 1
SINGLE 29   : OPEN LINE FROM BUS 44 [SEMF        30.000] TO BUS 84 [S. CIDADES  30.000] CKT 2
SINGLE 30   : OPEN LINE FROM BUS 44 [SEMF        30.000] TO BUS 85 [S.ROQUE     30.000] CKT 1
SINGLE 31   : OPEN LINE FROM BUS 44 [SEMF        30.000] TO BUS 85 [S.ROQUE     30.000] CKT 2
SINGLE 32   : OPEN LINE FROM BUS 44 [SEMF        30.000] TO BUS 86 [COVOADA     30.000] CKT 1
SINGLE 33   : OPEN LINE FROM BUS 44 [SEMF        30.000] TO BUS 86 [COVOADA     30.000] CKT 2
SINGLE 34   : OPEN LINE FROM BUS 45 [SECL        30.000] TO BUS 93 [LIVRAMENTO  30.000] CKT 1
SINGLE 35   : OPEN LINE FROM BUS 45 [SECL        30.000] TO BUS 93 [LIVRAMENTO  30.000] CKT 2
SINGLE 36   : OPEN LINE FROM BUS 45 [SECL        30.000] TO BUS 94 [RIBEIRA SECA30.000] CKT 1
SINGLE 37   : OPEN LINE FROM BUS 45 [SECL        30.000] TO BUS 94 [RIBEIRA SECA30.000] CKT 2
```

Figure E-1: *Contingency analysis outcomes for the 30 kV lines, Scenario 1.*

Appendix F: Scenario 2-Contingency Results (Low Demand)

For Scenario 2, tripping each one of the lines of 60 kV, are observed the branches with over loadings and buses with violations in voltage rates. In this Scenario case, there were not monitored voltage violations, whereas violations on line thermal constraints were observed for each one single contingency and with the highest rating occurred with disconnecting the line among 2 CGRG and 4 SEFO buses. Results are provided in Figure F-1.

Moreover, tripping the lines of 30 kV, is monitored once again the transmission branch of 3 CGPV-GPP and 30 SEFO rated at this voltage value being overloaded for each one contingency case. In more details, the contingency with the worst consequences on the system is to consider the outage of the subterranean circuit line from bus 3 CGPV-GPP to bus 30 SEFO and brings about an overloading rated at 171.2% on the overhead circuit. Figure F-2 illustrates the respective results.

Concluding, there are no any voltage breakings against the initial values. In both Scenarios 1&2, voltage sags do not occur in low load demand profiles while in high demand schemes do. Transmission line between CGRG-GPP and SEFO is rather affected, as the geothermal generator is connected to the one end of the branch and in case of disconnecting the line, the supplied power has to follow a longer path inducing greater total losses.

```
<---------------- MULTI-SECTION LINE ----------------> <----------------- MONITORED BRANCH -----------------> CONTINGENCY
   RATING      FLOW       %
                                                        3 CGPV-GPP    30.000     30*SEFO        30.000 2  BASE CASE
     14.8      19.1     134.3                          3 CGPV-GPP    30.000     30*SEFO        30.000 2  SINGLE 1
     14.8      19.0     133.6                          3 CGPV-GPP    30.000     30*SEFO        30.000 2  SINGLE 2
     14.8      19.1     134.4                          3 CGPV-GPP    30.000     30*SEFO        30.000 2  SINGLE 3
     14.8      19.1     134.4                          3 CGPV-GPP    30.000     30*SEFO        30.000 2  SINGLE 4
     14.8      19.1     134.3                          3 CGPV-GPP    30.000     30*SEFO        30.000 2  SINGLE 5
     14.8      19.1     134.3                          3 CGPV-GPP    30.000     30*SEFO        30.000 2  SINGLE 6
     14.8      19.1     134.3                          3 CGPV-GPP    30.000     30*SEFO        30.000 2  SINGLE 7
     14.8      19.4     136.4                          3 CGPV-GPP    30.000     30*SEFO        30.000 2  SINGLE 8
     14.8      19.0     133.1                          3 CGPV-GPP    30.000     30*SEFO        30.000 2  SINGLE 9
     14.8      19.1     134.3                          3 CGPV-GPP    30.000     30*SEFO        30.000 2  SINGLE 10
     14.8      19.1     134.3                          3 CGPV-GPP    30.000     30*SEFO        30.000 2  SINGLE 11
     14.8      19.1     134.3

MONITORED VOLTAGE REPORT:
SYSTEM                          CONTINGENCY  <-------- B U S --------->   V-CONT   V-INIT   V-MAX    V-MIN

CONTINGENCY LEGEND:
LABEL         EVENTS
SINGLE 1    : OPEN LINE FROM BUS 1 [CTCL-FPP    60.000] TO BUS 4 [SEFO        60.000] CKT 1
SINGLE 2    : OPEN LINE FROM BUS 1 [CTCL-FPP    60.000] TO BUS 11 [SELG        60.000] CKT 1
SINGLE 3    : OPEN LINE FROM BUS 1 [CTCL-FPP    60.000] TO BUS 11 [SELG        60.000] CKT 2
SINGLE 4    : OPEN LINE FROM BUS 1 [CTCL-FPP    60.000] TO BUS 27 [SEMF        60.000] CKT 1
SINGLE 5    : OPEN LINE FROM BUS 1 [CTCL-FPP    60.000] TO BUS 37 [SEAR        60.000] CKT 1
SINGLE 6    : OPEN LINE FROM BUS 1 [CTCL-FPP    60.000] TO BUS 39 [SESR        60.000] CKT 1
SINGLE 7    : OPEN LINE FROM BUS 2 [CGRG-GPP    60.000] TO BUS 4 [SEFO        60.000] CKT 1
SINGLE 8    : OPEN LINE FROM BUS 4 [SEFO        60.000] TO BUS 11 [SELG        60.000] CKT 1
SINGLE 9    : OPEN LINE FROM BUS 27 [SEMF        60.000] TO BUS 35 [SEPD1       60.000] CKT 1
SINGLE 10   : OPEN LINE FROM BUS 27 [SEMF        60.000] TO BUS 36 [SEPD2       60.000] CKT 1
SINGLE 11   : OPEN LINE FROM BUS 27 [SEMF        60.000] TO BUS 39 [SESR        60.000] CKT 1
```

Figure F-1: *Contingency analysis outcomes for the 60 kV lines, Scenario 2.*

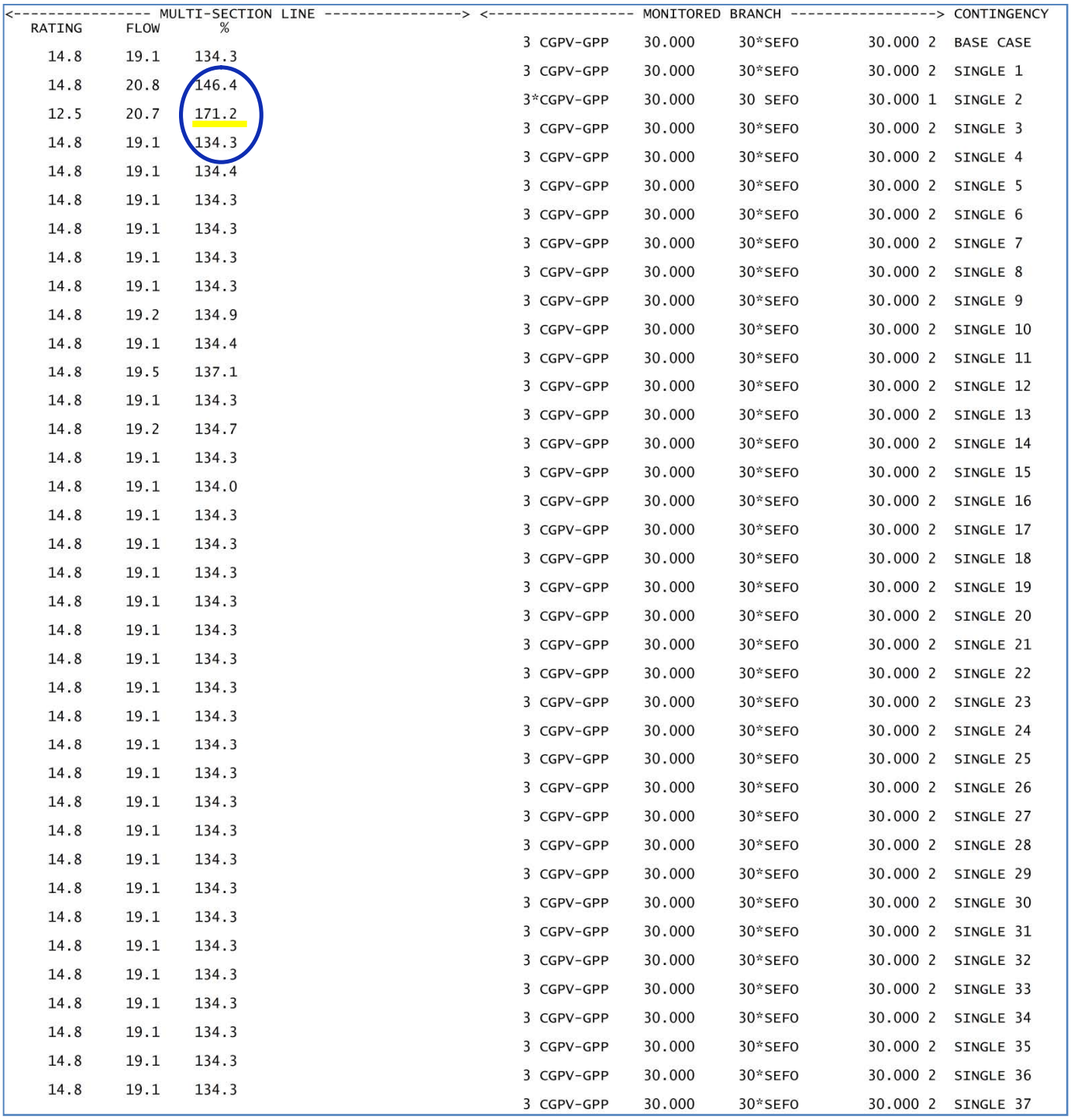

<---------- MULTI-SECTION LINE ----------> RATING	FLOW	%	<---------- MONITORED BRANCH ---------->				CONTINGENCY
14.8	19.1	134.3	3 CGPV-GPP	30.000	30*SEFO	30.000 2	BASE CASE
14.8	20.8	146.4	3 CGPV-GPP	30.000	30*SEFO	30.000 2	SINGLE 1
12.5	20.7	171.2	3*CGPV-GPP	30.000	30 SEFO	30.000 1	SINGLE 2
14.8	19.1	134.3	3 CGPV-GPP	30.000	30*SEFO	30.000 2	SINGLE 3
14.8	19.1	134.4	3 CGPV-GPP	30.000	30*SEFO	30.000 2	SINGLE 4
14.8	19.1	134.3	3 CGPV-GPP	30.000	30*SEFO	30.000 2	SINGLE 5
14.8	19.1	134.3	3 CGPV-GPP	30.000	30*SEFO	30.000 2	SINGLE 6
14.8	19.1	134.3	3 CGPV-GPP	30.000	30*SEFO	30.000 2	SINGLE 7
14.8	19.1	134.3	3 CGPV-GPP	30.000	30*SEFO	30.000 2	SINGLE 8
14.8	19.2	134.9	3 CGPV-GPP	30.000	30*SEFO	30.000 2	SINGLE 9
14.8	19.1	134.4	3 CGPV-GPP	30.000	30*SEFO	30.000 2	SINGLE 10
14.8	19.5	137.1	3 CGPV-GPP	30.000	30*SEFO	30.000 2	SINGLE 11
14.8	19.1	134.3	3 CGPV-GPP	30.000	30*SEFO	30.000 2	SINGLE 12
14.8	19.2	134.7	3 CGPV-GPP	30.000	30*SEFO	30.000 2	SINGLE 13
14.8	19.1	134.3	3 CGPV-GPP	30.000	30*SEFO	30.000 2	SINGLE 14
14.8	19.1	134.0	3 CGPV-GPP	30.000	30*SEFO	30.000 2	SINGLE 15
14.8	19.1	134.3	3 CGPV-GPP	30.000	30*SEFO	30.000 2	SINGLE 16
14.8	19.1	134.3	3 CGPV-GPP	30.000	30*SEFO	30.000 2	SINGLE 17
14.8	19.1	134.3	3 CGPV-GPP	30.000	30*SEFO	30.000 2	SINGLE 18
14.8	19.1	134.3	3 CGPV-GPP	30.000	30*SEFO	30.000 2	SINGLE 19
14.8	19.1	134.3	3 CGPV-GPP	30.000	30*SEFO	30.000 2	SINGLE 20
14.8	19.1	134.3	3 CGPV-GPP	30.000	30*SEFO	30.000 2	SINGLE 21
14.8	19.1	134.3	3 CGPV-GPP	30.000	30*SEFO	30.000 2	SINGLE 22
14.8	19.1	134.3	3 CGPV-GPP	30.000	30*SEFO	30.000 2	SINGLE 23
14.8	19.1	134.3	3 CGPV-GPP	30.000	30*SEFO	30.000 2	SINGLE 24
14.8	19.1	134.3	3 CGPV-GPP	30.000	30*SEFO	30.000 2	SINGLE 25
14.8	19.1	134.3	3 CGPV-GPP	30.000	30*SEFO	30.000 2	SINGLE 26
14.8	19.1	134.3	3 CGPV-GPP	30.000	30*SEFO	30.000 2	SINGLE 27
14.8	19.1	134.3	3 CGPV-GPP	30.000	30*SEFO	30.000 2	SINGLE 28
14.8	19.1	134.3	3 CGPV-GPP	30.000	30*SEFO	30.000 2	SINGLE 29
14.8	19.1	134.3	3 CGPV-GPP	30.000	30*SEFO	30.000 2	SINGLE 30
14.8	19.1	134.3	3 CGPV-GPP	30.000	30*SEFO	30.000 2	SINGLE 31
14.8	19.1	134.3	3 CGPV-GPP	30.000	30*SEFO	30.000 2	SINGLE 32
14.8	19.1	134.3	3 CGPV-GPP	30.000	30*SEFO	30.000 2	SINGLE 33
14.8	19.1	134.3	3 CGPV-GPP	30.000	30*SEFO	30.000 2	SINGLE 34
14.8	19.1	134.3	3 CGPV-GPP	30.000	30*SEFO	30.000 2	SINGLE 35
14.8	19.1	134.3	3 CGPV-GPP	30.000	30*SEFO	30.000 2	SINGLE 36
14.8	19.1	134.3	3 CGPV-GPP	30.000	30*SEFO	30.000 2	SINGLE 37

Figure F-2: *Contingency analysis outcomes for the 30 kV lines (branch violations), Scenario 2.*

Appendix G: Short circuit calculations-Scenario 2 (High Demand)

This appendix represents the three-phase fault summary reports of some selective nodes for case Scenario 2, CGPV, CGRG and SEFO. In more details, Tables G-1 & G-2 concentrate the short circuit summary report for the 11/30 kV CGPV substation node. Tables G-3 to G-5 illustrate the three-phase fault current calculations for the 10/60 CGRG substation node and Tables G-6 to G-8 for the 30/60 kV SEFO substation bus.

Such reports list the resistive and reactive parts of the sequence Thevenin impedances that would be measured by observations made at each bus in turn without the influence of the prescribed set of unbalances. The calculation process interconnects the three sequence networks to represent the unbalanced condition and solves for the sequence voltages. Following solution, a summary report is printed for each unbalance applied with various blocks of output included such as: 1) fault type and buses involved, 2) sequence and phase voltages at the bus, 3) series branch currents flowing in each branch (including any generator contributions) connected to the faulted node. Currents may be expressed either in pu or amperes. In our study, short circuit currents are expressed in amperes. Sequence and phase components are illustrated, 4) the algebraic ´´sum of contributions´´ of all elements are tabulated.

UNBALANCES APPLIED:						
LINE TO GROUND FAULT AT BUS 96 [CGPV-GPP 11.000] PHASE 1						
L-G Z = 0.000 0.000						
LINE TO LINE TO GROUND FAULT AT BUS 96 [CGPV-GPP 11.000] EXCLUDED PHASE 1						
L-L Z = 0.000 0.000 L-G Z = 0.000 0.000						
SEQUENCE THEVENIN IMPEDANCES AT FAULTED BUSES						
BUS# X-- NAME --X BASKV ZERO POSITIVE NEGATIVE						
96 CGPV-GPP 11.000 0.03083 0.30769 0.04828 0.36672 0.08236 0.52878						
THREE PHASE FAULT AT BUS 96 [CGPV-GPP 11.000]:						
SEQUENCE /V0/ AN(V0) /V+/ AN(V+) /V-/ AN(V-) /3V0/ AN(3V0)						
PHASE /VA/ AN(VA) /VB/ AN(VB) /VC/ AN(VC)						
96 (KV L-G) 0.000 0.00 0.000 0.00 0.000 0.00 0.000 0.00						
CGPV-GPP 11.000 0.000 0.00 0.000 0.00 0.000 0.00						
SEQUENCE /I0/ AN(I0) /I+/ AN(I+) /I-/ AN(I-) /3I0/ AN(3I0)						
PHASE /IA/ AN(IA) /IB/ AN(IB) /IC/ AN(IC)						
MACHINE 1 0.0 0.00 4795.7 -81.78 0.0 0.00 0.0 0.00						
4795.7 -81.78 4795.7 158.22 4795.7 38.22						
MACHINE 2 0.0 0.00 4795.7 -81.78 0.0 0.00 0.0 0.00						
4795.7 -81.78 4795.7 158.22 4795.7 38.22						
FROM 3 CKT 1 0.0 0.00 2301.8 -85.04 0.0 0.00 0.0 0.00						
CGPV-GPP 30.000 2301.8 -85.04 2301.8 154.96 2301.8 34.96						
FROM 3 CKT 2 0.0 0.00 2301.8 -85.04 0.0 0.00 0.0 0.00						
CGPV-GPP 30.000 2301.8 -85.04 2301.8 154.96 2301.8 34.96						
SUM OF CONTRIBUTIONS INTO BUS 96 [CGPV-GPP 11.000]:						
96 0.0 0.00 14189.9 -82.83 0.0 0.00 0.0 0.00						
CGPV-GP 11.000 14189.9 -82.83 14189.9 157.17 14189.9 37.17						
FAULT CURRENT AT BUS 96 [CGPV-GPP 11.000]:						
96 0.0 0.00 14189.9 -82.83 0.0 0.00 0.0 0.00						
CGPV-GPP 11.000 14189.9 -82.83 14189.9 157.17 14189.9 37.17						

Phase A Phase B Phase C

ATable G-1: Fault currents (A) at CGP 11 kV node.

UNBALANCES APPLIED:						
LINE TO GROUND FAULT AT BUS 3 [CGPV-GPP 30.000] PHASE 1						
L-G Z = 0.000 0.000						
LINE TO LINE TO GROUND FAULT AT BUS 3 [CGPV-GPP 30.000] EXCLUDED PHASE 1						
L-L Z = 0.000 0.000	L-G Z = 0.000 0.000					
SEQUENCE THEVENIN IMPEDANCES AT FAULTED BUSES						
BUS# X-- NAME --X BASKV	**ZERO**		**POSITIVE**		**NEGATIVE**	
3 CGPV-GPP 30.000	0.00000	0.07618	0.39064	0.10725	0.48663	
THREE PHASE FAULT AT BUS 3 [CGPV-GPP 30.000]:						
SEQUENCE /V0/ AN(V0)	/V+/ AN(V+)		/V-/ AN(V-)		/3V0/ AN(3V0)	
PHASE /VA/ AN(VA)	/VB/ AN(VB)		/VC/ AN(VC)			
3 (KV L-G) 0.000 0.00	0.000 0.00		0.000 0.00		0.000 0.00	
CGPV-GPP 30.000 0.000 0.00	0.000 0.00		0.000 0.00			
SEQUENCE /I0/ AN(I0)	**/I+/ AN(I+)**		**/I-/ AN(I-)**		**/3I0/ AN(3I0)**	
PHASE /IA/ AN(IA)	**/IB/ AN(IB)**		**/IC/ AN(IC)**			
FROM 30 CKT 1 0.0 0.00	181.4 -104.11		0.0 0.00		0.0 0.00	
SEFO 30.000 181.4 -104.11	**181.4 135.89**		**181.4 15.89**			
FROM 30 CKT 2 0.0 0.00	2011.5 -80.11		0.0 0.00		0.0 0.0	
SEFO 30.000 2011.5 -80.11	**2011.5 159.89**		**2011.5 39.89**			
FROM 96 CKT 1 0.0 0.00	1266.3 -81.23		0.0 0.00		0.0 0.00	
CGPV-GPP 11.000 1266.3 -81.23	**1266.3 158.77**		**1266.3 38.77**			
FROM 96 CKT 2 0.0 0.00	1266.3 -81.23		0.0 0.00		0.0 0.00	
CGPV-GPP 11.000 1266.3 -81.23	**1266.3 158.77**		**1266.3 38.77**			
SUM OF CONTRIBUTIONS INTO BUS 3 [CGPV-GPP 30.000]:						
3 0.0 0.00	4710.9 -81.61		0.0 0.00		0.0 0.00	
CGPV-GPP 30.000 4710.9 -81.61	**4710.9 158.39**		**4710.9 38.39**			
FAULT CURRENT AT BUS 3 [CGPV-GPP 30.000]:						
3 0.0 0.00	4710.9 -81.61		0.0 0.00		0.0 0.00	
CGPV-GPP 30.000 4710.9 -81.61	**4710.9 158.39**		**4710.9 38.39**			
Phase A	Phase B		Phase C			

ATable G-2: Fault currents (A) at CGP 30 kV node.

UNBALANCES APPLIED:						
LINE TO GROUND FAULT AT BUS 2 [CGRG-GPP 60.000] PHASE 1						
L-G Z = 0.000 0.000						
LINE TO LINE TO GROUND FAULT AT BUS 2 [CGRG-GPP 60.000] EXCLUDED PHASE 1						
L-L Z = 0.000 0.000	L-G Z = 0.000 0.000					
SEQUENCE THEVENIN IMPEDANCES AT FAULTED BUSES						
BUS# X-- NAME --X BASKV	ZERO		POSITIVE		NEGATIVE	
2 CGRG-GPP 60.000	0.00000	0.05489	0.20998	0.05874	0.22016	
THREE PHASE FAULT AT BUS 2 [CGRG-GPP 60.000]:						
SEQUENCE /V0/ AN(V0)	/V+/ AN(V+)		/V-/ AN(V-)		/3V0/ AN(3V0)	
PHASE /VA/ AN(VA)	/VB/ AN(VB)		/VC/ AN(VC)			
2 (KV L-G) 0.000 0.00	0.000 0.00	0.000 0.00	0.000 0.00	0.000 0.00		
CGRG-GPP 60.000 0.000	0.00	0.000 0.00	0.000 0.00	0.000 0.00		
SEQUENCE /I0/ AN(I0)	**/I+/ AN(I+)**		**/I-/ AN(I-)**		**/3I0/ AN(3I0)**	
PHASE /IA/ AN(IA)	**/IB/ AN(IB)**		**/IC/ AN(IC)**			
FROM 4 CKT 1 0.0 0.00	3304.3 -76.39		0.0 0.00		0.0 0.00	
SEFO 60.000 **3304.3 -76.39**	**3304.3 163.61**		**3304.3 43.61**			
FROM 95 CKT 1 0.0 0.00	285.9 -67.28		0.0 0.00		0.0 0.00	
CGRG-GPP 10.000 **285.9 -67.28**	**285.9 172.72**		**285.9 52.72**			
FROM 95 CKT 2 0.0 0.00	287.3 -67.25		0.0 0.00		0.0 0.00	
CGRG-GPP 10.000 **287.3 -67.25**	**287.3 172.75**		**287.3 52.75**			
FROM 95 CKT 3 0.0 0.00	285.9 -67.28		0.0 0.00		0.0 0.00	
CGRG-GPP 10.000 **285.9 -67.28**	**285.9 172.72**		**285.9 52.72**			
FROM 95 CKT 4 0.0 0.00	287.3 -67.25		0.0 0.00		0.0 0.00	
CGRG-GPP 10.000 **287.3 -67.25**	**287.3 172.75**		**287.3 52.75**			
SUM OF CONTRIBUTIONS INTO BUS 2 [CGRG-GPP 60.000]:						
2 0.0 0.00	4440.0 -74.05		0.0 0.00		0.0 0.00	
CGRG-GPP 60.000 **4440.0 -74.05**	**4440.0 165.95**		**4440.0 45.95**			
FAULT CURRENT AT BUS 2 [CGRG-GPP 60.000]:						
2 0.0 0.00	4440.0 -74.05		0.0 0.00		0.0 0.00	
CGRG-GPP 60.000 **4440.0 -74.05**	**4440.0 165.95**		**4440.0 45.95**			
Phase A	Phase B		Phase C			

ATable G-3: Fault currents (A) at CGRG 60 kV node.

UNBALANCES APPLIED:						
LINE TO GROUND FAULT AT BUS 95 [CGRG-GPP 10.000] PHASE 1						
L-G Z = 0.000 0.000						
LINE TO LINE TO GROUND FAULT AT BUS 95 [CGRG-GPP 10.000] EXCLUDED PHASE 1						
L-L Z = 0.000 0.000	L-G Z = 0.000 0.000					
SEQUENCE THEVENIN IMPEDANCES AT FAULTED BUSES						
BUS# X-- NAME --X BASKV	ZERO		POSITIVE		NEGATIVE	
95 CGRG-GPP 10.000	0.12489 0.11542		0.05198 0.28132		0.05348 0.28836	
THREE PHASE FAULT AT BUS 95 [CGRG-GPP 10.000]:						
SEQUENCE /V0/ AN(V0)	/V+/ AN(V+)		/V-/ AN(V-)		/3V0/ AN(3V0)	
PHASE /VA/ AN(VA)	/VB/ AN(VB)		/VC/ AN(VC)			
95 (KV L-G) 0.000 0.00	0.000 0.00		0.000 0.00		0.000 0.00	
CGRG-GPP 10.000 0.000 0.00	0.000 0.00		0.000 0.00			
SEQUENCE /I0/ AN(I0)	**/I+/ AN(I+)**		**/I-/ AN(I-)**		**/3I0/ AN(3I0)**	
PHASE /IA/ AN(IA)	**/IB/ AN(IB)**		**/IC/ AN(IC)**			
MACHINE 1 0.0 0.00	1482.2 -63.97		0.0 0.00		0.0 0.00	
1482.2 -63.97	**1482.2 176.03**		**1482.2 56.03**			
MACHINE 2 0.0 0.00	1482.2 -63.97		0.0 0.00		0.0 0.00	
1482.2 -63.97	**1482.2 176.03**		**1482.2 56.03**			
MACHINE 3 0.0 0.00	1482.2 -63.97		0.0 0.00		0.0 0.00	
1482.2 -63.97	**1482.2 176.03**		**1482.2 56.03**			
MACHINE 4 0.0 0.00	1482.2 -63.97		0.0 0.00		0.0 0.00	
1482.2 -63.97	**1482.2 176.03**		**1482.2 56.03**			
MACHINE 5 0.0 0.00	623.8 -69.47		0.0 0.00		0.0 0.00	
623.8 -69.47	**623.8 170.53**		**623.8 50.53**			
MACHINE 6 0.0 0.00	623.8 -69.47		0.0 0.00		0.0 0.00	
623.8 -69.47	**623.8 170.53**		**623.8 50.53**			
MACHINE 7 0.0 0.00	623.8 -69.47		0.0 0.00		0.0 0.00	
623.8 -69.47	**623.8 170.53**		**623.8 50.53**			
MACHINE 8 0.0 0.00	623.8 -69.47		0.0 0.00		0.0 0.00	
623.8 -69.47	**623.8 170.53**		**623.8 50.53**			
MACHINE 9 0.0 0.00	623.8 -69.47		0.0 0.00		0.0 0.00	
623.8 -69.47	**623.8 170.53**		**623.8 50.53**			
MACHINE : 0.0 0.00	623.8 -69.47		0.0 0.00		0.0 0.00	
623.8 -69.47	**623.8 170.53**		**623.8 50.53**			

ATable G-4: Fault currents (A) at CGRG 10 kV node (1).

FROM 2 CKT 1	0.0	0.00	2670.8	-81.76	0.0	0.00	0.0	0.00		
CGRG-GPP 60.000	**2670.8**	**-81.76**	**2670.8**	**158.24**	**2670.8**	**38.24**				
FROM 2 CKT 2	0.0	0.00	2684.2	-81.73	0.0	0.00	0.0	0.00		
CGRG-GPP 60.000	**2684.2**	**-81.73**	**2684.2**	**158.27**	**2684.2**	**38.27**				
FROM 2 CKT 3	0.0	0.00	2670.8	-81.76	0.0	0.00	0.0	0.00		
CGRG-GPP 60.000	**2670.8**	**-81.76**	**2670.8**	**158.24**	**2670.8**	**38.24**				
FROM 2 CKT 4	0.0	0.00	2684.2	-81.73	0.0	0.00	0.0	0.00		
CGRG-GPP 60.000	**2684.2**	**-81.73**	**2684.2**	**158.27**	**2684.2**	**38.27**				
SUM OF CONTRIBUTIONS INTO BUS 95 [CGRG-GPP 10.000]:										
95	0.0	0.00	20181.7	-74.33	0.0	0.00	0.0	0.00		
CGRG-GPP 10.000	**20181.7**	**-74.33**	**20181.7**	**165.67**	**20181.7**	**45.67**				
FAULT CURRENT AT BUS 95 [CGRG-GPP 10.000]:										
95	0.0	0.00	20181.7	-74.33	0.0	0.00	0.0	0.00		
CGRG-GPP 10.000	**20181.7**	**-74.33**	**20181.7**	**165.67**	**20181.7**	**45.67**				
	Phase A		Phase B		Phase C					

ATable G-5: Fault currents (A) at CGRG 10 kV node (2).

UNBALANCES APPLIED:						
LINE TO GROUND FAULT AT BUS 4 [SEFO 60.000] PHASE 1						
L-G Z = 0.000 0.000						
LINE TO LINE TO GROUND FAULT AT BUS 4 [SEFO 60.000] EXCLUDED PHASE 1						
L-L Z = 0.000 0.000	L-G Z = 0.000 0.000					
SEQUENCE THEVENIN IMPEDANCES AT FAULTED BUSES						
BUS# X-- NAME --X BASKV ZERO POSITIVE NEGATIVE						
4 SEFO 60.000 0.00000 0.04340 0.18110 0.04819 0.19210						
THREE PHASE FAULT AT BUS 4 [SEFO 60.000]:						
SEQUENCE /V0/ AN(V0) /V+/ AN(V+) /V-/ AN(V-) /3V0/ AN(3V0)						
PHASE /VA/ AN(VA) /VB/ AN(VB) /VC/ AN(VC)						
4 (KV L-G) 0.000 0.00 0.000 0.00 0.000 0.00 0.000 0.00						
SEFO 60.000 0.000 0.00 0.000 0.00 0.000 0.00						
SEQUENCE /I0/ AN(I0) /I+/ AN(I+) /I-/ AN(I-) /3I0/ AN(3I0)						
PHASE /IA/ AN(IA) /IB/ AN(IB) /IC/ AN(IC)						
FROM 1 CKT 1 0.0 0.00	1843.2 -77.19	0.0 0.00	0.0 0.00			
CTCL-FPP 60.000 1843.2 -77.19	1843.2 162.81	1843.2 42.81				
FROM 2 CKT 1 0.0 0.00	1076.7 -66.12	0.0 0.00	0.0 0.00			
CGRG-GPP 60.000 1076.7 -66.12	1076.7 173.88	1076.7 53.88				
FROM 11 CKT 1 0.0 0.00	1611.2 -77.43	0.0 0.00	0.0 0.00			
SELG 60.000 1611.2 -77.43	1611.2 162.57	1611.2 42.57				
FROM 29 CKT 1 0.0 0.00	0.0 0.00	0.0 0.00	0.0 0.00			
SEFO 10.000 0.0 0.00	0.0 0.00	0.0 0.00				
FROM 29 CKT 2 0.0 0.00	0.0 0.00	0.0 0.00	0.0 0.00			
SEFO 10.000 0.0 0.00	0.0 0.00	0.0 0.00				
FROM 29 CKT 3 0.0 0.00	0.0 0.00	0.0 0.00	0.0 0.00			
SEFO 10.000 0.0 0.00	0.0 0.00	0.0 0.00				
FROM 30 CKT 1 0.0 0.00	652.8 -86.19	0.0 0.00	0.0 0.00			
SEFO 30.000 652.8 -86.19	652.8 153.81	652.8 33.81				
SUM OF CONTRIBUTIONS INTO BUS 4 [SEFO 60.000]:						
4 0.0 0.00	5156.7 -76.10	0.0 0.00	0.0 0.00			
SEFO 60.000 5156.7 -76.10	**5156.7 163.90**	**5156.7 43.90**				
FAULT CURRENT AT BUS 4 [SEFO 60.000]:						
4 0.0 0.00	5156.7 -76.10	0.0 0.00	0.0 0.00			
SEFO 60.000	**5156.7 -76.10**	**5156.7 163.90**	**5156.7 43.90**			

Phase A Phase B Phase C

ATable G-6: Fault currents (A) at SEFO 60 kV node.

UNBALANCES APPLIED:
LINE TO GROUND FAULT AT BUS 30 [SEFO 30.000] PHASE 1
L-G Z = 0.000 0.000
LINE TO LINE TO GROUND FAULT AT BUS 30 [SEFO 30.000] EXCLUDED PHASE 1
L-L Z = 0.000 0.000 L-G Z = 0.000 0.000
SEQUENCE THEVENIN IMPEDANCES AT FAULTED BUSES
BUS# X-- NAME --X BASKV ZERO POSITIVE NEGATIVE
30 SEFO 30.000 0.00001 -0.00142 0.07633 0.38963 0.10552 0.48483
PTI INTERACTIVE POWER SYSTEM SIMULATOR--PSS(R)E WED, MAY 09 2012 16:59
THREE PHASE FAULT AT BUS 30 [SEFO 30.000]:
SEQUENCE /V0/ AN(V0) /V+/ AN(V+) /V-/ AN(V-) /3V0/ AN(3V0)
PHASE /VA/ AN(VA) /VB/ AN(VB) /VC/ AN(VC)
30 (KV L-G) 0.000 0.00 0.000 0.00 0.000 0.00 0.000 0.00
SEFO 30.000 0.000 0.00 0.000 0.00 0.000 0.00
SEQUENCE /I0/ AN(I0) /I+/ AN(I+) /I-/ AN(I-) /3I0/ AN(3I0)
PHASE /IA/ AN(IA) /IB/ AN(IB) /IC/ AN(IC)
FROM 3 CKT 1 0.0 0.00 209.9 -102.78 0.0 0.00 0.0 0.00
CGPV-GPP 30.000 209.9 -102.78 209.9 137.22 209.9 17.22
FROM 3 CKT 2 0.0 0.00 2328.5 -78.77 0.0 0.00 0.0 0.00
CGPV-GPP 30.000 2328.5 -78.77 2328.5 161.23 2328.5 41.23
FROM 4 CKT 1 0.0 0.00 2193.1 -82.52 0.0 0.00 0.0 0.00
SEFO 60.000 2193.1 -82.52 2193.1 157.48 2193.1 37.48

ATable G-7: Fault currents (A) at SEFO 30 kV node (1).

FROM 75 CKT 1	0.0	0.00	0.0	0.00	0.0	0.00	0.0	0.00		
CALHETAS 30.000	0.0	0.00	0.0	0.00	0.0	0.00				
FROM 75 CKT 2	0.0	0.00	0.0	0.00	0.0	0.00	0.0	0.00		
CALHETAS 30.000	0.0	0.00	0.0	0.00	0.0	0.00				
FROM 76 CKT 1	0.0	0.00	0.0	0.00	0.0	0.00	0.0	0.00		
NORDESTE 30.000	0.0	0.00	0.0	0.00	0.0	0.00				
FROM 76 CKT 2	0.0	0.00	0.0	0.00	0.0	0.00	0.0	0.00		
NORDESTE 30.000	0.0	0.00	0.0	0.00	0.0	0.00				
FROM 77 CKT 1	0.0	0.00	0.0	0.00	0.0	0.00	0.0	0.00		
RIBEIRINHA 30.000	0.0	0.00	0.0	0.00	0.0	0.00				
FROM 77 CKT 2	0.0	0.00	0.0	0.00	0.0	0.00	0.0	0.00		
RIBEIRINHA 30.000	0.0	0.00	0.0	0.00	0.0	0.00				
SUM OF CONTRIBUTIONS INTO BUS 30 [SEFO 30.000]:										
30	0.0	0.00	4714.3	-81.55	0.0	0.00	0.0	0.00		
SEFO 30.000	**4714.3**	**-81.55**	**4714.3**	**158.45**	**4714.3**	**38.45**				
SHUNT + LOAD CURRENT AT BUS 30 [SEFO 30.000]:										
30	0.0	0.00	0.0	0.00	0.0	0.00	0.0	0.00		
SEFO 30.000	**0.0**	**0.00**	**0.0**	**0.00**	**0.0**	**0.00**				
FAULT CURRENT AT BUS 30 [SEFO 30.000]:										
30	0.0	0.00	4714.3	-81.55	0.0	0.00	0.0	0.00		
SEFO 30.000	**4714.3**	**-81.55**	**4714.3**	**158.45**	**4714.3**	**38.45**				
	Phase A		Phase B		Phase C					

ATable G-8: Fault currents (A) at SEFO 30 kV node (2).

Appendix H: Connection of wind farm at bus SEFO rated at 30 kV

Concentrating the power flow results, there are voltage violations indicated as buses with voltage levels less than 0.95 pu (Fig. H-1). Moreover, the branch between CGPV and SEFO rated at 30 kV is overloaded at the rate of 126.0% (Fig. H-2). Voltage profile -at all nodes- has not improved substantially and the system losses amount for 1.5 MW+9.3 MVAr, higher than in Scenario 2, year 2015. Generally, a few differences/changes in voltages by 5.5% are noted with the wind energy contribution. The worst voltage level appears to have bus PSFU at 0.945 pu (Fig. H-1). Table H-1 concentrates the case summary results.

```
BUSES WITH VOLTAGE GREATER THAN 1.0500:

   BUS# X-- NAME --X BASKV AREA   V(PU)   V(KV)

                  * NONE *


BUSES WITH VOLTAGE LESS THAN 0.9500:

   BUS# X-- NAME --X BASKV AREA   V(PU)   V(KV)
     32 SEVF         10.000    1 0.9475   9.475
     79 POVOAÇÃO     30.000    1 0.9446  28.337
     81 FURNAS 2     30.000    1 0.9446  28.337
     92 VF I         10.000    1 0.9475   9.475

BUS# X-- NAME --X BASKV    AREA    V(PU)     V(KV)
 33      PSFU      30.000     1    0.9446    28.337
 80    FURNAS 1    30.000     1    0.9446    28.337
 88     VF II      10.000     1    0.9475     9.475
```

Figure H-1: *Voltage violations, addition node SEFO 30 kV.*

```
                              branch limits
BRANCH LOADINGS ABOVE  80.0 % OF RATING SET A (MVA FOR TRANSFORMERS,
CURRENT FOR NON-TRANSFORMER BRANCHES):

X---------- FROM BUS ----------X X---------- TO BUS ----------X
  BUS# X-- NAME --X BASKV  AREA   BUS# X-- NAME --X BASKV  AREA CKT
LOADING  RATING PERCENT
     3 CGPV-GPP    30.000     1     30 SEFO        30.000*    1  2
18.7    14.8   126.0
```

Figure H-2: *Branch-Check limits, addition node SEFO 30 kV.*

ATable H-1: Case summary power flow outcomes

Total	Generation	PQLoad	Shunts	Charging	Losses	Swing
MW	105.1	102.9	0.7	0	1.5	48.4
MVAr	37.6	35.7	-1.9	5.6	9.3	30.8

Appendix I: Connection of wind farm at bus SEFO rated at 60 kV

According to power flow results, there are voltage violations whereas the branch between CGPV and SEFO rated at 30 kV is overloaded at the rate of 127.8%. Voltage profile- at all nodes- has not improved significantly and the system losses amount for 1.3 MW+9.5 MVAr, higher than in Scenario 2, year 2015. In overall, there are noted decreases in voltages by 5.5% with the wind energy contribution like previously. The lowest voltage is dictated again at bus 33 of PSFU, which value is even smaller than in the case study before. Figures I-1 & I-2 depict the voltage and branch limits checkout reports in PSS/E, whereas Table H-1 concentrates the case summary results.

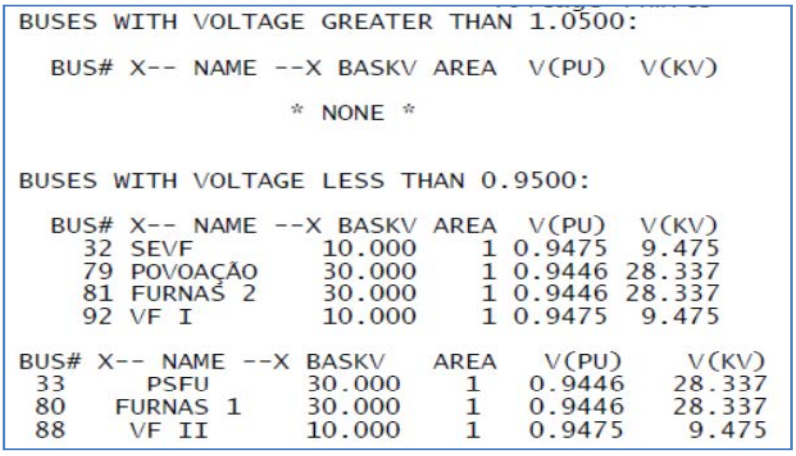

```
BUSES WITH VOLTAGE GREATER THAN 1.0500:

   BUS# X-- NAME --X BASKV AREA   V(PU)   V(KV)

                  * NONE *


BUSES WITH VOLTAGE LESS THAN 0.9500:

   BUS# X-- NAME --X BASKV AREA   V(PU)   V(KV)
     32 SEVF         10.000    1 0.9475   9.475
     79 POVOAÇÃO     30.000    1 0.9446  28.337
     81 FURNAS 2     30.000    1 0.9446  28.337
     92 VF I         10.000    1 0.9475   9.475

BUS# X-- NAME --X BASKV    AREA    V(PU)     V(KV)
 33      PSFU      30.000     1    0.9446    28.337
 80    FURNAS 1    30.000     1    0.9446    28.337
 88     VF II      10.000     1    0.9475     9.475
```

Figure I-1: *Voltage violations, addition node SEFO 60 kV.*

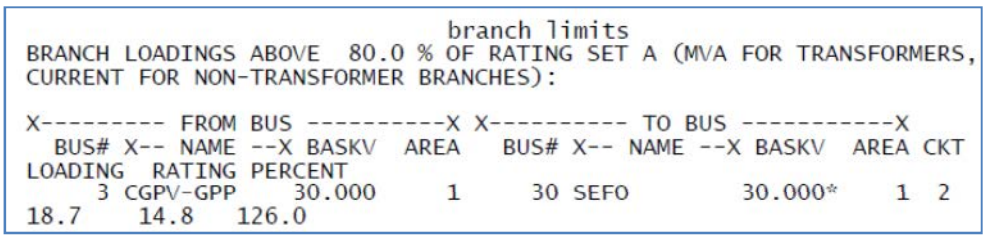

```
                                branch limits
BRANCH LOADINGS ABOVE  80.0 % OF RATING SET A (MVA FOR TRANSFORMERS,
CURRENT FOR NON-TRANSFORMER BRANCHES):

X--------- FROM BUS ----------X X---------- TO BUS ----------X
  BUS# X-- NAME --X BASKV  AREA   BUS# X-- NAME --X BASKV  AREA CKT
LOADING  RATING PERCENT
     3 CGPV-GPP    30.000     1     30 SEFO        30.000*    1  2
18.7    14.8   126.0
```

Figure I-2: *Branch limits checking, addition node SEFO 60 kV.*

ATable I-1: Case summary power flow outcomes

Total	Generation	PQLoad	Shunts	Charging	Losses	Swing
MW	105.1	102.9	0.7	0	1.5	48.4
MVAr	37.6	35.7	-1.9	5.6	9.3	30.8

Appendix J: Connection of wind farm at bus PSFU rated at 30 kV

The steady-state results indicate that there are no any voltage violations, whereas the branch between CGPV and SEFO rated at 30 kV is overloaded at the rate of 128.1% as it can be seen in Fig. J-1, similarly to Scenario 2. Voltage profile is improved at all nodes and the reactive system losses are now smaller totalling at 1.5 MW+8.3 MVAr. With the introduction of wind energy in this node, its voltage is improved, in addition to the nearby nodal voltages. In more details, the lowest voltage of 0.954 pu is noticed at the substation bus SEVF rated at 10 kV and the highest of 1.002 pu at the substation of the geothermal plant CGRG rated at 60 kV. Table J-1 concentrates the case summary results.

Furthermore, contingency analysis and three-phase fault current calculation results at this bus are given beneath.

```
BRANCH LOADINGS ABOVE  80.0 % OF RATING SET A (MVA FOR TRANSFORMERS,
CURRENT FOR NON-TRANSFORMER BRANCHES):

X--------- FROM BUS ----------X X---------- TO BUS ----------X
  BUS# X-- NAME --X BASKV  AREA    BUS# X-- NAME --X BASKV  AREA CKT
LOADING  RATING PERCENT
     3 CGPV-GPP    30.000     1     30 SEFO        30.000*    1  2
19.0    14.8   128.1
```

Figure J-1: *Branch-Check limits, addition node PSFU 30 kV.*

ATable J-1: Case summary power flow outcomes

Total	Generation	PQLoad	Shunts	Charging	Losses	Swing
MW	105	102.9	0.7	0	1.5	48.3
MVAr	36.5	35.7	-1.9	5.6	8.3	28.8

A) Contingency Analysis (N-1)

Tripping the lines of 60 kV one by one, are observed the branches with over loadings and buses with violations in voltage rates. In more details, the contingencies with the worst, once again, branch overloading by 131.2 % on the system is to open the line from bus 2 CGRG-GPP to bus 4 SEFO which interconnects the central geothermal plant to this big substation. The worst single contingency is disconnecting the line among bus 1 CTCL-FPP and bus 27 SEMF. This results in voltage drops under the minimum acceptable value of 0.95 pu. The red parallelogram denotes the contingency voltages whereas the blue one the line violations. It is worthy to mention that the bus 27 SEMF rated at 60 kV is connected to the substation of SEPD rated also at 60 kV. Thus, the far nodes connected to the latter mark notable voltage drops as they constitute the very end of the distribution lines. Fig. J-2 represents the relative results.

Tripping the lines of 30 kV one by one, are observed the two transmission branches between 3 CGPV-GPP and 30 SEFO rated at this voltage value being overloaded. In more details, the contingencies with the worst consequences on the system are to open the overhead and subterranean line from bus 3 CGPV-GPP to bus 30 SEFO (single contingencies 1&2). The effects of this tripping are violations on current ratings by 139.7% % and 159.3 % respectively. Voltage drops are not denoted. The blue circle describes line violations. The results are showed beneath in Fig. J-3.

B) Fault Current Calculation

After installing 14 MW of wind energy units that are assumed to operate for the 80% of their installed capacity, namely 11.2 MW, the fault current is expected to rise up. Actually, it is increased by 369 A that is an unacceptably

high value. Moreover, it should be noted that the fault current at the same node for Scenario 1 was at the figure of 1435 A. Table J-2 depicts the three-phase current values at PSFU substation node for Scenarios 2&3 respectively.

ATable J-2: Three-phase fault current at PSFU, Scenarios 2 &3

Scenarios	Voltage level (kV)	I (A)
2	30	1456
3	30	1825

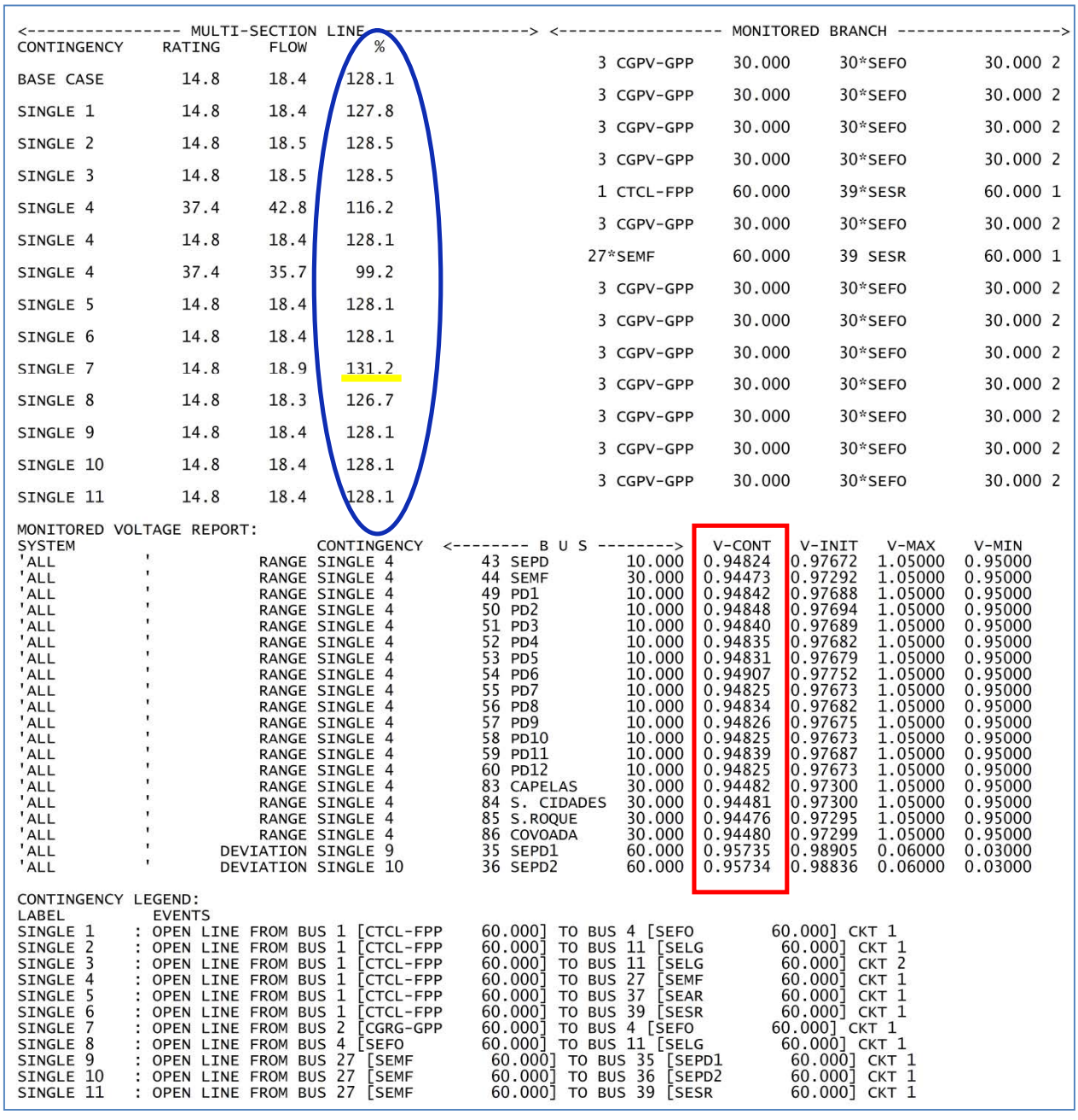

```
<---------------- MULTI-SECTION LINE ----------------> <----------------- MONITORED BRANCH ----------------->
CONTINGENCY    RATING     FLOW      %                                    3 CGPV-GPP    30.000     30*SEFO        30.000 2
BASE CASE        14.8     18.4    128.1                                  3 CGPV-GPP    30.000     30*SEFO        30.000 2
SINGLE 1         14.8     18.4    127.8                                  3 CGPV-GPP    30.000     30*SEFO        30.000 2
SINGLE 2         14.8     18.5    128.5                                  3 CGPV-GPP    30.000     30*SEFO        30.000 2
SINGLE 3         14.8     18.5    128.5                                  1 CTCL-FPP    60.000     39*SESR        60.000 1
SINGLE 4         37.4     42.8    116.2                                  3 CGPV-GPP    30.000     30*SEFO        30.000 2
SINGLE 4         14.8     18.4    128.1                                 27*SEMF        60.000     39 SESR        60.000 1
SINGLE 4         37.4     35.7     99.2                                  3 CGPV-GPP    30.000     30*SEFO        30.000 2
SINGLE 5         14.8     18.4    128.1                                  3 CGPV-GPP    30.000     30*SEFO        30.000 2
SINGLE 6         14.8     18.4    128.1                                  3 CGPV-GPP    30.000     30*SEFO        30.000 2
SINGLE 7         14.8     18.9    131.2                                  3 CGPV-GPP    30.000     30*SEFO        30.000 2
SINGLE 8         14.8     18.3    126.7                                  3 CGPV-GPP    30.000     30*SEFO        30.000 2
SINGLE 9         14.8     18.4    128.1                                  3 CGPV-GPP    30.000     30*SEFO        30.000 2
SINGLE 10        14.8     18.4    128.1                                  3 CGPV-GPP    30.000     30*SEFO        30.000 2
SINGLE 11        14.8     18.4    128.1

MONITORED VOLTAGE REPORT:
SYSTEM                    CONTINGENCY  <-------- B U S --------->  V-CONT   V-INIT   V-MAX    V-MIN
'ALL         '            RANGE SINGLE 4        43 SEPD        10.000  0.94824  0.97672  1.05000  0.95000
'ALL         '            RANGE SINGLE 4        44 SEMF        30.000  0.94473  0.97292  1.05000  0.95000
'ALL         '            RANGE SINGLE 4        49 PD1         10.000  0.94842  0.97688  1.05000  0.95000
'ALL         '            RANGE SINGLE 4        50 PD2         10.000  0.94848  0.97694  1.05000  0.95000
'ALL         '            RANGE SINGLE 4        51 PD3         10.000  0.94840  0.97689  1.05000  0.95000
'ALL         '            RANGE SINGLE 4        52 PD4         10.000  0.94835  0.97682  1.05000  0.95000
'ALL         '            RANGE SINGLE 4        53 PD5         10.000  0.94831  0.97679  1.05000  0.95000
'ALL         '            RANGE SINGLE 4        54 PD6         10.000  0.94907  0.97752  1.05000  0.95000
'ALL         '            RANGE SINGLE 4        55 PD7         10.000  0.94825  0.97673  1.05000  0.95000
'ALL         '            RANGE SINGLE 4        56 PD8         10.000  0.94834  0.97682  1.05000  0.95000
'ALL         '            RANGE SINGLE 4        57 PD9         10.000  0.94826  0.97675  1.05000  0.95000
'ALL         '            RANGE SINGLE 4        58 PD10        10.000  0.94825  0.97673  1.05000  0.95000
'ALL         '            RANGE SINGLE 4        59 PD11        10.000  0.94839  0.97687  1.05000  0.95000
'ALL         '            RANGE SINGLE 4        60 PD12        10.000  0.94825  0.97673  1.05000  0.95000
'ALL         '            RANGE SINGLE 4        83 CAPELAS     30.000  0.94482  0.97300  1.05000  0.95000
'ALL         '            RANGE SINGLE 4        84 S. CIDADES  30.000  0.94481  0.97300  1.05000  0.95000
'ALL         '            RANGE SINGLE 4        85 S.ROQUE     30.000  0.94476  0.97295  1.05000  0.95000
'ALL         '            RANGE SINGLE 4        86 COVOADA     30.000  0.94480  0.97299  1.05000  0.95000
'ALL         '         DEVIATION SINGLE 9        35 SEPD1       60.000  0.95735  0.98905  0.06000  0.03000
'ALL         '         DEVIATION SINGLE 10       36 SEPD2       60.000  0.95734  0.98836  0.06000  0.03000

CONTINGENCY LEGEND:
LABEL          EVENTS
SINGLE 1    : OPEN LINE FROM BUS 1 [CTCL-FPP    60.000] TO BUS 4 [SEFO        60.000] CKT 1
SINGLE 2    : OPEN LINE FROM BUS 1 [CTCL-FPP    60.000] TO BUS 11 [SELG        60.000] CKT 1
SINGLE 3    : OPEN LINE FROM BUS 1 [CTCL-FPP    60.000] TO BUS 11 [SELG        60.000] CKT 2
SINGLE 4    : OPEN LINE FROM BUS 1 [CTCL-FPP    60.000] TO BUS 27 [SEMF        60.000] CKT 1
SINGLE 5    : OPEN LINE FROM BUS 1 [CTCL-FPP    60.000] TO BUS 37 [SEAR        60.000] CKT 1
SINGLE 6    : OPEN LINE FROM BUS 1 [CTCL-FPP    60.000] TO BUS 39 [SESR        60.000] CKT 1
SINGLE 7    : OPEN LINE FROM BUS 2 [CGRG-GPP    60.000] TO BUS 4 [SEFO        60.000] CKT 1
SINGLE 8    : OPEN LINE FROM BUS 4 [SEFO        60.000] TO BUS 11 [SELG        60.000] CKT 1
SINGLE 9    : OPEN LINE FROM BUS 27 [SEMF        60.000] TO BUS 35 [SEPD1       60.000] CKT 1
SINGLE 10   : OPEN LINE FROM BUS 27 [SEMF        60.000] TO BUS 36 [SEPD2       60.000] CKT 1
SINGLE 11   : OPEN LINE FROM BUS 27 [SEMF        60.000] TO BUS 39 [SESR        60.000] CKT 1
```

Figure J-2: Contingency analysis outcomes for the 60 kV lines, Scenario 3.

MONITORED BRANCH				CONTINGENCY	RATING	FLOW	%
3 CGPV-GPP	30.000	30*SEFO	30.000 2	BASE CASE	14.8	18.4	128.1
3 CGPV-GPP	30.000	30*SEFO	30.000 2	SINGLE 1	14.8	20.1	139.7
3 CGPV-GPP	30.000	30*SEFO	30.000 1	SINGLE 2	12.5	19.1	159.3
3 CGPV-GPP	30.000	30*SEFO	30.000 2	SINGLE 3	14.8	18.4	128.1
3 CGPV-GPP	30.000	30*SEFO	30.000 2	SINGLE 4	14.8	18.4	128.1
3 CGPV-GPP	30.000	30*SEFO	30.000 2	SINGLE 5	14.8	18.4	128.1
3 CGPV-GPP	30.000	30*SEFO	30.000 2	SINGLE 6	14.8	18.4	128.1
3 CGPV-GPP	30.000	30*SEFO	30.000 2	SINGLE 7	14.8	18.4	128.1
3 CGPV-GPP	30.000	30*SEFO	30.000 2	SINGLE 8	14.8	18.4	128.1
3 CGPV-GPP	30.000	30*SEFO	30.000 2	SINGLE 9	14.8	18.6	128.9
3 CGPV-GPP	30.000	30*SEFO	30.000 2	SINGLE 10	14.8	18.5	128.2
3 CGPV-GPP	30.000	30*SEFO	30.000 2	SINGLE 11	14.8	18.6	129.1
3 CGPV-GPP	30.000	30*SEFO	30.000 2	SINGLE 12	14.8	18.5	128.2
3 CGPV-GPP	30.000	30*SEFO	30.000 2	SINGLE 13	14.8	18.5	128.7
3 CGPV-GPP	30.000	30*SEFO	30.000 2	SINGLE 14	14.8	18.5	128.2
3 CGPV-GPP	30.000	30*SEFO	30.000 2	SINGLE 15	14.8	18.5	128.4
3 CGPV-GPP	30.000	30*SEFO	30.000 2	SINGLE 16	14.8	18.4	128.1
3 CGPV-GPP	30.000	30*SEFO	30.000 2	SINGLE 17	14.8	18.4	128.1
3 CGPV-GPP	30.000	30*SEFO	30.000 2	SINGLE 18	14.8	18.4	128.1
3 CGPV-GPP	30.000	30*SEFO	30.000 2	SINGLE 19	14.8	18.4	128.1
3 CGPV-GPP	30.000	30*SEFO	30.000 2	SINGLE 20	14.8	18.4	128.1
3 CGPV-GPP	30.000	30*SEFO	30.000 2	SINGLE 21	14.8	18.4	128.1
3 CGPV-GPP	30.000	30*SEFO	30.000 2	SINGLE 22	14.8	18.4	128.1
3 CGPV-GPP	30.000	30*SEFO	30.000 2	SINGLE 23	14.8	18.4	128.1
3 CGPV-GPP	30.000	30*SEFO	30.000 2	SINGLE 24	14.8	18.4	128.1
3 CGPV-GPP	30.000	30*SEFO	30.000 2	SINGLE 25	14.8	18.4	128.1
3 CGPV-GPP	30.000	30*SEFO	30.000 2	SINGLE 26	14.8	18.4	128.1
3 CGPV-GPP	30.000	30*SEFO	30.000 2	SINGLE 27	14.8	18.4	128.1
3 CGPV-GPP	30.000	30*SEFO	30.000 2	SINGLE 28	14.8	18.4	128.1
3 CGPV-GPP	30.000	30*SEFO	30.000 2	SINGLE 29	14.8	18.4	128.1
3 CGPV-GPP	30.000	30*SEFO	30.000 2	SINGLE 30	14.8	18.4	128.1
3 CGPV-GPP	30.000	30*SEFO	30.000 2	SINGLE 31	14.8	18.4	128.1
3 CGPV-GPP	30.000	30*SEFO	30.000 2	SINGLE 32	14.8	18.4	128.1
3 CGPV-GPP	30.000	30*SEFO	30.000 2	SINGLE 33	14.8	18.4	128.1
3 CGPV-GPP	30.000	30*SEFO	30.000 2	SINGLE 34	14.8	18.4	128.1
3 CGPV-GPP	30.000	30*SEFO	30.000 2	SINGLE 35	14.8	18.4	128.1
3 CGPV-GPP	30.000	30*SEFO	30.000 2	SINGLE 36	14.8	18.4	128.1
3 CGPV-GPP	30.000	30*SEFO	30.000 2	SINGLE 37	14.8	18.4	128.1

CONTINGENCY LEGEND:

LABEL	EVENTS
SINGLE 1	: OPEN LINE FROM BUS 3 [CGPV-GPP 30.000] TO BUS 30 [SEFO 30.000] CKT 1
SINGLE 2	: OPEN LINE FROM BUS 3 [CGPV-GPP 30.000] TO BUS 30 [SEFO 30.000] CKT 2
SINGLE 3	: OPEN LINE FROM BUS 13 [SELG 30.000] TO BUS 31 [SEVF 30.000] CKT 1
SINGLE 4	: OPEN LINE FROM BUS 13 [SELG 30.000] TO BUS 31 [SEVF 30.000] CKT 2
SINGLE 5	: OPEN LINE FROM BUS 13 [SELG 30.000] TO BUS 70 [LIVRAMENTO 30.000] CKT 1
SINGLE 6	: OPEN LINE FROM BUS 13 [SELG 30.000] TO BUS 70 [LIVRAMENTO 30.000] CKT 2
SINGLE 7	: OPEN LINE FROM BUS 13 [SELG 30.000] TO BUS 82 [RIBEIRA CHΓ 30.000] CKT 1
SINGLE 8	: OPEN LINE FROM BUS 13 [SELG 30.000] TO BUS 82 [RIBEIRA CHΓ 30.000] CKT 2
SINGLE 9	: OPEN LINE FROM BUS 30 [SEFO 30.000] TO BUS 75 [CALHETAS 30.000] CKT 1
SINGLE 10	: OPEN LINE FROM BUS 30 [SEFO 30.000] TO BUS 75 [CALHETAS 30.000] CKT 2
SINGLE 11	: OPEN LINE FROM BUS 30 [SEFO 30.000] TO BUS 76 [NORDESTE 30.000] CKT 1
SINGLE 12	: OPEN LINE FROM BUS 30 [SEFO 30.000] TO BUS 76 [NORDESTE 30.000] CKT 2
SINGLE 13	: OPEN LINE FROM BUS 30 [SEFO 30.000] TO BUS 77 [RIBEIRINHA 30.000] CKT 1
SINGLE 14	: OPEN LINE FROM BUS 30 [SEFO 30.000] TO BUS 77 [RIBEIRINHA 30.000] CKT 2
SINGLE 15	: OPEN LINE FROM BUS 31 [SEVF 30.000] TO BUS 33 [PSFU 30.000] CKT 1
SINGLE 16	: OPEN LINE FROM BUS 31 [SEVF 30.000] TO BUS 89 [V F III 30.000] CKT 1
SINGLE 17	: OPEN LINE FROM BUS 31 [SEVF 30.000] TO BUS 90 [FURNAS 30.000] CKT 1
SINGLE 18	: OPEN LINE FROM BUS 31 [SEVF 30.000] TO BUS 90 [FURNAS 30.000] CKT 2
SINGLE 19	: OPEN LINE FROM BUS 31 [SEVF 30.000] TO BUS 91 [P. GARHA 30.000] CKT 1
SINGLE 20	: OPEN LINE FROM BUS 31 [SEVF 30.000] TO BUS 91 [P. GARHA 30.000] CKT 2
SINGLE 21	: OPEN LINE FROM BUS 33 [PSFU 30.000] TO BUS 79 [POVOAHΓO 30.000] CKT 1
SINGLE 22	: OPEN LINE FROM BUS 33 [PSFU 30.000] TO BUS 79 [POVOAHΓO 30.000] CKT 2
SINGLE 23	: OPEN LINE FROM BUS 33 [PSFU 30.000] TO BUS 80 [FURNAS 1 30.000] CKT 1
SINGLE 24	: OPEN LINE FROM BUS 33 [PSFU 30.000] TO BUS 80 [FURNAS 1 30.000] CKT 2
SINGLE 25	: OPEN LINE FROM BUS 33 [PSFU 30.000] TO BUS 81 [FURNAS 2 30.000] CKT 1
SINGLE 26	: OPEN LINE FROM BUS 44 [SEMF 30.000] TO BUS 83 [CAPELAS 30.000] CKT 1
SINGLE 27	: OPEN LINE FROM BUS 44 [SEMF 30.000] TO BUS 83 [CAPELAS 30.000] CKT 2
SINGLE 28	: OPEN LINE FROM BUS 44 [SEMF 30.000] TO BUS 84 [S. CIDADES 30.000] CKT 1
SINGLE 29	: OPEN LINE FROM BUS 44 [SEMF 30.000] TO BUS 84 [S. CIDADES 30.000] CKT 2
SINGLE 30	: OPEN LINE FROM BUS 44 [SEMF 30.000] TO BUS 85 [S.ROQUE 30.000] CKT 1
SINGLE 31	: OPEN LINE FROM BUS 44 [SEMF 30.000] TO BUS 85 [S.ROQUE 30.000] CKT 2
SINGLE 32	: OPEN LINE FROM BUS 44 [SEMF 30.000] TO BUS 86 [COVOADA 30.000] CKT 1
SINGLE 33	: OPEN LINE FROM BUS 44 [SEMF 30.000] TO BUS 86 [COVOADA 30.000] CKT 2
SINGLE 34	: OPEN LINE FROM BUS 45 [SECL 30.000] TO BUS 93 [LIVRAMENTO 30.000] CKT 1
SINGLE 35	: OPEN LINE FROM BUS 45 [SECL 30.000] TO BUS 93 [LIVRAMENTO 30.000] CKT 2
SINGLE 36	: OPEN LINE FROM BUS 45 [SECL 30.000] TO BUS 94 [RIBEIRA SECA 30.000] CKT 1
SINGLE 37	: OPEN LINE FROM BUS 45 [SECL 30.000] TO BUS 94 [RIBEIRA SECA 30.000] CKT 2

Figure J-3: Contingency analysis outcomes for the 30 kV lines, Scenario 3.

Appendix K: Connection of wind farm at bus SEMF rated at 30/60 kV

Firstly, the wind turbine generators (WTG) are added to the 30 kV SEMF substation voltage node. Concentrating the power flow results, voltage violations are observed, whereas the branch between CGPV and SEFO rated at 30 kV is overloaded at the rate of 129%. Nodal voltage profile has not improved and the system losses amount for 1.1 MW+8.9 MVAr, equal to Scenario 2, year 2015. Once again are observed decreases in voltage values by 5% with the wind energy contribution. The lowest voltage is dictated again at bus 33 of PSFU holding the figure of 0.944 pu. Tables K-1 & K-2 give the case summary results for this study.

Introducing wind turbine generators either at bus SEMF of 30 kV or at bus of 60 kV the consequences retain the same, except that is observed a slight drop in reactive losses by 0.1 MVAr. Summary results are following:

ATable K-1: Case summary power flow outcomes: Addition node SEMF 30 kV

Total	Generation	PQLoad	Shunts	Charging	Losses	Swing
MW	104.7	102.9	0.7	0	1.1	59.2
MVAr	37.1	35.7	-1.9	5.6	8.9	29.1

ATable K-2: Case summary power flow outcomes: Addition node SEMF 60 kV

Total	Generation	PQLoad	Shunts	Charging	Losses	Swing
MW	104.6	102.9	0.7	0	1.1	59.1
MVAr	37	35.7	-1.9	5.6	8.8	29

Appendix L: Connection of wind farm at bus SEPD rated at 10/60 kV

A similar effect on system voltages has the addition of wind energy at the bus of SEPD rated at 60 kV as on the SEMF substation node. In overall, there are noted decreases in voltage values by 5% with the lowest being at bus 33 PSFU and holds the figure of 0.944 pu (Fig. L-1). Tables L-1 concentrates the case summary results.

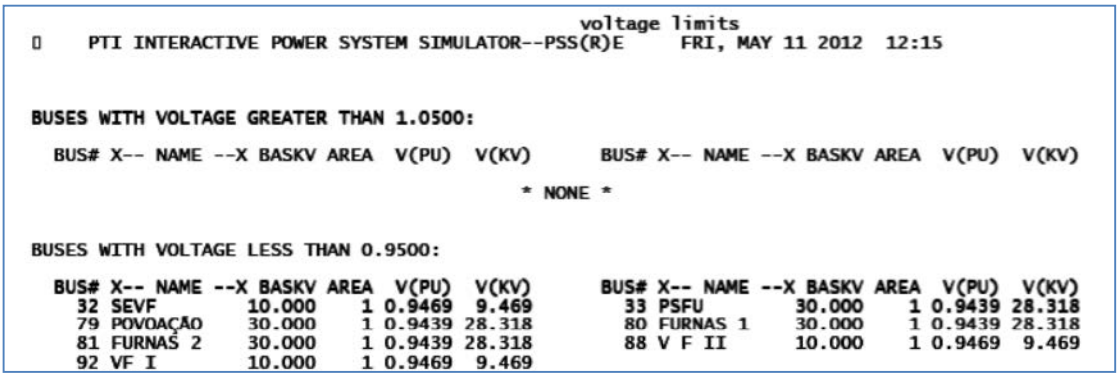

Figure L-1: *Voltage violations, addition node SEPD 60 kV.*

ATable L-1: Case summary power flow outcomes: Addition node SEPD 60 kV

Total	Generation	PQLoad	Shunts	Charging	Losses	Swing
MW	104.6	102.9	0.7	0	1.0	47.9
MVAr	36.9	35.7	-1.9	5.6	8.7	24.4

When the wind generation is connected to 10 kV SEPD bus, the lowest voltage of 0.944 pu remains at bus 33 PSFU, whereas reactive losses are higher by 0.1 MVar compared to the previous case study, but still less than Scenario 2 without adding extra renewable power into the system. This resulted from introducing wind machines as the swing generators. Without doing so, the losses raised up to 12.3 MVAr. Table L-2 gives the case summary results.

ATable L-2: Case summary power flow outcomes: Addition node SEPD 10 kV

Total	Generation	PQLoad	Shunts	Charging	Losses	Swing
MW	104.6	102.9	0.7	0	1.1	59.2
MVAr	37.1	35.7	-1.9	5.6	8.8	29.1

Appendix M: Connection of wind farm at bus SEVF rated at 30 kV

Concentrating the steady-state results, there are no any voltage violations whereas the branch between CGPV and SEFO rated at 30 kV is overloaded at the rate of 128.3%. All nodal voltages are improved and the reactive system losses are now totalling at 1.1 MW+8.6 MVAr. With the introduction of wind energy in this node, its voltage is improved and the ones at the nearby buses. Contingency analysis and three-phase fault current at this bus are following.

Compared to the case study, where wind generators are added on bus PSFU, active losses are minimized by 0.4 pu whereas reactive losses are increased by 0.3 pu. Moreover, the bus with the lowest voltage is again bus 33 PSFU with this value being at 0.954 pu. Table M-1 depicts the case summary results.

ATable M-1: Case summary power flow outcomes

Total	Generation	PQLoad	Shunts	Charging	Losses	Swing
MW	104.7	102.9	0.7	0	1.1	59.2
MVAr	36.8	35.7	-1.9	5.6	8.6	28.9

A) Contingency Analysis (N-1)

Tripping the 60 kV lines one by one, are observed the branches with over loadings and buses with violations in voltage rates. In more details, the contingencies with the worst branch overloading by 131.3 % on the system is to open the transmission line from bus 2 CGRG-GPP to bus 4 SEFO. The effect of tripping the 60 kV overhead line among bus 1 CTCL-FPP and bus 27 SEMF is that all voltages drop under the minimum acceptable value of 0.95 pu. It is worthy to mention that the bus 27 SEMF rated at 60 kV is connected to the substation of SEPD rated also at 60 kV. Thus, the far nodes of PD1 up to PD12 connected to SEPD substation mark voltage drops as they constitute the very end of these lines. Fig. M-1 represents the respective results;

Tripping the 30 kV lines one by one, are observed the two transmission branches between 3 CGPV-GPP and 30 SEFO rated at this voltage value being overloaded. Once again the contingencies with the worst consequences on the system is to open the overhead and subterranean line from bus 3 CGPV-GPP to bus 30 SEFO The effects of this tripping are violations on current ratings by 139.8% (139.7% in case study –Appendix J) and 159.5% (159.3% in case study –Appendix J) respectively. Voltage drops are denoted and all result from contingency single 4 (contingency legend, Fig. M-3), to open the subterranean circuit among buses 13 SELG and 31 SEVF. The results are showed beneath, in Fig. M-2;

```
<---------------- MULTI-SECTION LINE ----------------> <----------------- MONITORED BRANCH
-----------------> CONTINGENCY    RATING      FLOW       %
                                                          3 CGPV-GPP     30.000     30*SEFO
30.000 2  BASE CASE          14.8      18.5     128.3
                                                          3 CGPV-GPP     30.000     30*SEFO
30.000 2  SINGLE 1           14.8      18.4     128.1
                                                          3 CGPV-GPP     30.000     30*SEFO
30.000 2  SINGLE 2           14.8      18.5     128.8
                                                          3 CGPV-GPP     30.000     30*SEFO
30.000 2  SINGLE 3           14.8      18.5     128.8
                                                          1 CTCL-FPP     60.000     39*SESR
60.000 1  SINGLE 4           37.4      42.8     116.2
                                                          3 CGPV-GPP     30.000     30*SEFO
30.000 2  SINGLE 4           14.8      18.5     128.2
                                                         27*SEMF         60.000     39 SESR
60.000 1  SINGLE 4           37.4      35.7      99.2
                                                          3 CGPV-GPP     30.000     30*SEFO
30.000 2  SINGLE 5           14.8      18.5     128.2
                                                          3 CGPV-GPP     30.000     30*SEFO
30.000 2  SINGLE 6           14.8      18.5     128.2
                                                          3 CGPV-GPP     30.000     30*SEFO
30.000 2  SINGLE 7           14.8      18.9     131.3
                                                          3 CGPV-GPP     30.000     30*SEFO
30.000 2  SINGLE 8           14.8      18.2     126.7
                                                          3 CGPV-GPP     30.000     30*SEFO
30.000 2  SINGLE 9           14.8      18.5     128.2
                                                          3 CGPV-GPP     30.000     30*SEFO
30.000 2  SINGLE 10          14.8      18.5     128.2
                                                          3 CGPV-GPP     30.000     30*SEFO
30.000 2  SINGLE 11          14.8      18.5     128.2

MONITORED VOLTAGE REPORT:
SYSTEM                        CONTINGENCY  <-------- B U S --------->   V-CONT   V-INIT   V-MAX    V-MIN
'ALL         '           RANGE SINGLE 4        43 SEPD         10.000  0.94824  0.97672  1.05000  0.95000
'ALL         '           RANGE SINGLE 4        44 SEMF         30.000  0.94473  0.97292  1.05000  0.95000
'ALL         '           RANGE SINGLE 4        49 PD1          10.000  0.94842  0.97688  1.05000  0.95000
'ALL         '           RANGE SINGLE 4        50 PD2          10.000  0.94848  0.97694  1.05000  0.95000
'ALL         '           RANGE SINGLE 4        51 PD3          10.000  0.94840  0.97689  1.05000  0.95000
'ALL         '           RANGE SINGLE 4        52 PD4          10.000  0.94835  0.97682  1.05000  0.95000
'ALL         '           RANGE SINGLE 4        53 PD5          10.000  0.94831  0.97679  1.05000  0.95000
'ALL         '           RANGE SINGLE 4        54 PD6          10.000  0.94907  0.97752  1.05000  0.95000
'ALL         '           RANGE SINGLE 4        55 PD7          10.000  0.94825  0.97673  1.05000  0.95000
'ALL         '           RANGE SINGLE 4        56 PD8          10.000  0.94834  0.97682  1.05000  0.95000
'ALL         '           RANGE SINGLE 4        57 PD9          10.000  0.94826  0.97675  1.05000  0.95000
'ALL         '           RANGE SINGLE 4        58 PD10         10.000  0.94825  0.97673  1.05000  0.95000
'ALL         '           RANGE SINGLE 4        59 PD11         10.000  0.94839  0.97687  1.05000  0.95000
'ALL         '           RANGE SINGLE 4        60 PD12         10.000  0.94825  0.97673  1.05000  0.95000
'ALL         '           RANGE SINGLE 4        83 CAPELAS      30.000  0.94482  0.97300  1.05000  0.95000
'ALL         '           RANGE SINGLE 4        84 S. CIDADES   30.000  0.94481  0.97300  1.05000  0.95000
'ALL         '           RANGE SINGLE 4        85 S.ROQUE      30.000  0.94476  0.97295  1.05000  0.95000
'ALL         '           RANGE SINGLE 4        86 COVOADA      30.000  0.94480  0.97299  1.05000  0.95000
'ALL         '       DEVIATION SINGLE 9        35 SEPD1        60.000  0.95735  0.98905  0.06000  0.03000
'ALL         '       DEVIATION SINGLE 10       36 SEPD2        60.000  0.95734  0.98836  0.06000  0.03000

CONTINGENCY LEGEND:
LABEL          EVENTS
SINGLE 1    : OPEN LINE FROM BUS 1 [CTCL-FPP    60.000] TO BUS 4 [SEFO        60.000] CKT 1
SINGLE 2    : OPEN LINE FROM BUS 1 [CTCL-FPP    60.000] TO BUS 11 [SELG        60.000] CKT 1
SINGLE 3    : OPEN LINE FROM BUS 1 [CTCL-FPP    60.000] TO BUS 11 [SELG        60.000] CKT 2
SINGLE 4    : OPEN LINE FROM BUS 1 [CTCL-FPP    60.000] TO BUS 27 [SEMF        60.000] CKT 1
SINGLE 5    : OPEN LINE FROM BUS 1 [CTCL-FPP    60.000] TO BUS 37 [SEAR        60.000] CKT 1
SINGLE 6    : OPEN LINE FROM BUS 1 [CTCL-FPP    60.000] TO BUS 39 [SESR        60.000] CKT 1
SINGLE 7    : OPEN LINE FROM BUS 2 [CGRG-GPP    60.000] TO BUS 4 [SEFO        60.000] CKT 1
SINGLE 8    : OPEN LINE FROM BUS 4 [SEFO        60.000] TO BUS 11 [SELG        60.000] CKT 1
SINGLE 9    : OPEN LINE FROM BUS 27 [SEMF        60.000] TO BUS 35 [SEPD1        60.000] CKT 1
SINGLE 10   : OPEN LINE FROM BUS 27 [SEMF        60.000] TO BUS 36 [SEPD2        60.000] CKT 1
SINGLE 11   : OPEN LINE FROM BUS 27 [SEMF        60.000] TO BUS 39 [SESR        60.000] CKT 1
```

Figure M-1: *Contingency analysis outcomes for the 60 kV lines, Scenario 3.*

<---------- MULTI-SECTION LINE ---------->					<---------- MONITORED BRANCH			
----------> CONTINGENCY		RATING		FLOW	%			
30.000 2	BASE CASE	14.8	18.5	128.3	3 CGPV-GPP	30.000	30*SEFO	
30.000 2	SINGLE 1	14.8	20.1	139.8	3 CGPV-GPP	30.000	30*SEFO	
30.000 1	SINGLE 2	12.5	19.1	159.5	3 CGPV-GPP	30.000	30*SEFO	
30.000 2	SINGLE 3	14.8	18.5	128.3	3 CGPV-GPP	30.000	30*SEFO	
30.000 2	SINGLE 4	14.8	18.5	128.3	3 CGPV-GPP	30.000	30*SEFO	
30.000 2	SINGLE 5	14.8	18.5	128.2	3 CGPV-GPP	30.000	30*SEFO	
30.000 2	SINGLE 6	14.8	18.5	128.2	3 CGPV-GPP	30.000	30*SEFO	
30.000 2	SINGLE 7	14.8	18.5	128.2	3 CGPV-GPP	30.000	30*SEFO	
30.000 2	SINGLE 8	14.8	18.5	128.2	3 CGPV-GPP	30.000	30*SEFO	
30.000 2	SINGLE 9	14.8	18.6	129.0	3 CGPV-GPP	30.000	30*SEFO	
30.000 2	SINGLE 10	14.8	18.5	128.4	3 CGPV-GPP	30.000	30*SEFO	
30.000 2	SINGLE 11	14.8	18.6	129.2	3 CGPV-GPP	30.000	30*SEFO	
30.000 2	SINGLE 12	14.8	18.5	128.3	3 CGPV-GPP	30.000	30*SEFO	
30.000 2	SINGLE 13	14.8	18.5	128.8	3 CGPV-GPP	30.000	30*SEFO	
30.000 2	SINGLE 14	14.8	18.5	128.3	3 CGPV-GPP	30.000	30*SEFO	
30.000 2	SINGLE 15	14.8	18.4	127.9	3 CGPV-GPP	30.000	30*SEFO	
30.000 2	SINGLE 16	14.8	18.5	128.2	3 CGPV-GPP	30.000	30*SEFO	
30.000 2	SINGLE 17	14.8	18.5	128.2	3 CGPV-GPP	30.000	30*SEFO	
30.000 2	SINGLE 18	14.8	18.5	128.2	3 CGPV-GPP	30.000	30*SEFO	
30.000 2	SINGLE 19	14.8	18.5	128.2	3 CGPV-GPP	30.000	30*SEFO	
30.000 2	SINGLE 20	14.8	18.5	128.2	3 CGPV-GPP	30.000	30*SEFO	
30.000 2	SINGLE 21	14.8	18.5	128.2	3 CGPV-GPP	30.000	30*SEFO	
30.000 2	SINGLE 22	14.8	18.5	128.2	3 CGPV-GPP	30.000	30*SEFO	
30.000 2	SINGLE 23	14.8	18.5	128.2	3 CGPV-GPP	30.000	30*SEFO	
30.000 2	SINGLE 24	14.8	18.5	128.2	3 CGPV-GPP	30.000	30*SEFO	
30.000 2	SINGLE 25	14.8	18.5	128.2	3 CGPV-GPP	30.000	30*SEFO	
30.000 2	SINGLE 26	14.8	18.5	128.2	3 CGPV-GPP	30.000	30*SEFO	
30.000 2	SINGLE 27	14.8	18.5	128.2	3 CGPV-GPP	30.000	30*SEFO	
30.000 2	SINGLE 28	14.8	18.5	128.2	3 CGPV-GPP	30.000	30*SEFO	
30.000 2	SINGLE 29	14.8	18.5	128.2	3 CGPV-GPP	30.000	30*SEFO	
30.000 2	SINGLE 30	14.8	18.5	128.2	3 CGPV-GPP	30.000	30*SEFO	
30.000 2	SINGLE 31	14.8	18.5	128.2	3 CGPV-GPP	30.000	30*SEFO	
30.000 2	SINGLE 32	14.8	18.5	128.2	3 CGPV-GPP	30.000	30*SEFO	
30.000 2	SINGLE 33	14.8	18.5	128.2	3 CGPV-GPP	30.000	30*SEFO	
30.000 2	SINGLE 34	14.8	18.5	128.2	3 CGPV-GPP	30.000	30*SEFO	
30.000 2	SINGLE 35	14.8	18.5	128.2	3 CGPV-GPP	30.000	30*SEFO	
30.000 2	SINGLE 36	14.8	18.5	128.2	3 CGPV-GPP	30.000	30*SEFO	
30.000 2	SINGLE 37	14.8	18.5	128.2	3 CGPV-GPP	30.000	30*SEFO	

MONITORED VOLTAGE REPORT:

SYSTEM		CONTINGENCY	<-------- B U S -------->		V-CONT	V-INIT	V-MAX	V-MIN
'ALL	'	RANGE SINGLE 4	32	SEVF	10.000	0.94872	0.95697	1.05000	0.95000
'ALL	'	RANGE SINGLE 4	33	PSFU	30.000	0.94577	0.95404	1.05000	0.95000
'ALL	'	RANGE SINGLE 4	79	POVOAHΓO	30.000	0.94577	0.95405	1.05000	0.95000
'ALL	'	RANGE SINGLE 4	80	FURNAS 1	30.000	0.94577	0.95405	1.05000	0.95000
'ALL	'	RANGE SINGLE 4	81	FURNAS 2	30.000	0.94577	0.95405	1.05000	0.95000
'ALL	'	RANGE SINGLE 4	88	V F II	10.000	0.94872	0.95698	1.05000	0.95000
'ALL	'	RANGE SINGLE 4	92	VF I	10.000	0.94872	0.95698	1.05000	0.95000

Figure M-2: *Contingency analysis outcomes for the 30 kV lines, Scenario 3.*

```
CONTINGENCY LEGEND:
LABEL          EVENTS
SINGLE 1    : OPEN LINE FROM BUS 3 [CGPV-GPP    30.000] TO BUS 30 [SEFO        30.000] CKT 1
SINGLE 2    : OPEN LINE FROM BUS 3 [CGPV-GPP    30.000] TO BUS 30 [SEFO        30.000] CKT 2
SINGLE 3    : OPEN LINE FROM BUS 13 [SELG        30.000] TO BUS 31 [SEVF        30.000] CKT 1
SINGLE 4    : OPEN LINE FROM BUS 13 [SELG        30.000] TO BUS 31 [SEVF        30.000] CKT 2
SINGLE 5    : OPEN LINE FROM BUS 13 [SELG        30.000] TO BUS 70 [LIVRAMENTO  30.000] CKT 1
SINGLE 6    : OPEN LINE FROM BUS 13 [SELG        30.000] TO BUS 70 [LIVRAMENTO  30.000] CKT 2
SINGLE 7    : OPEN LINE FROM BUS 13 [SELG        30.000] TO BUS 82 [RIBEIRA CHΓ 30.000] CKT 1
SINGLE 8    : OPEN LINE FROM BUS 13 [SELG        30.000] TO BUS 82 [RIBEIRA CHΓ 30.000] CKT 2
SINGLE 9    : OPEN LINE FROM BUS 30 [SEFO        30.000] TO BUS 75 [CALHETAS    30.000] CKT 1
SINGLE 10   : OPEN LINE FROM BUS 30 [SEFO        30.000] TO BUS 75 [CALHETAS    30.000] CKT 2
SINGLE 11   : OPEN LINE FROM BUS 30 [SEFO        30.000] TO BUS 76 [NORDESTE    30.000] CKT 1
SINGLE 12   : OPEN LINE FROM BUS 30 [SEFO        30.000] TO BUS 76 [NORDESTE    30.000] CKT 2
SINGLE 13   : OPEN LINE FROM BUS 30 [SEFO        30.000] TO BUS 77 [RIBEIRINHA  30.000] CKT 1
SINGLE 14   : OPEN LINE FROM BUS 30 [SEFO        30.000] TO BUS 77 [RIBEIRINHA  30.000] CKT 2
SINGLE 15   : OPEN LINE FROM BUS 31 [SEVF        30.000] TO BUS 33 [PSFU        30.000] CKT 1
SINGLE 16   : OPEN LINE FROM BUS 31 [SEVF        30.000] TO BUS 89 [V F III     30.000] CKT 1
SINGLE 17   : OPEN LINE FROM BUS 31 [SEVF        30.000] TO BUS 90 [FURNAS      30.000] CKT 1
SINGLE 18   : OPEN LINE FROM BUS 31 [SEVF        30.000] TO BUS 90 [FURNAS      30.000] CKT 2
SINGLE 19   : OPEN LINE FROM BUS 31 [SEVF        30.000] TO BUS 91 [P. GARHA    30.000] CKT 1
SINGLE 20   : OPEN LINE FROM BUS 31 [SEVF        30.000] TO BUS 91 [P. GARHA    30.000] CKT 2
SINGLE 21   : OPEN LINE FROM BUS 33 [PSFU        30.000] TO BUS 79 [POVOAHΓO    30.000] CKT 1
SINGLE 22   : OPEN LINE FROM BUS 33 [PSFU        30.000] TO BUS 79 [POVOAHΓO    30.000] CKT 2
SINGLE 23   : OPEN LINE FROM BUS 33 [PSFU        30.000] TO BUS 80 [FURNAS 1    30.000] CKT 1
SINGLE 24   : OPEN LINE FROM BUS 33 [PSFU        30.000] TO BUS 80 [FURNAS 1    30.000] CKT 2
SINGLE 25   : OPEN LINE FROM BUS 33 [PSFU        30.000] TO BUS 81 [FURNAS 2    30.000] CKT 1
SINGLE 26   : OPEN LINE FROM BUS 44 [SEMF        30.000] TO BUS 83 [CAPELAS     30.000] CKT 1
SINGLE 27   : OPEN LINE FROM BUS 44 [SEMF        30.000] TO BUS 83 [CAPELAS     30.000] CKT 2
SINGLE 28   : OPEN LINE FROM BUS 44 [SEMF        30.000] TO BUS 84 [S. CIDADES  30.000] CKT 1
SINGLE 29   : OPEN LINE FROM BUS 44 [SEMF        30.000] TO BUS 84 [S. CIDADES  30.000] CKT 2
SINGLE 30   : OPEN LINE FROM BUS 44 [SEMF        30.000] TO BUS 85 [S.ROQUE     30.000] CKT 1
SINGLE 31   : OPEN LINE FROM BUS 44 [SEMF        30.000] TO BUS 85 [S.ROQUE     30.000] CKT 2
SINGLE 32   : OPEN LINE FROM BUS 44 [SEMF        30.000] TO BUS 86 [COVOADA     30.000] CKT 1
SINGLE 33   : OPEN LINE FROM BUS 44 [SEMF        30.000] TO BUS 86 [COVOADA     30.000] CKT 2
SINGLE 34   : OPEN LINE FROM BUS 45 [SECL        30.000] TO BUS 93 [LIVRAMENTO  30.000] CKT 1
SINGLE 35   : OPEN LINE FROM BUS 45 [SECL        30.000] TO BUS 93 [LIVRAMENTO  30.000] CKT 2
SINGLE 36   : OPEN LINE FROM BUS 45 [SECL        30.000] TO BUS 94 [RIBEIRA SECA30.000] CKT 1
SINGLE 37   : OPEN LINE FROM BUS 45 [SECL        30.000] TO BUS 94 [RIBEIRA SECA30.000] CKT 2
```

Figure M-3: *Single contingencies legend for the 30 kV lines, Scenario 3.*

B) Fault Current Calculation

The fault current increased by 239.7 A that is also an unacceptably high value. The results are given in Table M-2.

ATable M-2: Three-phase fault current at SEVF, Scenarios 2 &3

Scenarios	Voltage level (kV)	I (A)
2	30	2344.6
3	30	2584.3

Appendix N: Connection of wind farm at bus SELG rated at 60 kV

Concentrating the power flow results, they do exist voltage violations whereas the branch between CGPV and SEFO rated at 30 kV is overloaded by 128.2%. Nodal voltages have not improved and the system losses amount for 1.1 MW+9.0MVAr, a bit higher than in Scenario 2, year 2015. In general, there are noted decreases in voltages by 5.5% with the wind energy contribution. The lowest voltage is dictated again at bus 33 of PSFU, at the figure of 0.945 pu. Figures N-1 & N-2 depict the results from branch and voltage limit checking reports, whereas Table N-1 concentrates the case summary outcomes.

```
                                    voltage limits
BUSES WITH VOLTAGE LESS THAN 0.9500:

   BUS# X-- NAME --X BASKV    AREA   V(PU)   V(KV)
   32        SEVF     10.000     1  0.9482   9.482
   33        PSFU     30.000     1  0.9452  28.357
   79     POVOAHГO    30.000     1  0.9452  28.357
   80     FURNAS 1    30.000     1  0.9452  28.357
   81     FURNAS 2    30.000     1  0.9452  28.357
   88       VF II     10.000     1  0.9482   9.482
   92       VF I      10.000     1  0.9482   9.482
```

Figure N-1: *Voltage violations, addition node SELG 60 kV.*

```
                                    branch limits
BRANCH LOADINGS ABOVE  80.0 % OF RATING SET A (MVA FOR TRANSFORMERS,
CURRENT FOR NON-TRANSFORMER BRANCHES):

X--------- FROM BUS ----------X X---------- TO BUS -----------X
  BUS# X-- NAME --X BASKV  AREA    BUS# X-- NAME --X BASKV  AREA CKT
LOADING  RATING PERCENT
     3 CGPV-GPP    30.000     1     30 SEFO        30.000*    1  2
19.0    14.8   128.2
```

Figure N-2: *Branch-Check limits, addition node SELG 60 kV.*

ATable N-1: Case summary power flow outcomes

Total	Generation	PQLoad	Shunts	Charging	Losses	Swing
MW	104.7	102.9	0.7	0	1.1	59.2
MVAr	37.2	35.7	-1.9	5.6	9.0	29.4

Appendix O: Connection of wind farm at bus SELG rated at 30 kV

Summarising the steady-state results there are no any voltage violations, whereas the branch between CGPV and SEFO rated at 30 kV is overloaded at the rate of 128.3%. Voltage profile at the addition and nearby nodes is improved and the power system losses are now totalling to 1.1 MW+8.6 MVAr. Contingency analysis and three-phase fault current at this bus are following. Compared to case study where wind generators are added on bus 33 (Appendix J), active losses are minimized by 0.4 pu whereas reactive losses are increased by 0.3 pu. Moreover, the bus with the lowest voltage is again here bus 33 PSFU with this value being at 0.954 pu. Figure O-1- and Table O-1 represent the branch violations and case summary results respectively.

```
                                branch limits
BRANCH LOADINGS ABOVE  80.0 % OF RATING SET A (MVA FOR TRANSFORMERS,
CURRENT FOR NON-TRANSFORMER BRANCHES):

X--------- FROM BUS ----------X X---------- TO BUS -----------X
  BUS# X-- NAME --X BASKV     BUS# X-- NAME --X BASKV  LOADING  RATING
PERCENT
  3      CGPV-GPP   30.000     30      SEFO   30.000*    19.0    14.8
128.3
```

Figure O-1: *Branch-Check limits, addition node SELG 30 kV.*

ATable O-1: Case summary power flow outcomes

Total	Generation	PQLoad	Shunts	Charging	Losses	Swing
MW	104.7	102.9	0.7	0	1.1	56.3
MVAr	36.8	35.7	-1.9	5.6	8.6	27.9

A) Contingency Analysis (N-1)

Tripping the transmission lines of 60 kV one by one, are observed the branches with over loadings and buses with violations in voltage rates. In more details, the contingency with the worst branch overloading of 131.3 % on the system is to open the overhead line from bus 2 CGRG-GPP to bus 4 SEFO, which interconnects the central geothermal plant to this big substation. The effect of tripping the 60 kV line among bus 1 CTCL-FPP and bus 27 SEMF is that all voltages drop under the minimum acceptable value of 0.95 pu. The red circle denotes the contingency voltages whereas the blue one the line violations. Figure O-2 illustrates the results.

Tripping the lines of 30 kV one by one, are observed the two transmission branches between 3 CGPV-GPP and 30 SEFO rated at this voltage value are overloaded. In more details, the contingencies with the worst consequences on the system is to open the overhead and subterranean line from bus 3 CGPV-GPP to bus 30 SEFO The effects of this tripping are violations on current ratings by 139.8% and 159.5% respectively. Voltage drops are detected and all result from contingency- Single 4, to open the subterranean circuit among buses 13 SELG and 31 SEVF. The results are showed below (Fig. O-3);

B) Fault Current Calculation

The fault current is expected to rise up. Actually, it is increased by 239.4 A that is also an unacceptably high value. Before adding new distributed generators the fault level was at 2364.7 A. The results are given in Table O-2.

ATable O-2: Three-phase fault current at SELG, Scenarios 2 &3

Scenarios	Voltage level (kV)	I (A)
2	30	2364.7
3	30	2604.1

<---------- MULTI-SECTION LINE ---------->					<---------- MONITORED BRANCH		
----------> CONTINGENCY		RATING	FLOW	%			
30.000 2	BASE CASE	14.8	18.5	128.3	3 CGPV-GPP	30.000	30*SEFO
30.000 2	SINGLE 1	14.8	18.4	128.1	3 CGPV-GPP	30.000	30*SEFO
30.000 2	SINGLE 2	14.8	18.5	128.8	3 CGPV-GPP	30.000	30*SEFO
30.000 2	SINGLE 3	14.8	18.5	128.8	3 CGPV-GPP	30.000	30*SEFO
60.000 1	SINGLE 4	37.4	42.8	116.2	1 CTCL-FPP	60.000	39*SESR
30.000 2	SINGLE 4	14.8	18.5	128.2	3 CGPV-GPP	30.000	30*SEFO
60.000 1	SINGLE 4	37.4	35.7	99.2	27*SEMF	60.000	39 SESR
30.000 2	SINGLE 5	14.8	18.5	128.2	3 CGPV-GPP	30.000	30*SEFO
30.000 2	SINGLE 6	14.8	18.5	128.2	3 CGPV-GPP	30.000	30*SEFO
30.000 2	SINGLE 7	14.8	18.9	131.3	3 CGPV-GPP	30.000	30*SEFO
30.000 2	SINGLE 8	14.8	18.2	126.7	3 CGPV-GPP	30.000	30*SEFO
30.000 2	SINGLE 9	14.8	18.5	128.2	3 CGPV-GPP	30.000	30*SEFO
30.000 2	SINGLE 10	14.8	18.5	128.2	3 CGPV-GPP	30.000	30*SEFO
30.000 2	SINGLE 11	14.8	18.5	128.2	3 CGPV-GPP	30.000	30*SEFO

MONITORED VOLTAGE REPORT:

SYSTEM		CONTINGENCY	<-------- B U S -------->		V-CONT	V-INIT	V-MAX	V-MIN
'ALL	'	RANGE SINGLE 4	43	SEPD 10.000	0.94824	0.97672	1.05000	0.95000
'ALL	'	RANGE SINGLE 4	44	SEMF 30.000	0.94473	0.97292	1.05000	0.95000
'ALL	'	RANGE SINGLE 4	49	PD1 10.000	0.94842	0.97688	1.05000	0.95000
'ALL	'	RANGE SINGLE 4	50	PD2 10.000	0.94848	0.97694	1.05000	0.95000
'ALL	'	RANGE SINGLE 4	51	PD3 10.000	0.94840	0.97689	1.05000	0.95000
'ALL	'	RANGE SINGLE 4	52	PD4 10.000	0.94835	0.97682	1.05000	0.95000
'ALL	'	RANGE SINGLE 4	53	PD5 10.000	0.94831	0.97679	1.05000	0.95000
'ALL	'	RANGE SINGLE 4	54	PD6 10.000	0.94907	0.97752	1.05000	0.95000
'ALL	'	RANGE SINGLE 4	55	PD7 10.000	0.94825	0.97673	1.05000	0.95000
'ALL	'	RANGE SINGLE 4	56	PD8 10.000	0.94834	0.97682	1.05000	0.95000
'ALL	'	RANGE SINGLE 4	57	PD9 10.000	0.94826	0.97675	1.05000	0.95000
'ALL	'	RANGE SINGLE 4	58	PD10 10.000	0.94825	0.97673	1.05000	0.95000
'ALL	'	RANGE SINGLE 4	59	PD11 10.000	0.94839	0.97687	1.05000	0.95000
'ALL	'	RANGE SINGLE 4	60	PD12 10.000	0.94825	0.97673	1.05000	0.95000
'ALL	'	RANGE SINGLE 4	83	CAPELAS 30.000	0.94482	0.97300	1.05000	0.95000
'ALL	'	RANGE SINGLE 4	84	S. CIDADES 30.000	0.94481	0.97300	1.05000	0.95000
'ALL	'	RANGE SINGLE 4	85	S.ROQUE 30.000	0.94476	0.97295	1.05000	0.95000
'ALL	'	RANGE SINGLE 4	86	COVOADA 30.000	0.94480	0.97299	1.05000	0.95000
'ALL	'	RANGE SINGLE 4	43	SEPD 10.000	0.94824	0.97672	1.05000	0.95000
'ALL	'	RANGE SINGLE 4	44	SEMF 30.000	0.94473	0.97292	1.05000	0.95000
'ALL	'	RANGE SINGLE 4	49	PD1 10.000	0.94842	0.97688	1.05000	0.95000
'ALL	'	RANGE SINGLE 4	50	PD2 10.000	0.94848	0.97694	1.05000	0.95000
'ALL	'	RANGE SINGLE 4	51	PD3 10.000	0.94840	0.97689	1.05000	0.95000
'ALL	'	RANGE SINGLE 4	52	PD4 10.000	0.94835	0.97682	1.05000	0.95000
'ALL	'	RANGE SINGLE 4	53	PD5 10.000	0.94831	0.97679	1.05000	0.95000
'ALL	'	RANGE SINGLE 4	54	PD6 10.000	0.94907	0.97752	1.05000	0.95000
'ALL	'	RANGE SINGLE 4	55	PD7 10.000	0.94825	0.97673	1.05000	0.95000
'ALL	'	RANGE SINGLE 4	56	PD8 10.000	0.94834	0.97682	1.05000	0.95000
'ALL	'	RANGE SINGLE 4	57	PD9 10.000	0.94826	0.97675	1.05000	0.95000
'ALL	'	RANGE SINGLE 4	58	PD10 10.000	0.94825	0.97673	1.05000	0.95000
'ALL	'	RANGE SINGLE 4	59	PD11 10.000	0.94839	0.97687	1.05000	0.95000
'ALL	'	RANGE SINGLE 4	60	PD12 10.000	0.94825	0.97673	1.05000	0.95000
'ALL	'	RANGE SINGLE 4	83	CAPELAS 30.000	0.94482	0.97300	1.05000	0.95000
'ALL	'	RANGE SINGLE 4	84	S. CIDADES 30.000	0.94481	0.97300	1.05000	0.95000
'ALL	'	RANGE SINGLE 4	85	S.ROQUE 30.000	0.94476	0.97295	1.05000	0.95000
'ALL	'	RANGE SINGLE 4	86	COVOADA 30.000	0.94480	0.97299	1.05000	0.95000
'ALL	'	DEVIATION SINGLE 9	35	SEPD1 60.000	0.95735	0.98905	0.06000	0.03000
'ALL	'	DEVIATION SINGLE 9	35	SEPD1 60.000	0.95735	0.98905	0.06000	0.03000
'ALL	'	DEVIATION SINGLE 10	36	SEPD2 60.000	0.95734	0.98836	0.06000	0.03000
'ALL	'	DEVIATION SINGLE 10	36	SEPD2 60.000	0.95734	0.98836	0.06000	0.03000

CONTINGENCY LEGEND:

LABEL	EVENTS
SINGLE 1	: OPEN LINE FROM BUS 1 [CTCL-FPP 60.000] TO BUS 4 [SEFO 60.000] CKT 1
SINGLE 2	: OPEN LINE FROM BUS 1 [CTCL-FPP 60.000] TO BUS 11 [SELG 60.000] CKT 1
SINGLE 3	: OPEN LINE FROM BUS 1 [CTCL-FPP 60.000] TO BUS 11 [SELG 60.000] CKT 2
SINGLE 4	: OPEN LINE FROM BUS 1 [CTCL-FPP 60.000] TO BUS 27 [SEMF 60.000] CKT 1
SINGLE 5	: OPEN LINE FROM BUS 1 [CTCL-FPP 60.000] TO BUS 37 [SEAR 60.000] CKT 1
SINGLE 6	: OPEN LINE FROM BUS 1 [CTCL-FPP 60.000] TO BUS 39 [SESR 60.000] CKT 1
SINGLE 7	: OPEN LINE FROM BUS 2 [CGRG-GPP 60.000] TO BUS 4 [SEFO 60.000] CKT 1
SINGLE 8	: OPEN LINE FROM BUS 4 [SEFO 60.000] TO BUS 11 [SELG 60.000] CKT 1
SINGLE 9	: OPEN LINE FROM BUS 27 [SEMF 60.000] TO BUS 35 [SEPD1 60.000] CKT 1
SINGLE 10	: OPEN LINE FROM BUS 27 [SEMF 60.000] TO BUS 36 [SEPD2 60.000] CKT 1
SINGLE 11	: OPEN LINE FROM BUS 27 [SEMF 60.000] TO BUS 39 [SESR 60.000] CKT 1

Figure O-2: Contingency analysis outcomes for the 60 kV lines, Scenario 3.

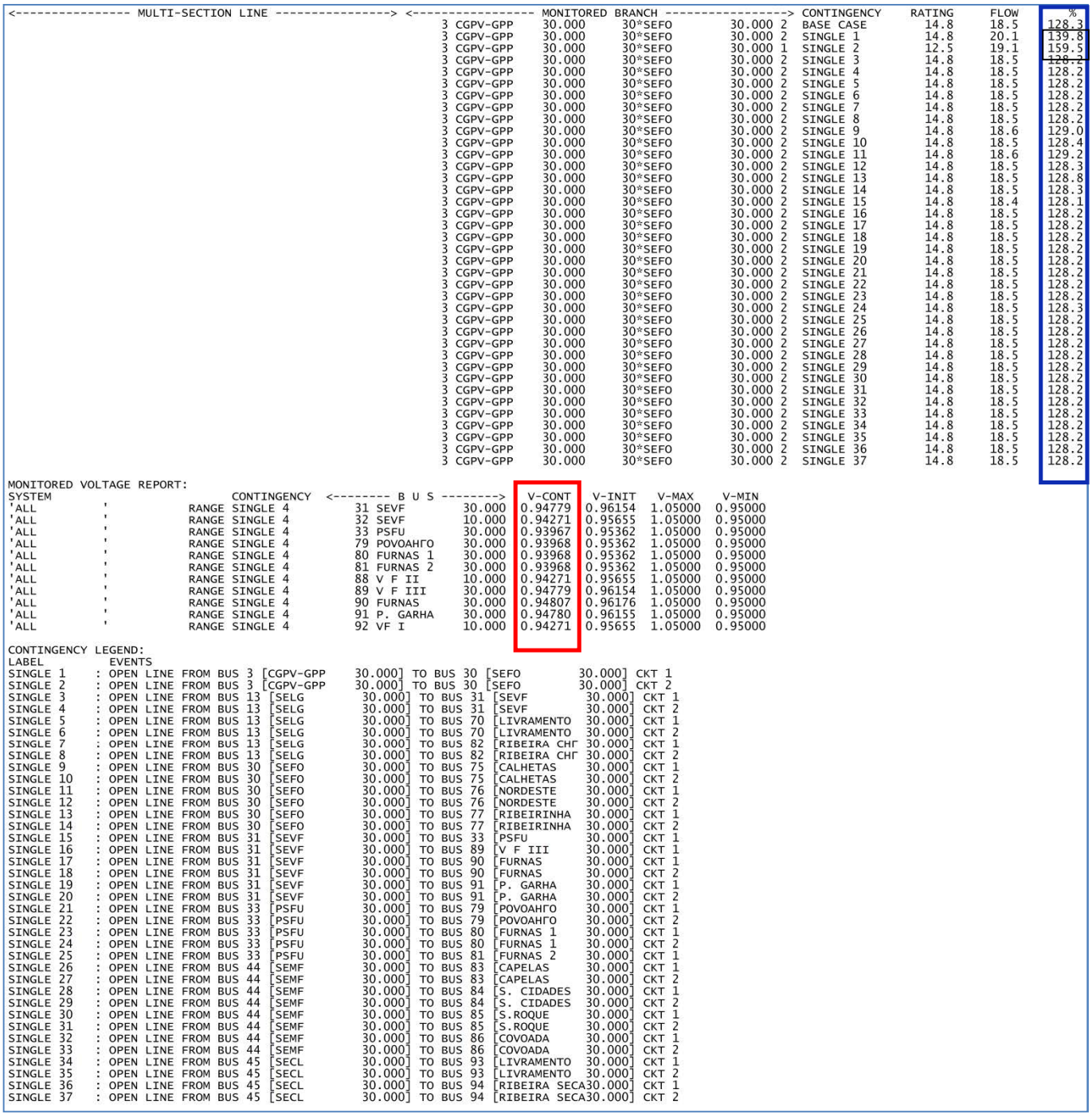

<---------- MULTI-SECTION LINE ---------->			<---------- MONITORED BRANCH ---------->			CONTINGENCY	RATING	FLOW	%
3 CGPV-GPP	30.000	30*SEFO	30.000	2		BASE CASE	14.8	18.5	128.3
3 CGPV-GPP	30.000	30*SEFO	30.000	2		SINGLE 1	14.8	20.1	139.8
3 CGPV-GPP	30.000	30*SEFO	30.000	1		SINGLE 2	12.5	19.1	159.5
3 CGPV-GPP	30.000	30*SEFO	30.000	2		SINGLE 3	14.8	18.5	128.2
3 CGPV-GPP	30.000	30*SEFO	30.000	2		SINGLE 4	14.8	18.5	128.2
3 CGPV-GPP	30.000	30*SEFO	30.000	2		SINGLE 5	14.8	18.5	128.2
3 CGPV-GPP	30.000	30*SEFO	30.000	2		SINGLE 6	14.8	18.5	128.2
3 CGPV-GPP	30.000	30*SEFO	30.000	2		SINGLE 7	14.8	18.5	128.2
3 CGPV-GPP	30.000	30*SEFO	30.000	2		SINGLE 8	14.8	18.5	128.2
3 CGPV-GPP	30.000	30*SEFO	30.000	2		SINGLE 9	14.8	18.6	129.0
3 CGPV-GPP	30.000	30*SEFO	30.000	2		SINGLE 10	14.8	18.5	128.4
3 CGPV-GPP	30.000	30*SEFO	30.000	2		SINGLE 11	14.8	18.6	129.2
3 CGPV-GPP	30.000	30*SEFO	30.000	2		SINGLE 12	14.8	18.5	128.3
3 CGPV-GPP	30.000	30*SEFO	30.000	2		SINGLE 13	14.8	18.5	128.8
3 CGPV-GPP	30.000	30*SEFO	30.000	2		SINGLE 14	14.8	18.5	128.3
3 CGPV-GPP	30.000	30*SEFO	30.000	2		SINGLE 15	14.8	18.4	128.1
3 CGPV-GPP	30.000	30*SEFO	30.000	2		SINGLE 16	14.8	18.5	128.2
3 CGPV-GPP	30.000	30*SEFO	30.000	2		SINGLE 17	14.8	18.5	128.2
3 CGPV-GPP	30.000	30*SEFO	30.000	2		SINGLE 18	14.8	18.5	128.2
3 CGPV-GPP	30.000	30*SEFO	30.000	2		SINGLE 19	14.8	18.5	128.2
3 CGPV-GPP	30.000	30*SEFO	30.000	2		SINGLE 20	14.8	18.5	128.2
3 CGPV-GPP	30.000	30*SEFO	30.000	2		SINGLE 21	14.8	18.5	128.2
3 CGPV-GPP	30.000	30*SEFO	30.000	2		SINGLE 22	14.8	18.5	128.2
3 CGPV-GPP	30.000	30*SEFO	30.000	2		SINGLE 23	14.8	18.5	128.2
3 CGPV-GPP	30.000	30*SEFO	30.000	2		SINGLE 24	14.8	18.5	128.3
3 CGPV-GPP	30.000	30*SEFO	30.000	2		SINGLE 25	14.8	18.5	128.2
3 CGPV-GPP	30.000	30*SEFO	30.000	2		SINGLE 26	14.8	18.5	128.2
3 CGPV-GPP	30.000	30*SEFO	30.000	2		SINGLE 27	14.8	18.5	128.2
3 CGPV-GPP	30.000	30*SEFO	30.000	2		SINGLE 28	14.8	18.5	128.2
3 CGPV-GPP	30.000	30*SEFO	30.000	2		SINGLE 29	14.8	18.5	128.2
3 CGPV-GPP	30.000	30*SEFO	30.000	2		SINGLE 30	14.8	18.5	128.2
3 CGPV-GPP	30.000	30*SEFO	30.000	2		SINGLE 31	14.8	18.5	128.2
3 CGPV-GPP	30.000	30*SEFO	30.000	2		SINGLE 32	14.8	18.5	128.2
3 CGPV-GPP	30.000	30*SEFO	30.000	2		SINGLE 33	14.8	18.5	128.2
3 CGPV-GPP	30.000	30*SEFO	30.000	2		SINGLE 34	14.8	18.5	128.2
3 CGPV-GPP	30.000	30*SEFO	30.000	2		SINGLE 35	14.8	18.5	128.2
3 CGPV-GPP	30.000	30*SEFO	30.000	2		SINGLE 36	14.8	18.5	128.2
3 CGPV-GPP	30.000	30*SEFO	30.000	2		SINGLE 37	14.8	18.5	128.2

MONITORED VOLTAGE REPORT:

SYSTEM	CONTINGENCY	<-------- B U S -------->		V-CONT	V-INIT	V-MAX	V-MIN
'ALL '	RANGE SINGLE 4	31 SEVF	30.000	0.94779	0.96154	1.05000	0.95000
'ALL '	RANGE SINGLE 4	32 SEVF	10.000	0.94271	0.95655	1.05000	0.95000
'ALL '	RANGE SINGLE 4	33 PSFU	30.000	0.93967	0.95362	1.05000	0.95000
'ALL '	RANGE SINGLE 4	79 POVOAHΓO	30.000	0.93968	0.95362	1.05000	0.95000
'ALL '	RANGE SINGLE 4	80 FURNAS 1	30.000	0.93968	0.95362	1.05000	0.95000
'ALL '	RANGE SINGLE 4	81 FURNAS 2	30.000	0.93968	0.95362	1.05000	0.95000
'ALL '	RANGE SINGLE 4	88 V F II	10.000	0.94271	0.95655	1.05000	0.95000
'ALL '	RANGE SINGLE 4	89 V F III	30.000	0.94779	0.96154	1.05000	0.95000
'ALL '	RANGE SINGLE 4	90 FURNAS	30.000	0.94807	0.96176	1.05000	0.95000
'ALL '	RANGE SINGLE 4	91 P. GARHA	30.000	0.94780	0.96155	1.05000	0.95000
'ALL '	RANGE SINGLE 4	92 VF I	10.000	0.94271	0.95655	1.05000	0.95000

CONTINGENCY LEGEND:

LABEL	EVENTS
SINGLE 1	: OPEN LINE FROM BUS 3 [CGPV-GPP 30.000] TO BUS 30 [SEFO 30.000] CKT 1
SINGLE 2	: OPEN LINE FROM BUS 3 [CGPV-GPP 30.000] TO BUS 30 [SEFO 30.000] CKT 2
SINGLE 3	: OPEN LINE FROM BUS 13 [SELG 30.000] TO BUS 31 [SEVF 30.000] CKT 1
SINGLE 4	: OPEN LINE FROM BUS 13 [SELG 30.000] TO BUS 31 [SEVF 30.000] CKT 2
SINGLE 5	: OPEN LINE FROM BUS 13 [SELG 30.000] TO BUS 70 [LIVRAMENTO 30.000] CKT 1
SINGLE 6	: OPEN LINE FROM BUS 13 [SELG 30.000] TO BUS 70 [LIVRAMENTO 30.000] CKT 2
SINGLE 7	: OPEN LINE FROM BUS 13 [SELG 30.000] TO BUS 82 [RIBEIRA CHΓ 30.000] CKT 1
SINGLE 8	: OPEN LINE FROM BUS 13 [SELG 30.000] TO BUS 82 [RIBEIRA CHΓ 30.000] CKT 2
SINGLE 9	: OPEN LINE FROM BUS 30 [SEFO 30.000] TO BUS 75 [CALHETAS 30.000] CKT 1
SINGLE 10	: OPEN LINE FROM BUS 30 [SEFO 30.000] TO BUS 75 [CALHETAS 30.000] CKT 2
SINGLE 11	: OPEN LINE FROM BUS 30 [SEFO 30.000] TO BUS 76 [NORDESTE 30.000] CKT 1
SINGLE 12	: OPEN LINE FROM BUS 30 [SEFO 30.000] TO BUS 76 [NORDESTE 30.000] CKT 2
SINGLE 13	: OPEN LINE FROM BUS 30 [SEFO 30.000] TO BUS 77 [RIBEIRINHA 30.000] CKT 1
SINGLE 14	: OPEN LINE FROM BUS 30 [SEFO 30.000] TO BUS 77 [RIBEIRINHA 30.000] CKT 2
SINGLE 15	: OPEN LINE FROM BUS 31 [SEVF 30.000] TO BUS 33 [PSFU 30.000] CKT 1
SINGLE 16	: OPEN LINE FROM BUS 31 [SEVF 30.000] TO BUS 89 [V F III 30.000] CKT 1
SINGLE 17	: OPEN LINE FROM BUS 31 [SEVF 30.000] TO BUS 90 [FURNAS 30.000] CKT 1
SINGLE 18	: OPEN LINE FROM BUS 31 [SEVF 30.000] TO BUS 90 [FURNAS 30.000] CKT 2
SINGLE 19	: OPEN LINE FROM BUS 31 [SEVF 30.000] TO BUS 91 [P. GARHA 30.000] CKT 1
SINGLE 20	: OPEN LINE FROM BUS 31 [SEVF 30.000] TO BUS 91 [P. GARHA 30.000] CKT 2
SINGLE 21	: OPEN LINE FROM BUS 33 [PSFU 30.000] TO BUS 79 [POVOAHΓO 30.000] CKT 1
SINGLE 22	: OPEN LINE FROM BUS 33 [PSFU 30.000] TO BUS 79 [POVOAHΓO 30.000] CKT 2
SINGLE 23	: OPEN LINE FROM BUS 33 [PSFU 30.000] TO BUS 80 [FURNAS 1 30.000] CKT 1
SINGLE 24	: OPEN LINE FROM BUS 33 [PSFU 30.000] TO BUS 80 [FURNAS 1 30.000] CKT 2
SINGLE 25	: OPEN LINE FROM BUS 33 [PSFU 30.000] TO BUS 81 [FURNAS 2 30.000] CKT 1
SINGLE 26	: OPEN LINE FROM BUS 44 [SEMF 30.000] TO BUS 83 [CAPELAS 30.000] CKT 1
SINGLE 27	: OPEN LINE FROM BUS 44 [SEMF 30.000] TO BUS 83 [CAPELAS 30.000] CKT 2
SINGLE 28	: OPEN LINE FROM BUS 44 [SEMF 30.000] TO BUS 84 [S. CIDADES 30.000] CKT 1
SINGLE 29	: OPEN LINE FROM BUS 44 [SEMF 30.000] TO BUS 84 [S. CIDADES 30.000] CKT 2
SINGLE 30	: OPEN LINE FROM BUS 44 [SEMF 30.000] TO BUS 85 [S.ROQUE 30.000] CKT 1
SINGLE 31	: OPEN LINE FROM BUS 44 [SEMF 30.000] TO BUS 85 [S.ROQUE 30.000] CKT 2
SINGLE 32	: OPEN LINE FROM BUS 44 [SEMF 30.000] TO BUS 86 [COVOADA 30.000] CKT 1
SINGLE 33	: OPEN LINE FROM BUS 44 [SEMF 30.000] TO BUS 86 [COVOADA 30.000] CKT 2
SINGLE 34	: OPEN LINE FROM BUS 45 [SECL 30.000] TO BUS 93 [LIVRAMENTO 30.000] CKT 1
SINGLE 35	: OPEN LINE FROM BUS 45 [SECL 30.000] TO BUS 93 [LIVRAMENTO 30.000] CKT 2
SINGLE 36	: OPEN LINE FROM BUS 45 [SECL 30.000] TO BUS 94 [RIBEIRA SECA 30.000] CKT 1
SINGLE 37	: OPEN LINE FROM BUS 45 [SECL 30.000] TO BUS 94 [RIBEIRA SECA 30.000] CKT 2

Figure O-3: *Contingency analysis outcomes for the 30 kV lines, Scenario 3.*

Appendix P: Connection of wind farm at bus SECL rated at 30 kV

The power flow results indicate power losses at the rate of 1.1MW + 9.0 MVAr. The lowest voltage value belongs to the bus 33 PSFU and is 0.944 pu. Voltage, branch violations and case summary outcomes are stated beneath in Figures P-1, P-2 and Table P-1, respectively.

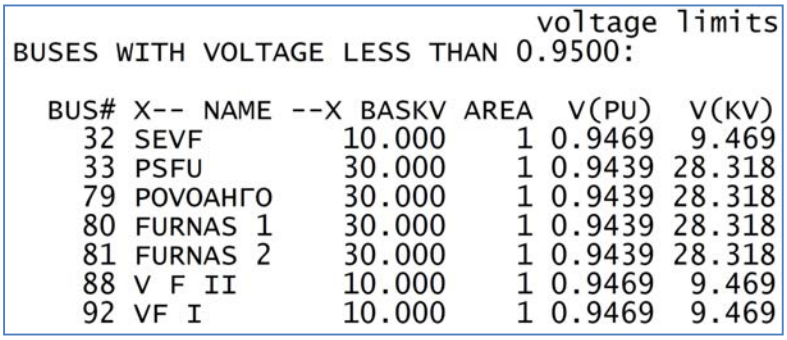

```
                                        voltage limits
BUSES WITH VOLTAGE LESS THAN 0.9500:

   BUS# X-- NAME --X BASKV AREA  V(PU)  V(KV)
     32 SEVF         10.000    1 0.9469  9.469
     33 PSFU         30.000    1 0.9439 28.318
     79 POVOAHГO     30.000    1 0.9439 28.318
     80 FURNAS 1     30.000    1 0.9439 28.318
     81 FURNAS 2     30.000    1 0.9439 28.318
     88 V F II       10.000    1 0.9469  9.469
     92 VF I         10.000    1 0.9469  9.469
```

Figure P-1: *Voltage violations, addition node SECL 30 kV.*

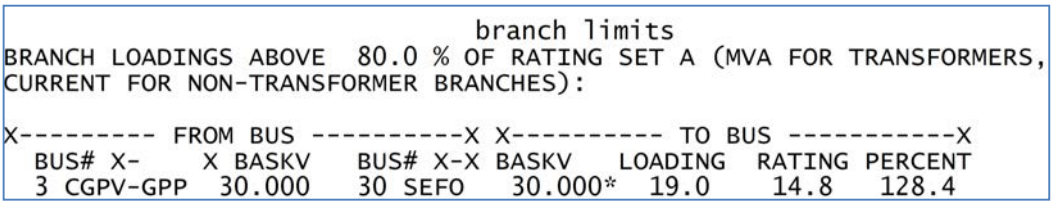

```
                                branch limits
BRANCH LOADINGS ABOVE  80.0 % OF RATING SET A (MVA FOR TRANSFORMERS,
CURRENT FOR NON-TRANSFORMER BRANCHES):

X--------- FROM BUS ----------X X---------- TO BUS -----------X
  BUS# X-     X BASKV   BUS# X-X BASKV   LOADING  RATING PERCENT
  3 CGPV-GPP  30.000    30 SEFO    30.000*  19.0    14.8   128.4
```

Figure P-2: *Branch-Check limits, addition node SECL 30 kV.*

ATable P-1: Case summary power flow outcomes

Total	Generation	PQLoad	Shunts	Charging	Losses	Swing
MW	104.7	102.9	0.7	0	1.1	59.2
MVAr	37.2	35.7	-1.9	5.6	9.0	29.2

Appendix Q: Connection of wind power at buses PSFU, SEVF and SEMF rated at 30 kV

In Scenario 2, the bus voltages with the lowest values were calculated and these belong to buses 33 PSFU, 31 SEVF and the corresponding very ends of the distribution branches they are connected to. Moreover, the substation node of SEMF (60/30 kV) rated at 30 kV faces a load requirement of 11.7 MW.

Within multiple simulation efforts to install wind power potential distributed throughout the whole energy system, it was chosen to penetrate two wind turbines of 2.0 MW into the 30 kV substation nodes of SEMF and SEVF and three machines into the 30 kV node of PSFU.

Concentrating the steady-state results there are no any voltage violations whereas the branch between CGPV and SEFO rated at 30 kV is overloaded at the rate of 128.1%. Voltage profile at all the nodes is improved and the reactive system losses are now smaller totalling at 1.1 MW+8.5 MVAr. With the introduction of wind energy in this node, its voltage is improved and also at the nearby buses. Compared to the case study where we added wind power potential solely at the substation node of 33 PSFU, voltage profile is advanced with the lowest voltage figure belonging to bus SEVF rated at 10 kV, 0.962 pu. In contrast, reactive losses are increased by 0.2 MVAr, whereas active power losses are smaller at the figure of 1.1 MW. It should be noted that in Scenario 2 without wind integration, system losses figured at 1.1 MW +8.9 MVAr. Figure Q-1 and Table Q-1 represent the branch limit checking report and case summary results respectively.

```
                                                branch limits
BRANCH LOADINGS ABOVE  80.0 % OF RATING SET A (MVA FOR TRANSFORMERS, CURRENT FOR NON-TRANSFORMER
BRANCHES):

X--------- FROM BUS ----------X X---------- TO BUS -----------X
  BUS# X-- NAME --X BASKV    BUS# X-- NAME --X BASKV  LOADING  RATING PERCENT
     3 CGPV-GPP     30.000     30 SEFO         30.000     19.0    14.8   128.1
```

Figure Q-1: *Branch limit checking report.*

ATable Q-1: Case summary power flow outcomes

Total	Generation	PQLoad	Shunts	Charging	Losses	Swing
MW	104.7	102.9	0.7	0	1.1	48
MVAr	36.7	35.7	-1.9	5.6	8.5	26.9

A) Contingency analysis N-1

Tripping the transmission lines of 60 kV one by one, are observed the branches with over loadings and buses with violations in voltage rates. In more details, the contingencies with the worst branch overloading by 131.2 % on the system is to open the overhead line from bus 2 CGRG-GPP to bus 4 SEFO. The effect of tripping the lines among bus SEMF and buses SEPD1 or SEPD2 are all voltage drops by 3.2 % but are still over the minimum acceptable value of 0.95 pu. The red circle denotes the contingency voltages whereas the blue one the line violations. It is worthy to mention that contingency analysis in this case study indicates that the inclusion of wind energy improves the system security with a transmission line loss because the extra power is distributed and is not concentrated in a substation node. Beneath are given the results. Figure Q-2 illustrates the relevant results.

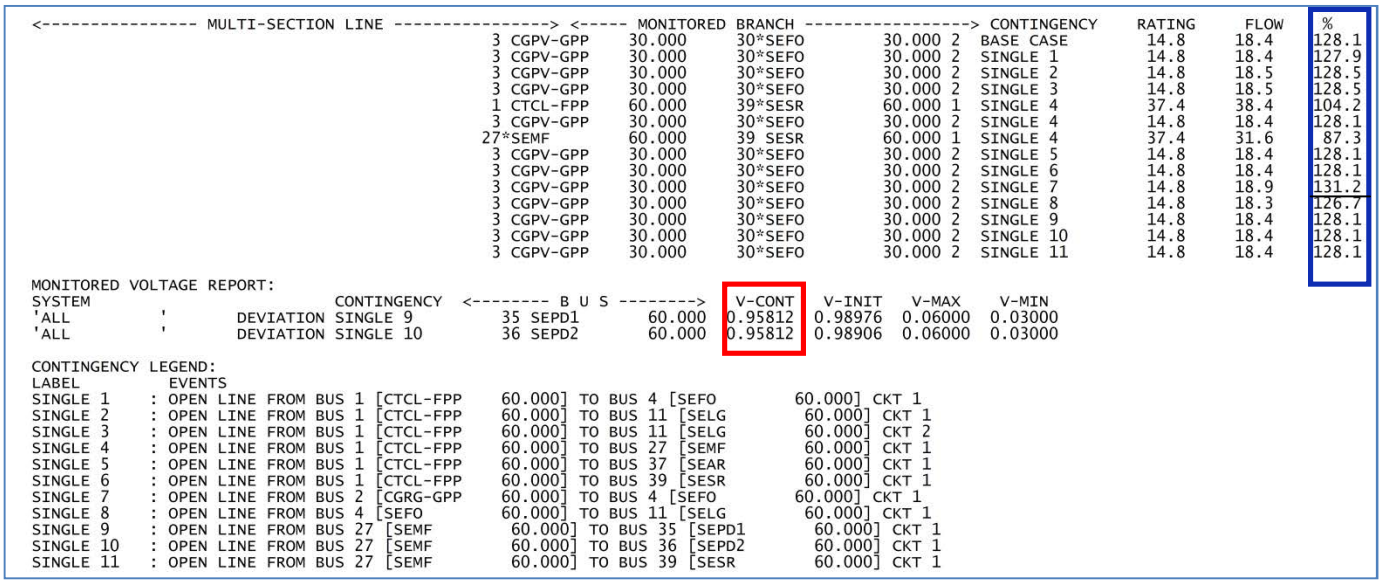

```
<---------------- MULTI-SECTION LINE ----------------> <----- MONITORED BRANCH -----------------> CONTINGENCY     RATING      FLOW      %
                                          3 CGPV-GPP     30.000     30*SEFO        30.000 2  BASE CASE       14.8      18.4     128.1
                                          3 CGPV-GPP     30.000     30*SEFO        30.000 2  SINGLE 1        14.8      18.4     127.9
                                          3 CGPV-GPP     30.000     30*SEFO        30.000 2  SINGLE 2        14.8      18.5     128.5
                                          3 CGPV-GPP     30.000     30*SEFO        30.000 2  SINGLE 3        14.8      18.5     128.5
                                          1 CTCL-FPP     60.000     39*SESR        60.000 1  SINGLE 4        37.4      38.4     104.2
                                          3 CGPV-GPP     30.000     30*SEFO        30.000 2  SINGLE 4        14.8      18.4     128.1
                                         27*SEMF         60.000     39 SESR        60.000 1  SINGLE 4        37.4      31.6      87.3
                                          3 CGPV-GPP     30.000     30*SEFO        30.000 2  SINGLE 5        14.8      18.4     128.1
                                          3 CGPV-GPP     30.000     30*SEFO        30.000 2  SINGLE 6        14.8      18.4     128.1
                                          3 CGPV-GPP     30.000     30*SEFO        30.000 2  SINGLE 7        14.8      18.9     131.2
                                          3 CGPV-GPP     30.000     30*SEFO        30.000 2  SINGLE 8        14.8      18.3     126.7
                                          3 CGPV-GPP     30.000     30*SEFO        30.000 2  SINGLE 9        14.8      18.4     128.1
                                          3 CGPV-GPP     30.000     30*SEFO        30.000 2  SINGLE 10       14.8      18.4     128.1
                                          3 CGPV-GPP     30.000     30*SEFO        30.000 2  SINGLE 11       14.8      18.4     128.1

MONITORED VOLTAGE REPORT:
SYSTEM                          CONTINGENCY  <-------- B U S --------->  V-CONT   V-INIT   V-MAX    V-MIN
'ALL         '       DEVIATION SINGLE 9         35 SEPD1       60.000  0.95812  0.98976  0.06000  0.03000
'ALL         '       DEVIATION SINGLE 10        36 SEPD2       60.000  0.95812  0.98906  0.06000  0.03000

CONTINGENCY LEGEND:
LABEL          EVENTS
SINGLE 1    : OPEN LINE FROM BUS 1 [CTCL-FPP    60.000] TO BUS 4 [SEFO        60.000] CKT 1
SINGLE 2    : OPEN LINE FROM BUS 1 [CTCL-FPP    60.000] TO BUS 11 [SELG        60.000] CKT 1
SINGLE 3    : OPEN LINE FROM BUS 1 [CTCL-FPP    60.000] TO BUS 11 [SELG        60.000] CKT 2
SINGLE 4    : OPEN LINE FROM BUS 1 [CTCL-FPP    60.000] TO BUS 27 [SEMF        60.000] CKT 1
SINGLE 5    : OPEN LINE FROM BUS 1 [CTCL-FPP    60.000] TO BUS 37 [SEAR        60.000] CKT 1
SINGLE 6    : OPEN LINE FROM BUS 1 [CTCL-FPP    60.000] TO BUS 39 [SESR        60.000] CKT 1
SINGLE 7    : OPEN LINE FROM BUS 2 [CGRG-GPP    60.000] TO BUS 4 [SEFO        60.000] CKT 1
SINGLE 8    : OPEN LINE FROM BUS 4 [SEFO        60.000] TO BUS 11 [SELG        60.000] CKT 1
SINGLE 9    : OPEN LINE FROM BUS 27 [SEMF        60.000] TO BUS 35 [SEPD1        60.000] CKT 1
SINGLE 10   : OPEN LINE FROM BUS 27 [SEMF        60.000] TO BUS 36 [SEPD2        60.000] CKT 1
SINGLE 11   : OPEN LINE FROM BUS 27 [SEMF        60.000] TO BUS 39 [SESR        60.000] CKT 1
```

Figure Q-2: *Contingency analysis outcomes for the 60 kV lines.*

Tripping the lines of 30 kV one by one, are observed the two transmission branches between 3 CGPV-GPP and 30 SEFO rated at this voltage value being overloaded. In more details, the contingencies with the worst consequences on the system are to open the overhead and subterranean line from bus 3 CGPV-GPP to bus 30 SEFO. The effects of this outage are violations on current ratings by 139.7% % and 159.3 % respectively (Fig. Q-3). Voltage violations are not denoted similarly to case study of adding wind generators solely at 33 PSFU bus.

B) Three- phase fault current at buses 33 PSFU, 31 SEVF & 44 SEMF

After installing 14 MW of wind energy units that are assumed to operate for the 80% of their installed capacity, 11.2 MW, the fault current is expected to rise up. Tables Q-2 to Q-4 depict the relative results.

Concluding, adding wind power to only one substation, namely the three nodes of 31, 33 and 44 would raise the SCL of the system by 692.6 A . On the other hand, distributing the additional power throughout different substations would raise this value at the same buses by 1089.1 A. Thus, a generation scattering may induce a better security and voltage profile in the system, but raises up the short circuit value at a very high level (Table Q-4).

<---------- MULTI-SECTION LINE ---------->	<---------- MONITORED BRANCH ---------->				CONTINGENCY	RATING	FLOW
	3 CGPV-GPP	30.000	30*SEFO	30.000 2	BASE CASE	14.8	18.4
128.1	3 CGPV-GPP	30.000	30*SEFO	30.000 2	SINGLE 1	14.8	20.1
139.7	3 CGPV-GPP	30.000	30*SEFO	30.000 1	SINGLE 2	12.5	19.1
159.3	3 CGPV-GPP	30.000	30*SEFO	30.000 2	SINGLE 3	14.8	18.4
128.1	3 CGPV-GPP	30.000	30*SEFO	30.000 2	SINGLE 4	14.8	18.4
128.1	3 CGPV-GPP	30.000	30*SEFO	30.000 2	SINGLE 5	14.8	18.4
128.1	3 CGPV-GPP	30.000	30*SEFO	30.000 2	SINGLE 6	14.8	18.4
128.1	3 CGPV-GPP	30.000	30*SEFO	30.000 2	SINGLE 7	14.8	18.4
128.1	3 CGPV-GPP	30.000	30*SEFO	30.000 2	SINGLE 8	14.8	18.4
128.1	3 CGPV-GPP	30.000	30*SEFO	30.000 2	SINGLE 9	14.8	18.6
128.9	3 CGPV-GPP	30.000	30*SEFO	30.000 2	SINGLE 10	14.8	18.5
128.2	3 CGPV-GPP	30.000	30*SEFO	30.000 2	SINGLE 11	14.8	18.6
129.1	3 CGPV-GPP	30.000	30*SEFO	30.000 2	SINGLE 12	14.8	18.5
128.2	3 CGPV-GPP	30.000	30*SEFO	30.000 2	SINGLE 13	14.8	18.5
128.7	3 CGPV-GPP	30.000	30*SEFO	30.000 2	SINGLE 14	14.8	18.5
128.2	3 CGPV-GPP	30.000	30*SEFO	30.000 2	SINGLE 15	14.8	18.5
128.2	3 CGPV-GPP	30.000	30*SEFO	30.000 2	SINGLE 16	14.8	18.4
128.1	3 CGPV-GPP	30.000	30*SEFO	30.000 2	SINGLE 17	14.8	18.4
128.1	3 CGPV-GPP	30.000	30*SEFO	30.000 2	SINGLE 18	14.8	18.4
128.1	3 CGPV-GPP	30.000	30*SEFO	30.000 2	SINGLE 19	14.8	18.4
128.1	3 CGPV-GPP	30.000	30*SEFO	30.000 2	SINGLE 20	14.8	18.4
128.1	3 CGPV-GPP	30.000	30*SEFO	30.000 2	SINGLE 21	14.8	18.4
128.1	3 CGPV-GPP	30.000	30*SEFO	30.000 2	SINGLE 22	14.8	18.4
128.1	3 CGPV-GPP	30.000	30*SEFO	30.000 2	SINGLE 23	14.8	18.4
128.1	3 CGPV-GPP	30.000	30*SEFO	30.000 2	SINGLE 24	14.8	18.4
128.1	3 CGPV-GPP	30.000	30*SEFO	30.000 2	SINGLE 25	14.8	18.4
128.1	3 CGPV-GPP	30.000	30*SEFO	30.000 2	SINGLE 26	14.8	18.4
128.1	3 CGPV-GPP	30.000	30*SEFO	30.000 2	SINGLE 27	14.8	18.4
128.1	3 CGPV-GPP	30.000	30*SEFO	30.000 2	SINGLE 28	14.8	18.4
128.1	3 CGPV-GPP	30.000	30*SEFO	30.000 2	SINGLE 29	14.8	18.4
128.1	3 CGPV-GPP	30.000	30*SEFO	30.000 2	SINGLE 30	14.8	18.4
128.1	3 CGPV-GPP	30.000	30*SEFO	30.000 2	SINGLE 31	14.8	18.4
128.1	3 CGPV-GPP	30.000	30*SEFO	30.000 2	SINGLE 32	14.8	18.4
128.1	3 CGPV-GPP	30.000	30*SEFO	30.000 2	SINGLE 33	14.8	18.4
128.1	3 CGPV-GPP	30.000	30*SEFO	30.000 2	SINGLE 34	14.8	18.4
128.1	3 CGPV-GPP	30.000	30*SEFO	30.000 2	SINGLE 35	14.8	18.4
128.1	3 CGPV-GPP	30.000	30*SEFO	30.000 2	SINGLE 36	14.8	18.4
128.1	3 CGPV-GPP	30.000	30*SEFO	30.000 2	SINGLE 37	14.8	18.4

MONITORED VOLTAGE REPORT:

SYSTEM	CONTINGENCY	<-------- B U S -------->	V-CONT	V-INIT	V-MAX	V-MIN

CONTINGENCY LEGEND:

LABEL	EVENTS
SINGLE 1	: OPEN LINE FROM BUS 3 [CGPV-GPP 30.000] TO BUS 30 [SEFO 30.000] CKT 1
SINGLE 2	: OPEN LINE FROM BUS 3 [CGPV-GPP 30.000] TO BUS 30 [SEFO 30.000] CKT 2
SINGLE 3	: OPEN LINE FROM BUS 13 [SELG 30.000] TO BUS 31 [SEVF 30.000] CKT 1
SINGLE 4	: OPEN LINE FROM BUS 13 [SELG 30.000] TO BUS 31 [SEVF 30.000] CKT 2
SINGLE 5	: OPEN LINE FROM BUS 13 [SELG 30.000] TO BUS 70 [LIVRAMENTO 30.000] CKT 1
SINGLE 6	: OPEN LINE FROM BUS 13 [SELG 30.000] TO BUS 70 [LIVRAMENTO 30.000] CKT 2
SINGLE 7	: OPEN LINE FROM BUS 13 [SELG 30.000] TO BUS 82 [RIBEIRA CHF 30.000] CKT 1
SINGLE 8	: OPEN LINE FROM BUS 13 [SELG 30.000] TO BUS 82 [RIBEIRA CHF 30.000] CKT 2
SINGLE 9	: OPEN LINE FROM BUS 30 [SEFO 30.000] TO BUS 75 [CALHETAS 30.000] CKT 1
SINGLE 10	: OPEN LINE FROM BUS 30 [SEFO 30.000] TO BUS 75 [CALHETAS 30.000] CKT 2
SINGLE 11	: OPEN LINE FROM BUS 30 [SEFO 30.000] TO BUS 76 [NORDESTE 30.000] CKT 1
SINGLE 12	: OPEN LINE FROM BUS 30 [SEFO 30.000] TO BUS 76 [NORDESTE 30.000] CKT 2
SINGLE 13	: OPEN LINE FROM BUS 30 [SEFO 30.000] TO BUS 77 [RIBEIRINHA 30.000] CKT 1
SINGLE 14	: OPEN LINE FROM BUS 30 [SEFO 30.000] TO BUS 77 [RIBEIRINHA 30.000] CKT 2
SINGLE 15	: OPEN LINE FROM BUS 31 [SEVF 30.000] TO BUS 33 [PSFU 30.000] CKT 1
SINGLE 16	: OPEN LINE FROM BUS 31 [SEVF 30.000] TO BUS 89 [V F III 30.000] CKT 1
SINGLE 17	: OPEN LINE FROM BUS 31 [SEVF 30.000] TO BUS 90 [FURNAS 30.000] CKT 1
SINGLE 18	: OPEN LINE FROM BUS 31 [SEVF 30.000] TO BUS 90 [FURNAS 30.000] CKT 2
SINGLE 19	: OPEN LINE FROM BUS 31 [SEVF 30.000] TO BUS 91 [P. GARHA 30.000] CKT 1
SINGLE 20	: OPEN LINE FROM BUS 31 [SEVF 30.000] TO BUS 91 [P. GARHA 30.000] CKT 2
SINGLE 21	: OPEN LINE FROM BUS 33 [PSFU 30.000] TO BUS 79 [POVOAHFO 30.000] CKT 1
SINGLE 22	: OPEN LINE FROM BUS 33 [PSFU 30.000] TO BUS 79 [POVOAHFO 30.000] CKT 2
SINGLE 23	: OPEN LINE FROM BUS 33 [PSFU 30.000] TO BUS 80 [FURNAS 1 30.000] CKT 1
SINGLE 24	: OPEN LINE FROM BUS 33 [PSFU 30.000] TO BUS 80 [FURNAS 1 30.000] CKT 2
SINGLE 25	: OPEN LINE FROM BUS 33 [PSFU 30.000] TO BUS 81 [FURNAS 2 30.000] CKT 1
SINGLE 26	: OPEN LINE FROM BUS 44 [SEMF 30.000] TO BUS 83 [CAPELAS 30.000] CKT 1
SINGLE 27	: OPEN LINE FROM BUS 44 [SEMF 30.000] TO BUS 83 [CAPELAS 30.000] CKT 2
SINGLE 28	: OPEN LINE FROM BUS 44 [SEMF 30.000] TO BUS 84 [S. CIDADES 30.000] CKT 1
SINGLE 29	: OPEN LINE FROM BUS 44 [SEMF 30.000] TO BUS 84 [S. CIDADES 30.000] CKT 2
SINGLE 30	: OPEN LINE FROM BUS 44 [SEMF 30.000] TO BUS 85 [S.ROQUE 30.000] CKT 1
SINGLE 31	: OPEN LINE FROM BUS 44 [SEMF 30.000] TO BUS 85 [S.ROQUE 30.000] CKT 2
SINGLE 32	: OPEN LINE FROM BUS 44 [SEMF 30.000] TO BUS 86 [COVOADA 30.000] CKT 1
SINGLE 33	: OPEN LINE FROM BUS 44 [SEMF 30.000] TO BUS 86 [COVOADA 30.000] CKT 2
SINGLE 34	: OPEN LINE FROM BUS 45 [SECL 30.000] TO BUS 93 [LIVRAMENTO 30.000] CKT 1
SINGLE 35	: OPEN LINE FROM BUS 45 [SECL 30.000] TO BUS 93 [LIVRAMENTO 30.000] CKT 2
SINGLE 36	: OPEN LINE FROM BUS 45 [SECL 30.000] TO BUS 94 [RIBEIRA SECA30.000] CKT 1
SINGLE 37	: OPEN LINE FROM BUS 45 [SECL 30.000] TO BUS 94 [RIBEIRA SECA30.000] CKT 2

Figure Q-3: Contingency analysis outcomes for the 30 kV lines.

ATable Q-2: Three-phase fault current values I(A)

Substation nodes	Voltage level (kV)	I (A)
PSFU	30	1811.4
SEVF	30	2781.9
SEMF	30	3956.6

ATable Q-3: Total system losses for Scenarios 2 & 3 with wind installed at 31, 33 & 44 buses

Network buses	System losses (P, Q)	
	Scenario 2, geothermal power	Scenario 3, geothermal & wind at PSFU, SEVF & SEMF (30 kV)
31 SEVF, 33 PSFU & 44 SEMF	1.1 MW+8.9 MVAr	1.1 MW+8.5 MVAr

ATable Q-4: SCL at the addition buses, Scenarios 2 & 3 with wind installed at 31, 33 & 44 buses

DG addition at bus	SCL (A)	
	Scenario 2, geothermal power	Scenario 3, geothermal & wind at PSFU, SEVF & SEMF (30 kV)
31 SEVF	2344.6	2781.9
33 PSFU	1455.8	1811.4
44 SEMF	3660.4	3956.6

Appendix R: Connection of wind power at buses PSFU, SEVF of 30 kV and SEMF rated at 60 kV

By adding the wind generators at bus 27 of the SEMF substation rated at 60 kV, system losses are even minimized to 1.0 MW+8.2 MVAr but voltages are variably improved. As it was expected, mainly the transmission voltages are now slightly higher. Transformer 0.69/60 kV power rating amounts at 40 MVA, resulting to the finding that the higher the current loading the higher will be and the reactive absorption. Contingency analysis does not influence the system´s security with any transmission or distribution line outage in terms of voltage overloads. However, thermal violations are noticed on the distribution line among 3 CGPV and 30 SEFO buses. On the other hand, short circuit level on the addition nodes is highly increased. Branch limit checking and case summary results are laid in Fig. R-1 and Table R-1 respectively.

```
                                branch limits
BRANCH LOADINGS ABOVE  80.0 % OF RATING SET A (MVA FOR TRANSFORMERS,
CURRENT FOR NON-TRANSFORMER BRANCHES):

X---FROM BUS -X X---------- TO BUS ----------X
 BUS# X-- NAME --X BASKV   BUS# X-- NAME --X BASKV LOADING  RATING PERCENT
   3 CGPV-GPP     30.00     30 SEFO         30.000*    19.0    14.8   128.1
```

Figure R-1: *Branch limit checking report.*

ATable R-1: Case summary power flow outcomes

Total	Generation	PQLoad	Shunts	Charging	Losses	Swing
MW	104.6	102.9	0.7	0	1.0	47.9
MVAr	36.3	35.7	-1.9	5.6	8.2	24.0

A) Contingency analysis N-1

Tripping the lines of 60 kV one by one, the branches with over loadings and buses with violations in voltage rates are observed. In more details, the contingencies with the worst branch overloading by 131.2 % on the system is to open the transmission line starting from bus 2 CGRG-GPP and ending to bus 4 SEFO. The effects of tripping the line among bus 27 SEMF and buses 35 SEPD1 or 36 SEPD2 are that all voltages drop by 3.2 % but are still over the minimum acceptable value of 0.95 pu.

Tripping the lines of 30 kV one by one, the two transmission branches between 3 CGPV-GPP and 30 SEFO rated at this voltage value are overloaded. In more details, the contingencies with the worst consequences on the system are to open the overhead and subterranean line from bus 3 CGPV-GPP to bus 30 SEFO. The effects of this tripping are violations on current ratings by 139.8% % and 159.4 % respectively. Voltage violations are not observed.

Figures R-2 & R-3 depict the relevant outcomes.

```
<---------------- MULTI-SECTION LINE ----------------> <----------------- MONITORED BRANCH
----------------> CONTINGENCY     RATING      FLOW        %
                                                          3 CGPV-GPP     30.000      30*SEFO
30.000 2   BASE CASE          14.8      18.4     128.1
                                                          3 CGPV-GPP     30.000      30*SEFO
30.000 2   SINGLE 1          14.8      18.4     128.0
                                                          3 CGPV-GPP     30.000      30*SEFO
30.000 2   SINGLE 2          14.8      18.5     128.6
                                                          3 CGPV-GPP     30.000      30*SEFO
30.000 2   SINGLE 3          14.8      18.5     128.6
                                                          1 CTCL-FPP     60.000      39*SESR
60.000 1   SINGLE 4          37.4      34.1      92.3
                                                          3 CGPV-GPP     30.000      30*SEFO
30.000 2   SINGLE 4          14.8      18.5     128.2
                                                          3 CGPV-GPP     30.000      30*SEFO
30.000 2   SINGLE 5          14.8      18.4     128.1
                                                          3 CGPV-GPP     30.000      30*SEFO
30.000 2   SINGLE 6          14.8      18.4     128.2
                                                          3 CGPV-GPP     30.000      30*SEFO
30.000 2   SINGLE 7          14.8      18.9     131.2
                                                          3 CGPV-GPP     30.000      30*SEFO
30.000 2   SINGLE 8          14.8      18.2     126.7
                                                          3 CGPV-GPP     30.000      30*SEFO
30.000 2   SINGLE 9          14.8      18.4     128.1
                                                          3 CGPV-GPP     30.000      30*SEFO
30.000 2   SINGLE 10         14.8      18.4     128.1
                                                          3 CGPV-GPP     30.000      30*SEFO
30.000 2   SINGLE 11         14.8      18.5     128.2

MONITORED VOLTAGE REPORT:
SYSTEM                          CONTINGENCY  <-------- B U S --------->  V-CONT   V-INIT   V-MAX    V-MIN
'ALL          '       DEVIATION SINGLE 9          35 SEPD1       60.000  0.95971  0.99123  0.06000  0.03000
'ALL          '       DEVIATION SINGLE 10         36 SEPD2       60.000  0.95971  0.99053  0.06000  0.03000

CONTINGENCY LEGEND:
LABEL          EVENTS
SINGLE 1    : OPEN LINE FROM BUS 1 [CTCL-FPP    60.000] TO BUS 4 [SEFO        60.000] CKT 1
SINGLE 2    : OPEN LINE FROM BUS 1 [CTCL-FPP    60.000] TO BUS 11 [SELG        60.000] CKT 1
SINGLE 3    : OPEN LINE FROM BUS 1 [CTCL-FPP    60.000] TO BUS 11 [SELG        60.000] CKT 2
SINGLE 4    : OPEN LINE FROM BUS 1 [CTCL-FPP    60.000] TO BUS 27 [SEMF        60.000] CKT 1
SINGLE 5    : OPEN LINE FROM BUS 1 [CTCL-FPP    60.000] TO BUS 37 [SEAR        60.000] CKT 1
SINGLE 6    : OPEN LINE FROM BUS 1 [CTCL-FPP    60.000] TO BUS 39 [SESR        60.000] CKT 1
SINGLE 7    : OPEN LINE FROM BUS 2 [CGRG-GPP    60.000] TO BUS 4 [SEFO        60.000] CKT 1
SINGLE 8    : OPEN LINE FROM BUS 4 [SEFO        60.000] TO BUS 11 [SELG        60.000] CKT 1
SINGLE 9    : OPEN LINE FROM BUS 27 [SEMF        60.000] TO BUS 35 [SEPD1       60.000] CKT 1
SINGLE 10   : OPEN LINE FROM BUS 27 [SEMF        60.000] TO BUS 36 [SEPD2       60.000] CKT 1
SINGLE 11   : OPEN LINE FROM BUS 27 [SEMF        60.000] TO BUS 39 [SESR        60.000] CKT 1
```

Figure R-2: *Contingency analysis outcomes for the 60 kV lines.*

B) Three- phase fault current at buses 33 PSFU, 31 SEVF & 27 SEMF

After installing 14 MW of wind energy units that are assumed to operate for the 80% of their installed capacity, 11.2 MW, the fault current is expected to rise up. Tables R-2 to R-4 concentrate the three-phase current values, total system losses, and short circuit level increase at each one of the addition substations for both Scenarios 2 & 3.

ATable R-2: Three-phase fault current values I(A)

Substation nodes	Voltage level (kV)	I (A)
PSFU	30	2038.4
SEVF	30	3072.8
SEMF	60	4970.7

ATable R-3: Total system losses for Scenarios 2 & 3 with wind installed at 31, 33 & 27 buses

Network buses	System losses (P, Q)	
	Scenario 2, geothermal power	Scenario 3, geothermal & wind at PSFU, SEVF & SEMF (60 kV)
31, 33 & 27	1.1 MW+8.9 MVAr	1.0MW+8.2 MVAr

ATable R-4: Short Circuit Level at the addition buses, Scenarios 2 & 3 with wind installed at 31, 33 & 44 buses

DG addition at bus	SCL (A)	
	Scenario 2, geothermal power	Scenario 3, geothermal & wind at PSFU, SEVF & SEMF (60 kV)
31	2344.6	3072.8
33	1455.8	2038.4
27	4768.8	4970.7

Concluding, adding wind power to only one of the substation nodes, i.e. 31, 33 and 27 would raise the total SCL by 856.8 A, whereas distributing the additional power throughout different substations would increase this value at the same buses by 1512.7 A. Thus, a generation scattering in transmission voltage may induce less active and reactive losses, but raises up the short circuit value at a very considerable level.

<---------- MULTI-SECTION LINE ---------->	<---------- MONITORED BRANCH ---------->				CONTINGENCY	RATING	FLOW
	3 CGPV-GPP	30.000	30*SEFO	30.000 2	BASE CASE	14.8	18.4
128.1	3 CGPV-GPP	30.000	30*SEFO	30.000 2	SINGLE 1	14.8	20.1
139.8	3 CGPV-GPP	30.000	30*SEFO	30.000 1	SINGLE 2	12.5	19.1
159.4	3 CGPV-GPP	30.000	30*SEFO	30.000 2	SINGLE 3	14.8	18.5
128.2	3 CGPV-GPP	30.000	30*SEFO	30.000 2	SINGLE 4	14.8	18.5
128.2	3 CGPV-GPP	30.000	30*SEFO	30.000 2	SINGLE 5	14.8	18.4
128.1	3 CGPV-GPP	30.000	30*SEFO	30.000 2	SINGLE 6	14.8	18.4
128.1	3 CGPV-GPP	30.000	30*SEFO	30.000 2	SINGLE 7	14.8	18.4
128.1	3 CGPV-GPP	30.000	30*SEFO	30.000 2	SINGLE 8	14.8	18.4
128.1	3 CGPV-GPP	30.000	30*SEFO	30.000 2	SINGLE 9	14.8	18.6
128.9	3 CGPV-GPP	30.000	30*SEFO	30.000 2	SINGLE 10	14.8	18.5
128.3	3 CGPV-GPP	30.000	30*SEFO	30.000 2	SINGLE 11	14.8	18.6
129.1	3 CGPV-GPP	30.000	30*SEFO	30.000 2	SINGLE 12	14.8	18.5
128.2	3 CGPV-GPP	30.000	30*SEFO	30.000 2	SINGLE 13	14.8	18.5
128.7	3 CGPV-GPP	30.000	30*SEFO	30.000 2	SINGLE 14	14.8	18.5
128.2	3 CGPV-GPP	30.000	30*SEFO	30.000 2	SINGLE 15	14.8	18.5
128.2	3 CGPV-GPP	30.000	30*SEFO	30.000 2	SINGLE 16	14.8	18.4
128.1	3 CGPV-GPP	30.000	30*SEFO	30.000 2	SINGLE 17	14.8	18.4
128.2	3 CGPV-GPP	30.000	30*SEFO	30.000 2	SINGLE 18	14.8	18.4
128.1	3 CGPV-GPP	30.000	30*SEFO	30.000 2	SINGLE 19	14.8	18.4
128.1	3 CGPV-GPP	30.000	30*SEFO	30.000 2	SINGLE 20	14.8	18.4
128.1	3 CGPV-GPP	30.000	30*SEFO	30.000 2	SINGLE 21	14.8	18.4
128.1	3 CGPV-GPP	30.000	30*SEFO	30.000 2	SINGLE 22	14.8	18.4
128.1	3 CGPV-GPP	30.000	30*SEFO	30.000 2	SINGLE 23	14.8	18.4
128.1	3 CGPV-GPP	30.000	30*SEFO	30.000 2	SINGLE 24	14.8	18.5
128.2	3 CGPV-GPP	30.000	30*SEFO	30.000 2	SINGLE 25	14.8	18.4
128.1	3 CGPV-GPP	30.000	30*SEFO	30.000 2	SINGLE 26	14.8	18.4
128.1	3 CGPV-GPP	30.000	30*SEFO	30.000 2	SINGLE 27	14.8	18.4
128.1	3 CGPV-GPP	30.000	30*SEFO	30.000 2	SINGLE 28	14.8	18.4
128.1	3 CGPV-GPP	30.000	30*SEFO	30.000 2	SINGLE 29	14.8	18.4
128.1	3 CGPV-GPP	30.000	30*SEFO	30.000 2	SINGLE 30	14.8	18.4
128.1	3 CGPV-GPP	30.000	30*SEFO	30.000 2	SINGLE 31	14.8	18.4
128.1	3 CGPV-GPP	30.000	30*SEFO	30.000 2	SINGLE 32	14.8	18.4
128.1	3 CGPV-GPP	30.000	30*SEFO	30.000 2	SINGLE 33	14.8	18.4
128.1	3 CGPV-GPP	30.000	30*SEFO	30.000 2	SINGLE 34	14.8	18.4
128.1	3 CGPV-GPP	30.000	30*SEFO	30.000 2	SINGLE 35	14.8	18.4
128.1	3 CGPV-GPP	30.000	30*SEFO	30.000 2	SINGLE 36	14.8	18.4
128.1	3 CGPV-GPP	30.000	30*SEFO	30.000 2	SINGLE 37	14.8	18.4

CONTINGENCY LEGEND:

LABEL	EVENTS
SINGLE 1	: OPEN LINE FROM BUS 3 [CGPV-GPP 30.000] TO BUS 30 [SEFO 30.000] CKT 1
SINGLE 2	: OPEN LINE FROM BUS 3 [CGPV-GPP 30.000] TO BUS 30 [SEFO 30.000] CKT 2
SINGLE 3	: OPEN LINE FROM BUS 13 [SELG 30.000] TO BUS 31 [SEVF 30.000] CKT 1
SINGLE 4	: OPEN LINE FROM BUS 13 [SELG 30.000] TO BUS 31 [SEVF 30.000] CKT 2
SINGLE 5	: OPEN LINE FROM BUS 13 [SELG 30.000] TO BUS 70 [LIVRAMENTO 30.000] CKT 1
SINGLE 6	: OPEN LINE FROM BUS 13 [SELG 30.000] TO BUS 70 [LIVRAMENTO 30.000] CKT 2
SINGLE 7	: OPEN LINE FROM BUS 13 [SELG 30.000] TO BUS 82 [RIBEIRA CHΓ 30.000] CKT 1
SINGLE 8	: OPEN LINE FROM BUS 13 [SELG 30.000] TO BUS 82 [RIBEIRA CHΓ 30.000] CKT 2
SINGLE 9	: OPEN LINE FROM BUS 30 [SEFO 30.000] TO BUS 75 [CALHETAS 30.000] CKT 1
SINGLE 10	: OPEN LINE FROM BUS 30 [SEFO 30.000] TO BUS 75 [CALHETAS 30.000] CKT 2
SINGLE 11	: OPEN LINE FROM BUS 30 [SEFO 30.000] TO BUS 76 [NORDESTE 30.000] CKT 1
SINGLE 12	: OPEN LINE FROM BUS 30 [SEFO 30.000] TO BUS 76 [NORDESTE 30.000] CKT 2
SINGLE 13	: OPEN LINE FROM BUS 30 [SEFO 30.000] TO BUS 77 [RIBEIRINHA 30.000] CKT 1
SINGLE 14	: OPEN LINE FROM BUS 30 [SEFO 30.000] TO BUS 77 [RIBEIRINHA 30.000] CKT 2
SINGLE 15	: OPEN LINE FROM BUS 31 [SEVF 30.000] TO BUS 33 [PSFU 30.000] CKT 1
SINGLE 16	: OPEN LINE FROM BUS 31 [SEVF 30.000] TO BUS 89 [V F III 30.000] CKT 1
SINGLE 17	: OPEN LINE FROM BUS 31 [SEVF 30.000] TO BUS 90 [FURNAS 30.000] CKT 1
SINGLE 18	: OPEN LINE FROM BUS 31 [SEVF 30.000] TO BUS 90 [FURNAS 30.000] CKT 2
SINGLE 19	: OPEN LINE FROM BUS 31 [SEVF 30.000] TO BUS 91 [P. GARHA 30.000] CKT 1
SINGLE 20	: OPEN LINE FROM BUS 31 [SEVF 30.000] TO BUS 91 [P. GARHA 30.000] CKT 2
SINGLE 21	: OPEN LINE FROM BUS 33 [PSFU 30.000] TO BUS 79 [POVOAHΓO 30.000] CKT 1
SINGLE 22	: OPEN LINE FROM BUS 33 [PSFU 30.000] TO BUS 79 [POVOAHΓO 30.000] CKT 2
SINGLE 23	: OPEN LINE FROM BUS 33 [PSFU 30.000] TO BUS 80 [FURNAS 1 30.000] CKT 1
SINGLE 24	: OPEN LINE FROM BUS 33 [PSFU 30.000] TO BUS 80 [FURNAS 1 30.000] CKT 2
SINGLE 25	: OPEN LINE FROM BUS 33 [PSFU 30.000] TO BUS 81 [FURNAS 2 30.000] CKT 1
SINGLE 26	: OPEN LINE FROM BUS 44 [SEMF 30.000] TO BUS 83 [CAPELAS 30.000] CKT 1
SINGLE 27	: OPEN LINE FROM BUS 44 [SEMF 30.000] TO BUS 83 [CAPELAS 30.000] CKT 2
SINGLE 28	: OPEN LINE FROM BUS 44 [SEMF 30.000] TO BUS 84 [S. CIDADES 30.000] CKT 1
SINGLE 29	: OPEN LINE FROM BUS 44 [SEMF 30.000] TO BUS 84 [S. CIDADES 30.000] CKT 2
SINGLE 30	: OPEN LINE FROM BUS 44 [SEMF 30.000] TO BUS 85 [S.ROQUE 30.000] CKT 1
SINGLE 31	: OPEN LINE FROM BUS 44 [SEMF 30.000] TO BUS 85 [S.ROQUE 30.000] CKT 2
SINGLE 32	: OPEN LINE FROM BUS 44 [SEMF 30.000] TO BUS 86 [COVOADA 30.000] CKT 1
SINGLE 33	: OPEN LINE FROM BUS 44 [SEMF 30.000] TO BUS 86 [COVOADA 30.000] CKT 2
SINGLE 34	: OPEN LINE FROM BUS 45 [SECL 30.000] TO BUS 93 [LIVRAMENTO 30.000] CKT 1
SINGLE 35	: OPEN LINE FROM BUS 45 [SECL 30.000] TO BUS 93 [LIVRAMENTO 30.000] CKT 2
SINGLE 36	: OPEN LINE FROM BUS 45 [SECL 30.000] TO BUS 94 [RIBEIRA SECA30.000] CKT 1
SINGLE 37	: OPEN LINE FROM BUS 45 [SECL 30.000] TO BUS 94 [RIBEIRA SECA30.000] CKT 2

Figure R-3: *Contingency analysis outcomes for the 30 kV lines.*

Appendix S: Bootstcap Maxwell Supercapacitor Test

Its maximum stored energy was 6.5 kJ with nominal capacitance of 58 F and nominal voltage of 15 V. The experiment consisted of charging the Supercapacitor at a current of 3 A, until the voltage reached the value of 30 V (two Supercapacitors connected in series), then the current was cut off for about 10 minutes. Following, with the assistance of a rheostat, a resistance of 10 Ohms was applied to the circuit to discharge the Supercapacitor. In that way, an experimental complete cycle of charging and discharging on a real energy storage device was executed in the Power Energy Systems laboratory in ICCS-NTUA.

. Fig. 5-25 shows the voltage profile of the complete cycle of charging and discharging on this real energy storage device whereas Fig. 5-26 represents only the discharging current.

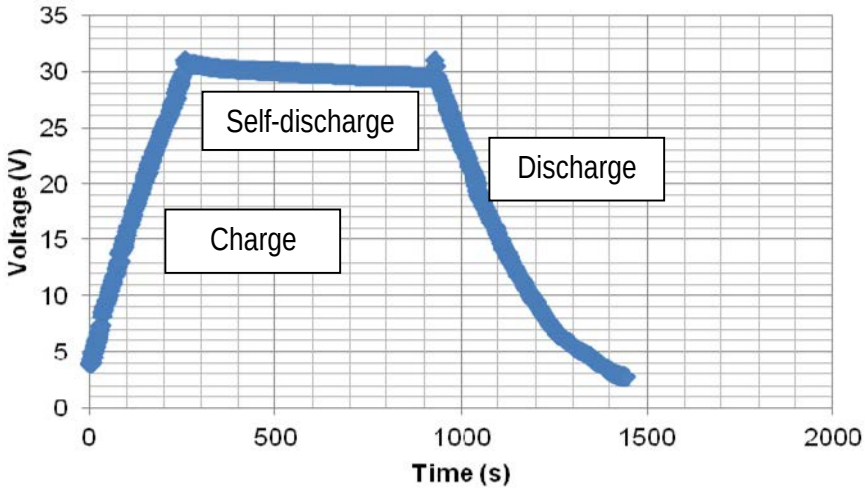

Figure S-1: *Voltage from screening test using Bootstcap Maxwell.*

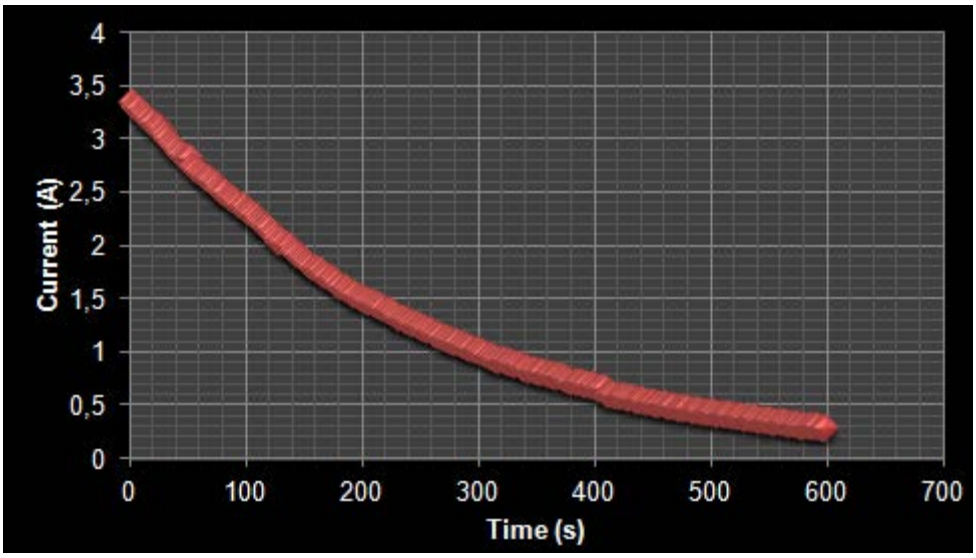

Figure S-2: *Current values during discharging.*

Appendix T: Current vector control

The three-phase inverter's control is actually based on the current vector control. The relevant equations are the ones that follow:

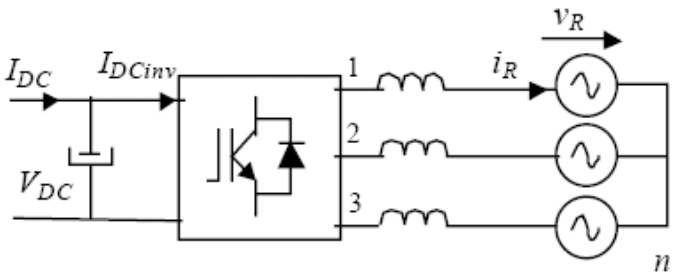

Figure T-1: *Three-phase inverter.*

$$V_{123} = V_L + V_{RST} = L \cdot \frac{di_{RST}}{dt} + V_{RST} \qquad \begin{cases} v_{123} = [v_{1n} v_{2n} v_{3n}]^T \\ i_{RST} = [i_R i_S i_T]^T \\ v_{RST} = [v_{Rn} v_{Sn} v_{Tn}]^T \end{cases} \tag{1}$$

$$V_{inv\_dq} = PV_{123} = P \cdot L \frac{d\left(P^{-1} i_{dq}\right)}{dt} + PV_{RST} = L \cdot P \frac{dP^{-1}}{dt} \cdot i_{dq} + L \cdot P \cdot P^{-1} \frac{di_{dq}}{dt} + V_{grid\_dq} =$$
$$= L\omega \begin{bmatrix} 0 & -1 \\ 1 & 0 \end{bmatrix} i_{dq} + L \frac{di_{dq}}{dt} + V_{grid\_dq} \Rightarrow \begin{cases} V_{inv\_d} = V_{grid\_d} - L \cdot \omega \cdot i_q + L \dfrac{di_d}{dt} \\ V_{inv\_q} = V_{grid\_q} + L \cdot \omega \cdot i_d + L \dfrac{di_q}{dt} \end{cases} \tag{2}$$

- R, S, T represent the three phases
- P and P^{-1} is the Park and Inverse Park transformation matrices which are given by equations 3 and 4 respectively [166, 167].

$$P = \sqrt{\frac{2}{3}} \begin{bmatrix} \cos\theta & \cos(\theta - \frac{2\pi}{3}) & \cos(\theta + \frac{2\pi}{3}) \\ -\sin\theta & -\sin(\theta - \frac{2\pi}{3}) & -\sin(\theta + \frac{2\pi}{3}) \\ \frac{1}{\sqrt{2}} & \frac{1}{\sqrt{2}} & \frac{1}{\sqrt{2}} \end{bmatrix} \tag{3}$$

$$P^{-1} = \sqrt{\frac{2}{3}} \begin{bmatrix} \cos\theta & -\sin\theta & \frac{1}{\sqrt{2}} \\ \cos(\theta - \frac{2\pi}{3}) & -\sin(\theta - \frac{2\pi}{3}) & \frac{1}{\sqrt{2}} \\ \cos(\theta + \frac{2\pi}{3}) & -\sin(\theta + \frac{2\pi}{3}) & \frac{1}{\sqrt{2}} \end{bmatrix} \quad (4)$$

The control is based on the idea of synchronising the inverter with the grid voltage vector (V_{red}), V_S and the d-axis as depicted in Fig. T-2 beneath. This process takes place through the Park transformation.

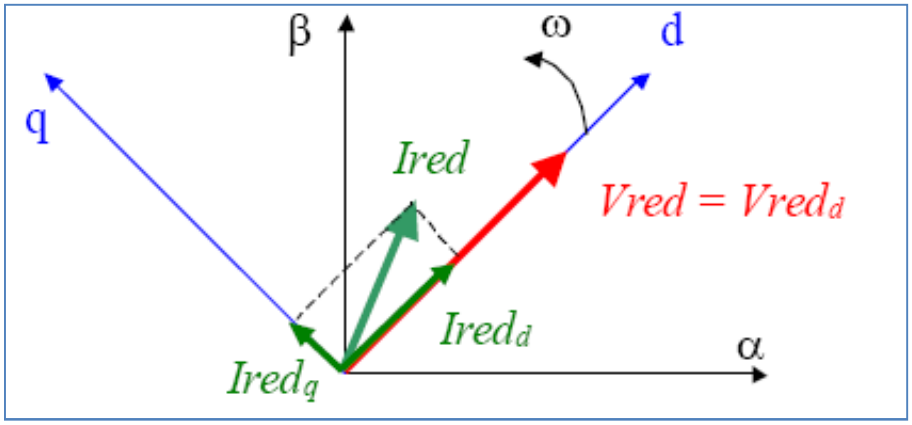

Figure T-2: *Current space vector and its component in (α, β) and in the d, q rotating reference frame [167].*

The following equations are derived:

$$P_{grid} = V_{grid\_d} \cdot I_{grid\_d} + V_{grid\_q} \cdot I_{grid\_q} \qquad Q_{grid} = V_{grid\_q} \cdot I_{grid\_d} - V_{grid\_d} \cdot I_{grid\_q} \quad (5)$$

$$V_{grid\_d} = V_{grid} \quad \& \quad V_{grid\_q} = 0 \quad (6)$$

$$P_{grid} = V_{grid\_d} \cdot I_{grid\_d} \quad \& \quad Q_{grid} = -V_{grid\_d} \cdot I_{grid\_q} \quad (7)$$

Appendix U: STATCOM & ESS Models

The STATCOM's control function block consists of four inputs, namely the DC reference voltage (V_{dc_ref}), the q-coordinate of the reference current (I_{q_ref}), the three-phase current and voltage measurements (I_{abc} & V_{abc}). The output of the inverter's control block is three signals that represent the three-phase voltages, i.e. V_a, V_b, V_c.

The three-phase sinusoidal current and voltage vectors are converted into their d and q coordinates via Park transformation (P block) as depicted below in Fig. T-1. In addition, the inverter's control consists of two regulation loops, one for the current and one for the voltage (Fig. 5-3 & 5-4).

The current regulation loop consists of two proportional-integral (PI) controllers that control the d-axis and q-axis currents. The controllers' outputs are the V_{d_ref} and V_{q_ref} voltages. The V_{d_ref} and V_{q_ref} voltages are converted into phase voltages V_a, V_b, V_c via the anti-park transformation (1/P block) and are used to feed the controllable voltage sources (Fig. T-2). The Id reference (in our case I_{d_ref}) comes from the DC-link voltage regulator. The I_q reference (in our case I_{q_ref}) comes from the q coordinate of the load current.

The voltage regulation loop consists of a DC voltage controller which keeps the DC link voltage constant to its nominal value using a PI controller maintaining. On the DC side, the inverter is modeled by a current source charging the DC capacitor (Fig. T-3). The DC reference current $I_{\_dc}$ is computed so that the instantaneous power at the AC input of the inverter remains equal to instantaneous power at the DC output (P_{AC}=P_{DC}).

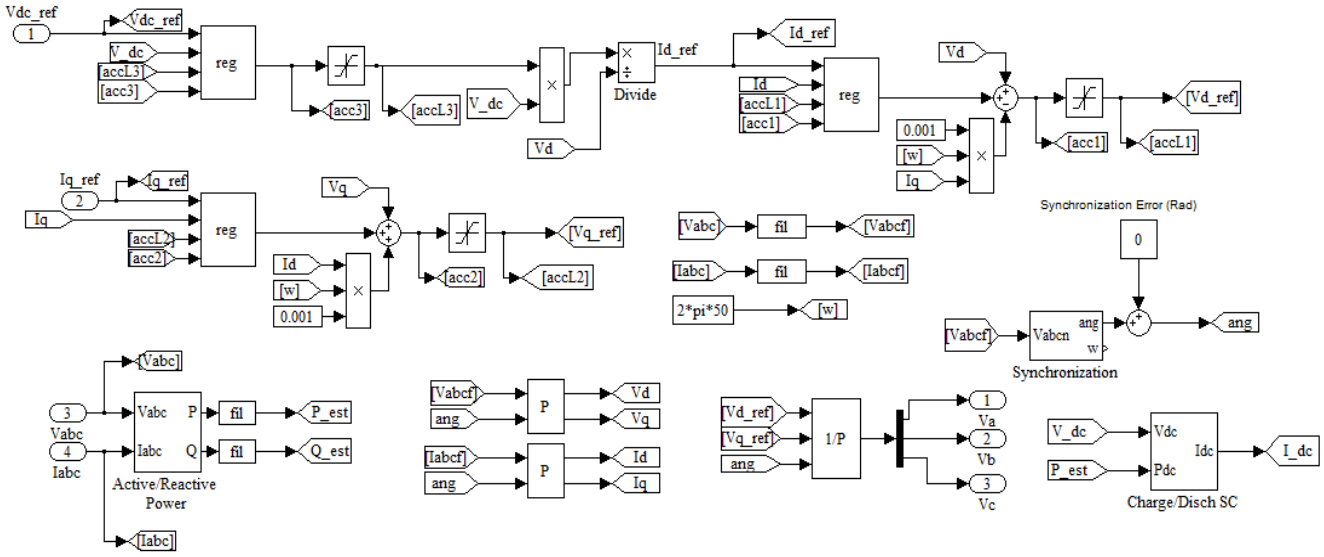

Figure U-1*: Control function blocks of the STATCOM Average Model [126].*

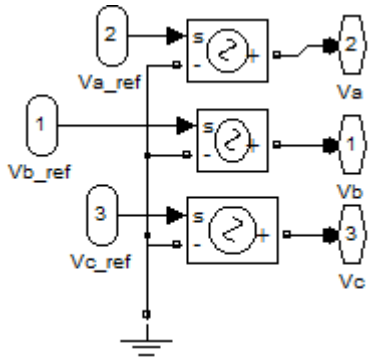

Figure U-2: *STATCOM Average Model [126].*

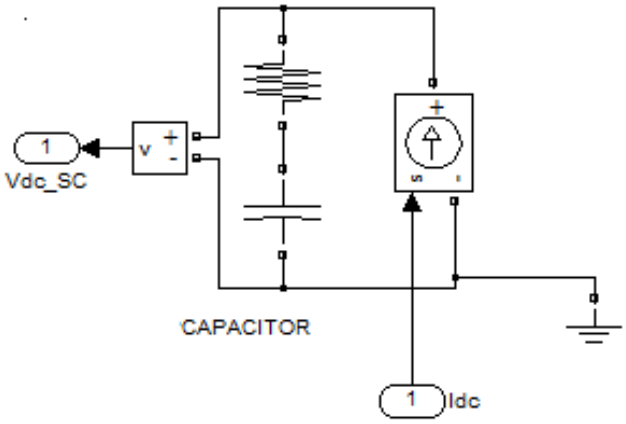

Figure U-3: *Capacitor Model [126].*

Appendix V: Publications

Herein, written articles are cited in the field of this thesis with the following order:

- Konstantina Mentesidi and Monica Aguado, "The potential integration of electrical distributed generation in an island power system," in *International Journal of Distributed Energy Resources and Smart Grids*, vol. 9, no. 4, pp. 341-366, 2013.

- Konstantina Mentesidi, Evangelos Rikos, Vasilis Kleftakis, Panos Kotsampopoulos and Monica Aguado, "Real time Simulation Technique of a Microgrid Model for DER Penetration", in *EAI Endorsed Transactions on Energy Web. In Press.*

- Konstantina Mentesidi, Mikel Santamaria, Athanassios Vassilakis, Alexandros Rigas, Vasilis Kleftakis, Panos Kotsampopoulos and Monica Aguado, "Power Hardware-In-The-Loop technique applied to a LV Network for integrating a Supercapacitor with an Average Model of STATCOM," in *IEEE International Workshop on Intelligent Energy Systems (IWIES 2013)* Vienna, Austria, November, 2013, pp. 167-172. *IEEE Indexed Conference Paper.*

- Konstantina Mentesidi and Monica Aguado, "Dynamic behavior analysis of distributed generation in an off-grid network with power system simulator for engineering (PSS/E)," in *IEEE International Energy Conference, ENERGYCON 2014*, Cavtat, Croatia, May 2014, pp. 1042-1049. *IEEE Indexed Conference Paper.*

- Konstantina Mentesidi, Evangelos Rikos, Vasilis Kleftakis, Panos Kotsampopoulos, Mikel Santamaria, and Monica Aguado, "Implementation of a Microgrid model for DER Integration in Real time Simulation Platform," in 23rd *International Symposium on Industrial Electronics (ISIE 2014)* Istanbul, Turkey, June, 2014, pp. 2274-2279. *IEEE Indexed Conference Paper.*

THE POTENTIAL INTEGRATION OF ELECTRICAL DISTRIBUTED GENERATION IN AN ISLAND POWER SYSTEM

Konstantina Mentesidi[1,2], Mónica Aguado[1,2]
[1]Grid Integration Department, National Renewable Energy Centre (CENER)
Ciudad de la Innovacion 7, 31621 Sarriguren-Spain
Phone (34) 948252800, Fax (34) 948270774
[2]Electrical & Electronic Engineering Department, Public University of Navarra
E-mail: kmentesidi@cener.com

Keywords: dynamic analysis; distributed generation; LV-grid; PSS®E

ABSTRACT

The sizing and allocation of distributed generation technologies into LV-grids creates a number of technical issues. In order to analyze a grid from an electrical point of view and define the potential sites suitable for distributed power penetration, considerations such as power quality, grid capacity and limits characterization need to be taken into account. In the current paper, Steady State and Dynamic Analysis configurations are proposed in order to determine the allocation, maximum capacity of non-conventional generation that may be inhabited within an Island low voltage grid. In addition, the dynamic behaviour of the system is checked under normal operation and against several disturbances onto the grid. Geothermal plants and wind farms employing Doubly-fed Induction Generator (DFIG) technology were chosen to investigate the impact may induce any units´ addition on the power system´s load flow, short circuit levels (SCL) and transient stability. A group of substations were proposed to introduce the dispersed generation with the extension in mind to suggest the voltage level to connect these units. The main issues addressed were the total system losses, fault level at the addition and nearby buses, whereas among the most critical perturbations was a three phase fault application at the connection point of the wind farm. PSS®E software simulation tool of Siemens PTI will be utilized throughout this work.

Este artículo ha sido eliminado por restricciones de derechos de autor

EAI Endorsed Transactions
on Energy Web
Editorial ICST.ORG

Real-Time Simulation Technique of a Microgrid Model for DER Penetration

Konstantina Mentesidi[1,*], Evangelos Rikos[2] , Vasilis Kleftakis[3] , Panos Kotsampopoulos[3] and Monica Aguado[1]

[1]K. Mentesidi and Monica Aguado are with the Grid Integration department of CENER, National Renewable Energy Centre, Navarra, Spain (kmentesidi@cener.com, maguado@cener.com).
[2]E. Rikos is with the department of Photovoltaics and Distributed Generation of CRES, Athens, Greece (vrikos@cres.gr).
[3]V.Kleftakis and P. Kotsampopoulos are with School of Electrical and Computer Engineering of the National Technical University of Athens, Greece (vkleft@mail.ntua.gr, kotsa@power.ece.ntua.gr).

Abstract

Comprehensive analysis of Distributed Energy Resources (DER) integration requires tools that provide computational power and flexibility. In this context, throughout this paper PHIL simulations are performed to emulate the energy management system of a real microgrid including a diesel synchronous machine and inverter-based sources. Moreover, conventional frequency and voltage droops were incorporated into the respective inverters. The results were verified at the real microgrid installation in the Centre for Renewable Energy Sources (CRES) premises. This research work is divided into two steps: A) Real time in RSCAD/RTDS and Power Hardware-in-the-Loop (PHIL) simulations where the diesel generator´s active power droop control is evaluated, the battery inverter´s droop curves are simulated and the load sharing for parallel operation of the system´s generation units is examined. B) microgrid experiments during which various tests were executed concerning the diesel generator and the battery inverters in order to examine their dynamic operation within the LV islanded power system.

Keywords: droop control, power hardware- in- the- loop (PHIL), RSCAD/ RTDS.

Received on DD MM YYYY, accepted on DD MM YYYY, published on DD MM YYYY

doi: 10.4108/_____

*Corresponding author. Email:kmentesidi@cener.com

1. Introduction

Due to the particular structure and characteristics of distributed networks, like islanded or autonomous power systems, the penetration of distributed generation and renewable energy sources may provoke problems and constraints which lead to limitations of their integration level into this type of power systems.

The transition to distributed generation systems requires dynamic and flexible tools for simulation and testing since the core of such active networks is depicted by the power converters. Thus, it is important to research on their control performance and the interaction of the devices connected to these grids since they may induce serious impacts on the power quality parameters.

An approach for studying such systems' dynamic behavior is by means of real time simulation [1]. The most considerable advantage of this type of simulation platform is that the system can be interfaced to real hardware components, generally called as hardware under test (HuT). This is widely known as hardware-in-the-loop simulation and particularly when the HuT is a power device, as Power hardware-in-the-loop simulation (PHIL) [2]. Real time simulations and especially PHIL allow for testing and validation of the electrical properties of power system devices such as converters, wind energy generators, hybrid and energy storage systems. This kind of experimenting gives the possibility to test repeatedly and analyze the behavior of the physical device, very

close to realistic conditions [3-5]. For instance, the hardware part can be subjected to several simulated fault incidents and its resulting response can be verified.

Several researches involve the PHIL concept using the Real Time Digital Simulation (RTDS) [6] as a powerful tool to perform flexible and high-speed real time simulations [1-3], [7-14]. RTDS uses a graphical environment to build up the simulated network of any complexity.

The deployment of RTDS/RSCAD simulations and PHIL laboratory tests as a data reference for verification in the domain of DER integration is relatively constrained up to now. Specifically, the existent literature is very limited regarding this kind of tests that study the control strategy of LV islanded power networks with the integration of inverter-based devices and even energy storage systems. The prevalent advantage of this kind of experimenting is that at the end is viable the implementation and development of a methodology that characterizes the energy supply devices and system analysis for decentralized grid services.

An implementation of real time simulation of distributed generation systems in RTDS was accomplished by NTUA [3]. Within this research work, a thorough description of the design and development of a PHIL set-up for DER devices is validated through laboratory experiments. Specifically, a PHIL implementation of a voltage divider was performed and the closed-loop synergy between a simulated LV network and hardware such as PVs and inverter was demonstrated.

The objective of the current paper is to execute real time simulations in RSCAD/RTDS of a LV islanded power system's energy management, to study its control strategy i.e. droop control and conduct PHIL laboratory tests as a data reference for verification. The hardware part utilized throughout these experiments was a variable resistive load of 105.8 Ohm. Moreover, for tests aiming at analyzing the energy transfer in an **AC** microgrid, a set of experiments were conducted related to the diesel generator and the battery inverters that were available in CRES premises. Hence, real time simulations will be reinforced and this will not only allow us to size and locate the distributed generation systems, but also will let us optimize MV/LV networks and in generally autonomous powers networks, and likely introduce energy storage.

The paper is structured as follows: Section 2 describes the microgrid case study for the simulations. An overview of the real-time simulation and the implementation of the PHIL environment for executing the tests described in this paper are given in Section 3. Section 4 describes the simulation, PHIL laboratory and experimental test results, whereas Section 5 summarizes the conclusions.

2. Microgrid Case Study

The present research work was jointly completed by ICCS-NTUA and CRES research infrastructures. In the former PHIL simulations were executed to emulate the behavior of a LV islanded power system including a diesel genset and inverter-based sources. Moreover, f-P and V-Q droops were incorporated into the respective inverters. The results were then verified at the real microgrid site in CRES premises. Fig. 1 illustrates the CRES microgrid infrastructure.

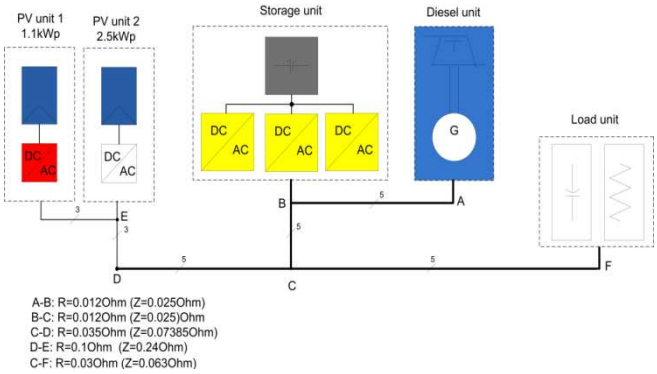

Figure 1. CRES microgrid topology.

The microgrid was setup and used either in single or in three-phase configuration according to the specific test. Unbalanced loading was also examined.

The DER units that were used for the tests include 3 battery inverters (13.5kWp), 1 diesel generator (12.5kVA), one load bank (13.5kW), 2 PV panels (1.1 and 2.5kW) and one three-phase capacitor. The operation and supervision of each unit is done using the local SCADA system, while for some measurements, portable equipment like current clamps and oscilloscopes were used. The fast transients and waveforms were measured by using oscilloscope.

The battery inverters used in the experimental tests are the SMA-Sunny Island 4500 inverters. By default, one of the inverters is connected to the appropriate grid phase and can operate in all possible modes such as grid-forming and grid-connected with droop characteristics. The other two inverters were reconfigured appropriately so that they operate under different modes.

The loads used in the experimental tests are 3 groups of resistors (2.5, 1.5 and 0.5kW), which are combined appropriately in order to obtain the maximum number of combinations.

2.1. Diesel Generator Droop Characteristics and Tests

The diesel unit´s droop for the microgrid experiments is considered arbitrarily as **-0.06Hz/kW** according to its governor's settings. Moreover, it is defined by (1) where Δf is the absolute change in the frequency (Hz) and ΔP is the absolute difference in the output power (kW) that caused the subsequent change in the frequency.

$$R = -\frac{\Delta f}{\Delta P} \quad (1)$$

The diesel generator is studied in islanded mode under load variations where an increase in load demand imposes an increase in diesel power output and a subsequent reduction in torque frequency.

In order to determine the frequency droop curve, one has to vary the active power exchanged by the generator with the microgrid and measure the corresponding frequency at the output of the diesel genset. Thus, its f-P droop curve was experimentally derived under symmetric and asymmetric loads.

2.2. Battery Inverter Characteristics and Tests

The f-P and V-Q droops of the SI inverter [15] are given by (2) and (3) respectively where the parameters are set to: i) Δf_{pu}=-2%, ii) ΔV_{pu}=-6%. Moreover, these droop curves were utilized for the RSCAD simulations.

$$f = 50 - \frac{1}{3.3} P \Leftrightarrow P = 3.3(50 - f) \quad (2)$$

$$V = 230 - 4.1818Q \Leftrightarrow Q = 0.239(230 - V) \quad (3)$$

The frequency droop curve was experimentally derived. In order to obtain each inverter's droop curve, data sets consisting of inverter's output frequency and active power have to be available. Not only the f-P droop calculation was evaluated but also the frequency, active and reactive power responses with static load changes.

3. Real-Time Simulations & PHIL Set-Up

Fig. 2 depicts the PHIL topology as implemented in NTUA research infrastructure.

In order to demonstrate the actual test with the PHIL setup, a series of preliminary actions had had to be pursued. The first simulation task was implemented on a three phase LV distribution network with and without the integration of the battery inverter. Subsequently, the system´s frequency was checked upon load changes with and without the storage penetration. In order to verify the frequency and power responses at the diesel generator´s terminals, a change of 105.8 Ohm was implemented in the resistive load at each phase with the utilization of a breaker.

The Power Hardware in the Loop experiments involved the following steps:

- The protection modules were added into the RSCAD/RTDS simulated model to ensure the safe operation of the RTDS during the PHIL tests
- The physical setup was verified
- The power amplifier was tested and the simulation was executed in open loop
- The loop was closed and the experiments were performed

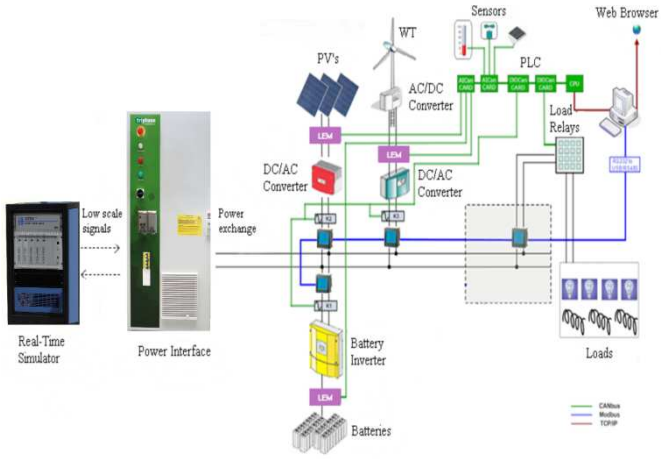

Figure 2. PHIL environment in NTUA Lab for DER devices.

Fig. 3 shows the power system model during the PHIL test. The network topology includes a diesel generator, 2 LV lines, a bank of restive loads and a three-phase inverter.

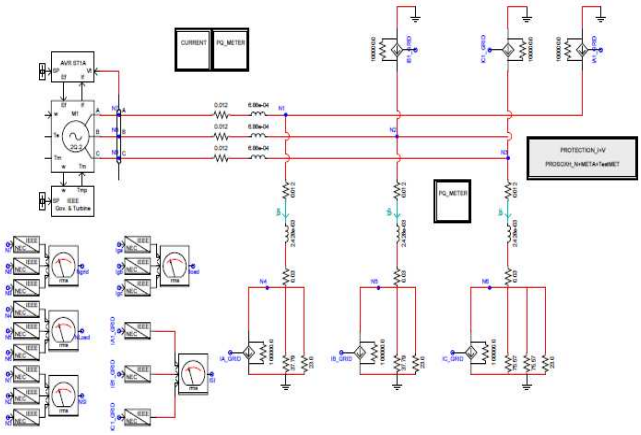

Figure 3. RSCAD/RTDS model during the PHIL test.

Table 1, 2 and 3 summarize the network parameter values and the diesel generator internal characteristics necessary for the execution of the real time simulations. The diesel unit's droop is considered as **-6%** (in percentage rates) for the RSCAD simulations.

Table 1. System parameters

Network Parameters	Values
$Vg_{\_rms\ ph\text{-}ph}$	400 V
RL_{line1}	0.012+j6.88E-4 Ohm
RL_{line2}	0.042+j2.428E-4 Ohm
Diesel genset	13.164 kVA
Battery S_{nom}	3.3 kVA
R_{load}	12.6 kW
R_{HuT}	105.8 Ohm

Table 2. Diesel generator parameters (A)

Ratings		
3-phase Output	**Sn**	13.164 kVA
Voltage	**Un**	230.94 V
Current	**In**	19 A
Frequency	**f**	50 Hz
Speed	**n**	1500 rpm
Pair poles	**p**	4
Inertia Constant	**H**	1.7 MWs/MVA

Table 3. Diesel generator parameters (B)

Resistances		
Stator Winding	**Ra**	0.0096 Ohm
Reactances		
Stator leakage reactance	**Xa**	0.0576 pu
Synchronous - Direct Axis	**Xd**	2.9619 pu
Synchronous - Quadrature Axis	**Xq**	1.2067 pu
Transient - Direct Axis	**X'd**	0.2304 pu
Transient - Quadrature Axis	**X'q**	0.228 pu
Subtransient - Direct Axis	**X''d**	0.0932 pu
Subtransient - Quadrature Axis	**X''q**	0.1097 pu
Time Constants		
D: Open Circuit-Transient	**T'do**	4.3 s

3.1. PHIL Interface Concerns

Power Hardware–in-the-Loop technique employs as hardware part a device that generates or absorbs power, such as a PV inverter or an induction motor. Here, the presence of a power interface is necessary since it exchanges low voltage signals with the simulated system and real power with the HuT, thus the digital to analogue and vice versa converters cannot participate sufficiently in this trade-off .

The power interface being used throughout this paper for the experimental procedure consisted of a single phase (5KVA) AC/DC/AC converter and enables the low power output signal (i.e. I_{HuT_low} and reference voltage labeled as V_{N*}) of the RTDS to be amplified to a higher voltage signal (i.e. V_N). This voltage is applied to the HuT device (in our case an actual load) and provokes a current flow through it. The current waveform is measured by the power interface's sensor and is fed back to the RTDS to close the loop (Fig. 4).

PHIL technique is a novel approach and offers great flexibility in arranging and performing various test scenarios for DER devices since the virtually simulated system can be modified without hardware adaptions, in addition to the fact that the tests can be repeated quickly and accomplished very close to realistic conditions.

However, PHIL simulations occupy a closed-loop interaction. Shortcomings that inherently lie in this closed-loop can reduce the accuracy of the simulation and may evoke instability. These imperfections in the closed-loop topology are mainly produced by the Power Interface, such as the time delay and the low pass filter of the amplifier, the time delay of the sensor and the sensor's noise [4]. Moreover, a time-delay is introduced by the RTDS.

3.1.1. Power Amplifier

The basic components of a power interface are the power amplifier and a sensor. The former amplifies the low level signals received from the RTS to the HuT at higher power ratings, thus high accuracy and small-time delay are key considerations.

The power amplifier used for this contribution is an unconventional single-phase bidirectional AC/DC/AC converter consisting of 3 IGBT half-bridges [4]. The converter is coupled to the utility grid on the one-side and runs as a voltage source of variable voltage and frequency on the other-side. Additionally, the analogue signals exchanging with the utility grid and the microgrid components is done on a conversion time of about 40μsec, 16 bit resolution and ± 10V range.

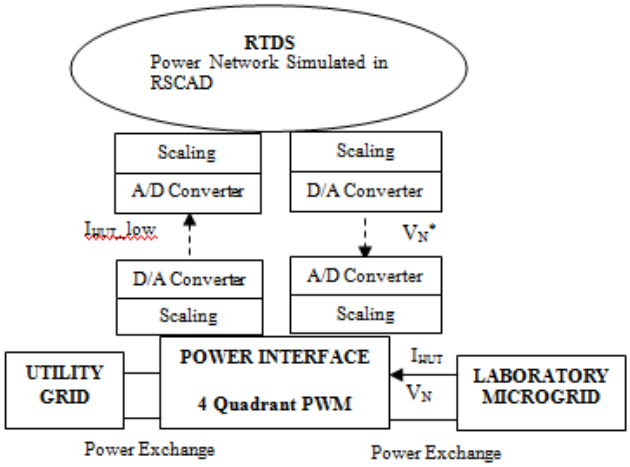

Figure 4. Representation of the PHIL environment.

The power electronic converter platform permits the user to model the control scheme in Matlab/Simulink, with access to the available measurements and the possibility to change some control parameters online. In this case, the control algorithm of the given converter was provided by the manufacturer and it was modified in order to fulfill the two basic functions which a power interface needs to provide with during a PHIL simulation, i.e. voltage amplification and supplying current feedback signal [4].

Equation (4) gives the transfer function of the power amplifier's second order output filter utilized throughout

the experiments. This transfer function is basically drawn from the introduced time delay and the output filter of the power converter [4].

$$T_f(s) = \frac{\omega_n^2}{s^2 + 2\xi \cdot \omega_n \cdot s + \omega_n^2} = \frac{(1500\pi)^2}{s^2 + 2100s + (1500\pi)^2} \quad (4)$$

- ω_n, the resonance angular frequency.
- ξ, the damping ratio.

The total time delay in the current PHIL experiments was about 750μsec.

3.1.2. Stability and Accuracy Considerations

Before performing a PHIL test, it is crucial to ensure that the experiment will be stable. Consequently, throughout this research work virtual hardware-in-the-loop experiments (off-line simulations) were performed in Matlab/Simulink to check the system's stability for the different test scenarios presented in the following section.

Furthermore, stability should be accompanied by an adequate accuracy of the experiments' outcomes. Therefore, the entire closed loop system was simulated, and the results were compared with the outputs from the PHIL tests in order to assess their accuracy.

Apart from the comparison of the PHIL results with the corresponding outcomes from the off-line simulations, the validity of monitored quantities (current and voltage rms values) was also obtained through comparison of several measurements at different points in the system. For instance, the current through the hardware impedance (105.8 Ohm) was monitored by measurements of the Power Interface, an oscilloscope, and the software of the RTDS.

3.1.3. Protection Issues

Over-current and over-voltage protection schemes are introduced into the RTDS/RSCAD at the shared node between the simulation and hardware. Fig. 5 beneath illustrates the protections implemented for the execution of the PHIL experiments conducted for this research work.

In case the pre-determined limits are exceeded, I_{HuT} becomes zero and the voltage reference sent to the amplifier is held constant to a specific value. Subsequently, the output of the RTDS will be maintained constant and the PHIL test will be terminated. Flip-flops are employed to ensure the safe operation of the system if an instability incident takes place.

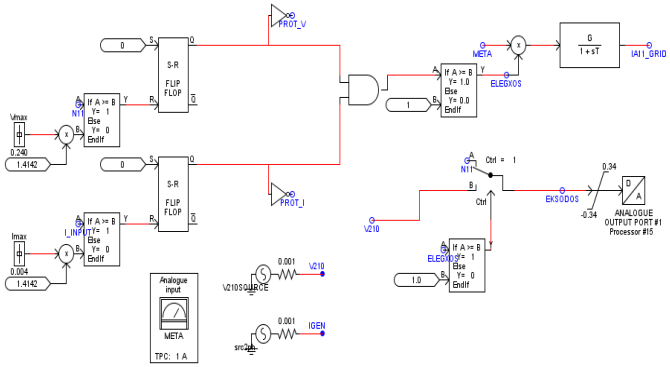

Figure 5. Protection design implemented in RTDS/RSCAD.

4. Results and Discussion

4.1. Experimental Results

The diesel generator suffers from frequency and voltage fluctuations due to harmonics distortion in the pulsating torque. Fig. 6 depicts the frequency oscillation upon an indicative step change from 6 to 12 kW and 12 to 0 kW respectively in load demand. In transducer's scale, 1V corresponds to Hz and 5V to 50 Hz.

Evidently, the diesel generator suffers from inherent frequency and voltage flickering. Moreover, the diesel f-P droop curve was experimentally derived under asymmetric and symmetric loads. The following captures (Fig. 7&8) illustrate these results respectively.

It is worth mentioning that under asymmetric loading the droop and idle frequency (fidle) differs from phase to phase where the biggest difference is detected on phase A. Table 4 summarizes this deviation in values. However, for a three-phase symmetric load the droop characteristic was confirmed at -0.06Hz/kW (Fig. 8).

Table 4. Asymmetric loads

Phase	Droop (Hz/kW)	Fidle (Hz)
A	-0.04422	50.2
B	-0.07529	50.35
C	-0.08298	50.375

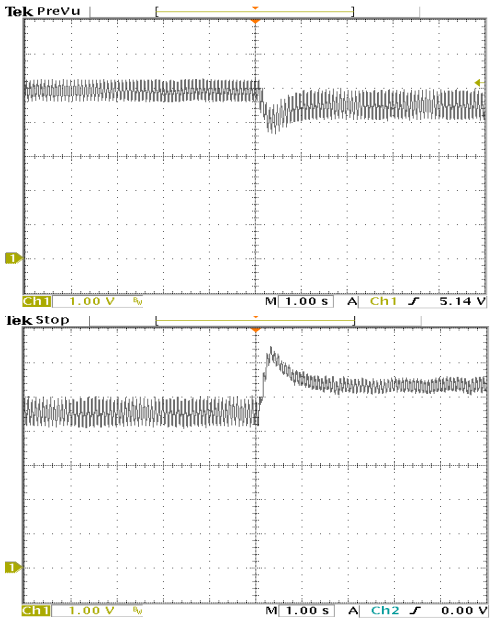

Figure 6. Diesel's frequency response under load stp change 6➔12 kW and 12➔0 kW.

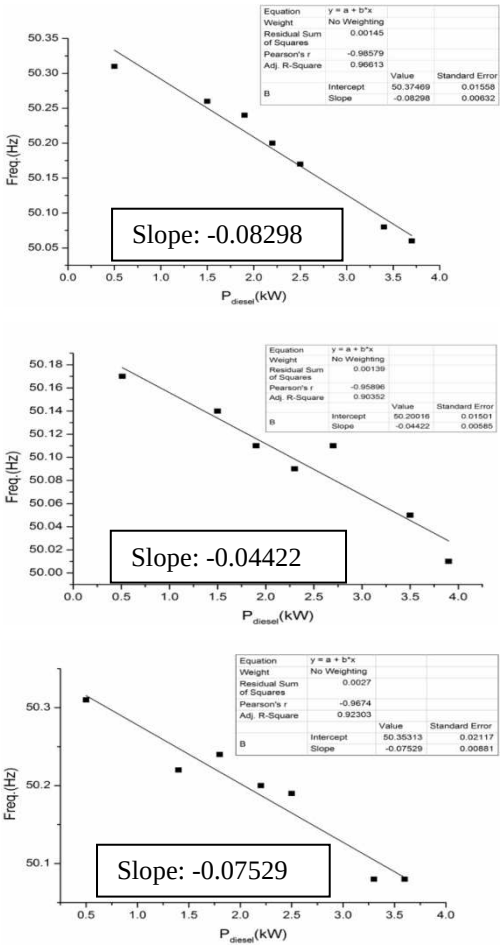

Figure 7. The measured f-P droop curve of the diesel genset for asymmetric loads.

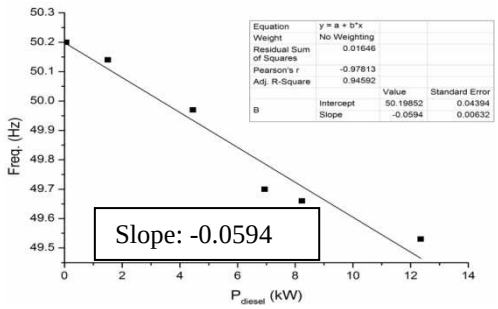

Figure 8. The measured f-P droop curve of the diesel genset for 3-phase symmetric loading.

It is hypothesized that this deviation is due to possible errors in data logging of the diesel genset´s droop and idle frequency potentiometers resulting in a slight change in the governor´s gains. This change can be attributed to environmental conditions, and especially temperature due to heat at the test site that can affect the results of the experiments.

The following figures (Fig. 9-11) illustrate the exerimental results from the battery inverters' tests. In order to obtain each inverter's droop curve, data sets consisting of inverter's output frequency and active power have to be available. In more details, the f-P droop calculation was evaluated with static load changes and only one inverter being in use. The Sunny Boy PV inverter is also included. Moreover, the f-P droop was measured for operation of the three inverters (master-slave) with static load variation and asymmetries.

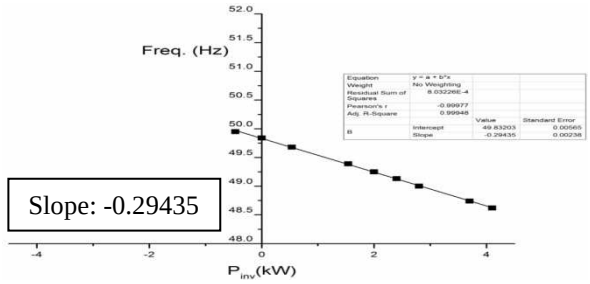

Figure 9. The f-P droop curve of one battery inverter (phase A).

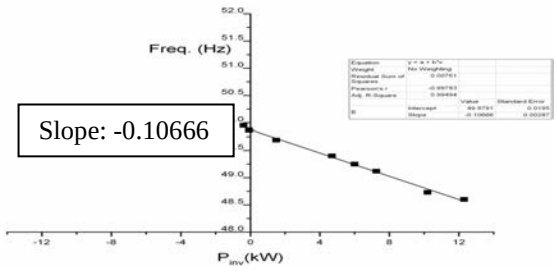

Figure 10. The f-P droop calculation for three-phase operation.

In general, the Master Inverter defines the frequency in both cases: Either when it is connected to one phase or when the three inverters are connected to the three phases

(master-slave operation); i.e. at 4.1 kW (single-phase) and 12.3 kW (three-phase) load demand, the frequency is the same at the figure of 48.6 Hz. In addition, under asymmetric loads any variation in the master inverter´s power output will once again define the change in the frequency. For instance, in our case the master inverter is connected to phase A, thus any changes in load demand at this phase and only in this phase will dominantly affect the frequency behavior. This result is evident in Fig. 11.

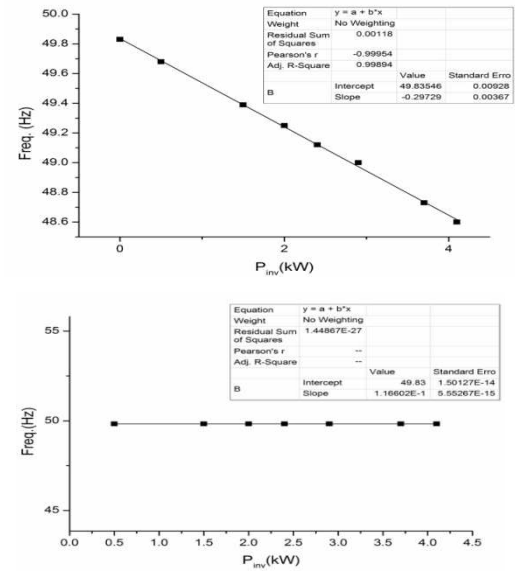

Figure 11. The f-P droop curve for asymmetric load variation with phase A (master inverter) and phases B, C (slave inverters).

Fig. 12 shows the f-P droop curve for the three inverters with a 2-hr load profile.

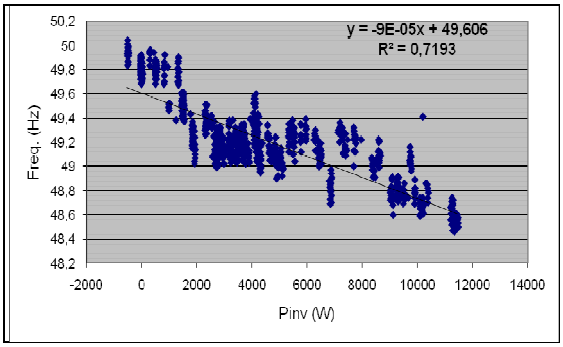

Figure 12. The battery inverters´ f-P droop curve for a 2-hr load profile.

One additional experiment included the investigation of the frequency and voltage behavior of the battery inverter by changing the load demand and switching the mode operation (grid connected to islanded transition). Fig. 13-15 depict these outcomes. First of all, in Fig. 13 only the master inverter is connected to phase A while the microgrid is islanded. The frequency and voltage fluctuations are derived from no-load to full load step change, i.e. 0 kW -4.1 kW.

Regarding the disconnection tests, the inverter´s voltage waveform does not change (Fig. 14) because the load is purely restive and not reactive, whereas its frequency suffers from a drop of 1.22 Hz, namely from 49.84 Hz to 48.62 Hz.

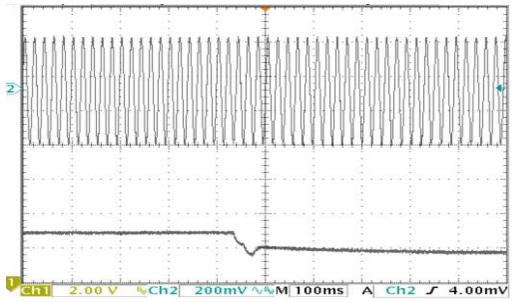

Figure 13. Battery inverter´s voltage and frequency response under step-change in the load.

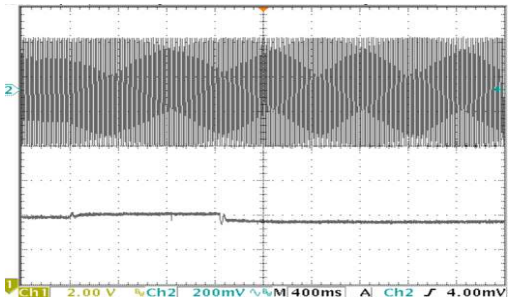

Figure 14. Master inverter´s voltage disturbance (DroopMains mode).

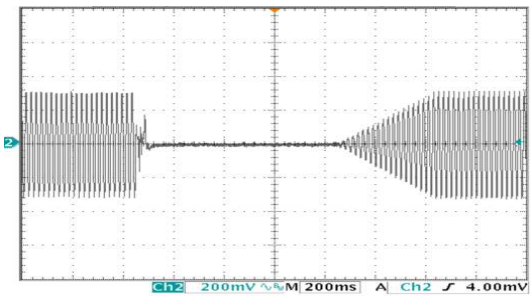

Figure 15. Master inverter´s voltage disturbance (Fast Mains mode).

In Fast Mains operation the voltage falls to zero as it was expected when switching from grid connected to disconnected operation and the Sunny Island is behaved as grid former. Contradictorily, in DroopMains operation the voltage is undisturbed and the frequency falls to 49.6 Hz.

The last experiment involved the load sharing for parallel operation of two SI inverters being both connected in one phase and demonstrate the concept of the battery inverters' active power control by changing the frequency droop (droop f) curve. For all the following

cases, the output power is measured: a) different droops (-2Hz/Pnom, -1Hz/Pnom) and fiddle (intersection of the droop f curve with the f axis) is of 50 Hz, b) same droop (-1Hz/Pnom) and fidle=50 Hz and c) same droop (-1Hz/Pnom) but the idle frequency is changed to 50.3 Hz. Figure 16 illustrates these results respectively.

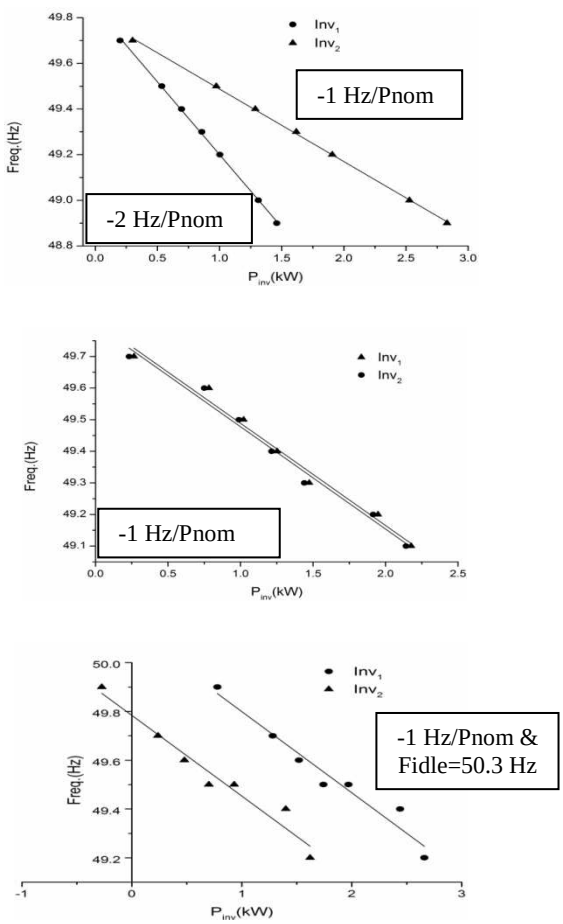

Figure 16. Load sharing for parallel operation of two Inverters.

4.2. Real-Time Simulations

Tables 5 and 6 summarize the real time simulation results without and with the storage inclusion respectively. As it can be easily seen from the frequency figures beneath, the battery inverter presence enhances the frequency stability by covering part of the load change.

Table 5. Numerical results without storage

Basic Load	Full Load
P_{diesel}= 10.92 kW	P_{diesel}=12.33 kW
f=50 Hz	f=49.68 Hz
Q_{diesel}= 0.689 kVAr	Q_{diesel}= 0.8933 kVAr
P_{load}= 10.88 kW	P_{load}=12.3 kW
P_{diesel}= 10.92 kW	P_{diesel}=12.33 kW

Table 6. Numerical results with storage

Basic Load	Full Load
P_{diesel}= 10.93 kW	P_{diesel}=11.74 kW
f=50 Hz	f=49.81 Hz
Q_{diesel}= 0.6898 kVAr	Q_{diesel}= 0.8601kVAr
P_{inv}= -0.05 kW	P_{inv}= 0.6173 kW
Q_{inv}= 0.3035 kVAr	Q_{inv}= 0.374 kVAr

Fig. 17 & 18 show the RSCAD/RTDS numerically transient responses with and without the battery inverter penetration respectively.

From (1) and considering that the diesel active power output is rated at Pdiesel= 10.92 kW, the diesel droop characteristic is given by (5) beneath. Moreover, it is confirmed at 6%.

$$P_{diesel} = 10.92 + \frac{13.164(50 - f)}{3} \quad (5)$$

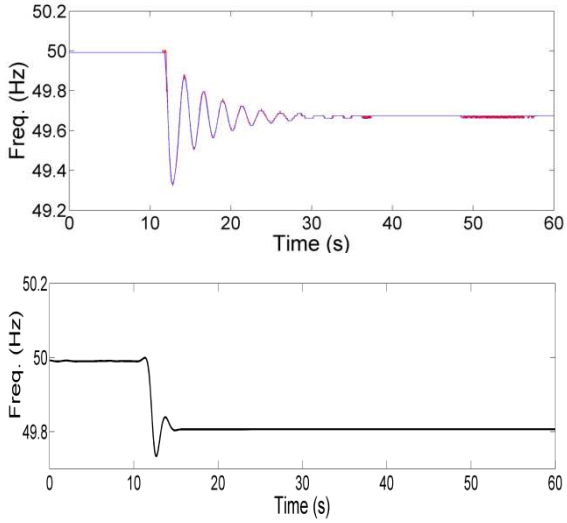

Figure 17. Frequency response (load change) without & with storage.

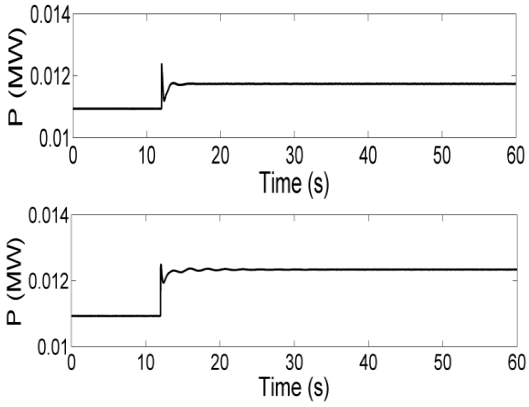

Figure 18. Diesel´s active power output with & without the battery inverter (load change).

4.3. PHIL Operation Outcomes

Fig. 19 & 20 show the RSCAD/RTDS transient responses with load change during the PHIL tests.

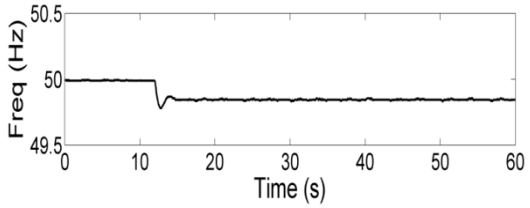

Figure 19. Frequency response during the load change.

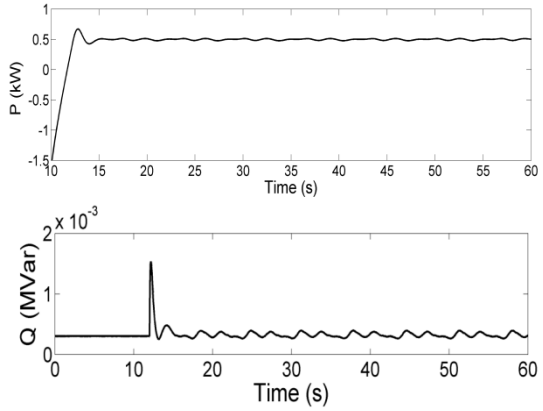

Figure 20. Battery Inverter active and reactive power responses.

Acknowledgements.
This work is co-funded by the European Commission within the Seventh Framework Programme (FP7/2007-2013) DERri under grant agreement n° 228449.

5. Conclusions

PHIL experiments render high flexibility in the research of the complex problems which concern the penetration of various energy systems with respect to network stability and security.

This study demonstrated an implementation of a microgrid model in real-time simulation platform for DER device integration. PHIL simulations were executed to emulate the energy management of a real microgrid system including a diesel synchronous machine and inverter-based sources.

Moreover, their dynamic behaviour was examined within the LV islanded power system and more than that the adequate performance of the laboratory set-up is verified through tests on a real experimental site.

Concluding, RSCAD/RTDS is an effective tool suitable for transient analysis due to its fast computation in real time and the laboratory hardware interfacing capability it offers. Additionally, at a later time, it is planned to extend the model in RSCAD/RTDS by including more simulations and experiments such as to examine the load sharing for parallel operation of two battery inverters being both connected in one phase and demonstrate the concept of the battery inverters' active power control by changing the frequency droop curve.

References

[1] P. Kotsampopoulos, A. Kapetanaki, G. Messinis, V. Kleftakis, N. Hatziargyriou, “A PHIL facility for microgrids”, International Journal of Distributed Energy Resources, vol. 9, no. 1, pp. 71-86, January-March 2013.

[2] P. Crolla, A.J. Roscoe, A.Dysko and G.M. Burt, “Methodology for testing loss of mains detection algorithms for microgrids and distributed generation using real-time power hardware-in-the-loop based technique”, The 8th International Conference on the Power Electronics-ECCE Asia, May 30-June 3, 2011, Korea.

[3] P. Kotsampopoulos, V. Kleftakis, G. Messinis, N. Hatziargyriou, “Design, development and operation of a PHIL environment for distributed energy resources”, The 38th Annual Conference of the IEEE Industrial Electronics Society IECON 2012.

[4] F. Lehfuss, G. Lauss, P. Kotsampopoulos, N. Hatziargyriou, P. Crolla and A.Roscoe., “Comparison of multiple power amplification types for Power Hardware-in-the-Loop applications”, IEEE Workshop on Complexity in Engineering (COMPENG 2012), June 11-13 2012, Aachen, Germany.

[5] A. Roscoe, A. Mackay, G. Burt and J. McDonald, “Architecture of a network-in-the-loop environment for characterizing AC power- system behavior”, IEEE Trans. Industrial Electronics, vol. 57, no 4, pp. 1245-1253, 2010.

[6] RTDS Technologies: http://www.rtds.com

[7] M. Steurer, F. Bogdan, W. Ren, M. Sloderbeck, S . Woodruff, “Controller and power hardware-in-loop methods for accelerating renewable energy integration”, Power Engineering Society General Meeting, IEEE , vol., no., pp.1-4, June 24-28 , 2007.

[8] V. Karapanos, S. de Haan, K. Zwetsloot, “Real Time Simulation of a Power System with VSG Hardware in the Loop”, Proc. IEEE Industrial Electronics Society IECON’2011, Australia, November 2011.

[9] M. Dargahi, A. Ghosh, G. Ledwich and F. Zare, “Studies in power hardware in the loop (PHIL) simulation using real-time digital simulator (RTDS)”, IEEE International Conference on Power Electronics, Drives and Energy Systems, December 16-19, 2012.

[10] P. McLaren, R. Kuffel, R. Wierckx, J. Giesbrecht and L.Arendt, “A real-time digital simulator for testing relays”, Power Delivery, IEEE Trans. on, vol. 7, pp. 207-2013, 1992.

[11] A. Sattar, A. Al-Durra and S. Muyeen, “Real time implementation of STATCOM to analyze transient and dynamic characteristics of wind farm”, 37th Annual Conference on IEEE Industrial Electronics Society, pp. 3742-3747, IECON 2011.

[12] G. Lauss, F. Lehfuss, A. Viehweider, and T. Strasser, “Power Hardware in the Loop Simulation with Feedback Current Filtering for Electric Systems,” 37th Annual Conference of the IEEE Industrial Electronics Society (IECON’2011), November 7-10, Australia, 2011.

[13] H. Li, M. Steurer , K.L. Shi , S. Woodruff, and D. Zhang,"Development of a Unified Design, Test, and Research Platform for Wind Energy Systems based on Hardware-In-the-Loop Real Time Simulation", IEEE Transactions on Industrial Electronics, Volume 53, Issue 4, June 2006 Page(s):1144 – 1151.

[14] O. Vodyakho, C.S Edrington, M. Steurer, S. Azongha, and F. Fleming,"Synchronization of three-phase converters and virtual microgrid implementation utilizing the Power-Hardware-in-the-Loop concept", 25th IEEE Applied Power Electronics Conference and Exposition (APEC), 2010.

[15] Sunny Island 4500 manual http://files.sma.de/dl/5614/SI4500-FEAT-11-EE4405.pdf

Konstantina Mentesidi, Evangelos Rikos, Vasilis Kleftakis, Panos Kotsampopoulos, Mikel Santamaria, and Monica Aguado, "Implementation of a Microgrid model for DER Integration in Real time Simulation Platform," in 23rd International Symposium on Industrial Electronics (ISIE 2014) Istanbul, Turkey, June, 2014, pp. 2274-2279. IEEE Indexed Conference Paper.

Konstantina Mentesidi and Monica Aguado, "Dynamic behavior analysis of distributed generation in an off-grid network with power system simulator for engineering (PSS/E)," in IEEE International Energy Conference, ENERGYCON 2014, Cavtat, Croatia, May 2014, pp. 1042-1049. IEEE Indexed Conference Paper.

Konstantina Mentesidi, Mikel Santamaria, Athanassios Vassilakis, Alexandros Rigas, Vasilis Kleftakis, Panos Kotsampopoulos and Monica Aguado, "Power Hardware-In-The-Loop technique applied to a LV Network for integrating a Supercapacitor with an Average Model of STATCOM," in IEEE International Workshop on Intelligent Energy Systems (IWIES 2013) Vienna, Austria, November, 2013, pp. 167-172. IEEE Indexed Conference Paper.